External Research Report ER74 [2022]

Recast Floors project

SESOC Journal Vol 35 No1 April 2022

Professor Ken Elwood et al

Project LR10207

University of Auckland, funded by the Building Research Levy

1222 Moonshine Road
RD1, Porirua 5381
Private Bag 50 908
Porirua 5240
New Zealand
branz.nz

This report provides a copy of the journal available at

https://www.sesoc.org.nz/library/sesoc-journals/vol-31-35/

Funded from the Building Research Levy

ISSN : 2423-0839

SESOC

RECAST FLOORS PROJECT PAPERS

SESOC takes great pleasure in publishing the following papers which have arisen from the ReCast Floors project. These papers relate to the performance of precast concrete floors in New Zealand including related design issues and retrofitting. The papers have been collated to provide comprehensive guidance for structural engineers and as stated in the introductory paper, ReCast Floors Project: Overview and Key Recommendations (Elwood, Brooke, Hogan), the Recast Floors project has two primary aims:

- Improving understanding of the likely behaviour of precast floors during earthquakes, including the performance of earthquake-damaged precast concrete floors, and
- Developing and validating methods for improving the performance of existing precast concrete floors.

SPECIAL EDITION
SESOC RECAST ISSUE

- **Recast Floors Project: Overview and Key Recommendations**
- **Overview of retrofit requirements and techniques for precast concrete floors**
- **Design recommendations for seating angles**
- **Design recommendations for strongback retrofits**
- **Seismic performance of precast hollow-core floors with modern detailing – A case study**
- **Real world experience of seismic performance and retrofits used in buildings with hollow-core floors**
- **Torsional capacity assessment of precast hollow-core floors**
- **Seismic damage observations of precast hollow-core floors from two full-scale super-assembly tests**
- **Load-path and stiffness degradation of floor diaphragms in reinforced concrete buildings subjected to lateral loading - Part I, Experimental Observations**
- **Load-path and stiffness degradation of floor diaphragms in reinforced concrete buildings subjected to lateral loading – Part II, Data Analysis**
- **Strategies for finite element modelling of precast pre-stressed hollow-core floors**

ISSN No. 2744-7871

RECAST FLOORS PROJECT: OVERVIEW AND KEY RECOMMENDATIONS

Elwood, K.J.[1], Brooke, N.J.[2], Hogan, L.S.[3]

1 INTRODUCTION

Precast concrete floors comprise precast floor units with in-situ (often lightly) reinforced concrete topping to form a composite floor system that generally also functions as a diaphragm. Such floors are a common feature of New Zealand buildings, being almost ubiquitous during the 1980s and early 1990s.

Four types of precast floor units are commonly encountered in New Zealand, namely

- hollow-core
- double tee
- ribs (with timber infill), and
- flat slabs.

All of these precast floor units are typically prestressed. Precast floors constructed using hollow-core and double tee units are distinguished by typically having longer spans and/or supporting heavier loads than rib or flat slab floors. Historically, a grey area existed regarding how responsibility for the design of precast concrete floors and their supports was divided between precast suppliers and the structural engineer for a building (Hare et al. 2009). Perhaps consequently, precast concrete floors were previously designed and constructed in ways that make the floors prone to poor performance during earthquakes, as has been documented previously (Corney et al. 2014; Fenwick et al. 2010; Hare et al. 2009; Henry et al. 2017; MBIE et al. 2018). Support conditions for units in existing buildings are likely to lead to significant damage and potentially collapse during design-level earthquakes.

Buildings with precast floors comprise a large percentage of the commercial building stock in all New Zealand cities. The Department of Building and Housing (now part of MBIE) found in 2007 that between Auckland, Wellington, and Christchurch, some 1.5 million square metres of hollow-core floor planks alone were supplied between 1981 and 2003 (DBH 2007). Anecdotal evidence based on post-earthquake inspections of buildings suggests that over 60% of commercial floor area in Wellington falls in this category. Observations suggest the proportion in Christchurch would have been similar until the earthquakes of 2010 and 2011, and there is no reason to think the situation is any different in Auckland and other major centres. While originally installed predominantly in commercial buildings, there are increasingly more residential buildings with older precast floor details as more buildings are being converted from commercial to residential use in major centres.

New Zealand's extensive use of precast floors in regions of high seismicity is unusual, with in-situ floors more commonly used internationally. Consequently, and in contrast to most other deficiencies found in existing buildings, little international research is available regarding the adequacy of existing precast floors. In this sense, the seismic performance of precast floors is "New Zealand's problem".

The collapse of double tee units in Statistics House (MBIE 2017, 2018) and widespread damage to other precast floors during the earthquakes that affected Christchurch and Wellington in recent years (Corney et al. 2014; Henry et al. 2017) has highlighted the risk that failure of precast floors can pose to building occupants. These events have also focussed attention on the difficulties of assessing and improving existing precast floors. The assessment of existing precast concrete floors is covered by Section C5 of the New Zealand seismic assessment guidelines (MBIE et al. 2017). The precast floor provisions saw a significant update in 2018 (MBIE et al. 2018) based in part on knowledge gained from the performance of precast floors in the Kaikoura Earthquake. The development of the update (MBIE et al. 2018) identified that significant unanswered questions existed regarding the performance and retrofit of precast concrete floors. The fact that no retrofit solutions for deficient precast concrete floors had been fully validated experimentally was a particular concern.

Recognising the urgent industry need for answers to these questions, funding was obtained from BRANZ in 2018 for an extensive three-year multi-agency research programme to address remaining questions about the performance and improvement of existing precast floors. The research programme, which has been dubbed the ReCast Floors (Retrofit of preCAST FLOORS) project, received further funding from EQC, QuakeCoRE, and Concrete NZ.

PAPER CLASS & TYPE: RESEARCH REFEREED

[1] *Professor, University of Auckland*
[2] *Managing Director, Compusoft Engineering*
[3] *Lecturer, University of Auckland*

The ReCast Floors project has two primary aims, namely:

- Improving understanding of the likely behaviour of precast floors during earthquakes, including the performance of earthquake-damaged precast concrete floors, and
- Developing and validating methods for improving the performance of existing precast concrete floors.

As outlined in this paper and summarised in Figure 1, ReCast Floors has investigated these topics in several different ways, including numerical simulations, full-scale laboratory tests, and 'real-world' investigations. These investigations have been undertaken by researchers from University of Auckland, University of Canterbury, and BRANZ, in close collaboration with structural engineering practitioners. The ReCast Floors project has supported four PhD students, one Masters student and several research assistants.

An industry advisory committee was assembled to ensure the focus and direction of the programme remained relevant to the needs of practicing structural engineers. This panel comprises representatives of stakeholder groups including SESOC, NZSEE, Concrete New Zealand Precast and Learned Society, Wellington City Council, and UC Quake Centre. The advisory group provided input on the direction of the research throughout the research programme, including during the development of potential retrofit solutions.

The ultimate goal of the ReCast Floors project was to assemble design guidance for the assessment and improvement of precast concrete floors. This special issue of the SESOC Journal achieves this goal by providing a summary of all aspects of ReCast Floors project to date, with a specific focus on recommendations of interest to structural engineers assessing and retrofitting building with precast floors. The purpose of this first paper is to provide an overview of the research programme and a summary of the key recommendations found in the rest of the special issue.

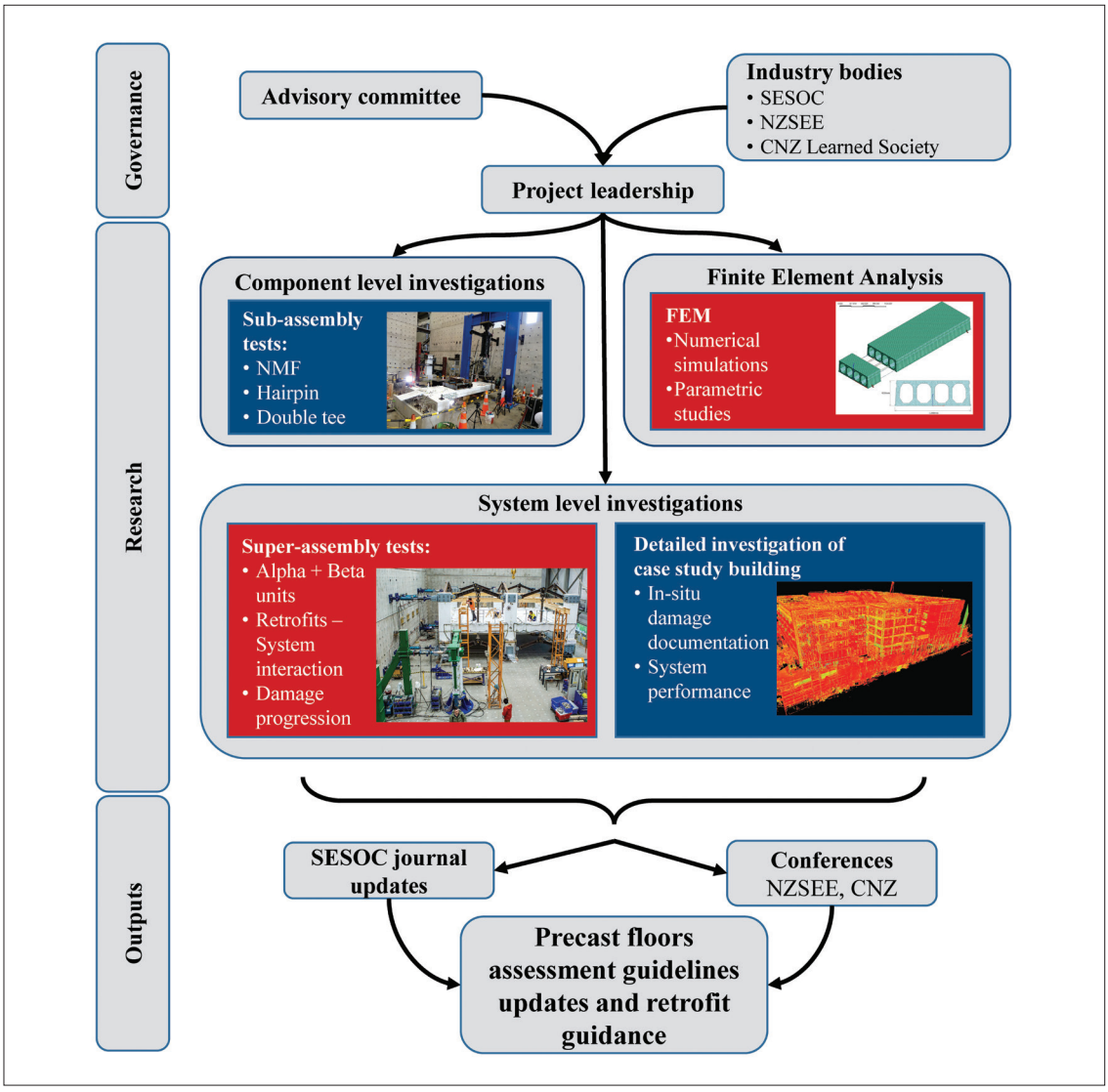

Figure 1: Overview of research projects, oversight arrangements, and outputs

2 SUMMARY OF RESEARCH PROGRAMME

As shown in Figure 1, research under the ReCast Floors project included:

- Finite element analysis of failures in hollow-core units.
- Component-level investigations using single-unit tests (Figure 2) to explore:
  - retrofits for negative moment failure of hollow-core,
  - performance of hollow-core with hairpin reinforcement, and
  - retrofits for flange-hung double-tee.
- System-level investigations via super-assembly tests (Figure 3) and detailed investigation of a damaged case study building to explore the interaction of the supporting frame and hollow-core units under three-dimensional demands.

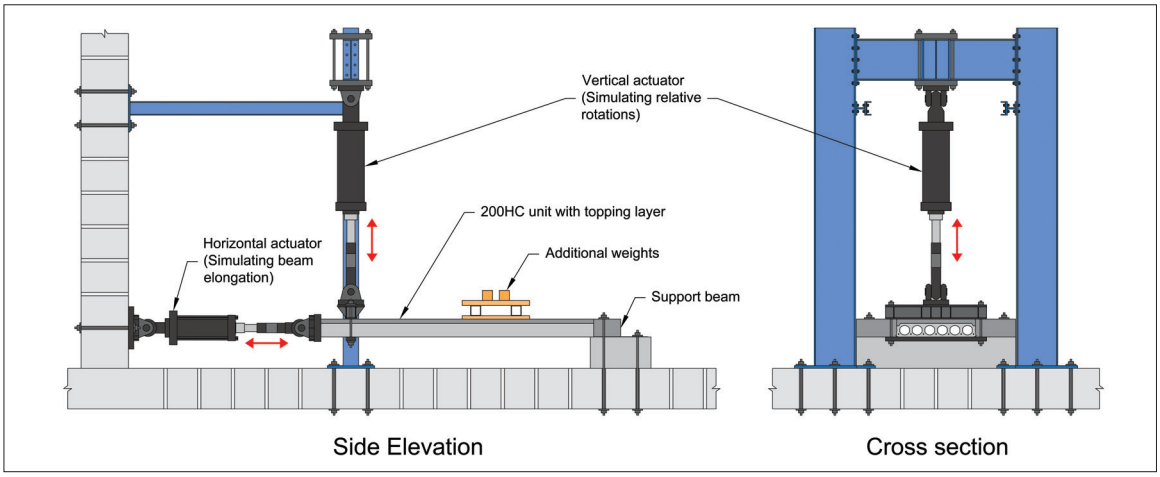

Figure 2: Example sub-assembly test arrangement

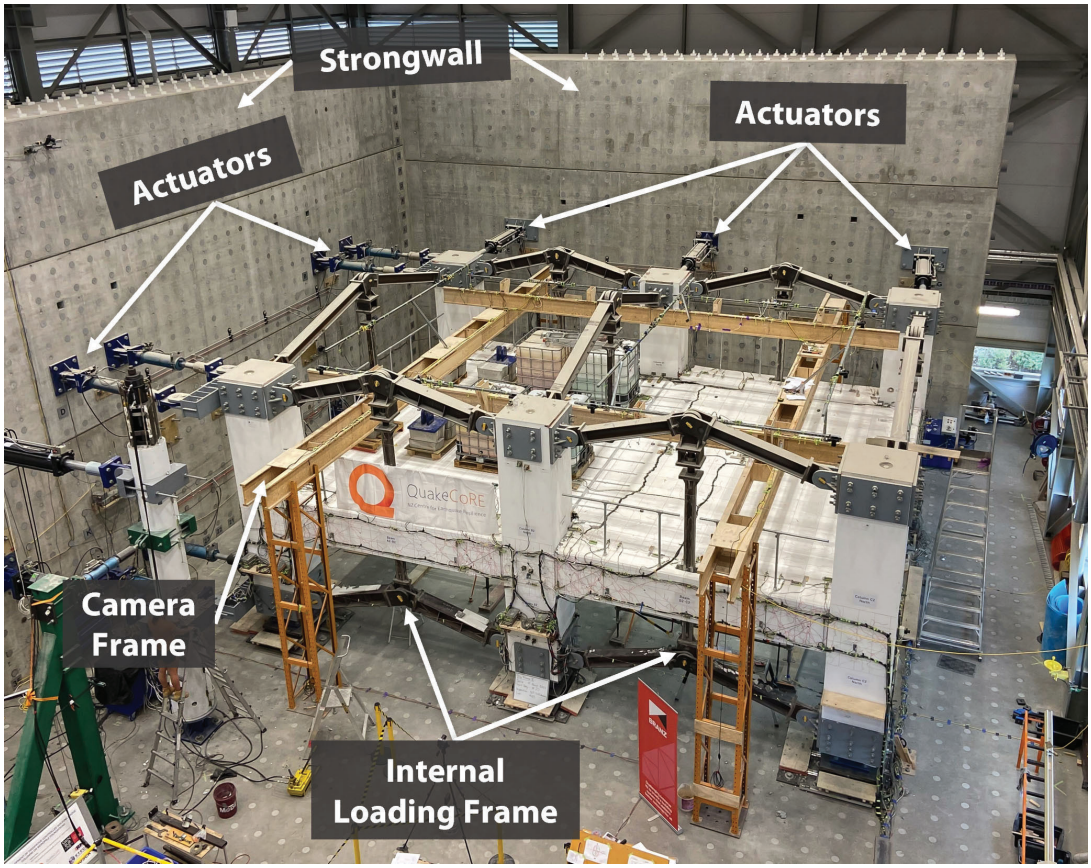

Figure 3: Super-assembly specimen (Büker et al 2022)

The experimental programme was very extensive including a total of 8 hollow-core shear tests, 10 hollow-core sub-assembly tests, 6 precast-tee single unit tests, and 2 super-assembly tests.

Furthermore, a very detailed damage survey of a building with hollow-core floors damaged during the Kaikoura earthquake was undertaken. The survey included 873 laser scans and over 105,000 photos, some of which were stitched together into three-dimensional renderings of the building, enabling a virtual post-earthquake inspection.

3 SESOC SPECIAL ISSUE

This issue of the SESOC Journal provides a summary of key outputs of the ReCast Floors project, with a specific focus on key observations and recommendations of interest to engineers engaged in seismic assessment and retrofit of buildings with precast floors. The intent is that this issue serves as a reference tool for engineers when facing challenges with assessment and retrofit of precast floors on future projects.Table 1 provides a list of all papers in the special issue. Papers have been organised by the following overarching themes: retrofits, building investigations, assessment and damage of hollow-core floors, diaphragm performance, and finite-element analysis.

Note that a further paper from the ReCast Floors project on the performance of double-tee floor systems and testing of retrofit solutions is expected to be published in the near future.

Table 1: Special issue papers

Topic	Paper No	Authors	Title	Page
Retrofits	1	Brooke, Büker, Bull, Elwood, Henry, Hogan	Overview of retrofit requirements and techniques for precast concrete floors	30
	2	Büker, Hogan, Brooke, Elwood, Bull	Design recommendations for seating angle retrofits	55
	3	Büker, Brooke, Hogan, Elwood, Bull, Sullivan	Design recommendations for strongback retrofits	69
Building investigations	4	Mostafa, Hogan, Elwood	Seismic performance of precast hollow-core floors with modern detailing – A case study	86
	5	Liu, Henry, Hogan, Brooke	Real world experience of seismic performance and retrofits used in buildings with hollow-core floors	102
Assessment and Damage of hollow-core floors	6	Mostafa, Hogan, Elwood	Torsional capacity assessment of precast hollow-core floors	109
	7	Büker, Parr, De Francesco, Hogan, Bull, Elwood, Liu, Sullivan	Seismic damage observations of precast hollow-core floors from two full-scale super-assembly tests	125
Diaphragm performance	8	Parr, Büker, De Francesco, Bull, Brooke, Elwood, Hogan, Liu, Sullivan	Load-path and stiffness degradation of floor diaphragms in reinforced concrete buildings subjected to lateral loading - Part I, Experimental observations	149
	9	Parr, Bull, Brooke, De Francesco, Elwood, Hogan, Liu, Sullivan	Load-path and stiffness degradation of floor diaphragms in reinforced concrete buildings subjected to lateral loading – Part II, Data analysis	172
Finite element analysis	10	Sarkis, Sullivan, Brunesi, Nascimbene	Strategies for finite element modelling of precast pre-stressed hollow-core floors	204

4 KEY RECOMMENDATIONS AND OBSERVATIONS

The following provides a quick overview of some of the key outcomes of the ReCast Floors project of value to the structural engineering community. These reference the paper number from Table 1 to facilitate quick reference to the appropriate paper within this special issue for more details. Recommendations are separated below between those that are applicable to all precast floors, those that apply specifically to hollow-core floors, and those applicable specifically to double tee floors.

4.1 GENERALLY APPLICABLE RECOMMENDATIONS

- Precast floor units in certain locations are more prone to damage during earthquakes. This includes "alpha units" that are immediately adjacent to a parallel beam, wall, or other structural element, and "beta units" that are supported at or adjacent to an intermediate column or a wall. The susceptibility of (particularly hollow-core) beta units to damage is not addressed in current assessment guidance (Papers 1, 4 and 7).
- It is typically not possible to retrofit precast concrete floors to achieve more than life safety performance during strong earthquake shaking. During such shaking, retrofitted floors are expected to sustain damage that may be difficult or impossible to repair (Paper 1).
- It is critical that deformation (in)compatibility between precast floor units, retrofit components and primary structure be considered when designing and detailing retrofits for precast floors (Paper 1).
- Strong preference should be given to retrofits that have been shown experimentally to be able to accommodate the interaction of deformations in three dimensions that affect the behaviour of precast floors (Paper 1).
- Load combination used for design of retrofits of precast floors should be different from that used for retrofits of the lateral system, reflecting the role of precast floors to provide gravity load support before, during, and after the earthquake (Paper 1).
- Retrofits should be designed and detailed so that they are not prone to brittle failure if overloaded (Papers 1, 2, 3).

Diaphragms were not a primary focus of the ReCast Floors project; however, the super-assembly tests offered a rare opportunity for experimental investigation of diaphragm behaviour. This produced a number of observations and recommendations (Papers 8 and 9):

- A previously unrecognised "rubble interlock" phenomenon allows compression forces to be transferred across wide cracks. However, the rubble interlock mechanism does not result in direct transfer of compression forces to columns as is often assumed in idealised strut-and-tie models of diaphragms.
- The behaviour of diaphragms can be greatly affected by the robustness of topping reinforcement crossing between adjacent beta units.
- Diaphragm load paths may be impacted by degradation of the torsional stiffness of beams at the diaphragm perimeter.
- Diaphragm stiffness degrades substantially as imposed diaphragm deformations are increased. Testing reported in Paper 9 indicates that the diaphragm stiffness can degrade by as much as 75% after drift demands exceed approximately 1%.

Further work is required to determine how these observations should be reflected in diaphragm assessment procedures.

4.2 HOLLOW-CORE FLOORS

Damage observations:

- While the seating details from NZS 3101:2006 Amendment 2 in the case study building addressed loss of seating, positive moment failure, and negative moment failure, they did not prevent severe damage to several beta units, including web cracking. The observed damage patterns are not directly accounted for in the assessment procedures of the Assessment Guidelines. Based on these observations, MBIE is currently initiating public consultation on changes to B1/VM1 such that the seating detail in Figure C18.4 NZS 3101:2006-A3 will not be considered a deemed-to-comply solution. (Paper 4).
- In full-scale super-assembly test, web-cracking was observed at 0.5% inter-storey drift but can be very difficult to detect after earthquake loading (Paper 7).
- Cracks emanating from a soffit crack can propagate at different angles through the webs, including at shallower angles than observed in previous experiments. (Paper 7).
- A gravity test of a web-cracked hollow-core unit demonstrated that such cracking reduces the gravity load capacity of hollow-core floors. Additional research is required to reliably quantify the reduction in the shear capacity (Paper 7).
- Transverse soffit cracks can form away from the support and beyond the typical seating retrofit, but the criticality of this crack depends on the

orientation of the crack and the concrete-to-strand bond on either side of the soffit crack. There is currently no known means of determining if the bond to the strand has been compromised (Paper 7).

Assessments:

- Tools have been provided to simplify torsion assessment of hollow-core units. It is recommended to only consider the equivalent tube section case for assessing the torsional capacity of hollow-core floor units and not consider the flange-only case. (Paper 6).
- Further research is required to improve the current torsional capacity assessment methodology. Limitations of the existing approach suggest that a cautious approach should be adopted when considering whether a retrofit to address torsion is required (Paper 6).
- The assessment guidelines C5 (MBIE et al. 2018) have been found to provide a good indication for the drift capacity of the tested hollow-core floors in full-scale super-assembly tests. However, in many instances, the observed damage patterns did not reflect the predicted governing failure modes (Paper 7).

Retrofits:

The recommendations below are discussed in Paper 1, and in more detail in other papers where noted:

- Retrofits that have been shown experimentally to address one or more failure modes comprise supplementary seating (Papers 2 and 7), strongback supports (Paper 3), the cable catch system, supplementary negative moment reinforcement, catch beams, and cutting of starter bar reinforcement.
- The shallow angle of some positive moment cracks noted in Paper 7 means that supplemental seating alone is not recommended to address positive moment failures (Paper 2).
- Supplementary transverse reinforcement is expected to be an effective retrofit technique, but has not yet been experimentally validated.
- Supplementary positive moment reinforcement has not been demonstrated to be an effective retrofit. It may be useful in conjunction with other measures, but this has not been experimentally validated.
- Infilling of cores and inducement of cracking at the ends of units are not effective retrofit techniques.

4.3 DOUBLE TEE FLOORS

- Double tee floors may be effectively retrofitted using supplementary corbels or articulating hangers. Post-installed Cazaly hangers may also be an effective retrofit, but this has not been demonstrated experimentally (Paper 1).

4.4 FLAT SLAB AND RIB AND INFILL FLOORS

- Retrofit techniques for flat slab and rib and infill floors would be broadly similar to those for hollow-core and double tee floors, respectively (Paper 1).

5 ACKNOWLEDGEMENTS

The primary funding committed by BRANZ, and supplemental funding from EQC, QuakeCoRE and Concrete New Zealand Learned Society for the ReCast Floors project is gratefully acknowledged. We also thank the project advisory group who generously donated their time and experience throughout the project. The project advisory group included: Alistair Cattanach, James Jensen, Jamie Macgregor, Ray Patton, Chris Poland, Peter Smith, Derek Baxter, Greg Preston and Rod Fulford.
We also thank the reviewers of the special issue papers for their detailed feedback which has helped improve the value of this special issue to structural engineering practice.

Special thanks is due to the PhD and Masters students who were key to the success of this research programme: Frank Büker, Matthew Jenkins, Mohamed Mostafa, Mike Parr and Ana Sarkis Fernandez. Furthermore, the successful delivery of the experimental programme would not have been possible without the countless hours and valuable advice of the technical staff at the University of Canterbury and University of Auckland, most notably Dave Carney, Alan Thirlwell, Russell McConchie, Norman King, Dave MacPherson, John Maley and Patrick Rogers. Also noteworthy is the contribution of the many students who helped with many long hours in the laboratory, namely Eldhose Thoyalinkara Paulose, Max Chirapattanakorn, Trevor Garrett, Abhishek Madan, Yuxin Huang, Claire Dong, Justin Brown, Jacob Nicholls, Alex Kirby, Trent Gawith and Kongson Zhong.

6 OTHER RECAST FLOORS REFERENCES

In addition to this SESOC Special Issue, the ReCast Floors project team and collaborators have published results of the research programme and associated activities in various journals and conferences. Below is a chronological list of additional papers either published, submitted, or in development, which may be of further interest to the readers of this special issue.

Corney, S. R., Elwood, K. J., Henry, R. S. Henry. 2018. “Residual capacity testing of damaged hollow-core precast concrete floors.” Proceedings of the 2018 NZSEE Annual Technical Conference, 9. Auckland, New Zealand: New Zealand Society for Earthquake Engineering.

Corney, S. R., Elwood, K. J., Henry, R. S., Nims, D. K. 2018. Assessment of existing concrete buildings in Wellington with precast floors. Kaikoura Earthquake Research Programme (2017-18). Lower Hutt, New Zealand: Natural Hazards Research Platform.

Hare, J., Elwood, K. J., Bull, D. K., Henry, R. S., and Brooke, N. J. 2019. “Precast Double Tee Support Systems - 10 Years On.” SESOC Journal, 32(1), pp.32–40.

Puranam, A., Bueker F., and Elwood, K. J. 2019. “Assessment of reinforced concrete buildings with hollow-core floors.” Proceedings of the 2019 Pacific Conference on Earthquake Engineering, 10. Auckland, New Zealand: New Zealand Society for Earthquake Engineering.

Parr, M., Elwood, K. J., Bull, D. K., Büker F., Hogan L. S., Puranam, A. Y., Henry R. S., and Brooke N. J. 2019. “Development and Testing of Retrofit Solutions for Hollow-core Floors in Existing Buildings.” Proceedings of the 2019 Concrete New Zealand Conference, 12. Dunedin, New Zealand: Concrete New Zealand

Büker, F., Poland C., and Brooke N. J. 2020. “Assessment of Existing Precast Concrete Floors: Hollow-core Worked Example - Revision 1.” Journal of the Structural Engineering Society New Zealand, 33 (2): 44–86.

De Francesco, G., and Sullivan,T. J. 2021. “Experimental loading protocols to evaluate the seismic performance of floor systems.” Proceedings of the 2021 NZSEE Annual Technical Conference, 12. Christchurch, New Zealand: New Zealand Society for Earthquake Engineering.

Sarkis, A. I., and Sullivan,T. J. 2021. “Finite element analyses of hollow-core units subjected to shear and torsion.” Proceedings of the 2021 NZSEE Annual Technical Conference, 8. Christchurch, New Zealand: New Zealand Society for Earthquake Engineering.

Büker, F., Brooke, N. J.,Elwood, K. J., Bull, D. K., Hogan, L. S. and Parr, M. 2021. “Development and Validation of Retrofit Techniques for Hollow-core Floors.” Proceedings of the 2021 SESOC Conference, 14. Hamilton, New Zealand: Structural Engineering Society New Zealand.

Corney, S. R., Puranam, A. Y., Elwood, K. J. Henry, R. S. and Bull, D. K. 2021. “Seismic Performance of Precast Hollow-Core Floors: Part 1—Experimental Data.” ACI Structural Journal, 118 (5): 49–64. https://doi.org/10.14359/51732821.

Puranam, A. Y., Corney, S. R., Elwood, K. J., Henry, R. S. and Bull, D. K. 2021. “Seismic performance of precast hollow-core floors: Part 2-assessment of existing buildings.” ACI Structural Journal, 118 (5): 65–77. https://doi.org/10.14359/51732822.

Mostafa, M. T., Büker, F., Hogan, L. S., Elwood, K. J., Bull, D. K. and Parr, M. 2022. “Seismic Performance of Precast Hollow-core Units Seated Within the Plastic Hinge Region (accepted).” Proceedings of the 2022 NZSEE Annual Technical Conference, 12. Wellington, New Zealand: New Zealand Society for Earthquake Engineering.

De Francesco, G., Sullivan, T. J., and Nievas, C. I. (Accepted). “Highlighting the need for multiple loading protocols in bi-directional testing.” Bulletin of the New Zealand Society for Earthquake Engineering, 15.

Sarkis Fernandez, A., Bueker F., Sullivan, T., Elwood, K. J., Brunesi, E., and Hogan, L. S. (Accepted). “Aspects affecting the nonlinear behavior of precast pre-stressed hollow-core units failing in shear.” Structural Concrete. https://doi.org/10.1002/suco.202100579.

Henry, R. S., and Jenkins, M. (In Development). “Retrofit Techniques for Double-Tee Floors: Experimental Investigation and Design Recommendations.” SESOC Journal.

Mostafa, M., Hogan, L. S., Stephens, M., Olsen, M. J., & Elwood, K. J. (In Development). “A Detailed Damage Investigation of an Instrumented Building Damaged During the M-7.8 Kaikoura Earthquake”. Earthquake Spectra.

7 REFERENCES

Corney, S. R., Henry, R. S., and Ingham, J. M. 2014. “Performance of Precast Concrete Floor Systems During the 2010/2011 Canterbury Earthquake Series.” Mag. Concr. Res., 66 (11): 563–575.

DBH. 2007. Hollowcore Floor Overview Report. 23. Wellington, New Zealand: Department of Building and Housing.

Fenwick, R. C., Bull, D. K., and Gardiner, D. R. 2010. Assessment of Hollow-Core Floors for Seismic Performance. 152. Christchurch, New Zealand: Department of Civil and Natural Resources Engineering, The University of Canterbury.

Hare, J., Fenwick, R. C., Bull, D. and Built, R. 2009. “Precast Double Tee Support Systems.” J. Struct. Eng. Soc. N. Z., 22 (1): 10–44.

Henry, R. S., Dizhur, D., Elwood, K. J., Hare, J. and Brunsdon, D. 2017. “Damage to Concrete Buildings with Precast Floors During the 2016 Kaikoura Earthquake.” Bull. N. Z. Soc. Earthq. Eng., 50 (2): 174–186.

MBIE. 2017. Investigation into the Performance of Statistics House in the 14 November 2016 Kaikoura Earthquake. 36. Wellington, New Zealand: Ministry of Business, Innovation, and Employment.

MBIE. 2018. Addendum: Investigation into the Performance of Statistics House in the 14 November 2016 Kaikoura Earthquake. 25. Wellington, New Zealand: Ministry of Business, Innovation, and Employment.

MBIE, NZSEE, EQC, NZGS, and SESOC. 2017. The Seismic Assessment of Existing Buildings: Technical Guidelines for Engineering Assessments. Technical Guidelines for Engineering Assessments. Wellington, New Zealand: Ministry of Business, Innovation, and Employment.

MBIE, NZSEE, EQC, NZGS, and SESOC. 2018. Technical Proposal to Revise the Engineering Assessment Guidelines - Part C5 Concrete Buildings. 252. Wellington, New Zealand: Ministry of Business, Innovation, and Employment.

ISSN No. 2744-7871

OVERVIEW OF RETROFIT REQUIREMENTS AND TECHNIQUES FOR PRECAST CONCRETE FLOORS

Brooke, N.J.[1], Büker, F.[2], Bull, D.K.[3], Elwood, K.J.[4], Henry, R.S.[5], Hogan, L.[6]

ABSTRACT

Despite development of detailed assessment procedures based on extensive past research, little guidance has previously been available regarding how to retrofit deficient precast floors. Additionally, prior to the ReCast floor project there had been little previous experimental validation of retrofit techniques for precast concrete floors. This paper outlines philosophical requirements affecting design and detailing of retrofits for precast concrete floors, and summarises the efficacy of known retrofits techniques for floors constructed using hollow-core, double tee, flat slab, or rib and infill precast units.

1 INTRODUCTION

The use of precast concrete elements to construct the floors of buildings became almost ubiquitous in New Zealand during the 1980s and through much of the 1990s (Bull 1999; fib Task Group 7.3 2003; CCANZ 2004). Hollow-core floor units were particularly commonly used, along with still-substantial extents of double tee, rib and infill, and flat-slab units. However, failures of precast concrete floors during the Northridge earthquake (Norton et al. 1994) and subsequent research at the University of Canterbury over an approximately 15 year period around the turn of the millennium revealed that then-typical hollow-core floor detailing was prone to poor seismic performance (Herlihy 1999; Jensen 2006; Liew 2004; Lindsay 2004; Matthews 2004; Woods 2008). Around the same time concerns were also raised regarding performance of some other precast floor configurations (Hare et al. 2009), with these concerns later confirmed and amplified by observed performance of floors of buildings in Christchurch (Cattanach and Thompson 2013; Cooper et al. 2012; Corney et al. 2014) and Wellington (Brunsdon et al. 2017; Henry et al. 2017; MBIE 2017, 2018).

Drawing on the extensive research undertaken at the University of Canterbury, detailed guidance on assessing the behaviour of existing precast concrete floors was first published for hollow-core floors (Fenwick et al. 2010), with less comprehensive guidance also produced for double tee floors (Hare et al. 2009). More recently these guidelines have been refined and extended to cover all major precast flooring types (MBIE et al. 2018), based in part on further research undertaken at the University of Auckland (Corney 2017) and understanding gained from observations in Wellington following the Kaikoura earthquake. While some areas of uncertainty remain about the performance of existing precast concrete floors, these guidelines permit thorough assessment of floors by practicing engineers.

In contrast to guidance on assessment of precast concrete floors, relatively little information has been published that provides a clear basis for the design of retrofit solutions for precast concrete floors. Available information largely comprises advice dispersed between various research reports (e.g. Jensen 2006; Liew 2004) and the useful, but non-specific and now rather dated, draft summary of retrofit techniques published by the 'Precast Concrete Floors Overview Group' (PCFOG 2009). This lack of guidance reflects the fact that few, if any, retrofit techniques for precast concrete floors have previously been robustly investigated through analyses and experiments.

The ReCast Floors project (Brooke et al. 2019) was established in 2018 with the primary aims of refining understanding of the behaviour of precast concrete floors and validating and documenting design methods for retrofit methods for such floors. The project is principally funded by BRANZ from the Building Levy, with additional financial support received from EQC via the UC Quake Centre, Concrete New Zealand Learned Society, and

PAPER CLASS & TYPE: GENERAL REFEREED

[1] *Managing Director, Compusoft Engineering Limited*
[2] *PhD Candidate, The University of Auckland*
[3] *Technical Director, Holmes Consulting*
[4] *Professor, The University of Auckland*
[5] *Associate Professor, The University of Auckland*
[6] *Lecturer, The University of Auckland*

QuakeCoRE. Various initial outputs from the project (e.g. Henry et al. 2018; Parr et al. 2019; Sarkis et al. 2019; Puranam et al. 2019; Corney et al. 2021; Puranam et al. 2021) have so far largely documented aspects of the performance of existing floors.

The purpose of this paper is to collate retrofit techniques for precast concrete floors that have been proposed in various forums, and to summarise what (if any) improvement can be gained from each technique. Details are also provided regarding the extent of analytical or experimental validation that has occurred for each technique, available sources of more detailed guidance, and other information as may be relevant. It is intended that this paper and companion papers supersede the retrofit guidance provided in Chapter 8 of the Precast Concrete Floors Overview Group report (PCFOG 2009).

The paper is divided into a number of sections. The first of these provides discussion on the design philosophies that need to be considered during design of retrofits for precast concrete floors. Retrofits addressing hollow-core floors are summarised in section 3, followed in section 4 by those specifically applicable to floors constructed using double tees units considered. Brief discussion of retrofit techniques for flat slab and rib and infill floors is presented in section 5.

This paper does not consider or address retrofit techniques and requirements for floor diaphragms.

1.1 UNIT DESIGNATIONS

Precast floor units in certain locations are more prone to damage during an earthquake. Notably this includes, with reference to Figure 1:

- 'Alpha' units that are immediately adjacent to a parallel beam, wall, or other structural element, and
- 'Beta' units that are supported at or adjacent to an intermediate column or a wall.

Beta units are notably not addressed at all in the current Appendix C5E assessment guidance (MBIE et al. 2018), but their susceptibility to damage has now been well documented both in the laboratory (Büker et al. 2022c) and in earthquake-damaged buildings (Mostafa et al. 2022; Siddiqui et al. 2019).

Concerns regarding the behaviour of alpha and beta units are most commonly raised in relation to hollow-core floors. However, other precast floor units in these locations may also be more prone to damage.

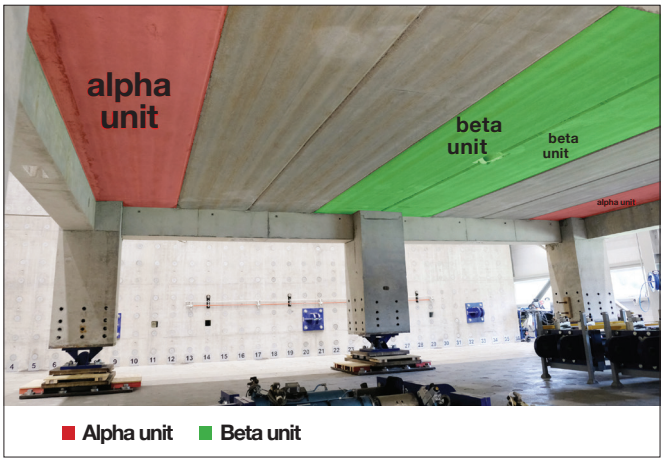

Figure 1: Underside of the 'super-assembly' specimen with alpha and beta units identified

2 RETROFIT PHILOSOPHY

Design of retrofit measures for precast concrete floors requires consideration of both the design philosophies that are generally applicable to all retrofits, as well as factors that are more specific to precast concrete floors. These philosophies are summarised in the following sections.

2.1 PERFORMANCE EXPECTATIONS AND REQUIREMENTS

Assessment of existing buildings in New Zealand is underpinned by *The Seismic Assessment of Existing Buildings: Technical Guidelines for Engineering Assessments* (MBIE et al. 2017 - the Guidelines). The Guidelines also consequently have an important role in setting the performance expectations for retrofits of structures, notwithstanding that the Guidelines contain relatively far less information pertaining to retrofit than assessment.

The Guidelines require earthquake scores (of building elements) and the consequent earthquake rating of a building to be expressed relative to the ultimate limit state (ULS) seismic demand used to design an equivalent new building on the same site, with these demands being tied for some purposes to those in effect on 1 July 2017. The resulting values are expressed as %NBS, i.e. the a percentage of New Building Standard calculated in accordance with the Guidelines. As a result of this assessment framework, it is typical that retrofits for structures (including precast concrete floors) are designed with the aim of increasing the earthquake scores of elements (and hence the earthquake rating of a building) to a specific %NBS value.

Section A10 of the Guidelines provides high level guidance regarding improvement of seismic performance, i.e. retrofit. Importantly, Section A10.2.4 notes that retrofit works must comply with the Building

Code (MBIE 2019). This is required by Section 17 of the Building Act (New Zealand Government 2004) because installing retrofits constitutes building work. In considering the requirement for compliance with the Building Code it is important that this not be confused with a requirement that the earthquake scores of retrofitted elements be 100%NBS. Rather, in summary, retrofit elements are required to resist demands associated with the ULS demands (factored where appropriate by the targeted %NBS rating, refer section 2.2) with design completed in accordance with Verification Method B1/BM1 or other appropriate Standards. Engineers are recommended to review Section A10.2.4 of the Guidelines, but for precast concrete floor retrofits the following points are pertinent:

- Demands on retrofit elements should be compared to the dependable strength of the element, i.e. the nominal strength, calculated using specified lower characteristic material strengths, multiplied by an appropriate strength reduction factor as specified in the relevant Standard, e.g. NZS 3101 or NZS 3404 (SNZ 2007, 2017).
- Anchors should typically be designed using provisions for seismic performance category C2 (CEN 2018), as described in section 2.5.
- Design of retrofit seating measures should be based on the required seating length specified in Chapter 18 of the New Zealand Concrete Structures Standard, NZS 3101 (SNZ 2017), with further guidance provided in a companion paper (Büker et al. 2022b).
- The earthquake scores of unretrofitted components (or for failure modes not affected by retrofits) should be assessed by relevant assessment guidance (MBIE et al. 2017, 2018) when determining the earthquake rating of the building after retrofit.

There are notable differences between the procedures used in design and assessment for determining the required seating length. At face value, the multiplier applied to drift demands for assessment (×2) appears greater than for design (×1.5/Sp) for some structures. However, other conservatisms in the design procedure are expected to result in the seating length required for design being larger than that required for assessment.

Engineers should clearly identify whether the design approach they adopt follows Verification Method B1/VM1, and hence is deemed to comply with the Building Code, or whether use of unreferenced Standards and guidance means that the retrofit design constitutes an Alternative Solution. This fact should be clearly communicated to reviewers and the building consent authority.

2.1.1 Targeting of retrofits

Retrofit measures should be well targeted to avoid unnecessary expense. For precast floors, this means that retrofit requirements should be determined on a unit-by-unit basis, or at least for groups of similar units. For example, the retrofits required for units within the elongation zone (MBIE et al. 2018) may be different to those outside that zone, and alpha and beta units typically warrant separate consideration. It may well be the case that the required retrofits varied markedly over the height of a building due to variation of drift demands at different levels.

It is also important to consider not just the critical mode of behaviour that defines the earthquake score for a particular precast unit, but the hierarchy of limiting behaviours that are expected as drift demand increases. Taking, for example, a hollow-core floor unit, assessment might show (with reference to section 3 for definitions) that LOS is expected at 1.2% drift and PMF at 1.8% drift, with NMF and WSF not anticipated. Installation of supplementary seating (section 3.1) would address the LOS. Whether this retrofit was sufficient would depend on the target drift capacity (i.e. %NBS). If the target drift capacity was (e.g.) 2%, then supplementary seating alone would not be a sufficient retrofit. As noted in section 3.1, supplementary seating does not address PMF. While it might be appealing to think that the expected occurrence of LOS at 1.2% drift would ‘protect’ against the occurrence of PMF, experimental evidence shows that this cannot be relied on. Consequently, for this example, retrofit would be required to address both LOS and PMF.

Consideration should also be given to non-structural items proximate to the precast floor. While retrofit is likely to disrupt existing services and fitout, the configuration of these items may inform the decision between alternative retrofit techniques that offer similar structural outcomes but different levels of disruption.

2.1.2 Expected performance of retrofits

Beyond simply achieving a selected %NBS target, Section A10.2.1 of the Guidelines emphasises the importance of understanding the requirements and expectations of the building owner. This may also necessitate improving the owner’s understanding of the likely outcomes of earthquake shaking of various intensities so that their expectations are realistic. This is certainly an important step in retrofit of precast concrete floors. Engineers should ensure that owners understand that:

- it is typically not possible to retrofit precast concrete floors to achieve more than life safety objectives during strong earthquake shaking
- Damage that may be difficult or impossible to repair is likely to occur even if a floor has been retrofitted, and
- Such damage could occur even during relatively low intensity shaking, i.e. shaking below that associated with the retrofitted %NBS.

Of particular note is that most retrofit techniques for precast concrete floors do not prevent failures from occurring, but instead are expected to reduce the life safety hazard to an acceptable level. Most retrofit techniques are more specifically "catch" systems that are expected to result in the floor unit displacing vertically but not collapsing. The term catch system is used at points through this paper in reference to such systems. As elaborated on in section 2.3, it is generally recommended to install a compressible layer between precast units and catch system retrofit components to reduce the suddenness of the expected vertical displacement associated with engagement of the retrofit.

2.1.3 Validation of retrofit techniques

As noted in the introduction to this paper, little robust investigation of retrofit techniques for precast floors existed prior to the ReCast Floors project. This paucity of information was a key motivator for the project.

As outlined elsewhere in this paper, and detailed in other companion papers (Büker et al. 2022a; b; c), several retrofit techniques have been extensively investigated by the ReCast Floors project. These investigations have comprised both analytical and experimental aspects, with experimental investigations further bifurcated between sub-assembly and super-assembly tests (Elwood and Hogan 2022).

Retrofit techniques that have been shown to perform satisfactorily in appropriate experiments and that have a sound analytical basis can be considered to be robustly validated. A number of such retrofit techniques are identified in this paper, in some cases with caveats about performance limitations and/or remaining uncertainties.

Inevitably, specific project circumstances may require consideration of retrofit techniques that have not been robustly investigated. Engineers should be cautious before adopting such techniques. The behaviour of precast floors and their retrofits is dependent on complex three-dimensional interaction of various components that are difficult to replicate from either analysis or sub-assembly testing alone. Alternative retrofit techniques must be based on sound engineering principles, with reference to experimental testing where possible and appropriate. Particular care is required to ensure that three-dimensional effects are adequately understood.

2.2 DESIGN ACTION COMBINATIONS

Building retrofits must be designed to resist appropriate combinations of design actions, with the combinations and actions requiring consideration generally following the requirements of the Structural Design Actions Standard, NZS 1170 (SNZ 2011).

In contrast to many retrofits that have their design governed by the seismic actions they are required to resist during an earthquake, precast floor retrofits are often primarily intended to provide reliable load paths for gravity actions both during and after a damaging earthquake.

Where precast floor retrofits are required to provide reliable load paths for gravity actions after the floor is damaged by an earthquake or other event, design should be consistent with the approach specified in AS/NZS 1170.0 for ULS gravity strength checks. AS/NZS 1170.0 requires that two gravity combinations be considered:

$$E_d = 1.35G \quad (1)$$

$$E_d = 1.2\mathrm{G} + 1.5Q \quad (2)$$

Where E_d is the design action effect, G is the permanent action (i.e. 'dead load') and Q is the imposed action ('live load'). The area reduction factor, ψ_α, is not included in this combination because it is required to be taken as 1.0 for one-way slabs such as precast concrete floors.

Focussing on Equation 2, a reasonable argument can be made that in some circumstances it is unrealistic for the full imposed action, Q, to act on a damaged floor during or (for temporary use) after an earthquake. In recognition, Equation 2 may be altered to:

$$E_d = 1.2\mathrm{G} + 1.5\psi_E Q \quad (3)$$

Where ψ_E is the combination factor for earthquake actions.

Before adopting Equation 3 as the basis of a retrofit design, engineers should consider the following factors:

1 It would be inappropriate to adopt the reduced demand suggested by Equation 3 for areas of floor that provide emergency egress routes, and consequently could be expected to be heavily loaded in the aftermath of an earthquake. Identification of such egress routes may be challenging, particularly for open plan spaces.

2 Engineers should be cautious about suggesting that a precast floor could remain usable after it had sustained damage that was sufficient to cause retrofits to be engaged. Notwithstanding, adoption of Equation 3 would be inappropriate if there was a desire to protect the potential for such post-damage usage. Where Equation 3 was used to design retrofits, it would be critical that careful post-earthquake inspection was undertaken to ascertain whether retrofits had been engaged.

Where retrofits are designed to resist seismic actions induced during an earthquake, design should consider the typical earthquake design action combination specified by AS/NZS 1170.0 but with the earthquake actions factored to reflect the targeted %NBS rating, i.e.:

$$E_d = \mathrm{G} + \psi_E Q + \psi_{\%NBS} E_u \qquad (4)$$

Where $\psi_{\%NBS}$ is a non-conventional notation introduced to reduce the ULS earthquake demand to reflect the targeted %NBS score.

For retrofits where the performance target is based on drift or displacement, the design demand should be based on the peak Maximum Considered Earthquake (MCE) drift as defined in the Concrete Structures Standard (SNZ 2017) factored to reflect the targeted %NBS rating. Thus the design drift demand should be:

$$\psi_{\%NBS}\,\delta_{peak.MCE} = \frac{1.5}{S_p}\,\psi_{\%NBS}\,\delta_{ULS} \qquad (5)$$

Where s_p is the structural performance factor used in the assessment, δ_{ULS} is the ULS interstorey drift for the structure, and $\delta_{peak.MCE}$ is the peak MCE interstorey drift demand for the structure.

It is not generally necessary to design retrofits to accommodate the 2.5% maximum ULS interstorey drift permitted by the Design Actions Standard (SNZ 2016), the exception of course being if analysis indicated that this level of drift occurred in the structure when it responded to the targeted %NBS level of shaking.

2.3 DEFORMATION COMPATIBILITY

For many retrofits it is necessary for designers to ensure that provided clearances are adequate to prevent unwanted interaction between the floor, retrofit, and/or superstructure of the building. Detailed guidance on the location and magnitude of clearances required for certain retrofit techniques can be found in other companion papers (Büker et al. 2022a; b). The principles and approaches outlined in these papers can be used as guidance for detailed consideration of other retrofit techniques.

Addressing differential vertical movement of retrofits and the floor is a particular challenge:

- If clearance is not provided, excessive demands could be induced on the floor or the retrofit. However,
- If clearance is provided consideration may be required regarding the potential for dynamic impact forces to be generated as a retrofit engages.

Avoiding the uncertainty of dynamic impact forces presents a strong argument for preferring retrofit techniques that are installed in contact with the floor. However, in many instances this is not practical due to the risk of generating problematically large forces due to deformation (in)compatibility. For such situations, i.e. where it is necessary to use a catch system as defined in section 2.1.2, it is considered that retrofit design could be undertaken without specific consideration of dynamic impact forces provided a deformable layer is included that provides a load path between the precast floor unit and the retrofit. Commentary on where such deformable layers are recommended are made in various parts of sections 3 and 4. The presence of the deformable layer will obviously result in forces being induced on the floor and retrofit when the building displaces laterally. While the magnitude of these forces will be less than if there was direct contact between the (e.g. steel) retrofit and the precast unit, it is critical that their impact be considered. An example of how to do so can be found in a companion paper (Büker et al. 2022b).

2.4 FAILURE HIERARCHY OF RETROFIT HARDWARE

The key concern with precast concrete floors is the brittle nature of most of the failure modes that they are susceptible to. Both for this reason, and in accordance with common structural engineering practice, it is highly desirable that retrofits for precast floors be designed so that they exhibit a ductile failure if subjected to demands larger than those anticipated during design.

The most dependable way of ensuring ductile behaviour is to employ a capacity design approach so that the force demands on potentially brittle components of a retrofit are limited by yielding of ductile components. Most commonly, this means that the strength of retrofits should be limited by yielding of steel components. Specific guidance appropriate to different retrofit techniques is given elsewhere in this paper and in companion papers, but given their brittle failure modes it is generally considered undesirable for either embedded anchors or fibre reinforced polymer (FRP) components to be the 'weakest link' that limits the strength of a retrofit.

Unless a secondary load path such as hanger bars can be provided, ductile behaviour is unlikely to be achievable where the failure mode involves loss of support. In such circumstances the required resilience should be provided by designing to accommodate peak MCE displacement demands as outlined in the previous section, which is consistent with the requirements for precast unit seating in the Concrete Structures Standard, NZS 3101 (SNZ 2017)

2.5 CONSIDERATION OF ANCHORAGE DESIGN FOR RETROFITS

Many retrofit techniques for precast floors require anchorage of new components to existing concrete elements. Chemical epoxy anchors are generally the recommended method for achieving this, though in some circumstances (Büker et al. 2022a) screw anchors may be beneficial.

Design of anchors should be undertaken in accordance with Chapter 17 of the Concrete Structures Standard (SNZ 2017) or another appropriate Standard. Chapter 17 makes reference to superseded guidance for design of post-installed anchors (European Organisation for Technical Approvals (EOTA) 2013). It is recommended that anchor design be undertaken using the replacement European Standard (CEN 2018), though this would result in the design representing an Alternative Solution. Irrespective of the guidance used, anchors will generally need to be designed using provisions for seismic performance category C2 as defined in the aforementioned European Standards.

Particular attention must be paid to anchors that are positioned in regions where plastic deformations are expected to occur during an earthquake:

- Anchors installed within half the beam depth away from the column are expected to be affected by substantial cracking and should not be relied on to resist shear and tension demands. Some consideration of anchors located in such locations may be warranted in specific situations (Büker et al. 2022a).
- For epoxy anchors installed less than one beam depth away from the column, the cover concrete should not be relied on and should be discounted from the effective embedment depth. This limitation is sufficient for reversing plastic hinges forming at the column face. Special attention is required where plastic hinges may form in other locations, for example where gravity dominance or reinforcement detailing results in potential plastic hinges forming within the beam span.

Where feasible, more robust anchorage can be achieved by drilling through an element and anchoring a threaded rod on the far side. This solution can be particularly appealing for internal support beams where the floors supported on each side require a seating extension retrofit.

Generally, where anchors are used to connect steel components to existing structural elements it will be beneficial to provide horizontally slotted holes in the steel components to simplify installation and mitigate potential clashes with existing reinforcement. Slotted holes are also recommended in regions where elongation of the supporting element could occur.

2.6 ASSESSMENT OF EXISTING RETROFITS

While not strictly related to design of new retrofits, comment is warranted on the subject of assessing the capacity of retrofits that already exist in a building.

For a variety of reasons, existing retrofits may not comply with the recommendations outlined in the preceding sections, other parts of this paper, and the more detailed companion papers (Büker et al. 2022a; b).

As with other aspects of assessment of existing structures, it is reasonable to assess existing retrofits on a less onerous basis than is suggested for the design of new retrofits. For aspects of retrofits such as the length of existing supplementary seating this can readily be achieved by applying the methods used for assessment of precast concrete floors (MBIE et al. 2018).

Existing anchors, for instance used to fix previously installed seating angles to beams, present a particularly problematic aspect to assess. Except when recently installed, existing anchors are likely to have been designed without adequate consideration of the deleterious impact of concrete cracking on anchor performance (Eligehausen et al. 2006). More

fundamentally, it will often be the case that no (or limited) information is available regarding the anchors and epoxy used in a building. There is currently no clear basis on which to determine an appropriate "probable" anchor strength for use in assessment. Some guidance on assessment and testing of anchors is available (MBIE et al. 2018), but further work to produce a more comprehensive methodology is required.

2.7 CONSIDERATION OF EXISTING DAMAGE

It is not unusual to encounter existing damage when assessing and retrofitting precast concrete floors. Cracking of topping concrete is routinely encountered, while damage to precast floor units or support ledges is less common but not unusual. Damage to both the topping concrete and precast floor units can be present in floors irrespective of whether the floor has been subject to strong earthquake shaking. Examples of damage to precast units that can occur in the absence of earthquakes includes:

- Spalling at the ends of units or of the support due to interaction between the unit and the seating ledge.
- Transverse cracking of hollow-core planks close to supports, which is particularly common where thermal strains cause repeated movement of the unit and may be an indicator of weak bond to the prestressing strand. The transverse cracks may extend further into the webs of the hollow-core unit and thus compromise the gravity capacity of the unit. Consequently it is essential that inspection with a borescope camera be undertaken where existing transverse cracks are identified.
- Longitudinal cracking of hollow-core planks. Longitudinal cracking may be associated with web cracking, particularly if the longitudinal crack is observed to cross between adjacent voids. It would be prudent to undertake borescope investigations of longitudinal cracks, with inspections focussing on the regions proximate to the supports where shear demands are highest and prestress lowest.
- Cracking of the flanges of 'flange hung' double tee units proximate to the supports, and
- Damage caused by corrosion of prestressing strands or other reinforcement.

Guidance on inspecting precast concrete floors is available in Appendix C5E (MBIE et al. 2018). Guidance on identification of web cracks can be found in a companion paper (Büker et al. 2022c).

Anecdotal evidence indicates that car park ramps constructed using hollow-core planks may be particularly susceptible to non-earthquake damage, and therefore warrant particularly careful inspection.

If the performance of a precast floor is expected to be significantly affected by existing damage, it is critical that these effects be taken into consideration when designing retrofits for the floor.

3 RETROFIT TECHNIQUES FOR HOLLOW-CORE FLOORS

Numerous retrofit techniques have been proposed for hollow-core floor units, including those summarised in earlier guidance (PCFOG 2009) and additional techniques conceptualised or developed since. These techniques are discussed in the following sub-sections, and are intended to address one or more the deficiencies that commonly affect hollow-core floor units, namely (MBIE et al. 2018):

- Loss of support **(LOS)**
- Positive moment failure **(PMF)**
- Negative moment failure **(NMF)**

While positive moment failure is identified in the assessment guidance (MBIE et al. 2018) as a single category, two criteria are used to define whether a unit is expected to experience positive moment failure, namely wide opening of a transverse soffit crack proximate to the support or presence of a transverse soffit crack along with web cracking. Web cracking is most commonly observed in alpha and beta units (Büker et al. 2022c) and may be caused by torsion or incompatible displacements. Different retrofit measures may be required depending on which of these failure sub-types are expected. In this paper, PMF will be used to refer to failure due to wide opening of a crack proximate to the support, while web splitting failure **(WSF)** will be used to refer to failures arising from web cracking.

Aspects of the positive moment response of hollow-core floors remain relatively poorly understood. As detailed in a companion paper (Büker et al. 2022c), recent experimental testing has shown that:

- Soffit cracks can form proximate to, but away from the face of the support. Units with cut outs to accommodate columns are particularly vulnerable to soffit cracks initiating at the corner formed by the cut out. In addition, poor strand-concrete bond can contribute to the likelihood of soffit cracks away from the support. However, further research is required to develop techniques to identify units with poor bond, and in any case anecdote suggests soffit cracks can exist without excessive bond degradation.

- Positive moment cracks can propagate at a shallow angle. It is not apparent that the possibility of shallow angle propagation can be excluded for any particular hollow-core unit.

Additionally, soffit cracking of units approximately 300 mm from the support and away from any unit cutouts has been observed in earthquake damaged buildings (Brunsdon et al. 2017; Henry et al. 2017). Attempts to reproduce such damage in the laboratory have been unsuccessful to date (Corney et al. 2018), and it remains uncertain whether such cracking is a result of earthquake shaking or other causes.

The uncertainties about the position and inclination of positive moment cracks must be accounted for when designing retrofit measures to address PMF.

Particular caution is required when assessing whether retrofit is required to address NMF. The potential for NMF is sensitive to the strength of reinforcement crossing the interface at the end of a hollow-core unit. This strength can be materially affected by common differences between the as-drawn and as-built configuration of a hollow-core floor, including:

- Starter bar configurations that differ from those shown on the drawings,
- Mesh reinforcement that is anchored over the support beam, rather than terminating prior to the end of the hollow-core unit, and
- "Paperclip" reinforcement used as a remedial measure where construction issues resulted in a unit having no effective seating (Bull 1999).

Various retrofit techniques for hollow-core floors are summarised in the following sections. Generally, retrofit techniques for hollow-core floors do not address all of the potential failure modes that can afflict hollow-core units. An overall summary of which failure modes are addressed by each retrofit technique discussed can be found below in Table 1.

Table 1: Summary of hollow-core retrofit techniques

Retrofit technique	Refer section:	Failure type			
		LOS	PMF	NMF	WSF
Supplementary seating	3.1	✓	✗	✗	✗
Strongback supports	3.2	✓	✓	✓	✓(1)
Cable catch system	3.3	✓	✓	✓	✗(2)
Supplementary negative moment reinforcement	3.4	✗	✗	✓	✗
Supplementary positive moment reinforcement	3.5	✗	✗(3)	✗	✗
Supplementary transverse reinforcement	3.6	✗	✗(3)	✗	✓(4)
Catch beams	3.7	✓	✓	✓	✓
Release of negative moment restraint	3.9	✗	✗	✗(5)	✗
Core filling	3.8	✗	✗	✗	✗

Notes to table

(1) Strongback supports address WSF within the length of the strongback. Other measures are required if WSF beyond the strongback requires addressing as described in a companion paper (Büker et al. 2022a).

(2) The cable catch does not necessarily address WSF, but can do depending on the configuration of cross beams used for the diverters.

(3) Supplementary positive moment reinforcement in conjunction with supplementary transverse reinforcement and supplementary seating may be able to address PMF, but this combination has not been validated experimentally.

(4) The ability of supplementary transverse reinforcement has not been validated experimentally.

(5) Table content reflects release of negative moment restraint by drilling/cutting concrete. Cutting of reinforcement at ends of hollow-core unit can prevent NMF.

While not included in Table 1 or discussed in the following sections, replacement of hollow-core units may be a viable retrofit technique in some circumstances, whether for particularly vulnerable units or for entire floors. Depending on floor span and demands, appropriate replacement floor systems may include rib and infill floors or steel beams with composite flooring. Other systems may also be structurally viable, but problematic from an access and/or construction perspective.

3.1 SUPPLEMENTARY SEATING

Supplementary seating refers to the technique of extending the seating of precast units by fixing new structural elements to the face of the existing seating ledge, typically by use of epoxy anchors. Detailed recommendations for the design of supplementary seating can be found in a companion paper (Büker et al. 2022b). The new seating element is most commonly a steel section but can also be made of another material such as concrete. Supplementary seating:

- Is an effective method of mitigating LOS.
- Cannot, on its own, mitigate NMF, PMF, or WSF.

Previously it was considered that installation of supplementary seating would mitigate PMF. This is no longer considered to reliably be the case for two reasons. Experimental testing has shown that positive moment cracks can form away from the face of the beam, i.e. beyond the length of supplemental seating. Additionally, even where positive moment cracks form at the beam face, testing has shown that positive moment cracks can propagate at a shallow angle as shown in Figure 2. The resulting slender unreinforced concrete section cannot be relied on to transfer the full weight of the floor to the supplementary seating.

While installation of supplementary seating has long been adopted as a measure to mitigate LOS, recent consideration outlined in a companion paper (Büker et al. 2022b) shows that design of supplementary seating is more challenging than had been previously understood due to the need to preclude potentially brittle failure of anchors.

Previous guidance (PCFOG 2009) suggested that rolled hollow sections (RHS) were the preferred form of supplementary seating, and that angle or channel sections were not recommended. This is no longer the case; either can be used. Provided the stiffness of the chosen section is appropriately considered in the design process, the choice of supplementary seating type can be made based on practical considerations related to ease of installation.

The companion detailed design guidance (Büker et al. 2022b) suggests two alternative approaches to the design of supplementary seating, as shown in Figure 3 :

1. Supplemental seating hard up against the soffit, which requires the post-installed anchors to be capacity designed, or
2. Supplemental seating set down from the soffit with a compressible layer provided between the supplemental seating and the floor unit.

For either configuration, it is recommended that the anchors be installed in slotted holes and that the supplemental seating span at least 75% of the width of the hollow-core unit as shown in Figure 4. It is also essential that the ability of the supported webs to resist the shear demand on the unit be checked.

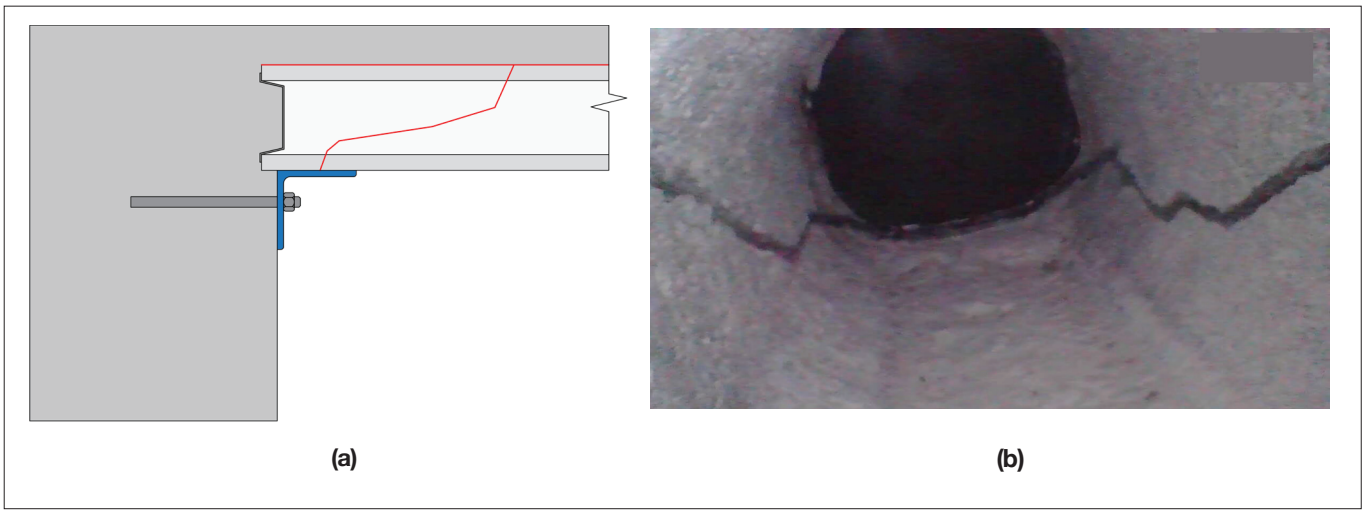

Figure 2: (a) Schematic and (b) borescope images showing potential shallow angle of positive moment cracks

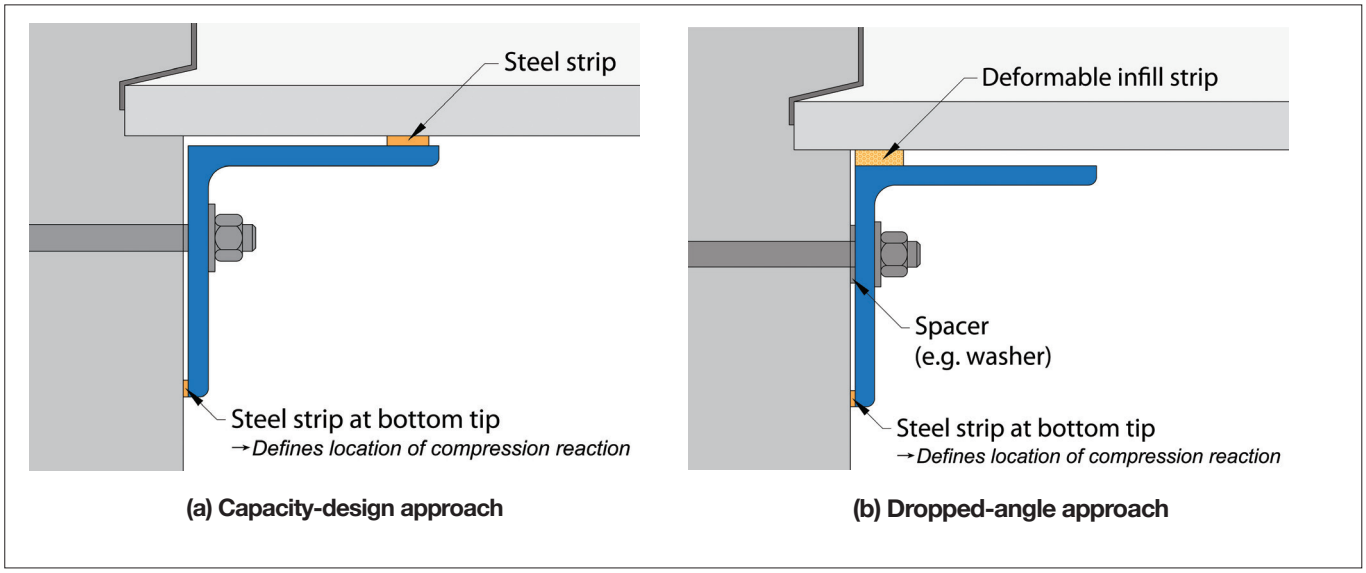

Figure 3: Detailing of the two recommended design approaches for supplementary seating angles (Büker et al. 2022b)

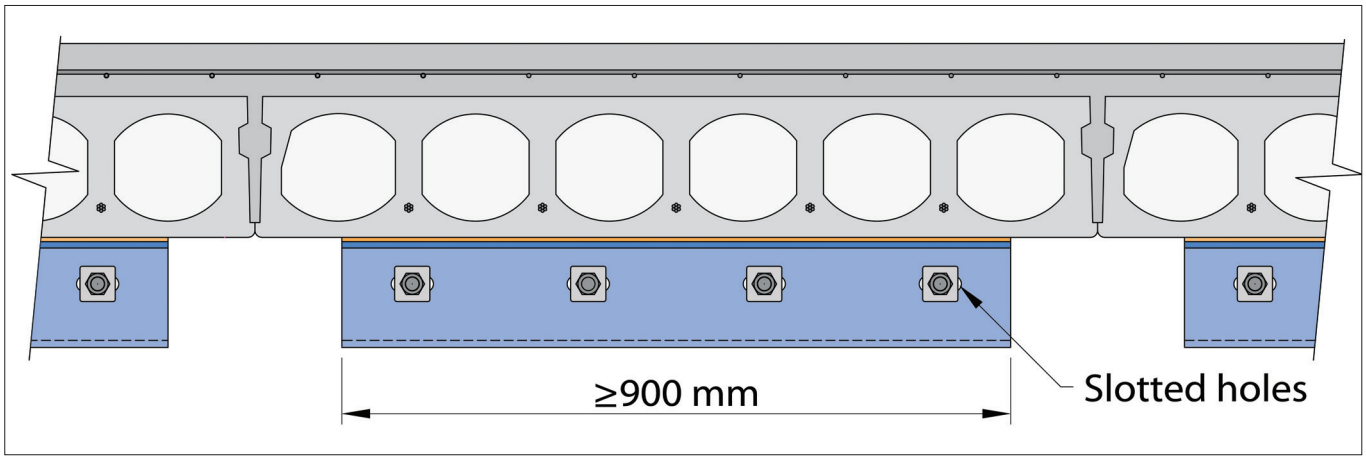

Figure 4: Elevation showing recommended supplemental support configuration

As outlined in the companion paper (Büker et al. 2022b) and assessment guidance (MBIE et al. 2018), supplementary seating elements can induce negative moment demands in the hollow-core units. Lateral drift of the building will cause this retrofit configuration to interact with the floor and induce a force in the hollow-core units that will increase the negative moment demand and may increase the propensity for NMF (Liew 2004; Parr et al. 2019). The significance of these forces needs consideration and is particularly significant for stiff supplementary supports (Parr et al. 2019). For new installations, guidance is provided in the companion paper. It is also important that the impact of previous supplementary seating retrofits that have been installed in contact with the soffit of the floor is accounted for during seismic assessments. Rational analysis accounting for the probable stiffness of the supplementary seating should be undertaken to quantify the significance of this interaction. This analysis should also account for the likelihood that the position of the reaction between the supplemental seating and the floor unit will be uncertain unless a steel strip (Figure 3a) or similar approach has been used to provide a defined reaction point.

3.2 STRONGBACK SUPPORTS

Strongback supports are a newly developed retrofit technique that utilise a number of steel beams to provide an alternative load path from the span of a hollow-core unit to the support beam. As shown in Figure 5 steel elements (in the case shown, I-beams) are fixed to a hollow-core unit and supported by a seating angle at the support beam. Further discussion of strongback configurations can be found in a companion paper (Büker et al. 2022a).

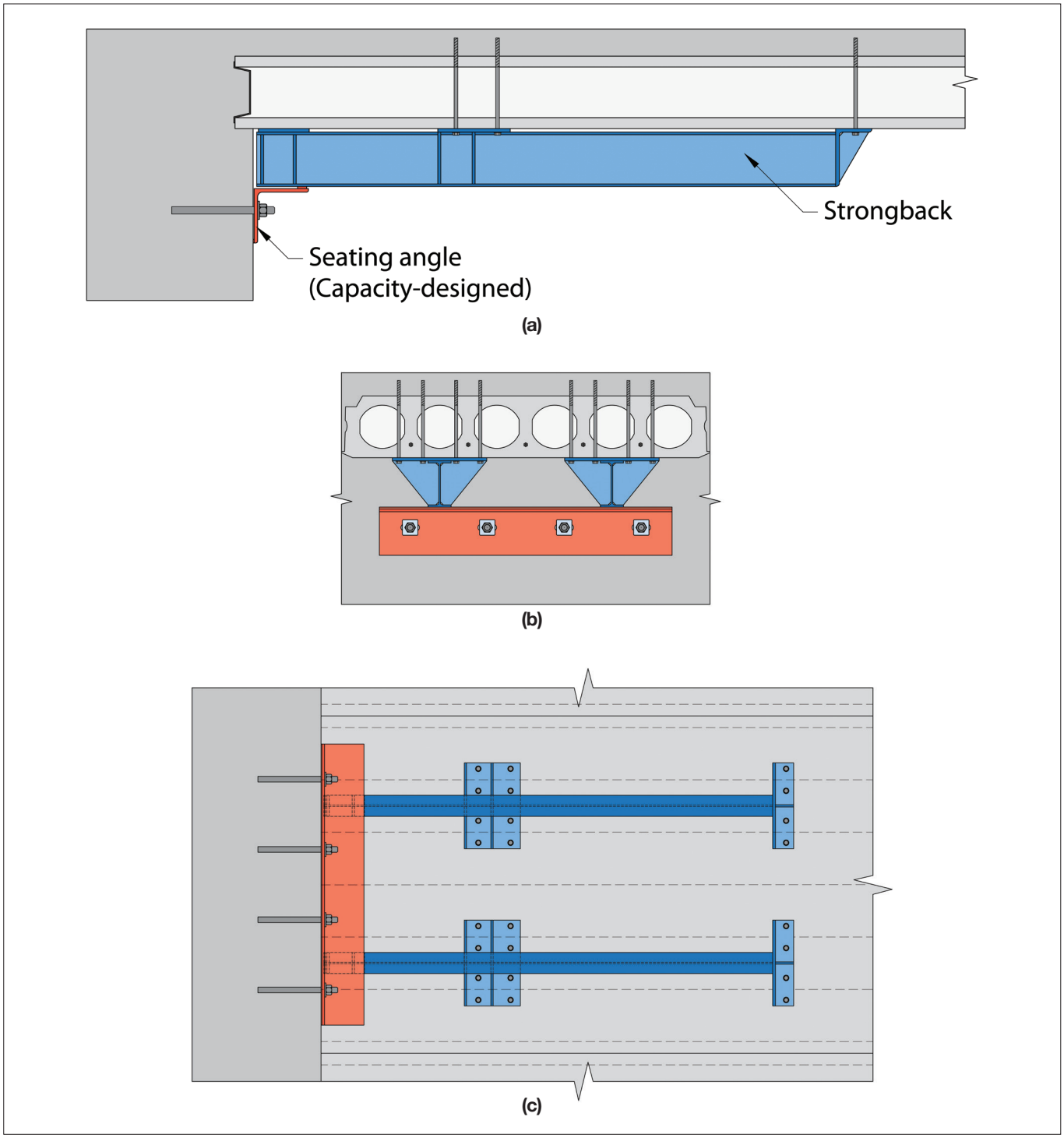

Figure 5: Strongback retrofit showing (a) side elevation, (b) cross section, and (c) plan view of soffit

Strongback supports:

- Can effectively address LOS, PMF, and NMF.
- Can address WSF within the length of the strongback, but other measures are required if WSF beyond the strongback is expected.

The performance of strongback supports has been verified by testing of a super-assembly specimen with strongback supports installed (Büker et al. 2021, 2022c). Detailed guidance for the design of strongback supports is available in a companion paper (Büker et al. 2022a).

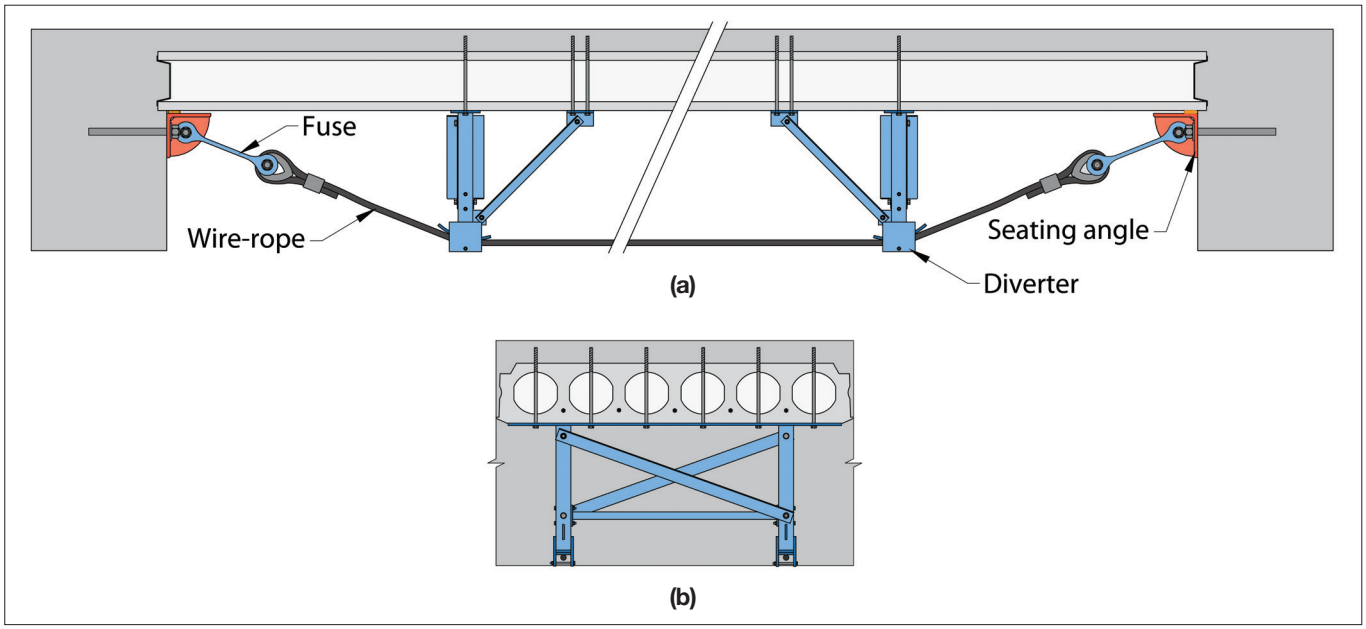

Figure 6: Cable catch system showing (a) side elevation and (b) cross section through diverter

3.3 CABLE CATCH SYSTEM

The cable catch system is a newly developed retrofit technique for hollow-core floors. Two wire ropes, spanning underneath and parallel to a hollow-core unit, are deflected by diverters located approximately one meter from each end of the unit. The wire ropes are connected to stiffeners welded to steel brackets that are anchored to the beams, which also act as supplementary seating and should be designed using the dropped-angle approach. The cable catch retrofit is shown schematically in Figure 6. Although the wire rope is shown to be taut in Figure 6, it is necessary to install the cable slack to allow for frame dilation. If sufficient slack is not provided elongation of the frame could induce upward forces on the diverters that would potentially 'break the back' of the hollow-core units. However, this must be finely balanced; too much slack would result in excessive drop of the floor before engagement of the retrofit.

The cable catch system is capable of mitigating LOS, PMF, and NMF. It does not necessarily address WSF, but can do provided the strength of a potentially detached soffit is considered when determining the configuration of cross beams used for the diverters.

The viability of the cable-catch system has been demonstrated during testing of a large scale super-assembly as detailed elsewhere (Büker et al. 2021, 2022c). As well as demonstrating the efficacy of the retrofit, this testing also confirmed that engagement of the cable-catch system occurs in conjunction with relatively large displacements and increased vertical flexibility of the floor.

While effective, the cable catch system is complex and is considered unlikely to be attractive as a practical solution. Consequently, there are no plans at the date of this publication to produce detailed design guidance for the cable catch system. Design can be undertaken from first principles, including those outlined in section 2. Aspects of the cable catch system that require particular consideration include:

- Determining the length of cables to ensure that sufficient slack is available to accommodate elongation of parallel beams,
- Design of the embedded anchors of the seating angle to resist the tensile forces in the cable. If possible, fastening of the seating angle should be achieved by drilling through an element and anchoring a threaded rod on the far side, and
- Providing a 'fuse' in the system is recommended to enable capacity design of the embedded anchors. The fuses used in the tested configuration also functioned as an efficient means of connecting the cables to the steel brackets.

3.4 SUPPLEMENTARY NEGATIVE MOMENT REINFORCEMENT

Supplementary negative moment reinforcement refers to the technique of installing additional reinforcement in or on the topping concrete close to the ends of hollow-core units. The intent of this technique is to increase the negative moment capacity of the floor at and beyond the end of the existing starter bars and consequently to prevent NMF.

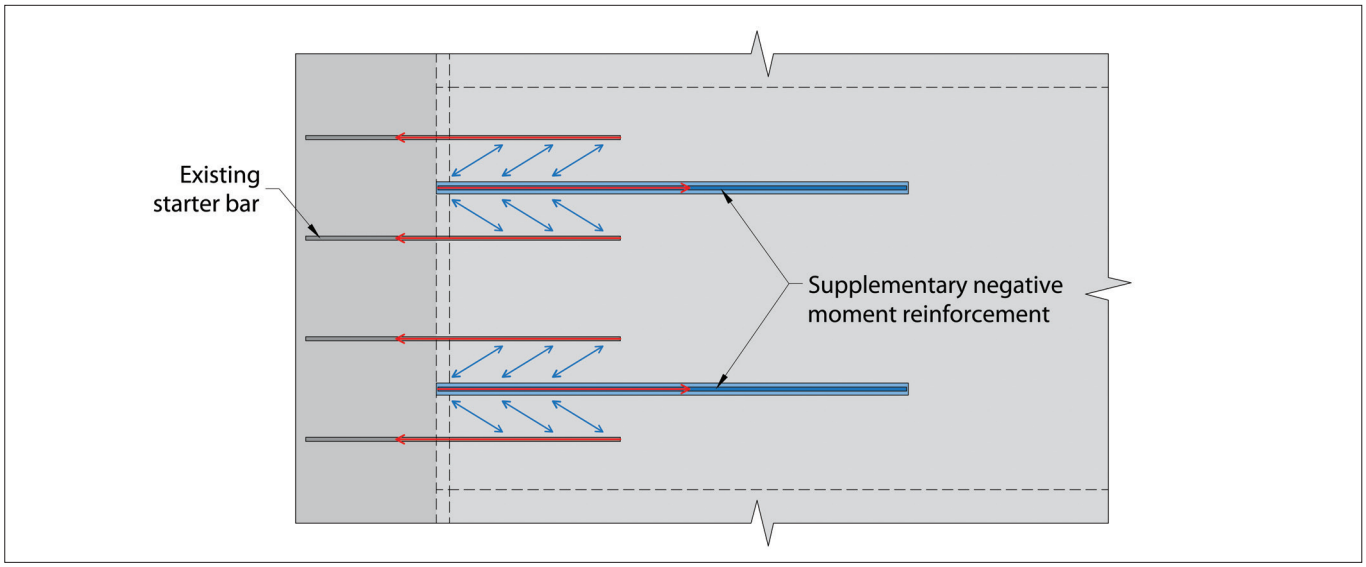

Figure 7: Example configuration of supplementary negative moment reinforcement (adapted from Parr et al. 2019)

Supplementary negative moment reinforcement can suppress NMF, with this being demonstrated in sub-assembly testing (Parr et al. 2019). In isolation, supplementary negative moment cannot prevent LOS, PMF, or WSF.

Supplementary negative moment reinforcement can consist of steel reinforcing bars chased into the topping concrete, FRP sheets or strips fixed to the topping concrete, or other configurations that provide the required tensile load paths. Testing of supplementary negative moment reinforcement has focussed mainly on solutions employing additional reinforcing bars, though an FRP configuration using FRP sheets worked satisfactorily in a sub-assembly test (Büker et al. 2020).

Supplementary negative moment reinforcement can be designed from first principles. Two key factors must be accounted for during design:

a. The supplementary negative moment reinforcement must not extend across the interface between the end of the hollow-core unit and the support beam, as this would increase the negative moment demand.

b. Forces must be able to reliably transfer between the existing starter bars and the supplementary negative moment reinforcement. Where discrete bars or FRP strips are used, consideration should be given to ensuring that this transfer can occur via a non-contact lap splice even if the existing starter bars are unfavourably positioned. As noted in section 3 it should not be assumed that starter bars are located precisely as indicated by drawings. Scanning to identify the actual locations may be beneficial.

Additionally, if FRP is being used as supplementary negative moment reinforcement it is important that FRP sheets not span across the interface between adjacent hollow-core units. If sheets do span between units this creates a risk that differential movement of the hollow-core units will cause the FRP to delaminate from the topping concrete. This restriction should not be assumed to apply if FRP is used for diaphragm strengthening, where different considerations may apply.

The use of steel reinforcing bars is generally preferable because, in comparison to FRP, these are more ductile, less reliant on bond of epoxy, and simpler to protect from wear and tear. Additionally:

- Design guidance for FRP (ACI Committee 440 2017) states that FRP sheets must not be anchored on a concrete surface that is expected to crack. This calls into question the ability of the FRP sheets from achieving full bond capacity within the region of topping concrete proximate to the end of a hollow-core unit.
- The use of steel reinforcement as a negative moment strengthening measure is particularly recommended over FRP products in regions where diagonal cracking in the topping of the floor is expected (e.g. in the vicinity of columns). This is because the ductile behaviour of steel reinforcing bars would be especially beneficial when subjected to local shear deformations as can occur across diagonal cracks.

3.5 SUPPLEMENTARY POSITIVE MOMENT REINFORCEMENT

Supplementary positive moment reinforcement refers to reinforcement, typically FRP sheets, that is applied to the soffit of hollow-core units. The intent of the reinforcement is to prevent positive moment cracking away from the

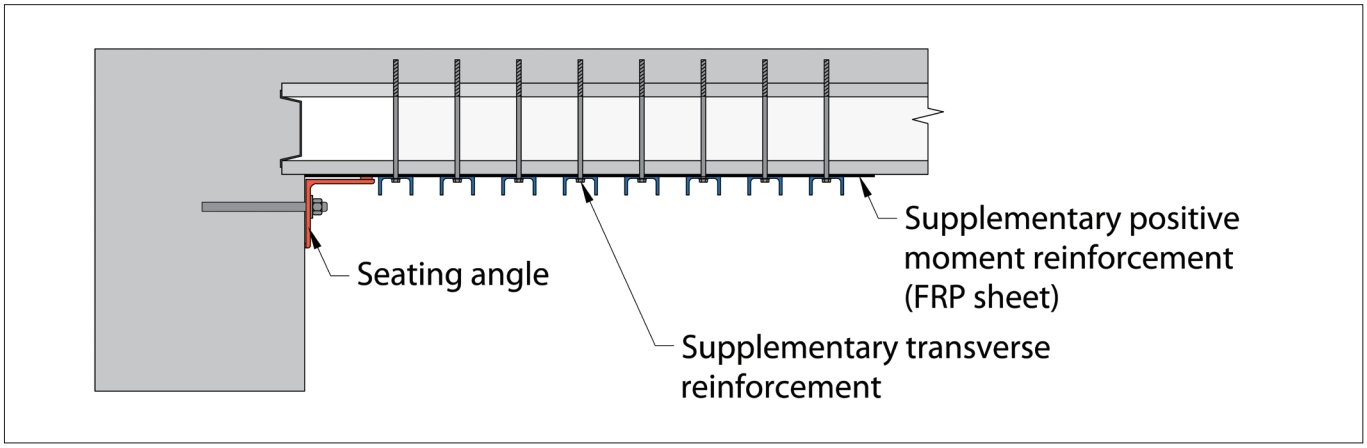

Figure 8: Example configuration of supplementary seating and supplementary positive moment and transverse reinforcement

support face. However, the reinforcement cannot prevent cracking close to the support face as sufficient bond length is required on either side of a potential crack in order for the supplementary reinforcement to be effective. Hence, supplementary positive moment reinforcement on its own is not considered an effective retrofit technique. However, used in conjunction with other techniques, structural mechanics suggest it may be effective as a means of addressing PMF, though this has not been validated experimentally. The additional measures required comprise:

- Supplementary seating (section 3.1) to prevent failure if a positive moment crack forms at the face of the support, i.e. beyond the point where post-installed supplementary positive moment reinforcement can suppress cracking, and
- Supplementary transverse reinforcement (section 3.6) of the end regions of the hollow-core to prevent failure if the crack from the support face propagates at a shallow angle as discussed in section 3.1.

Figure 8 shows an example of the configuration of retrofits envisaged. It must be emphasized here that this combined retrofit technique has not been tested in the laboratory. Further testing as outlined in section 2.1.3 is required to confirm that the combination of retrofit techniques described above can reliably prevent PMF. Until such testing is completed, the use of strongback supports (section 3.2) is recommended to address PMF.

As with supplementary negative moment reinforcement, FRP used as supplementary positive moment reinforcement should not span between hollow-core units.

3.6 SUPPLEMENTARY TRANSVERSE REINFORCEMENT

The brittle, unreinforced nature of the webs is one of the key vulnerabilities of hollow-core units. If correctly detailed, and depending on the nature and quantity provided, supplementary transverse reinforcement can:

a. Increase the shear strength of the hollow-core unit,

b. Prevent propagation of web cracks, as demonstrated during recent testing (Büker et al. 2022c), and

c. Prevent collapse of the bottom flange of a hollow-core unit in the event of WSF by providing a secondary load path to the topping and top flange.

Supplementary transverse reinforcement is likely to be an effective means of mitigating WSF, but this has not yet been experimentally validated. Ongoing research is likely to produce relevant results in the near future (Mostafa - In preparation).

Supplementary transverse reinforcement in conjunction with supplementary positive moment reinforcement and supplementary seating is also likely to provide an effective means of addressing PMF, though as discussed in the preceding section the efficacy of this combination has not been tested experimentally and strongback supports are recommended to address PMF. Supplementary transverse reinforcement is also an important part of the strongback support described in section 3.2 and a companion paper (Büker et al. 2022a).

Previous guidance (PCFOG 2009) recommended supplementary transverse reinforcement comprising either steel rods or FRP extending through holes drilled through the full depth of the floor. While the use of FRP supplementary transverse reinforcement is feasible, there appear to be no reasons that suggest it would be preferable to steel reinforcement and the anchorage

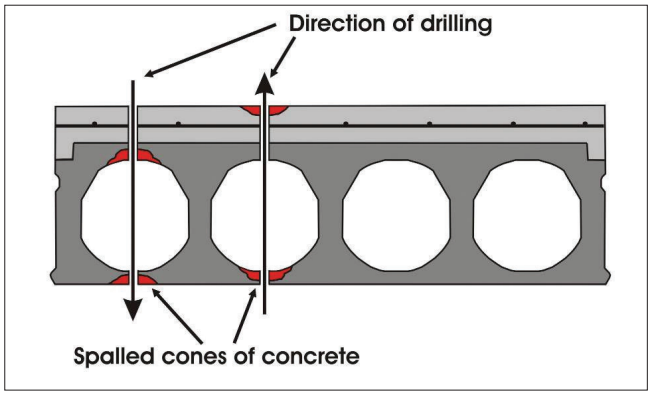

Figure 9: Illustration of the propensity for drilling through hollow-core units to cause spalling (Jensen 2006)

of FRP may be considered less reliable. The process of drilling holes for installation of either option risks damaging the hollow-core unit by causing concrete to spall as shown in Figure 9. Jensen (2006) investigated the process of drilling through hollow-core units, and recommends drilling from the underside on the basis that spalling of the topping concrete is less problematic than spalling of the unit near the strands and to minimise cosmetic impacts at the soffit. Drilling from the underside is also preferable as it simplifies alignment of the drilled holes with the voids of the hollow-core unit.

It remains critical that supplementary transverse reinforcement extend through the soffit of a hollow-core unit to ensure that the reinforcement engages with flexural tension forces in the soffit. Recent testing (Büker et al. 2022c) has shown, however, that satisfactory performance can be obtained through use of screw anchors installed from beneath and extending into, but not through, the topping concrete. As recommended in previous guidance (PCFOG 2009), supplementary transverse reinforcement could be tensioned to induce compression in the hollow-core webs, which can delay or arrest crack formation.

It is recommended that anchorage of supplementary transverse reinforcement at the soffit be achieved by use of steel sections that span across the hollow-core webs (Figure 10), rather than by washers as indicated in previous guidance. Steel plates or channel sections would both be viable options. The use of such cross beams provides an improved load path for compression struts through the webs, and also mitigates the risk of damage to the hollow-core unit that can occur when drilling holes in which to install supplementary transverse reinforcement (Jensen 2006).

Detailed design of supplementary transverse reinforcement depends on the purpose of the reinforcement:

- Where the purpose of supplementary transverse reinforcement is to prevent collapse in the event of WSF, the provided reinforcement must be sufficient to support the weight of the lower half of the hollow-core unit. The spacing of reinforcement must be such that the lower half of the unit can span between the reinforcement locations without failing. It is recommended that a minimum of two rows of reinforcement should be provided.
- Where the purpose of supplementary transverse reinforcement is to increase the shear strength of hollow-core units, design should be undertaken following the applicable provisions of the Concrete Structures Standard (SNZ 2017). In order to be effective as shear reinforcement the minimum spacing of reinforcement along the span of the hollow-core unit should not exceed half the effective depth of the floor (i.e. $s \leq d/2$).

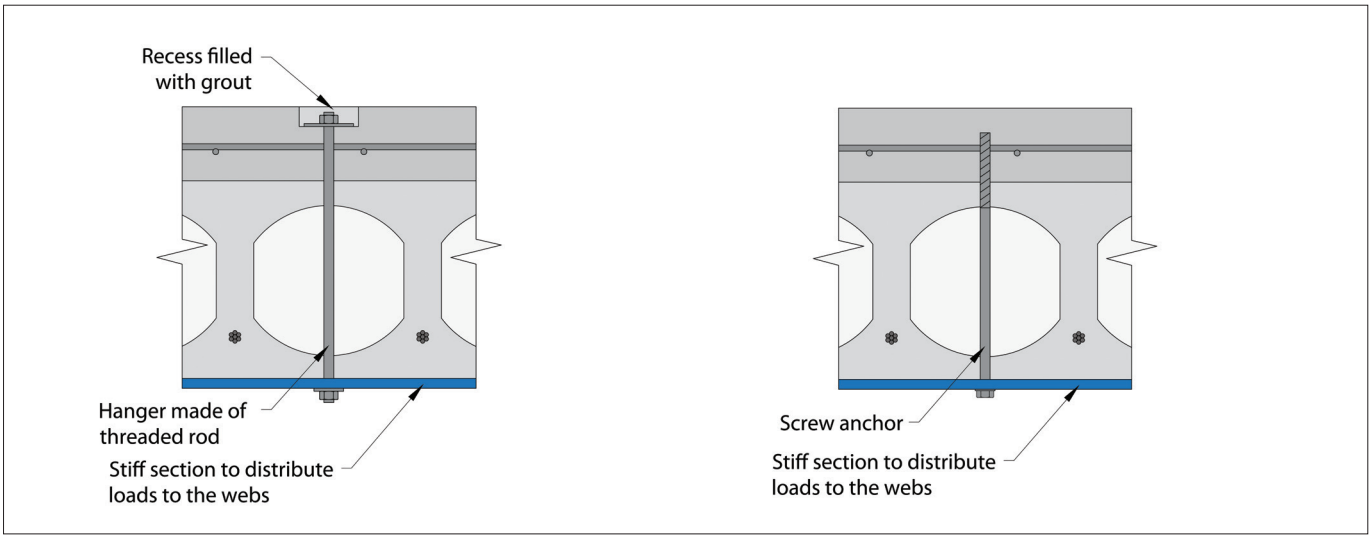

Figure 10: Steel supplementary transverse reinforcement configurations using screw anchors (left side) or threaded rods (right side)

3.6.1 Ineffective supplementary transverse reinforcement

Two forms of supplementary transverse reinforcement are identified in previous guidance (PCFOG 2009) as NOT being reliable retrofit techniques. These are:

a. Supplementary transverse reinforcement anchored into (filled) cores, and

b. Supplementary transverse reinforcement installed at the interface between adjacent units.

These retrofit techniques are still considered ineffective and are not recommended. They do not satisfactorily address LOS, PMF, NMF, or WSF.

The first technique is afflicted by the issues pertaining to infilling of cores that are discussed in section 3.8. Notably, the termination of the supplementary transverse reinforcement within the core means there is still no reliable load path between the top and bottom flanges of the unit should web cracking occur. This is elaborated on in section 3.8.

While supplementary transverse reinforcement at the interface between units would be expected to extend through the full depth of the floor, the widely spaced reinforcement is unlikely to adequately support the central parts of the bottom flange of the hollow-core unit. While this could conceptually be addressed by providing cross beams between the supplementary transverse reinforcement, it seems unlikely such a solution would be preferable to installing more closely spaced reinforcement. At most, this retrofit approach can only be used to try to stop a soffit from falling after failure since the wide spacing does not enable the supplementary transverse reinforcement to improve the shear resistance of the middle webs or limiting web crack propagation as observed with screw anchors (Büker et al. 2021).

3.7 CATCH BEAMS

Various retrofit techniques for hollow-core floors can collectively be described as catch beams. These include:

- 'Simply supported' catch beams illustrated in Figure 11. This configuration is similar to that described in previous guidance (PCFOG 2009), but has the notable addition of a deformable layer between the unit and catch beam. For this retrofit configuration it is important that the connection to the support beam is detailed to act as a (nominally) pinned support to avoid excess prying of the anchors. The ability of the adjacent hollow-core unit to support additional demands also requires careful checking,
- Catch beams designed to cantilever from adjacent primary structure (Figure 12), and
- Catch beams spanning directly between primary structural elements, such as the example shown in Figure 13 installed diagonally across the end of an alpha unit. To accommodate elongation of the supporting beams, such beams must be provided with the ability to rotate in the horizontal plane and to elongate. This has previously been achieved by provision of a sliding support at one end as indicated in Figure 13, or by use of telescoping steel hollow sections to provide elongation in conjunction with a support at one end that is detailed as a pin in the horizontal plane.

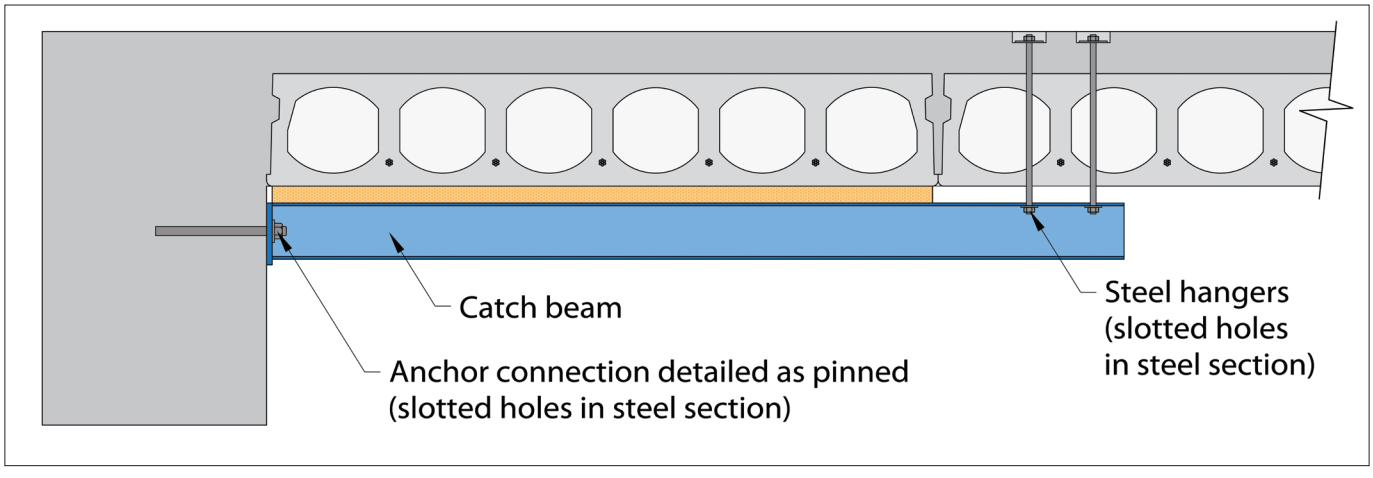

Figure 11: Simply supported catch beam

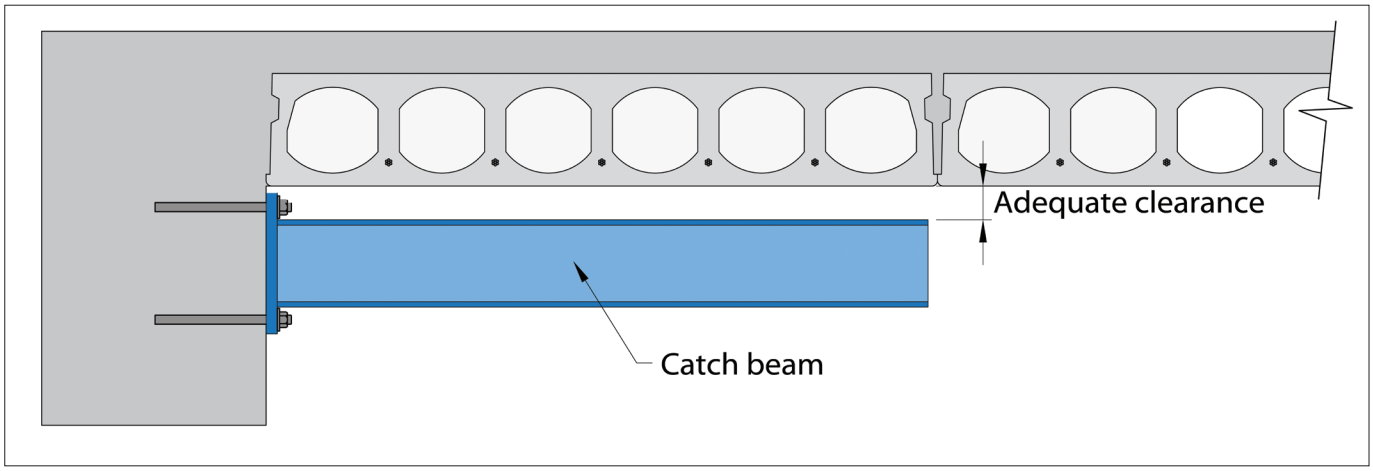

Figure 12: Cantilever catch beam

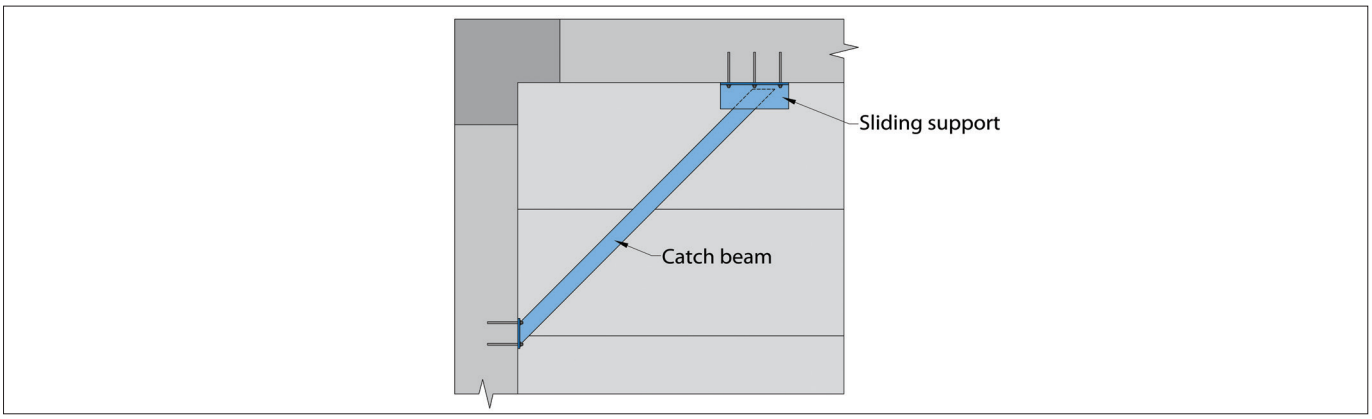

Figure 13: Diagonal alpha catch bracket with sliding support

Provided they are appropriately positioned, catch beams can address LOS, PMF, NMF, and WSF. As indicated by the name, catch beams function as a catch system as defined in section 2.1.2.

Key aspects of the design of catch beams that require consideration include:

1. The strength of the catch beam and the structure that supports it must be sufficient to support the ULS demands resulting from the weight of hollow-core unit(s) required to be caught. ULS demands should be determined based on the design action combinations outlined in section 2.2.
2. The spacing of catch beams must be sufficient so that the hollow-core unit (or parts thereof) can span reliably between the catch beams. This can also be achieved through a combination of catch beams and supplementary transverse reinforcement.
3. Compatibility of displacements and rotations between the catch beams, hollow-core units, and primary structure must be carefully considered. This can include both vertical movements, horizontal movements (e.g. due to beam elongation), as well as relative rotations between the support structure and the floor. The impact of forces arising from deformation (in)compatibility on the hollow-core unit and retrofit anchorages must be assessed.
4. If displacement compatibility is accommodated by providing clearance between the beams and the hollow-core units, consideration should be given to the potential for increased demands due to dynamic impact. It is recommended that a deformable layer be placed between the catch beam and the hollow-core unit, which removes the need to explicitly consider impact forces as outlined in section 2.3. For catch beams a relatively soft deformable layer such as polystyrene is likely to be appropriate.
5. The catch beam must be robustly supported. Particular attention is required for anchors used to fix the beams to the support structure. As outlined in section 2.5, these cannot be relied on to resist forces when installed in regions expected to experience substantial plastic deformation. This unreliability is not reflected in catch beam configurations suggested in previous guidance (PCFOG 2009 - refer Figure 8.14).

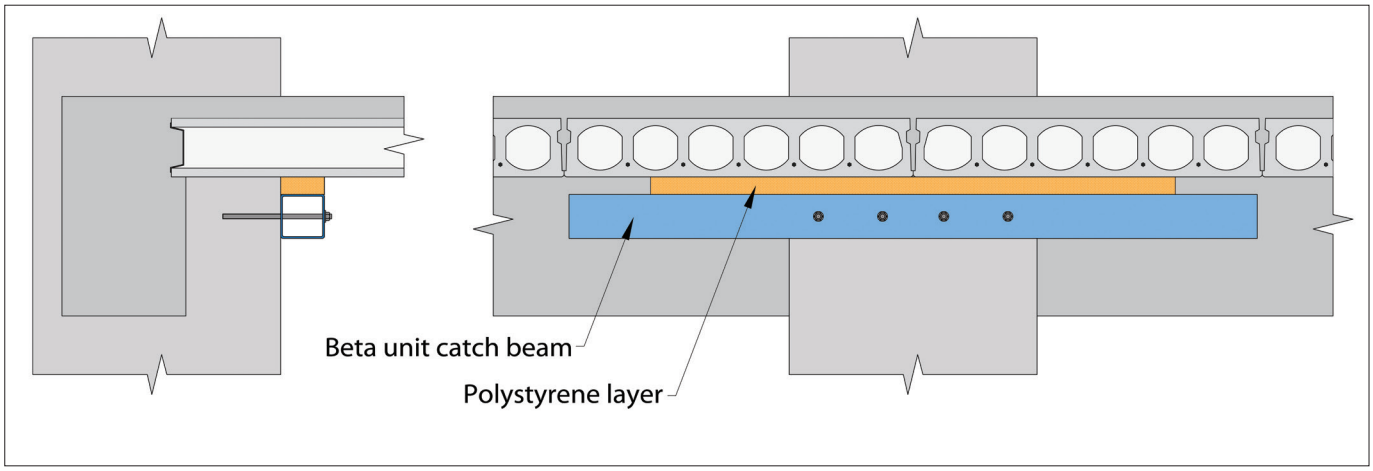

Figure 14: Example beta unit catch beam configuration

Provision of catch beams for beta units may pose particular challenges, in many cases requiring the catch beam to cantilever from the column that interacts with the beta unit. An example configuration is shown in Figure 14 that was demonstrated to be effective during super-assembly testing (Büker et al. 2022c). This catch beam extended to approximately 400 mm beyond the face of the support beam. As an interim recommendation until understanding of beta unit behaviour is refined, it is recommended that beta unit catch beams be detailed to support the beta unit a similar distance into the span, i.e. so that they extend to approximately twice the unit depth from the support beam face.

3.8 INFILLING OF CORES

Infilling of cores at the ends of hollow-core units is NOT considered an effective means of improving the performance of hollow-core floors.

Despite being identified as ineffective since at least 2009 (PCFOG 2009), discussion regarding retrofit techniques for hollow-core floors regularly turns to the concept of infilling cores. It is typically proposed that this will increase the shear strength of the hollow-core units, or otherwise enhance performance.

The previously-expressed rationale for deeming core infilling to be ineffective (PCFOG 2009) remains sound. However, this inadequacy warrants elaboration. Concerns about the approach are twofold:

- The presence of infilled cores will increase the flexural strength and stiffness of the end region of the hollow-core unit, which is likely to increase vulnerability to negative or positive moment failure outside the filled region.
- As illustrated in Figure 15a, for this infill to effectively increase the shear strength of the end of the unit it must contribute to resisting vertical tensile forces that have to anchor effectively into the top and bottom flanges where the flexural tension and compression forces are located. The infill material itself is not prestressed, and so depending on its composition it is unlikely to be able to reliably resist tension forces. Irrespective of its composition, the infill material is separated from the hollow-core unit by a cold joint. Even in favourable circumstances cold joints have greatly reduced tensile capacity compared to concrete (Torres et al. 2016). This reduction is likely to be even more significant in relation to the inside of a hollow-core unit that is likely to be old at the time that core infilling is undertaken, smooth/unroughened, and dusty.

The ineffectiveness of core infilling as a means of retrofit can be demonstrated by reference to previous testing that considered core infilling as a solution for new hollow-core (e.g. Liew 2004). For example, the test shown in Figure 15b clearly shows the clean separation of the core infill from the hollow-core unit. While the filled core in the unit shown in Figure 15b contained ‘paperclip’ reinforcement, this does not detract from the observation that no effective force transfer could occur across the cold joints at the top and bottom of the infill.

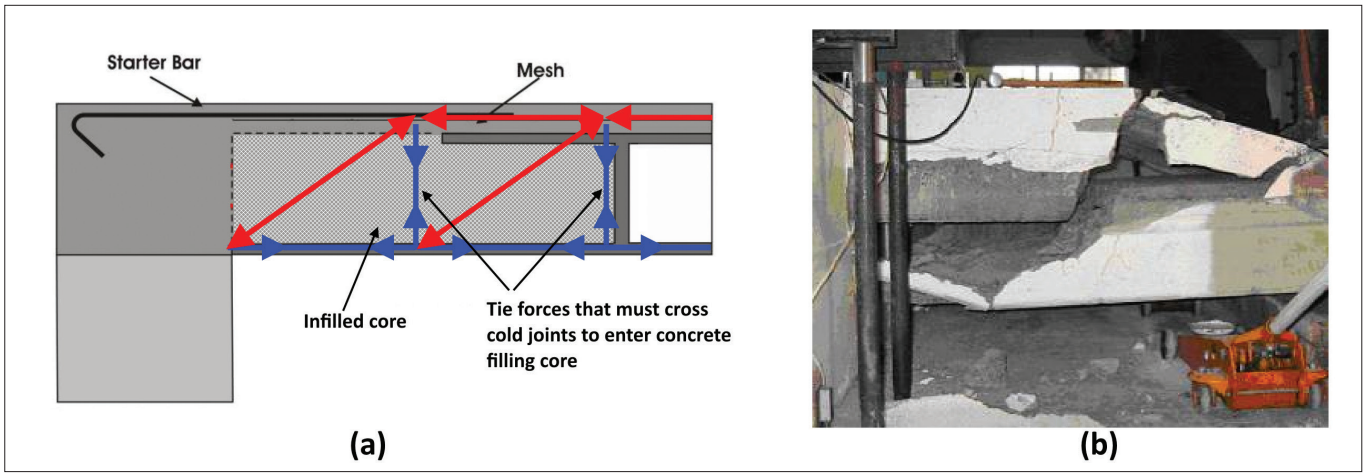

Figure 15: (a) Illustration of necessity of tension forces crossing cold joints at top and bottom of core and (b) failure during testing showing debonding of hollow-core unit from infilled core (adapted from Jensen 2006)

The discussion above applies equally irrespective of whether the proposed infilling material comprises plain concrete, fibre reinforced concrete, or other alternatives such as fibre reinforced polymer (FRP) tubes.

3.9 RELEASE OF NEGATIVE MOMENT RESTRAINT

In contrast to previous guidance on retrofit of hollow-core floors (PCFOG 2009), based on current knowledge it is concluded that:

- NMF cannot be prevented by inducing a crack in the topping concrete (and any core infills) at the end of a hollow-core unit, and that
- Cutting of reinforcement crossing the interface at the end of the hollow-core unit can be an effective retrofit technique provided that diaphragm capacity is maintained.

Inducement of a crack through the concrete at the end of a unit is not sufficient to prevent NMF. Inducement of the crack does not preclude yielding and strain hardening of reinforcement crossing the crack, and hence does not materially reduce the negative moment that can develop at the end of the unit and that dictates the propensity for NMF (Parr et al. 2019).

Cutting starter bars and other reinforcement that cross the end of the hollow-core unit can be a valid retrofit strategy for NMF as it reduces restraint and therefore negative moment demand at the end of the unit and consequently at the end of the starter bars. However, it also has the side effect of reducing the strength of the floor diaphragm. The impact of this reduction requires detailed consideration.

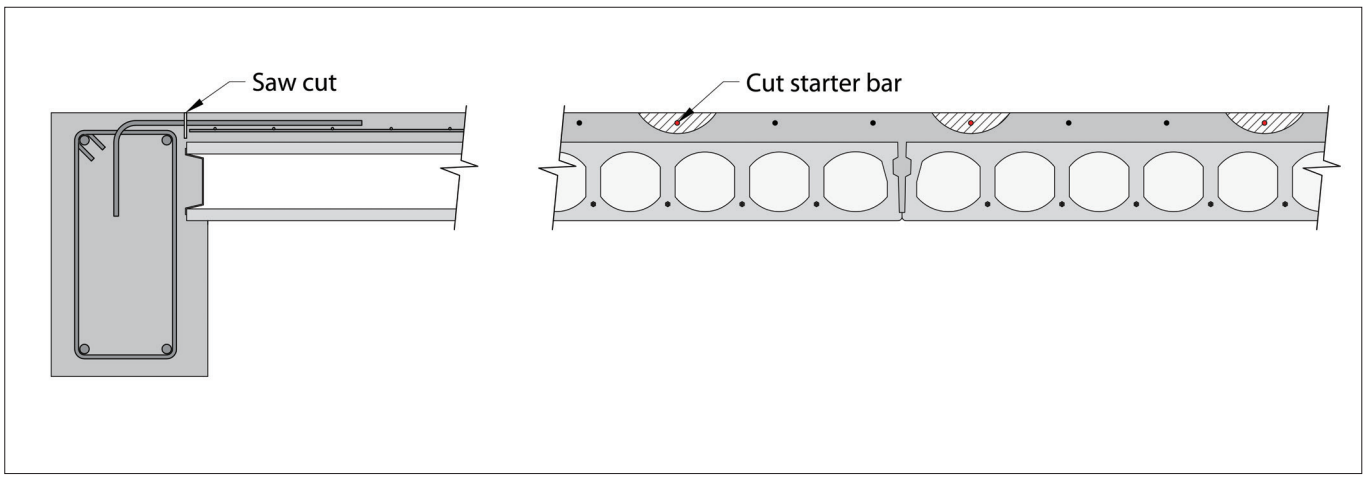

Figure 16: Illustration of cutting starter bars

4 RETROFIT TECHNIQUES FOR DOUBLE TEE FLOORS

In comparison to hollow-core floors, double tee floors are susceptible to fewer modes of failure. As outlined by the assessment guidance (MBIE et al. 2018), double tee floors:

- Are generally susceptible to loss of support (LOS) failure, and
- May be susceptible to failure of the flange support where units are supported by “loop bar” (i.e. “pigtail”) hanger details.

Hare et al. (2019) identified that there was no rational method for determining the reliable capacity of loop bar double tee supports. Despite further research since (Jenkins 2022), this remains the case.

Both of the above noted failure modes occur at the end of the unit and result in the unit dropping relative to the support beam. Consequently, similar retrofit techniques, outlined below, are applicable to both failure types.

It is essential that retrofit techniques for double tee units provide concentrated support to the webs of the unit because it is the webs that transfer the shear forces arising from gravity demands to the supporting structure. Techniques that provide remedial support only via the flanges of units are unlikely to effectively support the double tee unit after failure of the original load path. The flanges of double tee units are slender, and are not likely to have sufficient reinforcing to support the full weight of the floor or accommodate transfer of the web shear demands into the support.

Details regarding recent experimental investigations of double tee retrofit techniques along with more detailed design recommendations are expected to be described in a future paper (Henry and Jenkins - In preparation).

4.1 SUPPLEMENTARY BRACKETS

Supplementary brackets are a common retrofit technique for double tee floors that could be implemented for units that are originally either web or flange supported. As suggested by the name, the technique provides bracket supports at the end of each web of a double tee unit. Generally the supplementary brackets are installed as a catch mechanism with an initial gap between the web and bracket, i.e. they prevent collapse rather than preventing failure of the original support detail. An example support detail is shown in Figure 17.

Supplementary brackets for double tee units are typically more substantial than supplementary seating used for hollow-core floors (section 3.1). More substantial supports are required due to the concentration of support reactions in the two webs of the double tee unit, which contrasts with relatively even distribution of reactions across the width of hollow-core units.

When support beam rotation occurs that induces a negative moment in the connection of a flange hung double tee unit, there is potential for the webs of the double tee to bear against the face of the supporting beam and cause LOS due to prying. The tendency for this to occur is reduced or removed by the presence of a gap between the beam face and the end of the web. It is imperative that retrofit techniques do not encroach on this gap, as doing so would increase the chance of LOS occurring. Consequently, supplementary brackets should be installed such that components are located either under the double tee unit, or around the web as shown in Figure 17.

As noted, supplementary brackets should generally be designed as a catch system with a gap provided between the soffit of the double tee web and the support face of the supplementary bracket. The gap is required to prevent trapping the web in the retrofit and to avoid unpredictable large demands being placed on the

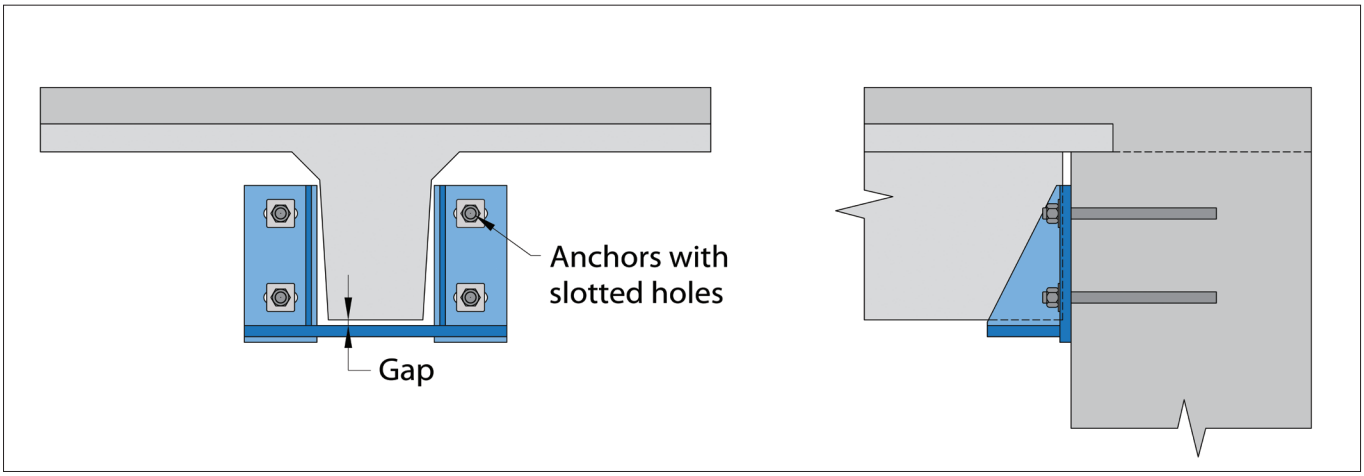

Figure 17: Example supplementary bracket

bracket due to relative displacement between the bracket and double tee when support beam rotation occurs.

Assuming that the supplementary bracket is designed so that it does not contact the double tee unit when the building sustains lateral drifts, it is not necessary to use capacity design to determine demands on the anchors for the bracket. Instead, they should be sized to resist the design action combinations discussed in section 2.2, with appropriate consideration given to dynamic impact forces that could arise if the double tee unit is able to drop onto the supplementary bracket. It is recommended that a deformable layer be placed between the bracket and double tee soffit to avoid the need to consider dynamic impact forces as outlined in section 2.3. Design of the deformable layer should follow the principles outlined for hollow-core supplementary seating in a companion paper (Büker et al. 2022b).

As with supplementary supports for hollow-core, horizontally slotted holes may be beneficial to simplify installation and mitigate potential clashes with existing reinforcement.

4.2 ARTICULATING HANGER SUPPORTS

Articulating hanger supports comprise a steel beam installed beneath the web soffit that is attached to the supporting structure at one end and to the web of a double tee unit via a pair of pinned links at the other end. Parallel flange channel (PFC) sections are likely to be appropriate for the steel beam. The links made from steel flats should be connected by rods inserted through the double tee web and the PFC and as long as practical to attach towards the top of web section. An example of the detail is shown in Figure 18. It is important that the connection of the PFC to the support beam is detailed to behave as a pin so that prying forces on the anchors are avoided.

The intent of the detail is that elongation demands can be accommodated by articulation of the links. Occurrence of this articulation requires a vertical clearance to be provided between the PFC and the double tee unit soffit which will close up as the links project at an angle due to elongation demands. The need for this gap means that the articulating hanger support acts as a catch system as defined in section 2.1.2.

An alternative detail has been proposed but not tested. The suggested difference involves placing a deformable plastic shim or other deformable layer on the PFC near to the end of the double tee web and with a nominal gap between the shim and web soffit. This gap would be sized so that the floor becomes supported when the hanger reaches its maximum extension.

If the magnitude of elongation is sufficient, the gap between the PFC and double tee soffit will close and the articulating hanger can bind as illustrated in Figure 19. Binding would be likely to overstress the anchors connecting the articulating hanger to the support structure. To mitigate against this risk it is recommended that:

- The potential elongation used when dimensioning the articulating hanger should be based on the peak MCE drift as discussed in section 2.2, and
- The demands on the anchors should be protected by a capacity design approach if practical.

Hanger retrofits of this type had been installed in Statistics House prior to the Kaikoura earthquake, but not in locations where double tee units lost support (MBIE 2017, 2018). Consequently the real-world performance of the retrofits was not tested by the Kaikoura earthquake.

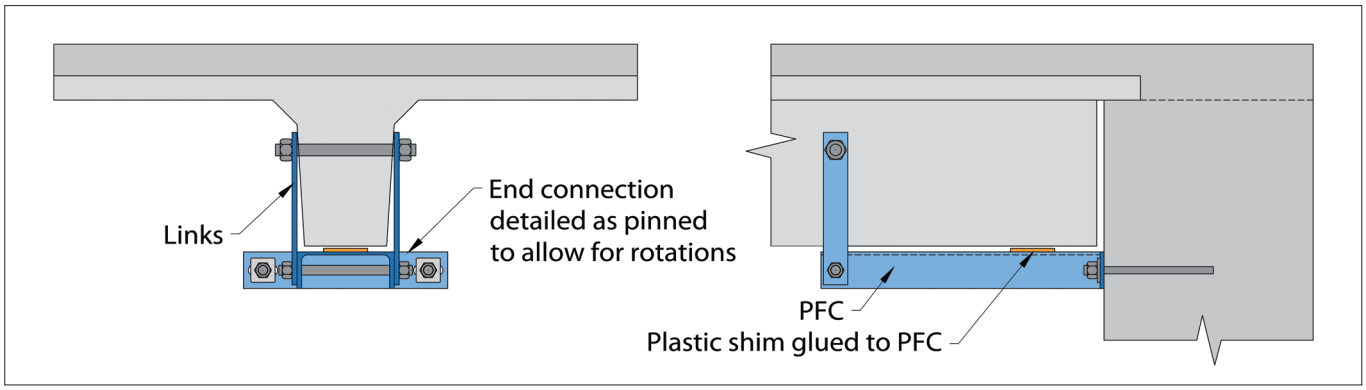

Figure 18: Example of articulating hanger configuration

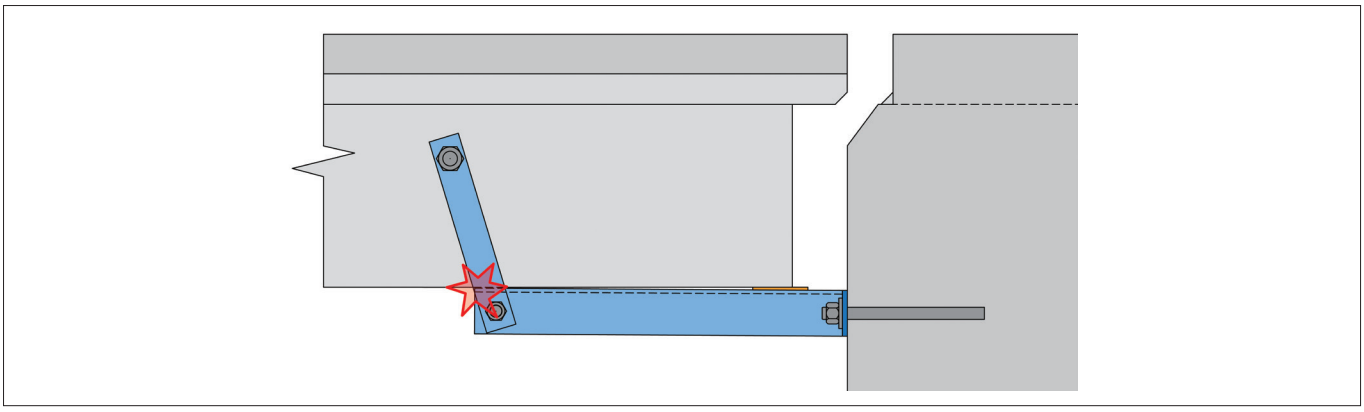

Figure 19: Illustration of potential for hanger binding (adapted from Jenkins 2022)

4.3 RETROFITTED CAZALY HANGER

Instead of providing a catch system for double tee units, it may be possible to provide an improved support system by retrofitting steel elements in a configuration similar to a Cazaly hanger (PCI Industry Handbook Committee 2010). The typical configuration of a Cazaly hanger is shown in Figure 20. Modifications would be required to enable this to be post-installed rather than cast in to the double tee unit:

- A hollow section, channel, or flat plate would need to be fixed in or on top of the topping concrete,
- A tie would be fixed at or near the soffit of the double tee unit (potentially externally mounted), and
- Rods, or other vertical ties, would be required to connect the top and bottom elements. These would logically be placed either side of the double tee web through holes cored in the flange.

Although a retrofitted Cazaly hanger presents a viable retrofit solution for flange hung double tees, it should be noted that no such solution has been designed or tested to validate the approach.

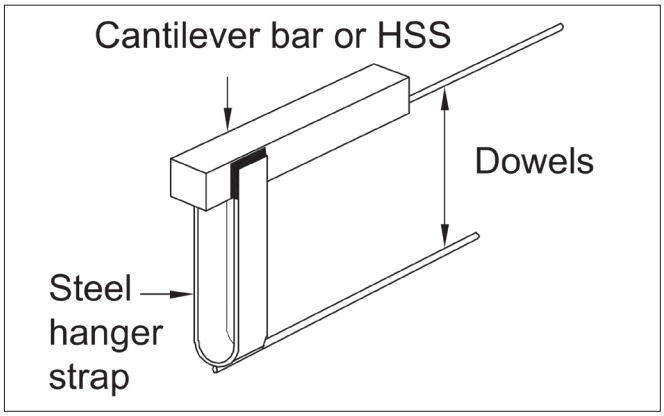

Figure 20: Cazaly hanger (PCI Industry Handbook Committee 2010)

5 RETROFIT TECHNIQUES FOR FLAT SLAB AND RIB AND INFILL FLOORS

In addition to the hollow-core and double tee floors discussed in the preceding sections, retrofit techniques may also be required for precast floors constructed using flat slab precast units or precast ribs with timber infills.

No specific research has been undertaken to investigate retrofit techniques for these other types of floors. However, it is reasonable to consider that:

- Flat slab floors have similarities to hollow-core floors, albeit flat slab floors are typically more robust due to the absence of voids and slender unreinforced webs which precludes WSF, and
- Rib and infill floors have similarities to double tee floors, but are vulnerable to a wider range of failure modes. Notably, rib and infill floors may be vulnerable to PMF if the ribs are ‘trapped’ at the supports.

In light of the comments above and the absence of specific research, it is recommended that retrofit techniques for hollow-core and double tee floors be adapted for use with flat slab and rib and infill floors respectively. For rib and infill floors care should be taken to ensure that retrofits extend far enough to mitigate PMF if a floor is vulnerable to this behaviour.

6 CONCLUSIONS

Design and detailing of efficient retrofits for precast concrete floors requires that retrofits be tailored to reflect the specific behaviour of individual precast units within the floor. It is unlikely to be efficient to assume that the same retrofit is applicable across an entire floor or building. Design of effective retrofits requires consideration of many factors, notably including the failure mode(s) expected to affect the unit considered and deformation (in)compatibility between the floor unit, retrofit components, and other elements of the existing structure.

In relation to hollow-core floors:

- Retrofits that have been shown experimentally to address one or more failure modes comprise supplementary seating, strongback supports, the cable catch system, supplementary negative moment reinforcement, catch beams, and cutting of starter bar reinforcement.
- Supplementary transverse reinforcement is expected to be an effective retrofit technique, but has not yet been experimentally validated.
- Supplementary positive moment reinforcement has not been demonstrated to be an effective retrofit. It may be useful in conjunction with other measures, but this has not been experimentally validated.
- Infilling of cores and inducement of cracking at the ends of units are not effective retrofit techniques.

Double tee floors may be effectively retrofitted using supplementary brackets or articulating hangers. Post-installed Cazaly hangers may also be an effective retrofit, but this has not been demonstrated experimentally.

Retrofit techniques for flat slab and rib and infill floors would be broadly similar to those for hollow-core and double tee floors respectively.

7 ACKNOWLEDGEMENTS

The ReCast Floors project is principally funded by BRANZ from the Building Levy, with additional financial support received from EQC via the UC Quake Centre and Concrete New Zealand Learned Society. The project was also supported by QuakeCoRE, a New Zealand Tertiary Education Commission-funded Centre.

Various images in this paper have been adapted from previous guidance (PCFOG 2009). The generosity of the creators of the original images in providing their source files is acknowledged.

The authors also gratefully acknowledge the contributions of all other members of the ReCast Floors research and oversight teams to the content of this paper.

8 REFERENCES

ACI Committee 440. (2017). Guide for the Design and Construction of Externally Bonded FRP Systems for Strengthening Concrete Structures (ACI PRC-440.2R-17). American Concrete Institute, Farmington Hills, Michigan, 112p.

Brooke, N. J., Elwood, K. J., Bull, D. K., Liu, A., Henry, R. S., Sullivan, T. J., Hogan, L. S., and del Rey Castillo, E. (2019). “ReCast Floors - Seismic Assessment and Improvement of Precast Concrete Floors.” SESOC Journal, 32(1), pp.50–59.

Brunsdon, D., Elwood, K. J., and Henry, R. S. (2017). Wellington City Council Targeted Assessment Programme following the Kaikoura Earthquake of 14 November 2016 Technical Report (Kestrel WCC TAP Technical Report 20170507). Kestrel Group, Wellington, New Zealand, 60p.

Büker, F., Brooke, N. J., Elwood, K. J., Bull, D. K., Hogan, L. S., and Parr, M. (2021). “Development and Validation of Retrofit Techniques for Hollow-core Floors.” Proc. SESOC Conference, Hamilton, New Zealand.

Büker, F., Brooke, N. J., Hogan, L. S., Elwood, K. J., Bull, D. K., and Sullivan, T. J. (2022a). “Design Recommendations for Strongback Retrofits.” SESOC Journal, 35(1).

Büker, F., Elwood, K. J., and Brooke, N. J. (2022b). “Design Recommendations for Seating Angle Retrofits.” SESOC Journal, 35(1).

Büker, F., Elwood, K. J., and Henry, R. S. (2020). “Testing of Retrofit Solutions for Vulnerable Hollow-Core Floor Connection Details.” Christchurch, New Zealand.

Büker, F., Parr, M., De Francesco, G., Hogan, L. S., Bull, D. K., Elwood, K. J., Liu, A., and Sullivan, T. J. (2022c). “Damage Progression Observed During Laboratory Testing of Hollow-Core Floor Super-Assembly Specimens.” SESOC Journal, 35(1).

Bull, D. K. (1999). Guidelines for the Use of Structural Precast Concrete in Buildings. Centre for Advanced Engineering, Christchurch, New Zealand, 143p.

Cattanach, A., and Thompson, J. (2013). “The Clarendon Tower Deconstruction: Lessons Learnt on 1980s Building Performance.” Proceedings of the New Zealand Concrete Industry Conference, Queenstown, New Zealand, 24p.

CCANZ. (2004). New Zealand Commentary on the Precast Concrete Handbook. Cement & Concrete Association of New Zealand & Precast New Zealand, Wellington, New Zealand.

CEN. (2018). Part 4: Design of Fastenings for Use in Concrete (Eurocode 2 - Design of Concrete Structures EN 1992-4:2018). European Committee for Standardization, Brussels, Belgium, 132p.

Cooper, M. C., Carter, R., and Fenwick, R. C. (2012). Final Report Volume 2: The Performance of Christchurch CBD Buildings. Canterbury Earthquakes Royal Commission, Christchurch, New Zealand, 236p.

Corney, S. R. (2017). Seismic Response of Precast Concrete Floor Systems (PhD Thesis). The University of Auckland, New Zealand.

Corney, S. R., Elwood, K. J., and Henry, R. S. (2018). "Residual Capacity Testing of Damaged Hollow-Core Precast Concrete Floors." Proceedings of the NZSEE Conference, New Zealand Society for Earthquake Engineering, Auckland, New Zealand, 9p.

Corney, S. R., Henry, R. S., and Ingham, J. M. (2014). "Performance of Precast Concrete Floor Systems During the 2010/2011 Canterbury Earthquake Series." Magazine of Concrete Research, 66(11), pp.563–575.

Corney, S. R., Puranam, A. Y., Elwood, K. J., Henry, R. S., and Bull, D. K. (2021). "Seismic Performance of Precast Hollow-Core Floors: Part 1—Experimental Data." ACI Structural Journal.

Eligehausen, R., Mallée, R., and Silva, J. F. (2006). Anchorage in Concrete Construction. Ernst & Sohn, Berlin, Germany, 391p.

Elwood, K. J., and Hogan, L. S. (2022). "ReCast Floors Project: Overview and Key Recommendations." SESOC Journal, 35(1).

European Organisation for Technical Approvals (EOTA). (2013). TR 45 - Design of Metal Anchors For Use In Concrete Under Seismic Actions (Technical Report TR 45). European Organisation For Technical Approvals, 15p.

Fenwick, R. C., Bull, D. K., and Gardiner, D. R. (2010). Assessment of Hollow-Core Floors for Seismic Performance (Research Report 2010-02). Department of Civil and Natural Resources Engineering, The University of Canterbury, Christchurch, New Zealand, 152p.

fib Task Group 7.3. (2003). Seismic Design of Precast Concrete Building Structures (fib Bulletin 27). International Federation for Structural Concrete (fib), Lausanne, Switzerland, 254p.

Hare, J., Elwood, K. J., Bull, D. K., Henry, R. S., and Brooke, N. J. (2019). "Precast Double Tee Support Systems - 10 Years On." SESOC Journal, 32(1), pp.32–40.

Hare, J., Fenwick, R. C., Bull, D., and Built, R. (2009). "Precast Double Tee Support Systems." Journal of the Structural Engineering Society New Zealand, 22(1), pp.10–44.

Henry, R. S., Dizhur, D., Elwood, K. J., Hare, J., and Brunsdon, D. (2017). "Damage to Concrete Buildings with Precast Floors During the 2016 Kaikoura Earthquake." Bulletin of the New Zealand Society for Earthquake Engineering, 50(2), pp.174–186.

Henry, R. S., and Jenkins, M. (- In preparation). "Retrofit Techniques for Double-Tee Floors: Experimental Investigation and Design Recommendations." SESOC Journal, In Preparation.

Henry, R. S., Parr, M., Brooke, N. J., Elwood, K. J., Liu, A., and Bull, D. K. (2018). "Progress Towards Experimental Validation of Precast Floor Retrofit Solutions." Proc. Concrete New Zealand Conference, Concrete New Zealand Learned Society, Hamilton, New Zealand.

Herlihy, M. D. (1999). Precast Concrete Floor Support and Diaphragm Action (PhD Thesis). The University of Canterbury, Christchurch, New Zealand, 344p.

Jenkins, M. (2022). Gravity & Seismic Investigation and Retrofit of Loop Bar Double Tee Precast Floors (Master's Thesis). The University of Auckland, New Zealand, 162p.

Jensen, J. P. (2006). The Seismic Behaviour of Existing Hollowcore Seating Connections Pre and Post Retrofit (Master's Thesis). The University of Canterbury, Christchurch, New Zealand, 292p.

Liew, H. Y. (2004). Performance of Hollowcore Floor Seating Connection Details (Master's Thesis). The University of Canterbury, Christchurch, New Zealand, 278p.

Lindsay, R. (2004). Experiments on the Seismic Performance of Hollow-Core Floor Systems in Precast Concrete Buildings (Master's Thesis). The University of Canterbury, Christchurch, New Zealand, 190p.

Matthews, J. (2004). Hollow-Core Floor Slab Performance Following a Severe Earthquake (PhD Thesis). The University of Canterbury, Christchurch, New Zealand, 521p.

MBIE. (2017). Investigation into the Performance of Statistics House in the 14 November 2016 Kaikoura Earthquake. Ministry of Business, Innovation, and Employment, Wellington, New Zealand, 36p.

MBIE. (2018). Addendum: Investigation into the Performance of Statistics House in the 14 November 2016 Kaikoura Earthquake. Ministry of Business, Innovation, and Employment, Wellington, New Zealand, 25p.

MBIE. (2019). Acceptable Solutions and Verification Methods for the New Zealand Building Code Clause B1 Structure (Amendment 19). Ministry of Business, Innovation, and Employment, Wellington, New Zealand, 94p.

MBIE, NZSEE, EQC, NZGS, and SESOC. (2017). The Seismic Assessment of Existing Buildings: Technical Guidelines for Engineering Assessments. Ministry of Business, Innovation, and Employment, Wellington, New Zealand.

MBIE, NZSEE, EQC, NZGS, and SESOC. (2018). Technical Proposal to Revise the Engineering Assessment Guidelines - Part C5 Concrete Buildings. Ministry of Business, Innovation, and Employment, Wellington, New Zealand, 252p.

Mostafa, M. T. (- In preparation). System-Level Seismic Performance of Precast-Prestressed Hollow-core Floors and Residual Shear Capacity of Web-Cracked Units (PhD Thesis). The University of Auckland, Auckland, New Zealand.

Mostafa, M. T., Hogan, L. S., and Elwood, K. J. (2022). "Seismic Performance of Hollow-Core Floors with Modern Detailing." SESOC Journal, 35(1).

New Zealand Government. (2004). Building Act (2004 No 72, Reprint as at 1 July 2019). New Zealand Government, Wellington, New Zealand, 343p.

Norton, J. A., King, A. B., Bull, D. K., Chapman, H. E., McVerry, G. H., Larkin, T. J., and Spring, K. C. (1994). "Northridge Earthquake Reconnaissance Report." Bulletin of the New Zealand National Society for Earthquake Engineering, 27(4), pp.235–344.

Parr, M., Bueker, F., Elwood, K. J., Hogan, L. S., Henry, R. S., Puranam, A., Bull, D. K., and Brooke, N. J. (2019). "Development and Testing of Retrofit Solutions for Hollow-core Floors in Existing Buildings." Proc. Concrete New Zealand Conference, Concrete New Zealand Learned Society, Dunedin, New Zealand.

PCFOG. (2009). Seismic Performance of Hollow Core Floor Systems: Guidelines for Design, Assessment, and Retrofit (www.nzsee.org.nz/db/PUBS/HollowCoreFloorSystems.pdf). Precast Concrete Floors Overview Group (SESOC, NZSEE, and NZCS), Wellington, New Zealand, 163p.

PCI Industry Handbook Committee. (2010). PCI Design Handbook Precast and Prestressed Concrete. Precast/Prestressed Concrete Institute, Chicago, Illinois, 828p.

Puranam, A., Büker, F., and Elwood, K. J. (2019). "Assessment of Reinforced Concrete Buildings with Hollow-core Floors." Proc. Pacific Conference on Earthquake Engineering, Auckland, New Zealand, 10p.

Puranam, A. Y., Corney, S. R., Elwood, K. J., Henry, R. S., and Bull, D. K. (2021). "Seismic Performance of Precast Hollow-Core Floors: Part 2—Assessment of Existing Buildings." ACI Structural Journal, 118(5).

Sarkis, A. I., Brunesi, E., Sullivan, T. J., and Nascimbene, R. (2019). "Numerical Seismic Performance Assessment of Precast Pre-stressed Hollow-core Concrete Floors." Proc. Concrete New Zealand Conference, Concrete New Zealand Learned Society, Dunedin, New Zealand.

Siddiqui, U., Parker, W., Davey, R., and Therkleson, S. (2019). "Seismic Response of BNZ Building in Wellington Following the 2016 Kaikoura Earthquake." Proc. SESOC Conference, Structural Engineering Society of New Zealand, Auckland, New Zealand.

SNZ. (2007). Steel Structures Standard (NZS 3404:1997 inc. Amendment 2). Standards Association of New Zealand, Wellington, New Zealand, 689p.

SNZ. (2011). Structural design actions, Part 0: General Principles (AS/NZS 1170.0 inc. A1-A5). Standards New Zealand, Wellington, New Zealand, 36p.

SNZ. (2016). Structural design actions, Part 5: Earthquake Actions - New Zealand (NZS 1170.5 inc. A1). Standards New Zealand, Wellington, New Zealand, 88p.

SNZ. (2017). Concrete Structures Standard (NZS 3101:2006 inc. A1-A3). Standards New Zealand, Wellington, New Zealand.

Torres, A., Ramos-Canon, A., Prada-Sarmiento, F., and Botia-Diaz, M. (2016). "Mechanical Behaviour of Concrete Cold Joints." Revista Ingeneria de Construccion, 31(3), pp.151–162.

Woods, L. J. (2008). The Significance of Negative Bending Moments in the Seismic Performance of Hollow-Core Flooring (Master's Thesis). The University of Canterbury, Christchurch, New Zealand, 294p.

ISSN No. 2744-7871

DESIGN RECOMMENDATIONS FOR SEATING ANGLE RETROFITS

Büker, F.[1,*], Hogan, L.S.[2], Brooke, N.J.[3], Elwood, K.J.[4], Bull, D.K.[5]

ABSTRACT

Existing precast hollow-core floors commonly have insufficient seating lengths, which makes them prone to Loss of Support failure when subjected to earthquake-imposed demands. A supplementary seating retrofit, such as a seating angle, can be used to prevent collapse when the floor unseats. The absence of design guidance for such seating retrofits has resulted in a wide range of different design and detailing approaches that often underestimate the demands on the post-installed anchors and seating angles. This paper addresses the lack of design guidance by introducing two design methodologies for seating angle retrofits. The first design approach entails design steps for seating angles installed hard up against the soffit of the floor. Capacity-design philosophy is used to ensure the post-installed anchors can withstand the force demands arising from earthquake-imposed deformations. The second recommended approach omits these high demands on the post-installed anchors by leaving a gap between the seating angle and the floor soffit and partially filling this gap with a deformable infill strip. Using these two proposed design recommendations ensures that the seating angle and post-installed anchors can safely support the precast flooring unit if it unseats.

1 BACKGROUND

Precast hollow-core floors are widespread in New Zealand's multi-storey building stock. Advantages such as low cost, lightweight, span capability and ease of construction made the hollow-core floor a popular flooring system, particularly during the construction boom in the 1980s. Until the early 2000s, there were no stringent provisions that outlined how to detail the support for the hollow-core floors. Consequently, the support conditions and seating lengths of hollow-core floors varied significantly, primarily depending on regional practice and contractors' preferences. A nominal seating length of 50 mm was typically specified, following 1970s North American practice, but a review of original drawings of hollow-core floor buildings in Wellington indicated that seating lengths as short as 30 mm were specified in a substantial number of cases (Puranam et al. 2021). In addition, the influence of tolerances during installation could cause the actual seating to be even shorter (MBIE et al. 2018; PCFOG 2009).

The super-assembly test conducted by Matthews (2003) exposed crucial shortcomings of the typical hollow-core floor connection detailing that was used since the 1980s. In response, the third amendment to the concrete structures standard NZS3101:1995 was published in 2004 (SNZ 2004a), making a seating length of at least 75 mm and the use of low-friction bearing strips mandatory. More recent updates to NZS3101 have further increased the required seating length depending on the configuration of a building.

Based on the findings from the Matthews experiment (2003) and subsequent testing on existing hollow-core floor details (Corney et al. 2018; Jensen 2006; Liew 2004; Woods 2008), procedures to assess the seismic capacity of hollow-core floors were developed. These assessment procedures were first published by Fenwick et al. (2010) and then adopted and refined for the technical proposal to revise Section C5 (Concrete Buildings) of the "Guidelines for Detailed Seismic Assessment of Buildings" (MBIE et al. 2018), subsequently referred to as assessment guidelines C5. Three primary failure modes were identified in these assessment procedures, namely Loss of Support (LOS), Negative Moment Failure (NMF) and Positive Moment Failure (PMF).

Seismic assessment of pre-2000s hollow-core floor buildings (using the assessment guidelines C5 (MBIE et al. 2018)) will often find LOS to be the controlling failure mode, though this depends on the provided seating length and other building characteristics (Puranam et al. 2021).

PAPER CLASS & TYPE: GENERAL REFEREED

1 *PhD Candidate, University of Auckland*
2 *Lecturer, University of Auckland*
3 *Managing Director, Compusoft Engineering Limited*
4 *Professor, University of Auckland*
5 *Technical Director, Holmes Consulting*
* *frank.bueker@auckland.ac.nz*

The factors taken into account when assessing for LOS are:

(a) Movements due to relative rotation of the supporting member/beam,

(b) Elongation of the adjacent beam or unit movement due to plastic strain in the starter bars,

(c) Spalling at the seating beam ledge and at the back face of the hollow-core unit,

(d) Creep, shrinkage and temperature-related deformations,

(e) Construction tolerances, and

(f) Required bearing length.

While the assessment procedures for hollow-core floors have been well established, only limited guidance was provided on retrofit techniques. In practice, a steel angle or hollow section affixed to the support member is the most-widespread solution to extend the short original seating and prevent collapse by LOS. However, the lack of design and detailing guidance for such angle retrofits resulted in a number of different seating angle configurations that have been installed in existing buildings. Several concerns have been raised on the adequacy of the design and detailing features of these typical seating angle configurations.

A floor-to-beam connection with a typical seating angle configuration is depicted in Figure 1. This connection is shown as undergoing an earthquake-induced negative support rotation and pull-off displacement due to the elongation of the adjacent beam. The relative rotation causes the floor to pry over the seating angle, generating a vertical reaction and an associated horizontal friction force at the top leg of the angle. The forces are transferred through the angle and resisted in shear and tension by the post-installed anchors and a compression reaction at the vertical leg.

The main concern associated with the design and detailing of this typical seating angle configuration is that it is not practical to accurately estimate the deformation-induced force on the post-installed anchors, which may lead to sudden brittle failure if the anchors are overloaded. The reasons it is not practical to accurately estimate the force demand are:

- As indicated in Figure 1, the imposed force demands on the anchors may be greater than just the gravity shear, $V_{Gravity}$. The shear force in the anchors, V_{Anchor}, is the sum of the gravity shear, $V_{Gravity}$, and the interface shear, $V_{Interface}$. While the gravity shear force is known, the interface shear force is highly variable. The interface shear consists of (1) the shear resistance from the starter bars acting in dowel action, (2) the shear resistance by the in-situ concrete plugs protruding from the beam into the cells and (3) the shear friction associated with a compression reaction at the back face of the floor. Because of the variability of the involved interface shear components combined with the high uncertainty of the as-built connection conditions, the interface shear resistance cannot reliably be quantified.
- There is uncertainty about at what distance x_1 along the horizontal leg this shear reaction will be transferred into the angle. Without knowing the location of the shear force, the tension force in the anchor, T_{Anchor}, cannot be determined.
- Similarly, the location of the compression reaction C_C, between the seating angle and the support beam is unknown. When the compression reaction, C_C, increases, angle deformations may cause the compression force to shift up towards the anchors. The smaller the lever arm between the compression

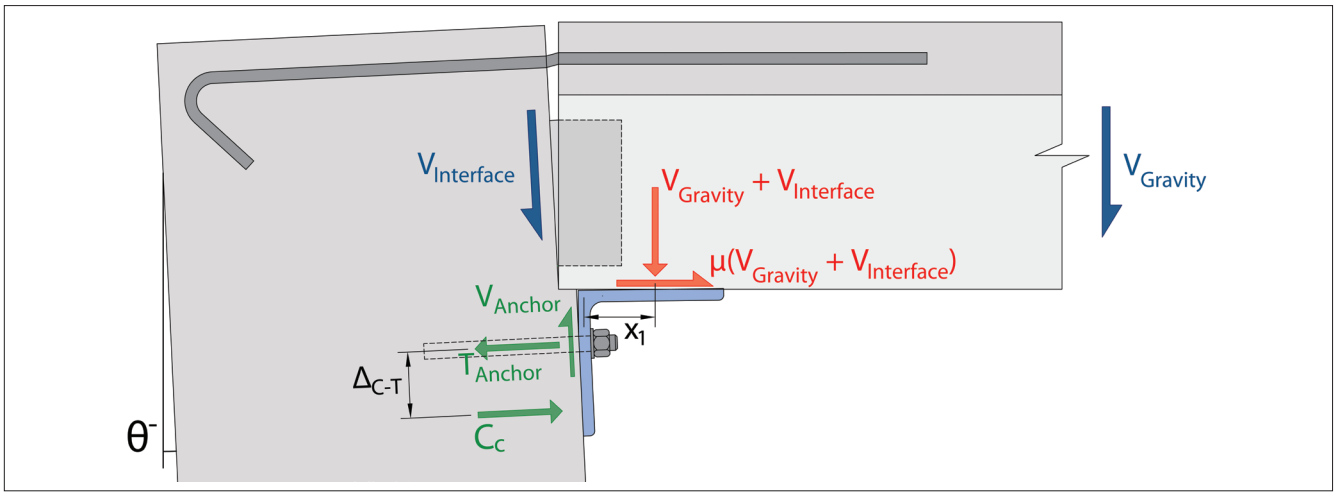

Figure 1: Hollow-core floor to beam connection with a typical existing seating angle under negative rotation

reaction and the post-installed anchors, $\Delta_{C\text{-}T}$, the larger the tension force in the anchors. This effect can result in anchor failure.

Additionally, until recently, guidance has not been provided on which load combinations appropriately represent the gravity load demands on the angle during and after the earthquake.

Furthermore, improper seating angle design and detailing may not only lead to retrofit failure but can also adversely affect the floor performance, i.e. triggering unexpected floor failure modes. Parr et al. (2019) demonstrated that NMF could be triggered when the seating retrofit is very stiff, not allowing for the expected deformations under negative rotations.

Many existing seating angles have been designed without consideration of the above concerns. Factors such as flexibility in the anchor connection and probable versus design anchor capacities may show that existing angles are sufficient to support the floor in an earthquake event. Future research is needed to quantify these factors. Nevertheless, practitioners are encouraged to review existing seating retrofits that may have critical deficiencies, such as shallow embedded anchors with little capacity or stiff seating retrofits installed hard up against the soffit.

1.1 EFFECTIVENESS OF SEATING ANGLES

While seating angles are an appropriate retrofit option for LOS, observations from a recently conducted super-assembly test (Büker et al. 2022b) highlight that seating angles alone cannot effectively address PMF. The companion paper by Brooke et al. (2022) provides recommendations on which additional retrofit components are required to sufficiently address PMF.

Brooke et al. also discuss the failure hierarchy of precast concrete floors and its implication for the choice of retrofit techniques. It is emphasised that LOS may often be the governing failure mode as per seismic assessment (i.e. failure mode with the lowest assessed drift capacity), but it is not guaranteed that this failure mode occurs. Consequently, an adequate combination of floor retrofits needs to be installed that addresses all failure modes for which the drift demands exceed the assessed drift capacities.

This paper provides design and detailing recommendations for new seating angles. Two design approaches are outlined that mitigate the aforementioned concerns and ensure resilience to withstand demands during and after the earthquake.

2 RECOMMENDED SEATING ANGLE VARIATIONS

Recommendations for two approaches to design and detail seating angle retrofits for hollow-core floors are outlined in this paper. The first procedure allows the angle to be installed hard-up against the soffit of the floor, and the second procedure has the angle set down with a deformable infill strip. The conceptual details of these two solutions are illustrated in Figure 2. A key factor of the proposed seating angle details is to maximise the understanding of forces on the post-installed anchors. Modification of the proposed details may affect the design procedures outlined in this paper and requires careful consideration.

For the first design procedure, the seating angle is installed hard-up against the floor soffit, and thus, all components need to be designed and detailed to endure the earthquake-imposed deformations of the

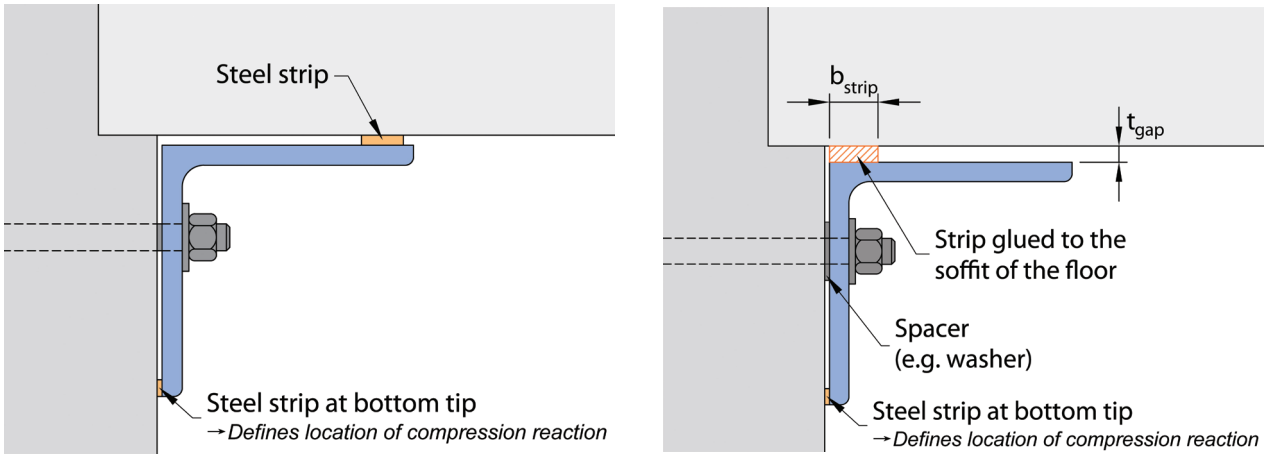

Figure 2: Detailing of the two recommended design approaches for seating angles

floor-to-support connection. As discussed in Section 1, these deformations can result in large force demands on the seating angle and the post-installed anchors. While ductile flexural behaviour can be expected from the steel angle, the post-installed anchors are likely to exhibit brittle performance when experiencing higher than expected demands. A 'capacity-design' procedure can be adopted to protect the post-installed anchors from overloading. Applying the concept of capacity design to the seating angle design ensures that an upper limit of the forces in the post-installed anchors can be determined from the flexural overstrength of the seating angle. The application of this design procedure is outlined in Section 3. To conduct the capacity-design procedure, the location of all applied forces must be known to reliably determine the shear and tension demands on the post-installed anchors. Therefore, steel bearing strips should be fixed (e.g. welded) near the toes of both legs, as demonstrated in Figure 2a. Other material could be used for the strip in lieu of the steel, provided it is stiff enough. It may be preferred to install a washer as a spacer between the beam face and back of the angle at the bolt connections for construction purposes, but such spacers are not crucial for the angle to perform as intended.

The advantage of the capacity-design approach is that there is no vertical drop once the floor unseats from its original support. This ensures that the diaphragm remains on the same level and may also limit additional damage to the floor, such as topping delamination or web-cracking.

The second detailing solution features a gap between the seating angle and the floor soffit and thereby avoids large forces in the anchors that could be generated by flexural deformation of the angle during negative support rotation. The detail incorporates a deformable infill strip of rubber or material of similar stiffness that is glued to the bottom of the floor, as shown in Figure 2b. The deformable infill strip can slide on the angle and ensures that the location of the vertical reaction is clearly defined. Furthermore, the deformable infill strip helps to limit the vertical drop of the floor and aids the installation process of the seating angle by ensuring a consistent gap to the floor soffit. Similarly to the capacity-design approach, a steel strip is recommended to be fixed (e.g. tack-welded) to the bottom toe of the vertical leg of the angle to ensure the location of the compression reaction is known.

A spacer in form of a washer or similar between the beam face and back of the angle at the bolt connections should be incorporated into the detailing

With this solution, the force demands on the anchors are generally lower compared to the capacity-design approach. Nonetheless, consideration should be given to the fact that, depending on the flexibility of the strip, the hollow-core unit will sustain a vertical drop if LOS occurs. This drop of the hollow-core unit can cause delamination of the floor topping and may promote web-cracking. The adverse effect of web-cracking on the floor performance and the gravity load-carrying capacity is currently not well understood. Furthermore, this solution has not been experimentally validated at the time of publication of this article. Consequently, the capacity-design method should be viewed as the preferred option.

Despite these recommendations exclusively covering the design of seating extensions using steel angle sections, it is also possible to use them, with slight modifications, to design supplemental seating employing rectangular hollow sections or other steel sections. In particular, for the capacity-design approach, some equations need to be modified to adjust for the different yield mechanisms of other sections.

2.1 LOAD COMBINATIONS

Precast floor retrofits need to be able to resist the loads that arise both during and after the earthquake. The load combinations outlined in this section are consistent with the overarching precast floor retrofit design recommendations outlined in the companion paper by Brooke et al. (2022).

Force demands during the earthquake can appropriately be represented by the ultimate limit state (ULS) load combination of permanent, earthquake and imposed actions as specified in NZS1170.0:2002-A5 (SNZ 2011):

$$E_d = \mathrm{G} + \psi_{\mathrm{E}}\mathrm{Q} + \psi_{\%\mathrm{NBS}}\mathrm{E_u} \qquad (1)$$

where E_d is the design action effect, G is the permanent action (i.e. 'dead' load), ψ_{E} is the combination factor for earthquake action, Q is the imposed action ('live' load), $\psi_{\%\mathrm{NBS}}$ is a non-conventional notation reflecting the reduction of demands by the targeted %NBS rating and $\mathrm{E_u}$ is the earthquake action[1]. The area reduction factor, ψ_a, can be omitted as it is taken as 1.0 for one-way slabs.

Besides the force demands, it is essential to take into account the displacements and rotations imposed on the support connection and seating angle during the earthquake. These demands should be evaluated based on the relevant peak drift for the maximum considered earthquake (MCE) as specified in NZS3101:2006-A3 (SNZ 2017) under consideration of the targeted %NBS.

[1] Vertical accelerations can be neglected for the seating angle design due to their high-frequency

$$\psi_{\%NBS}\,\delta_{peak.MCE} = \frac{1.5}{S_p}\,\psi_{\%NBS}\,\delta_{ULS} \quad (2)$$

where $\delta_{peak.MCE}$ is the peak MCE interstorey drift, S_p is the structural performance factor, δ_{ULS} is the ULS interstorey drift for the structure and all other variables have been defined previously.

In the post-earthquake scenario, the damaged floor must be able to support the gravity loads per NZS1170.0:2002-A5 (SNZ 2011):

$$E_d = 1.35G \quad (3)$$

$$E_d = 1.2G + 1.5Q \quad (4)$$

where all variables have been defined previously.

Designing the seating retrofit using the full ULS gravity load combination (Equations (3) and (4)) likely overestimates the actual load demands on the floor in a post-earthquake scenario. Brooke et al. (2022) argue that a reduction of the design live loads for the post-earthquake scenario may be reasonable on the basis that the damaged flooring units will have restricted access. In view of this argument, Equation (4) can be modified to:

$$E_d = 1.2G + 1.5\psi_E\,Q \quad (5)$$

where all variables have been defined previously.

Seating retrofits of hollow-core units that are part of an egress route should not be designed with the reduced live loads but always with the full ULS gravity loads (Equations (3) and (4)) for the post-earthquake scenario. Furthermore, engineers and building owners should note that unrestricted usage of the floor is not possible after LOS has occurred if the retrofit is designed with Equation (5).

3 DESIGN RECOMMENDATIONS FOR THE 'CAPACITY-DESIGN' SOLUTION

The 'capacity-design' approach for seating angles has the objective to protect the post-installed anchors by designing them to resist the maximum expected loads associated with the flexural overstrength of the seating angle. This procedure aligns with the design provisions for post-installed anchors as per EN1992-4 (2018), which has superseded TR045 that NZS3101:2006-A3 (SNZ 2017) refers to for the design of post-installed anchors.

The capacity-design procedure involves the following four design steps:

1. Determine the required additional seating length, $\delta_{s,ret,CD)}$.
2. Size the seating angle for the flexural demands.
3. Check if the angle is expected to yield.
4. Capacity design the post-installed anchors.

The design procedure allows for two different design pathways based on whether the seating angle is expected to yield or remain elastic. These two pathways are illustrated in the flowchart shown in Figure 3. After determining the required additional seating length and sizing the angle to withstand the flexural demands, the expected rotation demands at the support can be compared to the rotation at which the seating angle starts yielding. If yielding of the seating angle is expected, 'Pathway 1' should be followed. The design assumptions in 'Pathway 1' use the conventional capacity-design philosophy by assuming that the seating angle may reach flexural overstrength.

In cases where the seating angle is not expected to yield, 'Pathway 2' can be followed. 'Pathway 2' provides the option to omit the overstrength factor, ϕ_{oms} and size the anchors for the nominal flexural strength of the angle, M_s, in recognition of the limited expected rotation demands. Nonetheless, it should be noted that 'Pathway 2' does not abide by the conventional rules of the capacity-design philosophy and, thereby, entails the risk of anchor failure if the earthquake is bigger than expected. 'Pathway 1' is applicable regardless of whether the angle will yield or not and is generally the preferred procedure for new retrofits. 'Pathway 2' may be more suitable for the reassessment of existing retrofits.

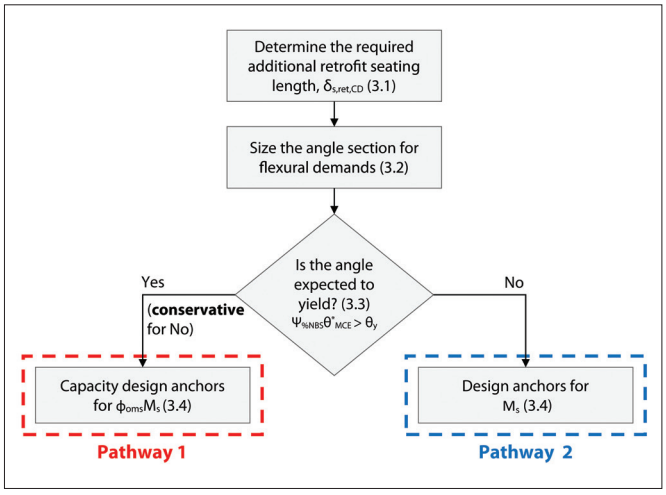

Figure 3: Flowchart of the design procedure for the capacity-design approach. Numbers in brackets refer to section numbers that follow.

The individual design steps for the capacity-design method are outlined in the following sub-sections.

3.1 REQUIRED SEATING LENGTH

The first design step is the determination of the additional retrofit seating length, $\delta_{s,ret,CD}$, that needs to be provided by the seating angle in addition to the existing seating. This length can be calculated as follows:

$$\delta_{s,ret,CD} \geq \delta_{s,\,NZS3101:2006A3} - \delta_{s,\,specified} \qquad (6)$$

where $\delta_{s,ret,CD}$ is the additional available seating as shown in Figure 4, $\delta_{s,specified}$ is the seating length specified in the original drawing[2], and $\delta_{s,NZS3101:2006A3}$ is the theoretically required seating length for the existing hollow-core unit to sustain a maximum considered earthquake according to NZS3101:2006-A3 (SNZ 2017), which includes demands due to spalling, creep, shrinkage and thermal actions as well as tolerances in accordance with NZS3109:1997-A2 (SNZ 2004b).

Existing buildings may have uneven strengths at each end of the unit (i.e. strong, ductile starter bars at one support and non-ductile mesh at the other support), which may lead to a concentration of elongation at one end. On this basis, and as required by NZS 3101:2006-A3 (SNZ 2017), it is prudent to design the seating angle considering that the total elongation generated by the plastic hinges along the span of the unit concentrates at one end.

3.2 BENDING CAPACITY CHECK

Based on the required additional seating, an adequate steel angle section can be selected under consideration of the detailing recommendations discussed in Section 5. The bending capacity of the selected angle section should be sufficient to support the gravity loads of the floor during and after the earthquake. The demands during the earthquake consist of a vertical gravity load from the seismic weight of the floor (Equation (1)) and an associated friction force generated by the elongation movement, as depicted in Figure 5a.

After the earthquake, only a vertical load component remains (Figure 5b), but this component reflects the expected shear demands defined by the relevant post-earthquake load combinations (Equation (3) and Equation (4) or (5)). The yield line is expected to run horizontally along the upper edge of the nuts of the post-installed anchors, marked with a red dot in Figure 5.

For the bending design check, the design moment capacity, ϕM_s, should be equal to or larger than the maximum of the flexural demands imposed during and after the earthquake:

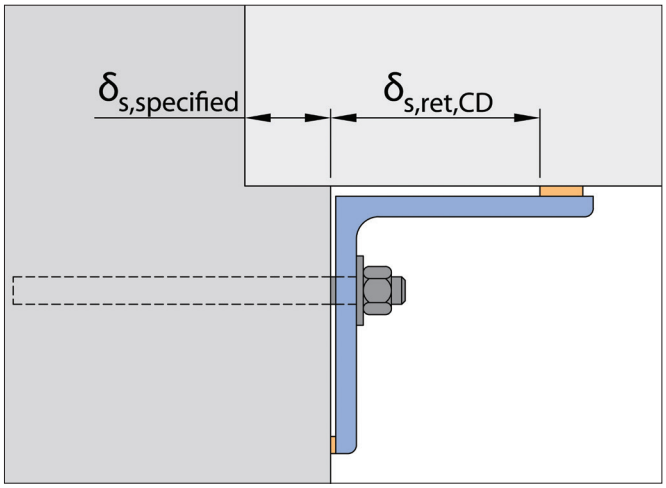

Figure 4: Required angle size to accommodate the seating demands.

$$\phi M_s \geq max\left(\begin{matrix} V_{EQ}\ x_{1,CD} + \mu V_{EQ}\ y_{1,CD} \\ V_{post\_EQ}\ x_{1,CD} \end{matrix}\right) \qquad (7)$$

where ϕ is the strength reduction factor as specified in NZS3404:1997-A2 (SNZ 2007), M_s is the nominal section moment capacity based on NZS3404:1997-A2 (SNZ 2007), V_{EQ} is the ULS shear demand at the support during the earthquake calculated with Equation (1), μ is the friction coefficient between concrete and the strip, $y_{1,CD}$ is the vertical distance from the top of the nut to the top of the strip, V_{post_EQ} is the post-earthquake shear demand at the support calculated with Equation (3) or Equation (4) and $x_{1,CD}$ has been defined previously.

3.3 YIELD ROTATION CHECK

To find out which of the two design pathways can be used for the anchor design, the yield rotation of the angle must be determined and compared to the expected rotation demands. This design step can be omitted if the intention is to follow 'Pathway 1' regardless of whether the angle is expected to yield.

The floor-to-support rotation at which the angle is expected to yield can be calculated as:

$$\theta_y = \theta_{y,1} + \theta_{y,2} = \frac{2\varepsilon_\gamma}{t} y'_{1,CD} + \frac{2\varepsilon_\gamma (x'_{1,CD})^2}{3tx_{1,CD}} \qquad (8)$$

where ε_γ is the yield strain of the steel grade used for the seating angle, t is the seating angle thickness, $y'_{1,CD}$ is the vertical distance between the top of the nut and the bottom edge of the root, $x_{1,CD}$ is the horizontal distance between the centreline of the strip to the centreline of the vertical leg of the angle section and $x'_{1,CD}$ is the horizontal distance from the centre of the strip to the edge of the root. The dimensions are also illustrated in Figure 6.

[2] If the actual seating has been measured, $\delta_{s,specified}$ can be replaced by the actual seating length and tolerances, creep and shrinkage can be omitted from $\delta_{s,NZS3101:2006A3}$.

If the rotation demands are greater than the seating angle yield rotation, 'Pathway 1' must be followed. Otherwise, if the expected rotation demands are smaller or equal to the seating angle yield rotation, both 'Pathway 1' and 'Pathway 2' are valid.

$$\psi_{\%NBS}\theta_{peak,MCE} \quad \begin{matrix} \leq \theta_y \rightarrow Pathway\ 1\ or\ 2 \\ > \theta_y \rightarrow only\ Pathway\ 1 \end{matrix} \qquad (9)$$

where $\psi_{\%NBS}\theta_{peak,MCE}$ is the floor-to-support rotation demand based on the peak MCE drift (Equation (2), factored by the targeted %NBS rating as defined in Equation (5) and θ_y is the floor-to-support rotation at which the angle is expected to yield as defined in Equation (8) . For a typical support arrangement in a strong-column weak-beam moment frame, the peak MCE floor-to-support rotation demand, $\theta_{peak,MCE}$, can be taken as equal to the peak MCE interstorey drift, $\delta_{peak,MCE}$.

3.4 CAPACITY DESIGN OF ANCHOR

The design loads of the anchors are determined following the capacity-design philosophy. Applying this philosophy to the seating angle configuration means that the angle must be able to accommodate the imposed demands during the earthquake through flexural deformations in a ductile manner. In order to prevent a brittle failure of the post-installed anchors, the anchors should be designed to withstand the upper-bound demands generated by bending of the angle. Therefore, it is recommended to keep the flexural demand to capacity ratio high when designing the seating angle for flexure because the greater the flexural strength of the seating angle, the higher the demands on the anchor.

The worst-case loading scenario for the post-installed anchors arises during negative support rotations when the interface shear resistance is still high. The forces

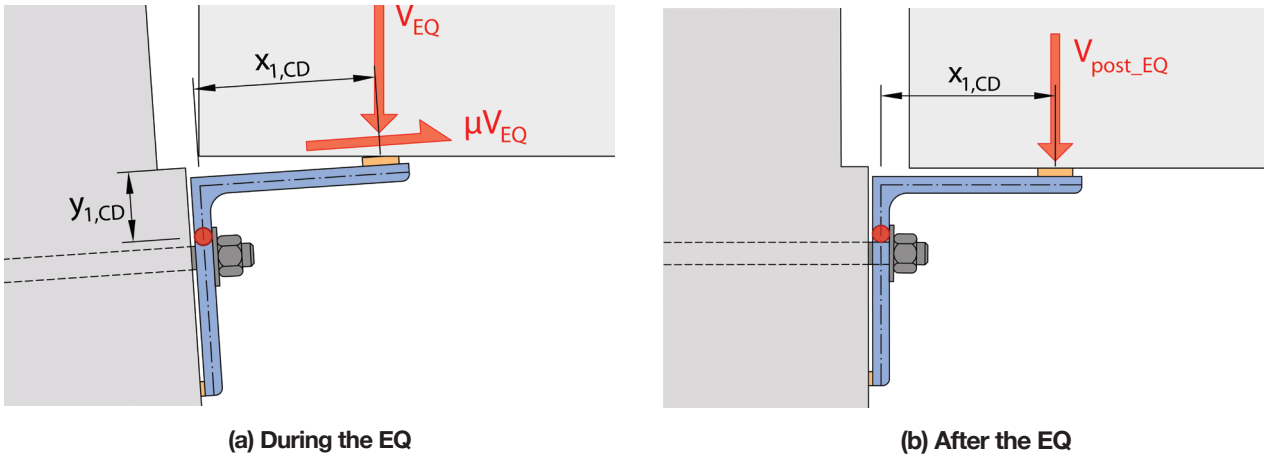

(a) During the EQ (b) After the EQ

Figure 5: Bending checks of capacity-designed seating angle.

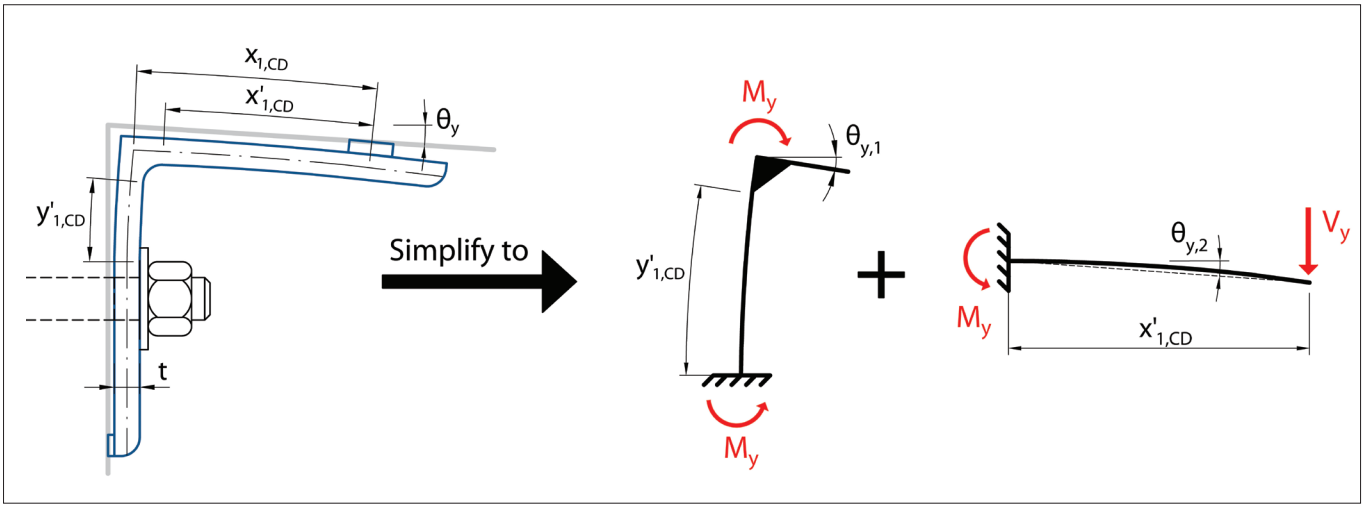

Figure 6: Estimation of the relative rotation between the supporting beam and the floor at which the angle starts yielding.

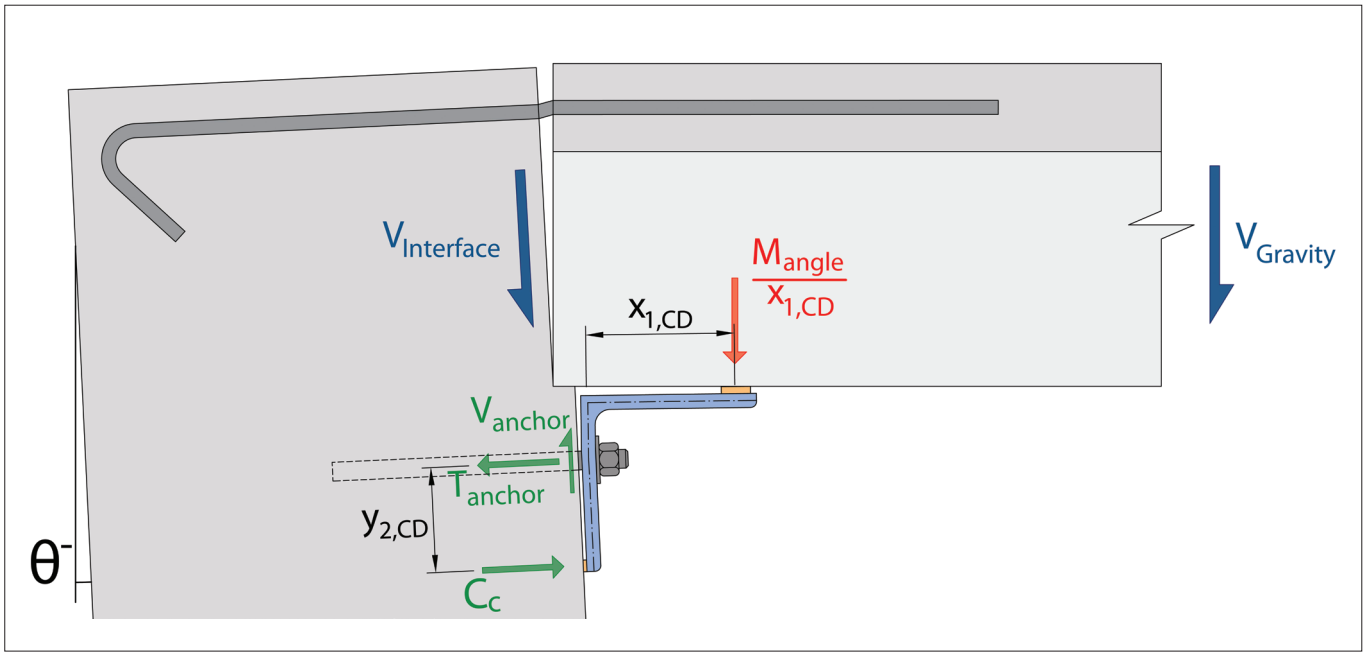

Figure 7: Capacity design of post-installed anchors.

acting on the seating angle assembly are shown in Figure 7. From the depicted scenario, the shear and tension demands on the post-installed anchors can be derived based on the flexural capacity of the seating angle:

$$V_{anchor} = \frac{M_{angle}}{x_{1,CD}} \quad (10)$$

$$T_{anchor} = \frac{M_{angle}}{y_{2,CD}} \quad (11)$$

where M_{angle} is the moment capacity of the seating angle at the top of the nut (for 'Pathway 1' use the overstrength moment capacity, $\phi_{oms}M_s$ as per NZS3404:1997-A2 (SNZ 2007), and for 'Pathway 2' use the unfactored nominal section moment capacity, M_s), $y_{2,CD}$ is the vertical distance between the centreline of the post-installed anchors and the centreline of the strip at the bottom toe of the angle and $x_{1,CD}$ has been defined previously.

Although the demands on the post-installed anchors are typically governed by the loading scenario elaborated above, the anchor capacity should also be evaluated for the forces generated by the floor sliding on the seating angle, in particular, in cases where the friction coefficient, μ, is high. For this loading scenario, which is depicted in Figure 8, the shear and tension demands on the anchors can be derived as:

$$V_{anchor} = V_{EQ} \quad (12)$$

$$T_{anchor} = \left(\frac{x_{1,CD} + \mu\, y_{3,CD}}{y_{2,CD}} + \mu\right) V_{EQ} \quad (13)$$

where $y_{3,CD}$ is the vertical distance from the anchor centreline to the top of the strip on the horizontal leg of the angle and all other parameters have been defined previously and are shown in Figure 8.

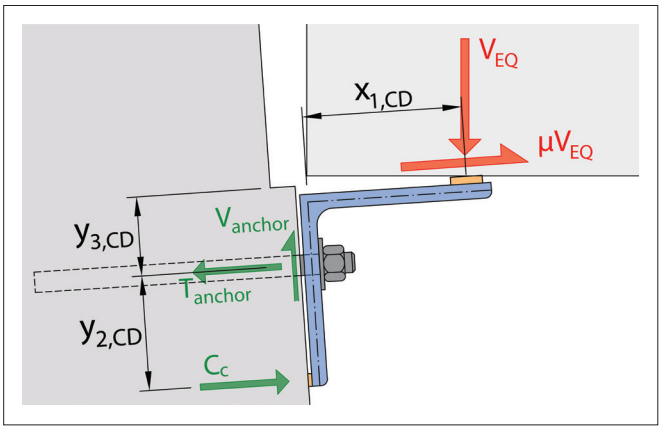

Figure 8: Forces in the post-installed anchors when the floor is sliding on the angle.

Seating angles designed with the capacity-design approach can be used in conjunction with the newly developed strongback retrofit discussed in the companion paper by Büker et al. (2022a). This retrofit combination was successfully tested in a super-assembly experiment recently conducted at the University of Canterbury (Büker et al. 2022b). When designing the seating angles for the strongback retrofit, modifications are required to the seating length check outlined in this Section 3.1. These modifications are described in the design recommendation for strongbacks (Büker et al. 2022a).

4 DESIGN RECOMMENDATIONS FOR THE 'DROPPED-ANGLE' APPROACH

As an alternative to the 'capacity-design' approach, the seating angle can also be designed using the 'dropped-angle' method. For this method, the seating angle is installed with a gap to the floor soffit and a deformable infill strip is glued to the floor, partially filling the gap as shown in Figure 2b. Installing the angle set-down has the advantage that demands on the post-installed anchors can be mitigated but, as discussed in Section 2, this method has several drawbacks, making it less reliable compared to the capacity-design solution.

The following sections outline the recommended design procedures for the dropped-angle approach. The naming convention of variables is kept consistent with the capacity-design approach, but for clarity, the subscript 'DA' for "dropped-angle" has been added.

4.1 REQUIRED SEATING LENGTH AND DESIGN OF THE STRIP

The deformable infill strip, fixed to the bottom of the hollow-core unit, needs to be fully supported on the seating angle even during large seating movements. To ensure the top leg of the seating angle has sufficient length, the earthquake-induced movements, namely the relative rotation between the support and the floor and beam elongation of the adjacent beam, need to be compared to the provided retrofit seating length, $\delta_{s,ret,DA}$:

$$\delta_{s,ret,DA} \geq \delta^*_{s,DA} \qquad (14)$$

where $\delta_{s,ret,DA}$ is the additional seating length provided by the seating angle measured from the edge of the deformable infill strip to the tip of the seating angle as indicated in Figure 9, and $\delta^*_{s,DA}$ is the sum of the displacement demands due to the elongation of the adjacent beam and displacement induced by the rotation of the support beam as defined in the current concrete design standard NZS3101:2006-A3 (SNZ 2017). The total elongation from the plastic hinges along the floor span should be assumed to concentrate at one support when sizing the seating angle, as elaborated in Section 3.1. The effects of spalling, creep, shrinkage and construction tolerances do not need to be considered here.

In cases where hollow-core floors are exposed to significant thermal variation, such as parking decks, the displacements caused by temperature changes should be added to the earthquake demands.

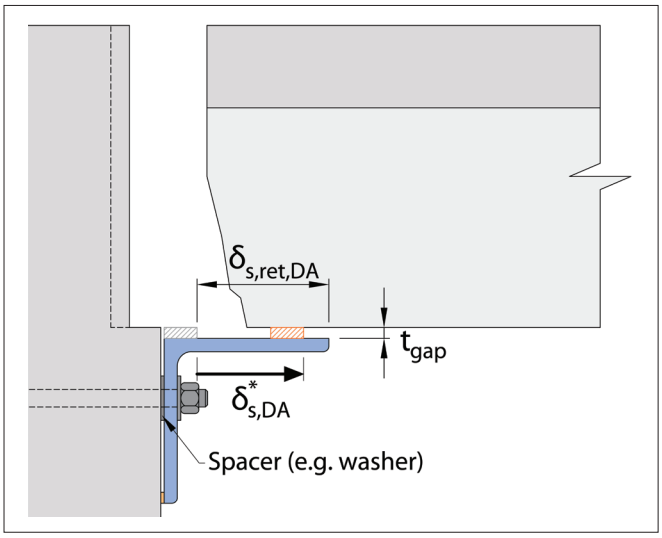

Figure 9: Required seating length for a dropped angle with deformable infill strip

The width of the gap between the seating angle and the floor soffit, t_{gap}, should generally be large enough so that the floor soffit does not come into contact with the tip of the horizontal leg of the angle during negative support rotation due to MCE peak inter-storey drifts (Equation (2)). To ensure that the angle is installed upright, a spacer (e.g. washer) should be added between the beam face and the back of the seating angle (Figure 9). If this spacer is intentionally omitted, the geometrical rotation resulting from the presence of the steel strip at the base of the vertical leg should be accounted for when sizing the gap, t_{gap}.

Considerations should also be given to the design and sizing of the deformable infill strip that is glued to the soffit of the floor. The recommended design and performance criteria for the deformable infill strip are as follows:

- The minimum recommended width of the deformable infill strip, b_{strip}, is 20 mm. A wider strip will generally provide more stability.
- The deformable infill strip should generally have the same length as the seating angle. However, if the seating angle is installed across several units, the deformable infill strip should be installed on a unit-by-unit basis.
- The choice of strip dimensions and material should be made under consideration of the following two criteria that ensure the strip performs as desired:
  - The deformable infill strip should be sufficiently stiff so that if the floor unseats and the strip

compresses under the floor loads, the tip of the angle does not come in contact with the bottom of the floor (Figure 10a). This scenario should be prevented because it is incompatible with the design procedures for the angle and anchor discussed in the following sub-sections. The material and dimension of the deformable infill strip should be selected so that this scenario will not occur. The deformation compatibility can be assessed geometrically assuming a scenario in which the floor-to-support connection is undergoing the maximum negative rotation (based on Equation (2)), and the floor has completely unseated, compressing the deformable infill strip under gravity load during the earthquake, V_{EQ} (based on Equation (1)). For simplicity, it can be assumed that the strip remains in the initial pre-earthquake position when unseating occurs. Alternatively, it is also valid to assume the likely location of the strip at the maximum negative rotation (based on Equation (2)) determined with the assessment guidelines C5 (MBIE et al. 2018) in lieu of NZS3101:2006-A3 (SNZ 2017) because it provides a more realistic estimate.

  - The deformable infill strip should be flexible enough to prevent excessive force demands on the post-installed anchors. When the maximum negative support rotation occurs while the interface shear capacity is still high, forces can be transferred directly through the strip into the anchors, as demonstrated in Figure 10b. The magnitude of this force depends on the strain demand on the strip and can therefore be derived for the maximum negative support rotation pivoting about the front tip of the seating ledge. The anchor capacity should then be checked against this force demand. Note that for stiffer strips, the forces from this scenario may be the governing demands for the post-installed anchor design.

- An appropriate adhesive should be used for the fixation of the deformable infill strip to the bottom of the hollow-core unit. The adhesive must withstand the expected maximum friction force that is generated by the strip sliding on the seating angle during the earthquake (μV_{EQ}).

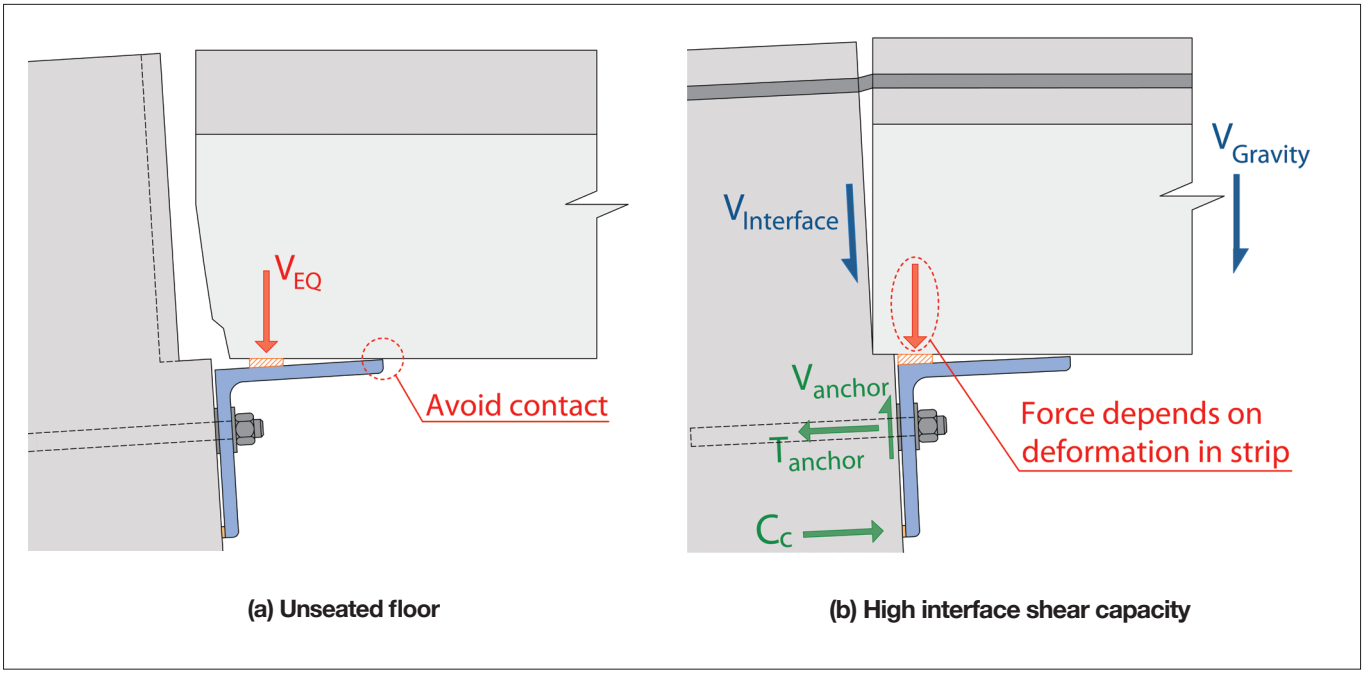

Figure 10: Scenarios to consider when sizing the deformable infill strip

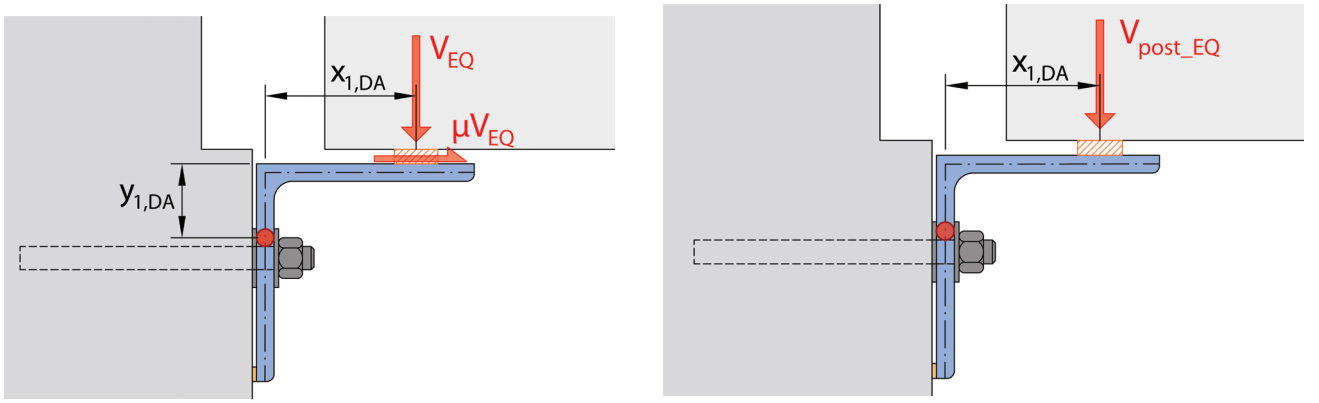

(a) During the EQ (b) After the EQ

Figure 11: Bending check of a seating angle designed with the dropped-angle approach

4.2 BENDING CAPACITY CHECK

For the flexural design of the seating angle, both loading scenarios, during the earthquake (Figure 11a) and after the earthquake (Figure 11b), should be considered. The bending capacity of the angle section must be greater or equal to the maximum generated moment demand from these two scenarios:

$$\phi M_s \geq \max \begin{pmatrix} V_{EQ}\ x_{1,DA} + \mu V_{EQ}\ y_{1,DA} \\ V_{post\_EQ}\ x_{1,DA} \end{pmatrix} \qquad (15)$$

where ϕ is the strength reduction factor as specified in NZS3404:1997-A2 (SNZ 2007), M_s is the nominal section moment capacity based on NZS3404:1997-A2 (SNZ 2007), V_{EQ} is the ULS shear demand at the support during the earthquake calculated using Equation (1), $x_{1,DA}$ is the horizontal distance from the centreline of the deformable infill strip to the centreline of the vertical leg of the seating angle, μ is the coefficient of friction between the seating angle and the strip, $y_{1,DA}$ is the vertical distance between the top of the nut and the top of the seating angle and V_{post_EQ} is the post-earthquake shear demand at the support calculated using Equation (3) and Equations (4) or (5).

4.3 ANCHOR CAPACITY CHECK

By leaving a gap between the angle and the bottom of the floor, overloading of the anchors is prevented. Thus, tension and shear in the anchors are limited to the gravity demands during the earthquake (Figure 12a, Equations (16) and (18)) and after the earthquake (Figure 12b, Equations (17) and (19)):

During the earthquake

$$V_{anchor} = V_{EQ} \qquad (16)$$

$$T_{anchor} = \left(\frac{x_{1,DA} + \mu\, y_{3,DA}}{y_{2,DA}} + \mu\right) V_{EQ} \qquad (18)$$

After the earthquake

$$V_{anchor} = V_{post\_EQ} \qquad (17)$$

$$T_{anchor} = \frac{x_{1,DA}}{y_{2,DA}}\, V_{post\_EQ} \qquad (19)$$

where $y_{3,DA}$ is the vertical distance between the centreline of the post-installed anchors and the top of the angle and all other variables have been defined previously.

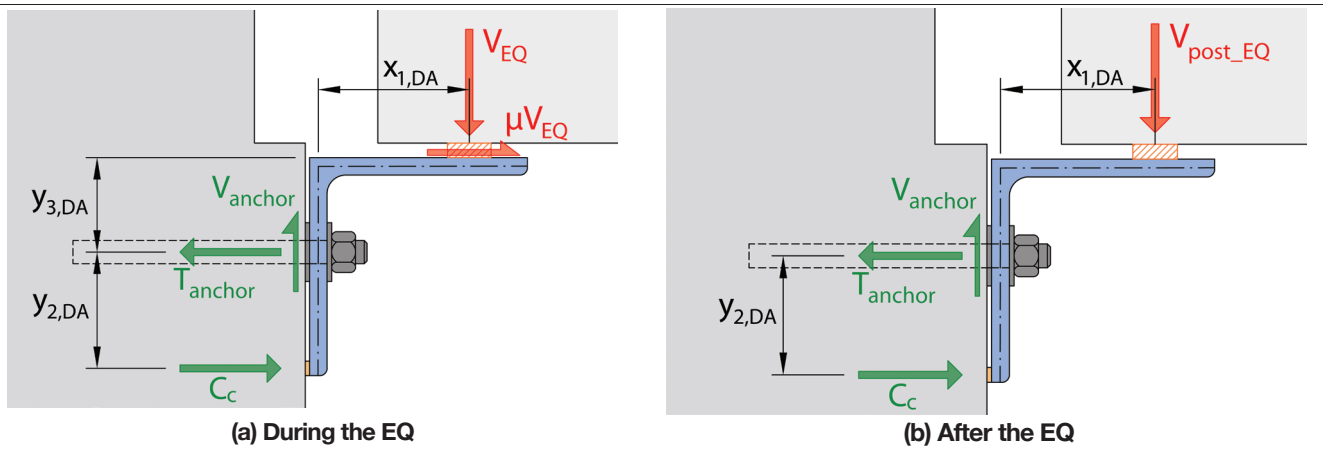

(a) During the EQ (b) After the EQ

Figure 12: Forces in the post-installed anchors for the dropped-angle approach

The dropped-angle approach can be used in conjunction with the cable catch system tested in the recent super-assembly experiment at the University of Canterbury (Büker et al. 2021). When designing the seating angles to be used with the cable catch retrofit, stiffeners can be welded to the angles that act as fixing points for the cables. Due to the presence of these stiffeners, the capacity-design approach is not applicable. Nevertheless, demands on the anchors are likely governed by the tension forces generated in the cable when the floor drops onto the cable catches.

5 DETAILING AND LIMITATIONS OF SEATING ANGLES

Regardless of which seating angle design procedure is being followed, appropriate detailing is essential to ensure the seating angle performs appropriately. A list of detailing recommendations can be found below, with many of these recommendations also being applicable to other precast floor retrofits.

- A rigid connection between the seating angle and the hollow-core unit must be avoided to allow the flooring unit to slide freely on the seating retrofit and accommodate relative movement between the unit and the supporting beam.
- Holes in the seating angle provided for the post-installed anchors should be slotted parallel to the longitudinal axis of the angle. The reasoning for this recommendation is twofold. Slotted holes firstly make it easier to avoid drilling through existing beam reinforcement during anchor installation and secondly provide an allowance for relative movements between the anchors and the seating angle that are caused by flexural deformations and elongation of the support beam. To ensure sufficient nut-bearing along the slotted holes, wide and thick square washers should be used. A washer thickness of at least 5 mm is recommended.
- Chemical epoxy anchors are generally the default anchor solution for seating angles. Where feasible, more robustness in terms of anchorage can be achieved by drilling through the support member and anchoring the threaded rod on the other side of the support. This solution can be particularly appealing for internal support beams where the floors supported on each side require a seating extension retrofit. Note that this method still requires the filling of the hole with (optionally lower grade) epoxy or similar to stabilise the bar in the hole.
- Caution is needed when using anchors in regions where cracking is anticipated. Figure 13 indicates the following recommendations for the typical case of plastic hinges adjacent to columns (adjustments needed for gravity-dominated frames experiencing non-reversing plastic hinges within the beam span):
  - Anchors installed within half the beam depth away from the column are expected to be impacted by substantial cracking and should not be relied on to resist shear and tension demands (Figure 13).
  - For epoxy anchors installed within one beam depth away from the column, the cover concrete should not be relied on and should be discounted from the effective embedment depth.
- The seating angle should ideally cover all the webs, but this may not always be practical. A minimum support length of 900 mm (supporting five webs for a 200 mm deep hollow-core unit) is recommended. If the seating angle does not cover all webs, the shear capacity of the reduced number of supported webs should be checked against the design loads specified in this paper. Furthermore, to prevent instability and unwanted torsion demands, the angle should always be placed in line with the centreline of the hollow-core unit.

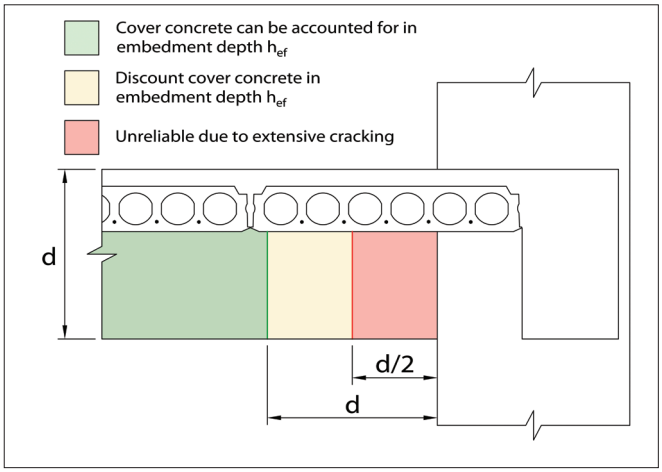

Figure 13: Anchorage in the plastic hinge region of the support beam

6 INFLUENCE OF THE SEATING ANGLE ON THE NEGATIVE MOMENT DEMANDS

With a seating angle installed hard up against the soffit of the hollow-core unit, the deformations of the seating angle during negative support rotations not only lead to large force demands in the post-installed anchors but also increased negative moment demands in the flooring unit itself. Parr et al. (2019) experimentally demonstrated that stiffened angles installed hard-up against the soffit are of particular concern and result in a significant increase in the negative moment demand, which can lead to NMF.

When designing the seating angle with the capacity-design approach, a certain degree of flexibility is assured through (1) the installation of bearing strips near the toes of the seating angle and (2) the incentive to limit the flexural strength and stiffness of the angle section to keep forces in the anchors low. In addition, the presence of the strips has the advantage that the location and upper limit of the force transferred into the floor by the seating angle can be determined with certainty. For seating angles installed without strips, both the location and the magnitude of the reaction at the top leg are challenging to determine, as elaborated in Section 1, and require additional research.

The increase in negative moment demand for capacity-designed seating angles may generally be low; nonetheless, a reassessment of the NMF vulnerability is necessary. Figure 14 demonstrates how to account for the additional negative moment demands induced on the floor. The moment demands in the flooring unit at the location of the bearing strip on the top leg of the angle can be determined as follows:

$$M_{o,angle\_tip} = M_{o,floor} + V_{end}\, x_{2,CD} - \frac{\omega x_{2,CD}^2}{2} \qquad (20)$$

where $M_{o,floor}$ is the overstrength moment at the back face of the hollow-core unit as defined for the NMF assessment in the assessment guidelines C5 (MBIE et al. 2018), V_{end} is the shear force at the back face of the hollow-core unit, which can be determined by solving the moment equilibrium about the opposite floor support, $x_{2,CD}$ is the distance from the back face of the hollow-core unit to the centre of the bearing strip at the top leg of the seating angle and ω is the gravity demand due to the un-factored self-weight (1.0G).

Parr et al. (2019) also showed that a potential increased NMF vulnerability can be counteracted by increasing the negative moment resistance through post-installing rebars into the topping concrete. Alternatively, to avoid the effect of increased negative moment demands, the dropped-angle approach can be used.

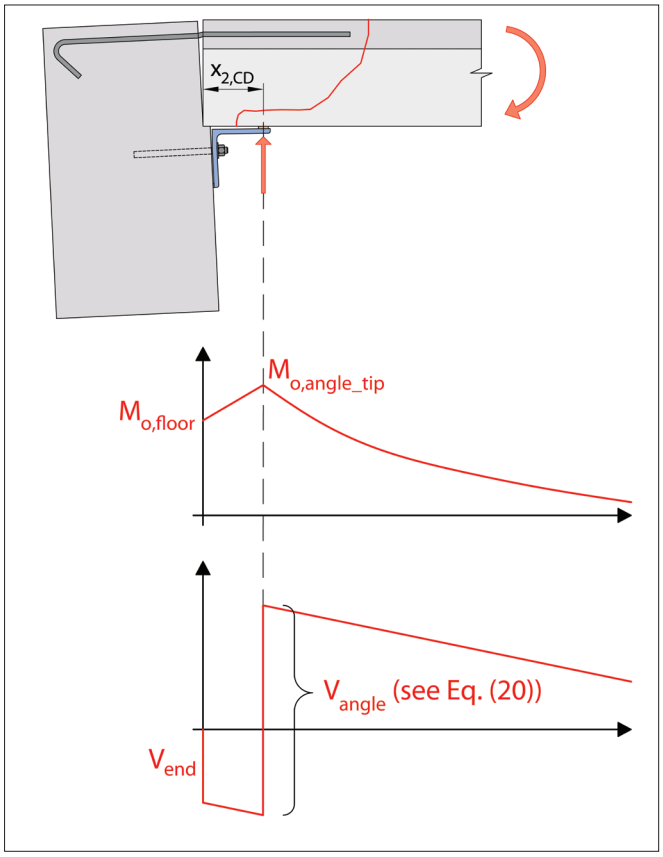

Figure 14: The influence of a seating angle on the negative moment demands.

7 CONCLUSIONS

Seating angles are a widely used retrofit solution to protect hollow-core floors against unseating during earthquakes. In this paper, concerns are raised about the appropriateness of the common design and detailing approach for seating angles, such as the uncertainty of the post-installed anchor demands generated by earthquake-imposed deformations.

Two design approaches for seating angles that aim to address these concerns are outlined in this paper. The first solution referred to as the 'capacity-design' approach, allows the seating angle to be installed hard-up against the soffit of the floor. A capacity-design philosophy is adopted to protect the post-installed anchors from being overloaded. The second solution, referred to as the 'dropped-angle' approach, avoids high anchor demands during negative support rotation by installing the seating angle with a gap to the hollow-core floor soffit and adding a deformable infill strip of rubber or similar material.

Both solutions are viable design approaches, but the capacity-design approach is the preferred option because it ensures that the diaphragm remains on the same level

and reduces the likelihood of delamination or web splitting. Also, a determinate and desirable hierarchy of failure is achieved using the 'capacity-design' approach. When designing the angle using the dropped-angle approach, it needs to be anticipated that a small drop of the floor could be sustained, with the potential consequence of promoting topping delamination and web-cracking.

8 ACKNOWLEDGEMENT

The authors would like to thank BRANZ, QuakeCORE, the Earthquake Commission (EQC) and Concrete NZ for providing the funding for the ReCast Floors project, from which these design recommendations were developed. The ReCast Floors team and the industry advisory group contributed with valuable feedback during the development of these recommendations. The Precast Floors Monitoring Group, chaired by Dave Brunsdon, also provided invaluable feedback which influenced the direction of these recommendations.

This project was (partially) supported by QuakeCoRE, a New Zealand Tertiary Education Commission-funded Centre. This is QuakeCoRE publication number 0737.

9 REFERENCES

Brooke, N. J., Büker, F., Bull, D. K., Elwood, K. J., Henry, R. S. and Hogan, L. S. 2022. "Overview of Retrofit Requirements and Techniques for Precast Concrete Floors." Journal of the Structural Engineering Society New Zealand, 35 (1).

Büker, F., Brooke, N. J., Elwood, K. J., Bull, D. K., Hogan, L. S. and Parr, M. 2021. "Development and Validation of Retrofit Techniques for Hollow-core Floors." Proceedings of the 2021 SESOC Conference, 14. Hamilton, New Zealand: Structural Engineering Society New Zealand.

Büker, F., Brooke, N. J., Hogan, L. S., Elwood, K. J., Bull, D. K. and Sullivan,T. J. 2022a. "Design Recommendations for Strongback Retrofits." Journal of the Structural Engineering Society New Zealand, 35 (1).

Büker, F., Parr, M., De Francesco, G., Hogan, L. S., Bull, D. K., Elwood, K. J., Liu, A. and Sullivan,T. J. 2022b. "Seismic Damage Observations of Precast Hollow-Core Floors from Two Full-Scale Super-Assembly Tests." Journal of the Structural Engineering Society New Zealand, 35 (1).

CEN (European Committee for Standardization). 2018. EN 1992-4: Eurocode 2 - Design of Concrete Structures - Part 4: Design of Fastenings for Use in Concrete. Brussels, Belgium: CEN.

Corney, S. R., Elwood, K. J., Henry, R. S. and Nims, D. K. 2018. Assessment of Existing Concrete Buildings in Wellington with Precast Floors. Kaikoura Earthquake Research Programme (2017-18). Lower Hutt, New Zealand: Natural Hazards Research Platform.

Fenwick, R., Bull, D. K. and Gardiner, D. 2010. Assessment of Hollow-Core Floors for Seismic Performance (Research Report 2010-02). University of Canterbury, Christchurch, New Zealand (https://ir.canterbury.ac.nz/handle/10092/4211).

Jensen, J. 2006. "The Seismic Behaviour of Existing Hollowcore Seating Connections Pre and Post Retrofitted." ME Thesis. University of Canterbury, Christchurch, New Zealand.

Liew, H. Y. 2004. "Performance of Hollow-core Floor Seating Connection Details." ME Thesis. University of Canterbury, Christchurch, New Zealand.

Matthews, J. 2003. "Hollowcore Floor Slab Performance Following a Severe Earthquake." PhD Thesis. University of Canterbury, Christchurch, New Zealand.

MBIE, EQC, NZSEE, SESOC, and NZGS. 2018. Technical Proposal to Revise the Engineering Assessment Guidelines - Part C5 Concrete Buildings. Wellington, New Zealand: Ministry of Business, Innovation, and Employment.

Parr, M., Elwood, K. J., Bull, D. K., Büker, F., Hogan, L. S., Puranam, A. Y., Henry, R. S. and Brooke, N. J. 2019. "Development and Testing of Retrofit Solutions for Hollow-core Floors in Existing Buildings." Proceedings of the 2019 Concrete New Zealand Conference, 12. Dunedin, New Zealand.

PCFOG. 2009. Seismic Performance of Hollow Core Floor Systems - Guidelines for Design Assessment and Retrofit (Preliminary Draft). Precast Concrete Floors Overview Group (SESOC, NZSEE, and NZCS), Wellington, New Zealand. http://www.nzsee.org.nz/db/PUBS/HollowCoreFloorSystems.pdf.

Puranam, A. Y., Corney, S. R., Elwood, K. J., Henry, R. S. and Bull, D. K. 2021. "Seismic Performance of Precast Hollow-Core Floors: Part 2 - Assessment of Existing Buildings." ACI Structural Journal, 118 (5): 65–77. https://doi.org/10.14359/51732822.

SNZ. 2004a. Amendment 3 to the Concrete Structures Standard. NZS 3101:1995-A3. Wellington, New Zealand: SNZ.

SNZ. 2004b. Concrete Construction (Incorporating Amendment No. 1 and No. 2). NZS 3109:1997. Wellington, New Zealand: SNZ.

SNZ. 2007. Steel Structures Standard (Incorporating Amendment No. 1 and Amendment No. 2). NZS 3404:1997. Wellington, New Zealand: SNZ.

SNZ. 2011. Structural Design Actions. Part 0: General Principles (Incorporating Amendments Nos 1,2,3,4 and 5). NZS1170.0:2002. Wellington, New Zealand: SNZ.

SNZ. 2017. Concrete Structures Standard (Incorporating Amendment No. 1,2 and 3). NZS 3101:2006. Wellington, New Zealand: SNZ.

Woods, L. J. 2008. "The Significance of Negative Bending Moments in the Seismic Performance of Hollow-Core Flooring." ME Thesis. University of Canterbury, Christchurch, New Zealand, 294p.

ISSN No. 2744-7871

DESIGN RECOMMENDATIONS FOR STRONGBACK RETROFITS

Büker, F.[1,*], Brooke, N.J.[2], Hogan, L.S.[3], Elwood, K.J.[4], Bull, D.K.[5], Sullivan, T.J.[6]

ABSTRACT

Since the early 2000s, it has been widely recognised that existing hollow-core floors can pose a threat to life during earthquakes, but only limited and mostly unvalidated guidance on how to retrofit the many existing hollow-core floors in New Zealand has since been provided. The lack of retrofit validation was emphasised by recent experimental findings showing that seating angles do not necessarily address positive moment failure within the precast floor unit, as has commonly been assumed.

A new retrofit solution referred to as 'strongback' retrofit has been developed and experimentally validated. The strongback retrofit consists of short steel beams running longitudinally underneath the hollow-core unit combined with a supplementary support. When the floor loses its gravity load-carrying capacity, the strongback retrofit can provide a robust alternative load path. Thereby, the strongback retrofit can address the majority of known hollow-core floor failure modes, including positive moment failure proximate to the support.

This paper provides design recommendations for the new strongback retrofit and describes the key performance observations from the validation test. The paper also discusses in what situations the strongback retrofit should be used.

1 BACKGROUND

Precast hollow-core floors were a widely used flooring solution in New Zealand, particularly during the 1980s to 2000s. However, the 1994 Northridge Earthquake and the 2016 Kaikoura earthquake (Henry et al. 2017) exposed critical vulnerabilities of these floors under seismic demands. Guidance for assessing the drift capacity of various failure modes is provided by Fenwick et al. (2010) and the Technical proposal to revise Section C5 (Concrete Buildings) of the "Guidelines for Detailed Seismic Assessment of Buildings" (MBIE et al. 2018). The assessment guidelines distinguish between three primary failure modes, namely loss of support (LOS), negative moment failure (NMF) and positive moment failure (PMF).

While there is well-considered guidance for the assessment of hollow-core floors available, only limited guidance has been provided on retrofit solutions for the many existing poorly detailed hollow-core floors in New Zealand. To date, the most commonly used retrofit has been supplementary seating retrofits placed under the soffit of the floor unit and bolted to the face of the supporting beam. The primary intent of this retrofit has been to address failure due to LOS, but it has also been widely assumed to address PMF. However, the success of a supplemental seating retrofit in addressing PMF depends on two conditions. Firstly, the positive moment crack needs to form close to the beam face, and secondly, the crack needs to be steep so that the broken end of the floor still has sufficient shear capacity to transfer the gravity loads into the seating angle. The PMFs observed in early hollow-core floor tests (Bull and Matthews 2003; Matthews 2003) fulfilled these two conditions, as shown in Figure 1. As a result, it was commonly assumed that supplemental seating retrofits can address PMF.

Figure: 1 Steep positive moment crack along the ledge of the seating resulted in floor collapse (Bull and Matthews 2003)

PAPER CLASS & TYPE: GENERAL REFEREED

1 PhD Candidate, University of Auckland
2 Managing Director, Compusoft Engineering Limited
3 Lecturer, University of Auckland
4 Professor, University of Auckland
5 Technical Director, Holmes Consulting
6 Professor, University of Canterbury
** frank.bueker@auckland.ac.nz*

(a) Transverse soffit cracking away from the support and seating angle (Henry et al. 2017)

(b) Internal cracking at a shallow angle (Büker et al. 2021)

Figure 2: Cracking in hollow-core floors

Despite the early indications that supplemental seating retrofits could mitigate the risk of collapse due to PMF, evidence from the 2016 Kaikoura earthquake (Henry et al. 2017) demonstrated that positive moment soffit cracks can form up to ~400 mm away from the support (e.g. Figure 2a), making the typical supplemental seating retrofit ineffective if damage progresses at this location. In addition, recent testing (Büker et al. 2021, 2022b) showed that the slope of the web cracks that extend from the positive moment soffit crack could, in fact, be shallower (approx. 30 degrees, as shown in Figure 2b) than previously observed. In such cases, even if the positive moment crack forms close to the beam face, the remaining shallow concrete wedge seated on the angle cannot reliably support the weight of the floor (Büker et al. 2021). Currently, neither the slope of the web crack nor the location of the transverse soffit crack can be predicted reliably. As a result, seating angles need to be viewed as insufficient for PMF (SESOC et al. 2021).

A new retrofit solution has been developed that can address the uncertainty of both the location of the positive moment crack and the slope of the associated web crack. This new retrofit is referred to as a 'strongback' retrofit and can, in fact, address the majority of hollow-core floor failure modes. The effectiveness of the strongback retrofit was successfully demonstrated in a super-assembly test recently conducted at the University of Canterbury (Büker et al. 2021, 2022b).

Design and detailing recommendations for the strongback retrofit have been developed under consideration of the performance observation from the experiment. These recommendations are described in the subsequent sections of this paper.

2 STRONGBACK RETROFIT CONCEPT

The strongback retrofit is a versatile retrofit solution that addresses most hollow-core floor failure modes. It is notably effective for flooring units prone to PMF and NMF. The strongback technique can also be used to reinstate a reliable load path where existing damage, such as web or soffit cracking, compromises the capacity of the end region of a hollow-core unit.

Experimental validation of the strongback retrofit was conducted as part of a super-assembly test (Büker et al. 2021, 2022b), which is subsequently referred to as the 'validation test'. The performance of the strongback retrofit observed during the validation test is described at various relevant points in this paper. The drawings in this section generally reflect the retrofit detailing used in the validation test, but modifications to improve the detailing are incorporated in the drawings shown in the following sections.

The main components of the strongback retrofit, illustrated in Figure 3, are steel members running longitudinally underneath the hollow-core unit. These steel members are seated on a seating angle bolted to the support structure and, at the opposite end, fixed to the floor by post-installed anchors. Another point of contact is provided by a steel plate with screw anchors located at the desired position of a compression reaction.

The conceptual idea of the strongback retrofit is to provide an alternative load path if the floor loses its gravity load capacity. During the formation of an NMF in the floor unit, for instance, the shear capacity of the end of the hollow-core unit diminishes in a sudden, brittle fashion. The strongback retrofit prevents floor collapse by transferring the loads from the intact part of the floor beyond the failed section to the supporting beam via the seating angle.

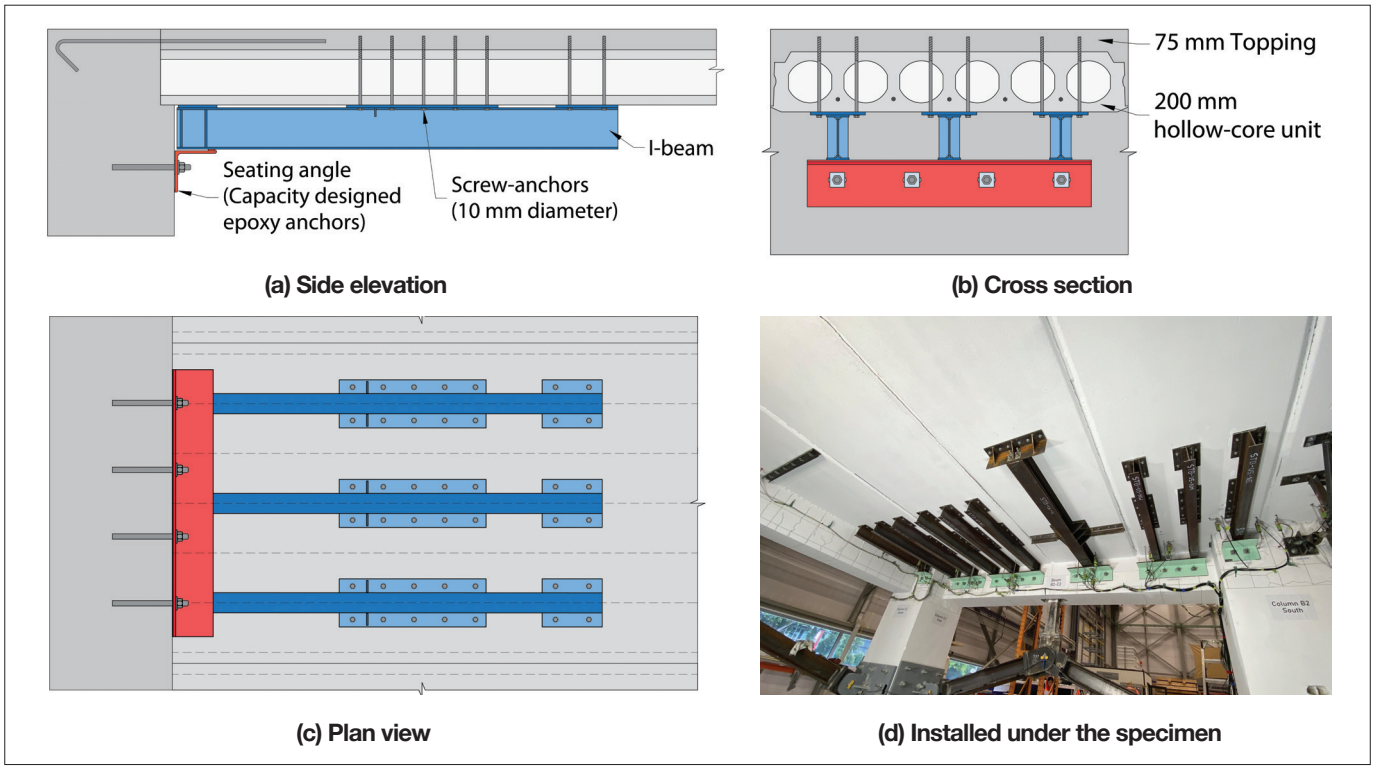

Figure 3: Strongback retrofit as used in the super-assembly test

This mechanism is demonstrated in Figure 4a, where the structurally unreliable part of the floor is shown as faded. Also indicated in this figure is the compression-tension force couple, which is required to resist the moment and shears generated by the transfer of forces from the hollow-core unit to the strongback. Similarly, this alternative load path can be utilised when a PMF occurs, as illustrated in Figure 4b.

In the validation test, the strongback retrofit was also installed under the hollow-core unit that spanned right next to the adjacent beam, which is commonly referred to as the 'alpha unit' (Brooke et al. 2022). An alpha unit undergoes incompatibility displacement demands with the adjoining beam deforming in double curvature while the alpha unit tries to remain straight. The relative displacement demands between the beam and the floor can lead to horizontal splitting of the hollow-core floor webs. When the web-splitting develops and propagates further under increased inter-storey drift demands, the bottom flange of the hollow-core unit may collapse (Matthews 2003). The strongback configuration tested in the validation test was able to restrain the web-splitting due to the presence of screw anchors. Despite the successful prevention of this failure mechanism in the validation test, it is important to recognise that the tested hollow-core units only spanned one bay. For an alpha unit spanning one bay, the largest deformation due to displacement incompatibility occurred towards the ends of the hollow-core unit, where the strongbacks with the screw-anchors were located. In cases where alpha units span two or more bays, large incompatibility displacements also develop close to the intermediate column, requiring additional retrofit measures (Büker et al. 2021).

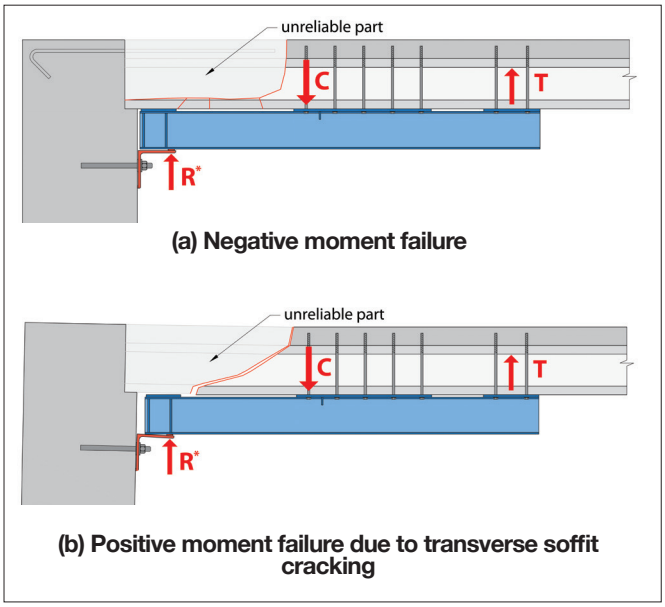

Figure 4: Alternative load paths for different failure mechanisms

The strongback retrofit's primary purpose is the assurance of life safety. It is crucial to acknowledge that, in common with other retrofit techniques for hollow-core floors, the strongback retrofit does not preclude floor damage (Büker et al. 2021). This fact should be communicated clearly to building owners. Notwithstanding, this retrofit is considered to provide a robust alternative load path, resulting in superior performance compared to many other hollow-core floor retrofits. Besides its overall versatility in addressing the potential failure mechanisms, the strongback solution offers many additional benefits, including:

1. Effectiveness at keeping the floor vertically at the same level as the support. This contrasts with most hollow-core floor retrofits that only engage once the floor unit sustains a considerable drop. The drop is likely to cause delamination of the topping concrete and potentially has detrimental effects on the diaphragm capacity and also compromises the functionality of the floor.
2. Improvements to the overall floor integrity through the presence of post-installed anchors. During the validation test, it was observed that web-cracking consistently terminated before the anchor rows. This positive effect can be attributed to the clamping action generated by tightening the anchors (see Section 3.5 for further elaboration).
3. Design of the strongbacks follows the principles of New Zealand Standards for the design of steel and concrete structures, meaning it should be straightforward to demonstrate compliance with the New Zealand building code,
4. Entire installation of the strongback retrofit can be conducted from the underside of the floor and thereby limits the impact on building operations, and
5. Ease of post-earthquake damage inspection due to the clearance between the seating angle and floor underside provided by the strongback steel beams. Critical damage, in contrast, may be missed when a seating angle installed hard up against the soffit hides this part of the floor.

While the strongback retrofit can significantly improve the life-safety performance of the floor, the material and installation costs are expected to be relatively high, particularly because the relocation of existing services may be required. Furthermore, the installation of the strongback members can be challenging, and attention should be paid to the member weight and how the parts will be lifted into place.

These disadvantages, particularly the cost aspect, draw into question whether the strongback retrofit is required for every hollow-core unit in a building. As discussed in Section 1, seating angles cannot sufficiently address PMF, but the strongback retrofit can do so (see Figure 4b) and has been recommended for this purpose by New Zealand's engineering societies (SESOC et al. 2021). To date, the strongback retrofit is the only experimentally validated retrofit that can dependably address PMF in hollow-core floors. Therefore, the strongback retrofit should at least be installed under hollow-core units for which the PMF drift capacity does not reach the %NBS target.

For cases where the PMF capacity reaches or exceeds the %NBS target, alternative retrofit solutions may be acceptable. For instance, hollow-core units that are only vulnerable to LOS can still sufficiently be retrofitted with just a supplemental seating retrofit (Büker et al. 2022a). Furthermore, hollow-core units that are prone to LOS and NMF (but not prone to PMF) can be retrofitted, for example, with a combination of a supplemental seating retrofit and floor strengthening with additional rebars post-installed in the concrete topping (Parr et al. 2019) as an alternative to the strongback retrofit.

Design and detailing of the strongbacks and their support angle can be challenging for 'alpha units'. Alternative retrofits for alpha units, such as 'catch beams', can be found in the companion paper by Brooke et al. (2022).

In the next section, comprehensive design and detailing recommendations for strongback retrofit are provided.

3 DESIGN AND DETAILING RECOMMENDATIONS

As noted in the previous section, the design of strongbacks follows the principles encompassed by the New Zealand Standards for the design of steel and concrete structures. Further detail regarding a recommended approach to the design and detailing is outlined in this section. This recommended approach incorporates the experience gained during the design, construction, and testing of the super-assembly specimen used for the validation test.

The steps encompassed in the design and detailing approach comprise:

1. Selection of load combination.
2. Supplemental seating design.
3. Preliminary sizing of required backspan and number of supported webs.
4. Shear and bending moment design checks of the hollow-core floor.

5. Design of tension anchors and supplemental shear enhancement.
6. Design and detailing of the strongback members.
7. Other considerations.

A flowchart visualising the design procedure with comments on the key considerations for individual design steps is shown in Figure 5. More detailed elaborations of each design step can be found in the following sub-sections.

A site inspection should be conducted prior to designing the strongback retrofit. Aspects to look out for during the inspection are highlighted throughout this section. The inspection is not included as a separate design stage as it is envisaged it may well have been completed as part of an earlier assessment of the floor.

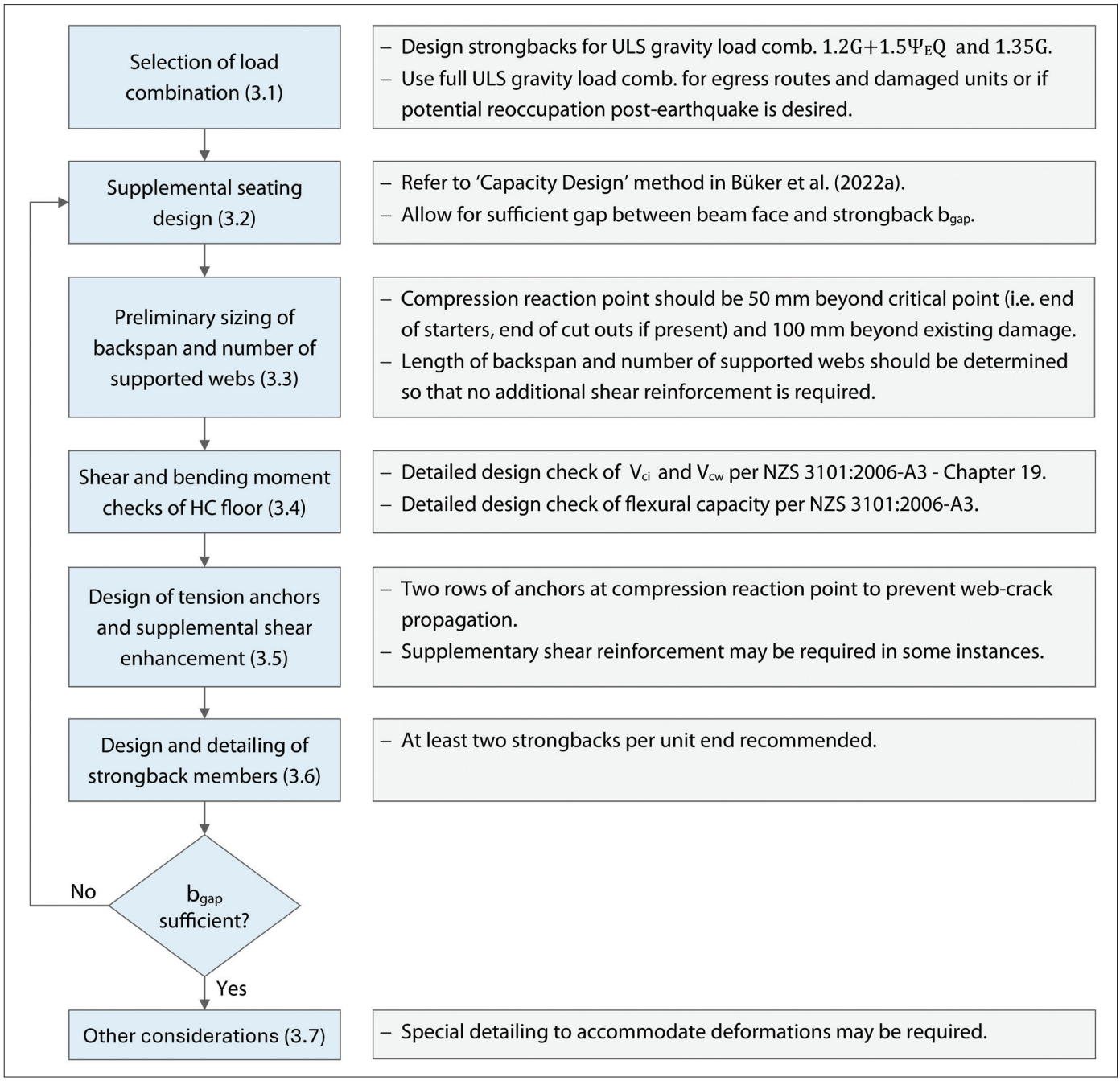

Figure 5: Flowchart outlining the recommended design and detailing procedure for the strongback retrofit. Numbers in brackets refer to section numbers that follow.

3.1 SELECTION OF LOAD COMBINATION

The first step of the design process is to select an appropriate load combination. The design of the strongback retrofit needs to meet the ultimate limit state (ULS) requirements defined in the Structural Design Action Standard NZS1170.0:2002-A5 (SNZ 2011). Based on this standard, the retrofit needs to be able to sustain two gravity load combinations:

$$E_d = 1.35G \quad (1)$$

$$E_d = 1.2G + 1.5Q \quad (2)$$

where G is the permanent action ('dead' load) and Q is the imposed action ('live' load).

In a companion paper, Brooke et al. (2022) argue that it is unlikely that the full imposed action, Q, acts on the damaged flooring units during or after the earthquake (provided access is restricted). Therefore, the following load combination as defined by Brooke et al. may be used instead of Equation (2) for the design of floor retrofits:

$$E_d = 1.2G + 1.5\psi_E Q \quad (3)$$

where ψ_E is the combination factor for earthquake action and all other parameters have been defined previously.

Before designing the strongback retrofit with Equation (3), the following factors should be considered:

- Strongback retrofits for hollow-core units that are part of an egress route should be designed for the full ULS gravity load (Equations (1) and (2)) because the gravity demands on such units may likely see high live loads during the evacuation in an earthquake event.
- It is crucial to recognise that the building will not be able to be re-occupied following an earthquake if the hollow-core units are supported by strongbacks designed with Equation (3). This constraint needs to be communicated clearly to building owners and tenants.
- In cases where a hollow-core unit shows existing damage that may impair the gravity load-carrying capacity (i.e. diagonal web-cracking), it is advisable to design the strongback retrofit (or any other retrofit) to support the full ULS gravity load (Equations (1) and (2)) for continued occupancy.

Refer to the companion paper by Brooke et al. (2022) for further discussion in regards to the selection of appropriate load combinations for the design of floor retrofits.

Once the appropriate design load combination is identified, the support reaction, R^*, can be determined.

3.2 SUPPLEMENTAL SEATING DESIGN

After choosing an appropriate load combination, the supplemental seating can be designed. It is recommended to follow the capacity-design approach[1] described in the seating angle design recommendations (Büker et al. 2022a).

The capacity design approach is generally applicable when used in conjunction with the strongback retrofit, but the seating length calculation requires special consideration in this case.

With the strongback being the point of contact to the seating angle, the additionally provided retrofitted seating length, $\delta_{s,ret}$, should be measured relative to the end of the strongback steel member as indicated in Figure 6. The seating movement demand, δ_s^*, may then be calculated as the sum of movement due to beam elongation and relative rotation at the height of the seating angle top flange based on the recommendations by Büker et al. (2022a). The demands on the seating must not exceed the available retrofitted seating:

$$\delta_s^* \leq \delta_{s,ret} \quad (4)$$

As indicated in Figure 6, a gap, b_{gap}, between the support structure and strongback retrofit is required to allow for movements due to relative rotations between the floor and the support beam. If the size of the gap is insufficient, the strongback may come into contact with the support beam, resulting in relative movements between the strongback and the floor. These relative movements can have the potential to shear off the heads of the post-installed vertical strongback anchors. This critical damage is of particular concern where large relative rotation demands between

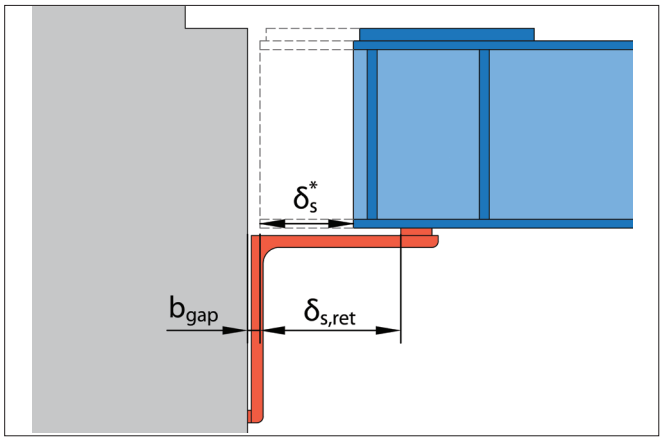

Figure 6: Seating conditions when using the seating angle with the strongback retrofit

[1] If using the capacity-design approach is impractical, the dropped-angle design approach as defined in the companion paper by Büker et al. (2022a) may be used as an alternative.

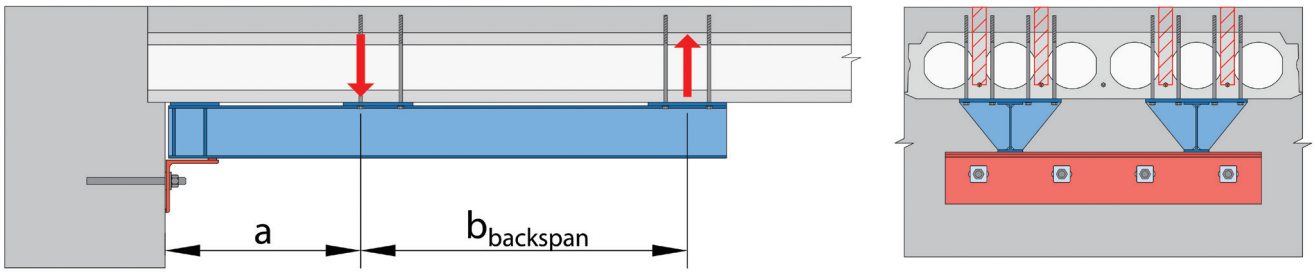

(a) Side elevation of strongback with key dimensions

(b) Cross section showing the engaged number of webs (marked with diagonal hatch pattern)

Figure 7: Key dimensions and design parameters for the strongback retrofit

the floor and support without the displacements due to elongation are possible. Without knowing the exact depth of the strongback retrofit, the gap size cannot be determined at this stage.

Therefore, a 15 mm gap may be assumed, which will need to be reviewed once the strongback depth is confirmed (refer to Section 3.6). To ensure the gap is implemented as specified, a block of low-density polystyrene or similar compressible material can be placed between the strongback and the face of the support beam during the installation.

If desirable for practical reasons, the total depth of the retrofit installation could be minimised by installing the seating angle upside down.

3.3 PRELIMINARY SIZING OF REQUIRED BACKSPAN AND NUMBER OF WEBS

A key design consideration for the strongback retrofit is to determine a configuration of strongbacks that ensures sufficient shear capacity of the hollow-core webs within the backspan, $b_{backspan}$, which is the region between the tension reaction, T, and compression reactions, C, as indicated in Figure 7a. Along the backspan, the shear demand on the webs is increased due to the transfer of forces out of the hollow-core unit and into the strongback. In addition, the number of engaged hollow-core webs, n, that can be relied upon for the shear capacity is reduced. As indicated in Figure 7b, only the webs supported by the strongback at the compression point, C, can be considered for the shear capacity. The figure also demonstrates that it is possible to support several webs with one strongback by adding outriggers at the compression point and tension point.

The distance between the beam face and the compression point (designated as distance "a"), depends on a number of factors, such as the floor dimensions, critical failure modes and potential existing damage. The following guidance is provided in the selection of distance a:

$$a \geq \max \begin{cases} 1.5\ h_{floor} & \\ l_{starters} + 50\ \text{mm} & \text{when NMF is possible,} \\ l_{cutout} + 50\ \text{mm} & \text{when the unit has cut-outs,} \\ l_{damage} + 100\ \text{mm} & \text{when there is pre-existing damage.} \end{cases} \quad (5)$$

where h_{floor} is the depth of the floor including the topping, $l_{starters}$ is the extension of the starter bars into the topping beyond the beam face, l_{cutout} is the length beyond the beam face of any cut-outs at the unit end (e.g. to accommodate a column) and l_{damage} is the distance from the beam face to the furthest point of existing external and internal damage in the unit. Note that all distances a and l are measured from the beam face.

Following the determination of distance a, the required backspan, $b_{backspan}$, and the number of webs engaged by the strongbacks, n, can be determined. Governing factors for the determination of these values are typically the web-shear capacity and the flexural-shear capacity as defined in Section 19 of NZS3101:2006-A3 (SNZ 2017). Further guidance on the determination of these shear capacities is provided in the subsequent Section 3.4.

An estimate for the required backspan length, $b_{backspan}$, based on distance a and the number of engaged webs, n, can be obtained from the preliminary design charts shown in Figure 8. These graphs were generated based on the shears and moments that can be withstood by the hollow-core floor without the installation of supplemental shear reinforcement. The applicability of these charts is limited to Equation (1) and the post-earthquake retrofit load combination (Equation (3)) with uniformly distributed live loads of 3 kPa for office use in accordance with NZS1170.1:2002-A2 (SNZ 2009). While these preliminary design charts may be useful for the initial sizing, the charts should not be used as a substitute for the detailed design checks described in the subsequent sections.

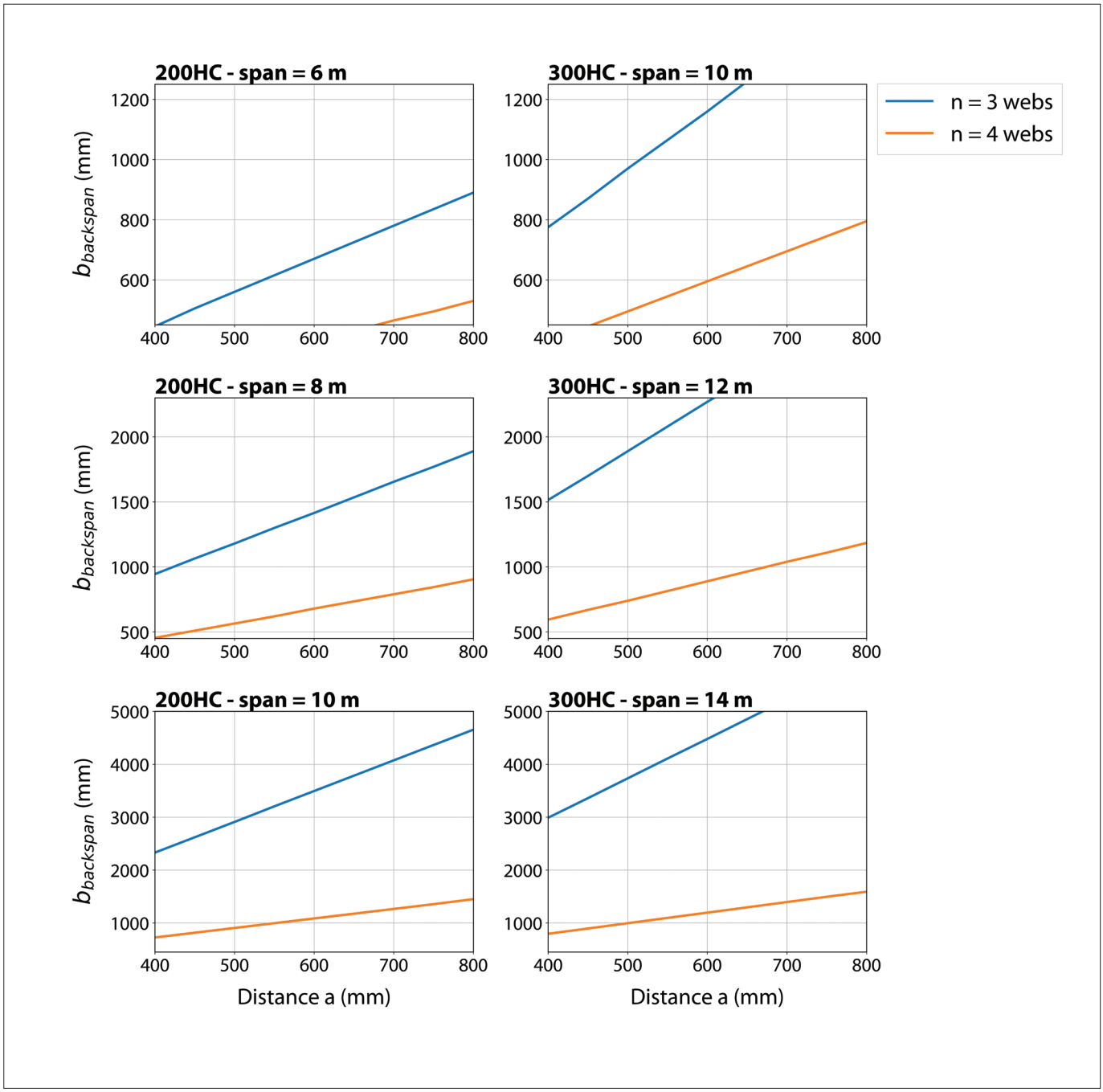

Figure 8: Preliminary design charts to determine the backspan length, $b_{backspan}$, and the number of engaged webs, n assuming no additional shear reinforcement (Not to be used for detailed design)

As a conservative assumption, distance a is defined as the distance from the beam face to the location of the compression reaction, C. This assumption is based on the possibility of the front end of the strongback coming into contact with the supplemental seating retrofit. This scenario has been observed at large lateral drifts in excess of 3% in the validation test and is further discussed in Section 3.6 and shown in Figure 14. A less conservative assumption for distance a may be warranted if contact between the front end of the strongback and the angle can be avoided, i.e. a sufficiently deep strip of steel is installed at the tip of the seating angle or supplemental seating alternative. If it can be demonstrated that this contact is prevented, the distance between the support reaction and the compression reaction point may be refined to:

$$a_{refined} = a - b_{gap} - \delta_{s,ret} + \delta_s^* \qquad (6)$$

where a is calculated based on Equation (4) and all other parameters have been defined previously.

The value of $a_{refined}$ can replace distance a and used with the preliminary design charts.

3.4 SHEAR AND BENDING MOMENT DESIGN CHECKS OF THE HOLLOW-CORE FLOOR

After the preliminary sizing, detailed design checks of the shear and moment demand in the floor unit should be conducted. These design checks require careful consideration because (1) a reduced number of webs is being relied on to resist the shear demands and (2) the shear demands are increased compared to a simply supported undamaged floor because the compression reaction C is the sum of the support reaction, R^*, and the tension reaction, T.

Earthquake damage is expected to concentrate between the support and the compression point (i.e. within span a). Consequently, the bond between prestressing strands and concrete along length a may be heavily impaired and, hence, unreliable. This implies that the transmission of the prestress now starts at the compression point (Figure 9b). The prestress transmission can be assumed as linear over the transfer length, L_t, as defined in NZS3101:2006-A3 (SNZ 2017). Taking this assumption into account, the shear capacity for both web-shear cracking, V_{cw}, and flexural-shear cracking, V_{ci}, as specified in Section 19 of NZS3101:2006-A3 (SNZ 2017), can be calculated. Only the selected number of engaged webs n should be considered when calculating the shear capacities (Figure 7b). An on-site inspection is required to determine the number of strands per unit and **specifically ensure that the webs engaged by the strongback retrofit contain strands.**

The concrete strength of existing hollow-core units has been found to be significantly greater than the specified 28-day strength, which is commonly specified as 45 MPa (Fenwick et al. 2010). Using this as a basis, it is appropriate to use the probable concrete strength, which can be determined by multiplying the specified 28-day concrete strength by 1.4 based on Section C5.4.2.2 in the Assessment Guidelines C5 (MBIE et al. 2018). For the determination of the shear capacity, NZS3101:2006-A3 (SNZ 2017) limits the concrete strength value to 50 MPa. Other standards (i.e. ACI318 (2019)) have higher concrete strength limits for the calculation of shear capacities and should be referred to when intending to utilise the full probable concrete strength for the shear design. If this approach is adopted, it should be noted that this would be considered an "Alternative Solution" because the other standards are not cited in the NZ Building Code B1/VM1 (MBIE 2019).

Furthermore, the flexural capacity according to NZS3101:2006-A3 (SNZ 2017) needs to be checked against the flexural demands along the backspan, $b_{backspan}$, and the rest of the floor. When calculating the flexural capacity of the floor, it is important to recognise the relocated development length location of the strands as outlined above.

The shear and bending moment distributions should be plotted along the length of backspan, $b_{backspan}$, as shown in the conceptual example in Figure 9. If it is found that the shear or bending demands exceed the capacity along the length of the floor, the assumed backspan, $b_{backspan}$, and number of engaged webs, n, can be increased or, alternatively, the shear capacity can be enhanced with supplemental shear reinforcement as discussed in the subsequent section.

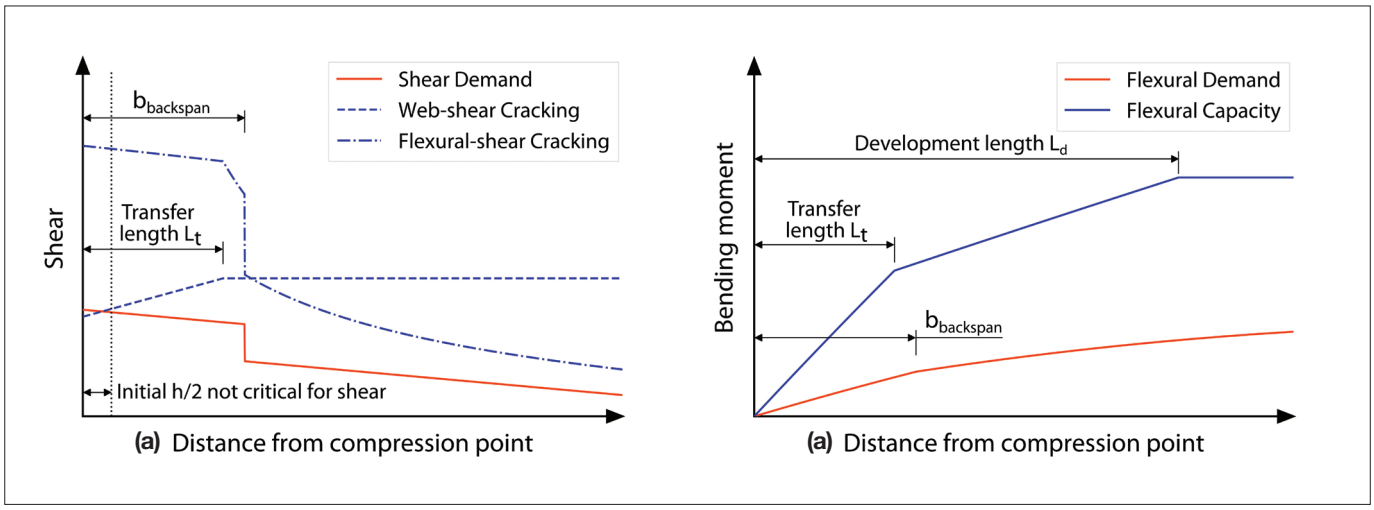

Figure 9: Example of shear and bending moment distribution plotted from the compression point towards mid-span of the floor

3.5 DESIGN OF TENSION ANCHORS AND SUPPLEMENTAL SHEAR ENHANCEMENT

Vertical anchors between the strongbacks and the hollow-core floor are an essential part of the strongback retrofit technique. The anchors have three critical functions, namely:

- Transfer of the tension force, T, from the far end of the strongback into the floor,
- Supplemental shear reinforcement, and
- Clamping action at the compression point.

The need for a tension load path at the far end of the strongback and the potential need for supplemental shear reinforcement is self-evident. The importance of the clamping action provided at the compression point is not as intuitively crucial; however, experimental evidence from previous studies highlights the importance of such a clamping mechanism to be present for the strongback retrofit. A number of studies have investigated the NMF mechanisms in hollow-core floors (Büker (In Preparation); Liew 2004; Parr et al. 2019; Woods 2008). As illustrated in Figure 10, the negative moment crack would typically propagate vertically through the webs, then branch horizontally in both directions – towards the support and towards the mid-span of the floor. Such horizontal web cracks would critically impair the shear resistance along the backspan, potentially resulting in a brittle shear failure.

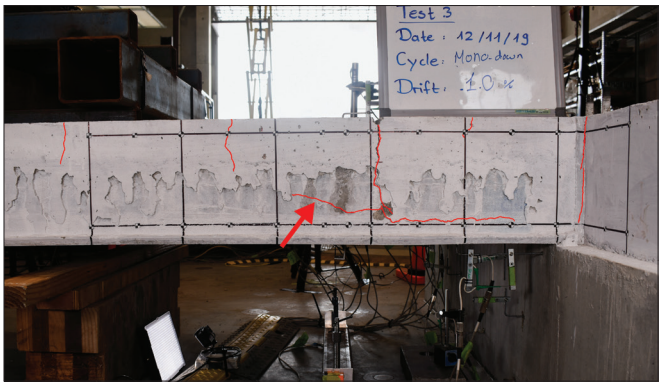

Figure 10: Side view of a hollow-core floor with a negative moment crack (marked in red) that propagates through the webs and branches horizontally towards and away from the support. ***(Photo taken at -1.0% inter-storey drift) (Büker 2022)***

Experimental observations from the validation test indicate that the clamping forces generated by the screw-anchors that were installed at the compression point effectively prevented the propagation of internal floor damage (i.e. web-cracking) beyond this point.

In the validation test, one of the hollow-core units sustained structurally non-critical damage to the unreinforced outer web when the specimen was loaded to 4% inter-storey drift. During subsequent loading to 5% inter-storey drift, parts of this outer web collapsed and thereby exposed the interior of the cell, which is illustrated in Figure 11. To the right of the compression point, C, a large web-crack caused by NMF can be seen branching from the top of the floor towards the support. No web-cracking was observed to propagate in the opposite direction beyond the vertical anchors, which provided the clamping action. This observation was not limited to the hollow-core unit illustrated in Figure 11 but was a consistent finding for all hollow-core units in the validation test.

Figure 11: Strongback retrofit carrying the load of the floor after a negative moment failure has occurred.
(Photo taken at 5% inter-storey drift)

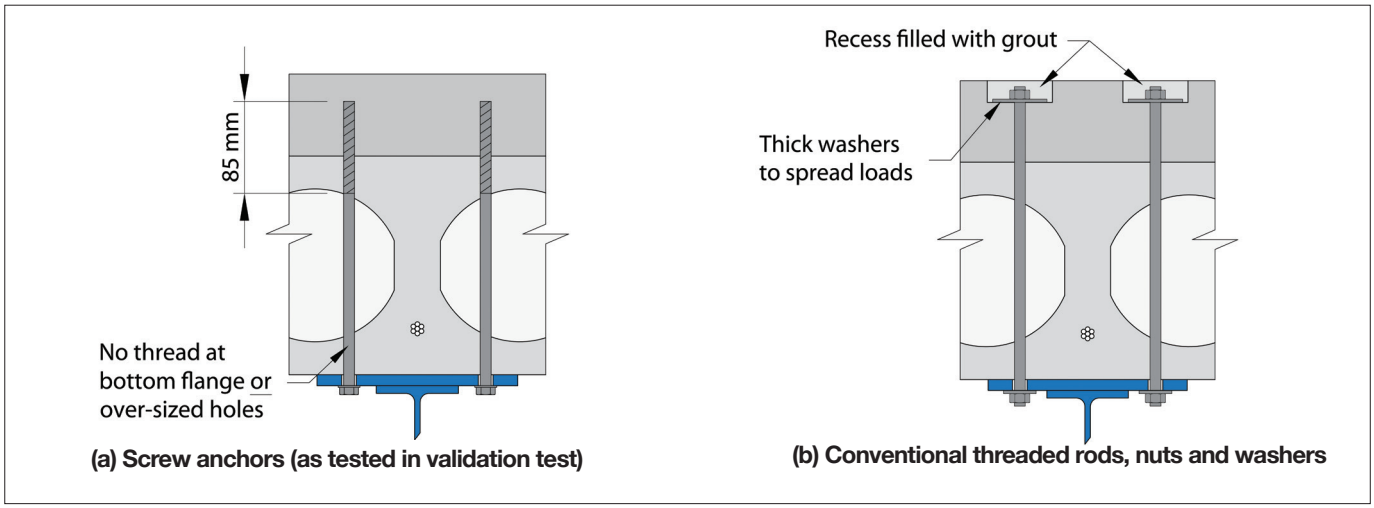

Figure 12: Example of different anchor solutions

To provide the clamping action, two rows of screw anchors with a diameter of 10 mm should be installed along each engaged web at the compression point (i.e. four anchors per engaged web). These anchors should be snug tight so that some degree of vertical pretension on the webs is provided. For the validation test, the screw-anchor product *fischer UltraCut FBSII-10x260* was used. If a different anchor solution or diameter is selected, it is recommended to determine the required number of anchors at the compression point based on the condition that the modified anchor configuration should provide an equivalent or greater stiffness per engaged web compared to four of the 10 mm screw-anchors used in the validation test. These four screw-anchors provided a stiffness of 0.36 kN/m over their unbonded length. No less than one row of anchors (i.e. one anchor on each side of an engaged web) should be installed at the compression.

If the shear capacity of the precast unit within the backspan is insufficient, supplemental shear reinforcement can be provided to ensure sufficient shear capacity. This can be achieved by installing additional anchor rows along the engaged webs. The arrangement of the supplemental anchors should satisfy shear reinforcement spacing provisions in NZS3101:2006-A3 (SNZ 2017).

In the validation test, five rows of anchors per engaged web were installed starting from the compression over a portion of the strongback's backspan (see Figure 11). The first two anchor rows had the main purpose of providing the clamping action that restrains cracking of the webs and contributes to the shear capacity. An additional three anchor rows were found to be required as supplemental shear reinforcement to enhance the shear capacity along this part of the backspan. While the anchors that provide the clamping action are always required, the number of additional supplemental shear anchors can be reduced or completely omitted by increasing the backspan length, $b_{backspan}$, or increasing the number of engaged webs, n.

If the strongback retrofit is intended to address web-splitting due to incompatibility displacement in alpha units, the anchor configuration should be similar to what was tested in the validation test (Figure 3) unless it can be shown that a detailing variation can successfully address this failure mechanism.

All post-installed anchors should be designed in accordance with EN 1992-4 (CEN 2018) (superseded EOTA TR045, which is referenced in NZS3101:2006-A3 – Cl. 17.5.5 (SNZ 2017)). The selected screw anchor product for the validation test had a partial thread that was embedded into the topping concrete and top flange of the unit, as shown in Figure 12a. The screw-anchors were located close to the webs to achieve a sufficient embedment in the curved portion of the cell and allow for a direct load transfer of the clamping force from the anchors to the webs.

Using screw-anchors has the benefit that the installation of the strongback retrofit only requires access to the floor underside. Nevertheless, some additional design and detailing considerations should be taken into account when using screw anchors. Firstly, it is important that screw-anchors only anchor into the top part of the floor in view of the fact that anchoring into the bottom flange may promote web-cracking. For screw-anchor solutions with a full-length thread, oversizing the holes in the bottom flange of the hollow-core unit can prevent this detrimental effect. Secondly, the validation test showed

that screw-anchors with a larger diameter (i.e. 10 mm or greater) generally provide more redundancy when crossed by cracks such as longitudinal splits. When short screw-anchors with a diameter of 6 mm were tested, it was found that longitudinal splits in the topping and top flanges of the hollow-core units significantly impaired their load capacity. As a result, some of the 6 mm diameter screw-anchors loosened to the extent that a few of the anchors fell out of the floor. Therefore, it is recommended to use larger diameter screw-anchors, which may lead to a low demand-capacity ratio.

As an alternative to using screw anchors, it may be more desirable to drill through the entire floor depth and use conventional threaded bars, nuts and washers as anchor solution. At the top, the washers and nuts can be recessed into the topping and the remaining pocket filled with high-strength grout, as depicted in the detailing example in Figure 12b. This anchor solution was conceptually tested by Jensen (2006). The experimental work by Jensen also showed that the holes should be drilled from the underside because drilling from the top can result in large concrete cone breakouts in the bottom flange of the hollow-core unit. Sizing of these conventional products should be conducted following recognised procedures.

While there may be other suitable anchor solution alternatives, the use of expanding anchors is discouraged as this type of anchor may promote longitudinal splitting or other cracking to form through the anchor lines due to the induced transverse tensile stresses from the anchor expansion.

Irrespective of the method used to post-install anchors and transverse reinforcement, it is critical that care be taken to avoid damage to the prestressing strands in the hollow-core units.

3.6 DESIGN AND DETAILING OF THE STRONGBACK MEMBERS

The strongback steel beams can be designed to resist the imposed demands, allowing for flexibility in the detailing. I-sections are generally preferred over hollow sections for the steel beams because I-sections have many benefits in terms of constructability. As shown in Figure 13, the I-beams in the validation test were set down by 10 mm from the soffit of the hollow-core unit with only three critical points of contact with the floor unit:

- A plate welded onto the top flange of the I-beam close to the support beam. If LOS occurs, a direct vertical load transfer from the unseated floor through the strongback into the seating angle can be established.
- A second point of contact is required where the compression force is designed to land. This contact point may be detailed with a flat plate that is fixed to the hollow-core unit by post-installed anchors. Ideally, this plate should not be rigidly connected to the I-beam so that relative sliding movements between the I-beam and the floor can be accommodated. In some cases, the plate at the compression point may need to be welded to the I-beam, for example, when a strongback is designed to support multiple webs. In order to prevent the anchor heads from getting sheared off due to the relative laminar shear sliding movements, the holes for the anchors need to have sufficient tolerances.
- The third point of contact is where the tension force needs to be transmitted between the floor and strongback. At the tension point, the holes for the anchors are also recommended to have sufficient tolerances for the aforementioned reasons.

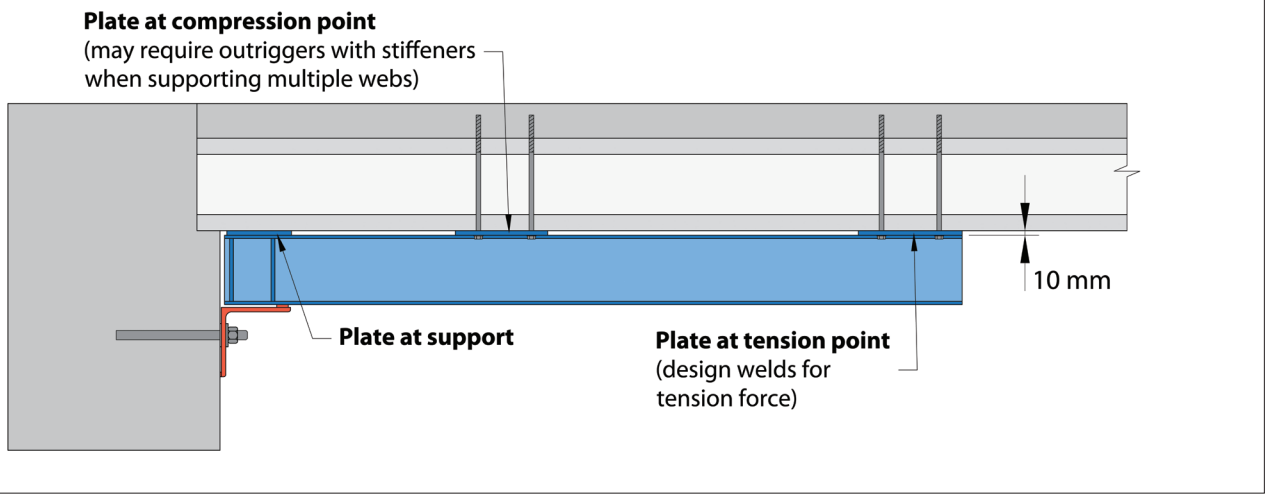

Figure 13: Typical strongback side elevation

Where a single strongback is intended to engage multiple webs, the flat plate at the compression point needs to be extended to the sides with vertical stiffeners that are welded to the flat plate and the I-beam. This arrangement forms wide outriggers that provide sufficient stiffness to support several webs (conceptually demonstrated in Figure 7b). When multiple webs are engaged by one strongback, the tension anchors at the far end of the strongback should be equally distributed to the engaged webs.

Although it may be possible to use a single strongback member per unit end and, in fact, has successfully been tested in the validation test, a minimum of two strongbacks per unit end is recommended to ensure torsional stability and to provide a degree of redundancy. This restriction is imposed due to the possibility of a longitudinal split forming directly above a single strongback. The longitudinal split could critically decrease the load-carrying mechanism of the strongback and may result in the collapse of the unit. Two or more strongbacks, in contrast, will provide the necessary redundancy.

The general design and detailing of the strongback members can be conducted utilising conventional steel design procedures and standards. Following these procedures, it can be found that the required section size of the steel beam is typically small. Consideration should also be given to the stiffness of the strongback elements in relation to the expected floor deflections. While no prescriptive criteria are suggested here, it is recommended to generally keep the deflections of the strongback low so that the diaphragm remains on the same level. The strongback and floor deflections should be assessed with the assumption that the unreliable part of the floor (refer to Figure 4) becomes completely ineffective. When sizing the steel members, it is important to ensure that the steel beam has sufficient capacity to withstand lateral-torsional buckling, particularly where distance a is of significant length. Furthermore, the potential of local buckling of the web of the strongback must be checked at (1) the compression point and, more importantly, (2) where the strongback is supported by the seating angle. It is crucial to recognise that the demand on the strongback webs at their front end is not limited to the support reaction, R^*. As discussed, in the seating angle design recommendations (Büker et al. 2022a), the compression reaction at the tip of the angle can grow as large as the force required to reach the overstrength moment of the seating angle. This higher force only needs to be considered for the local buckling check of the strongback webs at the steel strip of the supplemental seating retrofit. Note that the location of the force relative to the strongback shifts with increasing beam elongation demands.

During the validation test, it was observed that contact between the front tip of the strongback and the seating angle could occur at large inter-storey drifts (Figure 14). Due to the advanced floor damage at large inter-storey drifts, the floor-to-support connection will have softened significantly at this stage. On this basis, it can be assumed that the magnitude of this new reaction at the front end of the strongback is unlikely to significantly exceed the value of the support reaction, R^*. To ensure that the strongback remains undamaged in this critical location, it may be advisable to add stiffeners as a precautionary measure, as had been done for the tested strongbacks (see Figure 14). Alternatively, a sufficiently thick steel strip at the tip of the angle could be installed (refer to Section 3.3 for further discussion).

Figure 14: Front end of strongback in contact with the seating angle (first observed at 3% inter-storey drift).

Once the steel member dimensions are confirmed, the assumed required width of the gap between the support beam and strongback, b_{gap}, should be revisited. Knowing the depth of the strongback member, the required gap can be calculated as follows:

$$b_{gap} = h_{stb}\,\theta_{MCE} + 5 \text{ mm} \geq 15 \text{ mm} \qquad (7)$$

where h_{stb} is the depth of the strongback and θ_{MCE} is the peak MCE inter-storey drift demand, which is defined as the peak ULS inter-storey drift demand multiplied by $1.5/S_p$ based on the provisions in NZS3101:2006-A3 (SNZ 2017). If the calculated required gap exceeds the previously assumed gap, the seating angle design needs to be revised with the updated larger gap size.

The above recommendations on strongback detailing are based on what successfully worked in the validation test. The authors recognise that detailing deviations may be required based on floor and site conditions, material choice, etc.

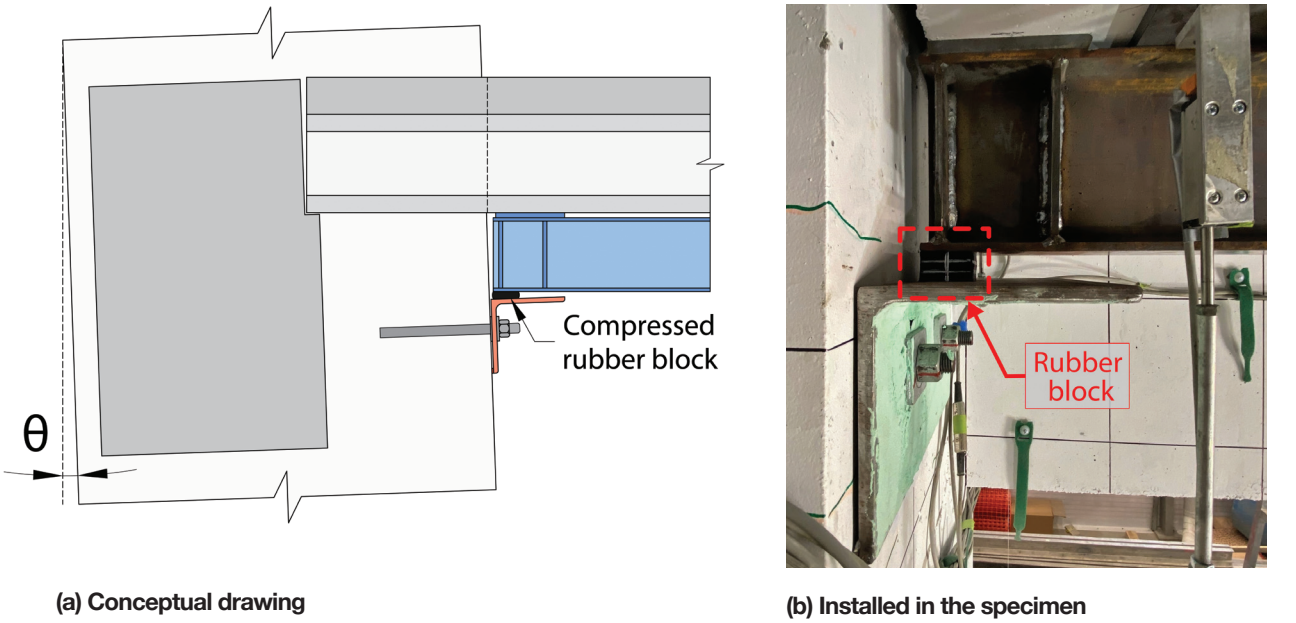

(a) Conceptual drawing

(b) Installed in the specimen

Figure 15: Rubber block detail used to accommodate relative vertical movements at the column face

3.7 OTHER CONSIDERATIONS

The preceding sections have dealt with the design approach required when strongback retrofits are considered for 'typical' hollow-core units. This section describes additional detailing considerations which may be required for specific floor support arrangements.

Detailing to accommodate displacement compatibility may require particular attention in the vicinity of the columns. The specimen for the validation test, for instance, required some of the floor units to have cut-outs allowing the columns to protrude into the floor. As a result, a number of strongbacks needed to be seated on a seating bracket attached to the column face (Büker et al. 2021). This detail, however, raises the issue that, due to the distance between the support beam and the column face, large relative vertical movements at the column face arise from lateral drifts (Figure 15a). These vertical movements have the potential to cause undesired critical damage to the angle anchor bolts and the floor unit. By adding a block of unreinforced natural rubber (Figure 15b), large forces could be avoided while still ensuring that the strongback is sufficiently supported.

These rubber blocks were designed with the assumption that the vertical deformation of the block at 2.5% inter-storey drift generates a force equal to the maximum ULS gravity load in accordance with Section 3.1. Simple compression tests were conducted to find the appropriate dimensions and suitable shore hardness of the rubber. The rubber block was glued to the underside of the strongback so that it can slide on the seating angle. The seating angle can be designed with the 'dropped angle' approach, which is described in Büker et al. (2022a). Note that while the rubber block is useful in this instance to prevent undesired damage, it is not recommended to use rubber blocks as a general alternative to the 'capacity design' solution for the strongback retrofit design.

Finally, when establishing a retrofit strategy for a given floor plate, a range of retrofit solutions may be used for different precast floor units. When selecting suitable retrofits, it is important to ensure compatibility between the individual retrofits. One of the main advantages of the strongback retrofit is the ability to keep the floor vertically at the same level as the support, while other retrofits may only engage once the floor drops. For this reason, the strongback retrofit should preferably only be used in conjunction with other retrofits that do not allow the units to drop.

4 CONCLUSION

The strongback retrofit addresses the majority of failure modes in hollow-core floors and, most notably, is a suitable retrofit for both negative moment failure and positive moment failure. Experimental testing has successfully validated the effectiveness of this new retrofit technique. The validation test highlighted the benefits of the strongback retrofits, such as the load path integrity provided by post-installed shear anchors and the ability

to keep the diaphragm on the same level. Due to the relatively high material and installation costs, the use of the strongback retrofit may be limited to the critical hollow-core units (i.e. where PMF is a concern).

The recommended design steps described in this paper offer a straightforward design procedure. The most important aspects to consider when designing the strongback retrofit are summarised as follows:

1. An appropriate load combination should be selected based on the performance objective.
2. The seating angle should be designed following the 'capacity design' procedure described by Büker et al. (2022a) with modifications for the seating length design (see Section 3.2).
3. The length of the strongbacks highly depends on the number of hollow-core floor webs engaged and the shear capacity of these webs. Preliminary design charts are provided in this paper, but a detailed design check of the floor capacities is still required as an essential part of the strongback design.
4. Two rows of screw anchors with a diameter of 10 mm (or anchors with equivalent stiffness to this configuration) should be installed at the compression point to prevent web-crack propagation. Supplemental shear reinforcement must be provided if the shear capacity of the hollow-core webs is insufficient.
5. Careful detailing of the steel components is required to ensure stable transfer of loads between the unit, strongback beam, and support angle.

5 ACKNOWLEDGEMENT

The authors want to acknowledge and thank the funders that made the development and experimental testing of the strongback retrofit possible. The main funders were BRANZ (from the Building Research Levy), QuakeCoRE, the Earthquake Commission (EQC), Concrete NZ and the University of Canterbury. Blacks Fasteners and fischer kindly sponsored the fasteners for the strongback retrofits. Thanks to the Advisory Group of the ReCast Floors project for the support in developing this retrofit solution. The authors also want to thank Stuart Oliver, Juliane Spaak and Javier Berrios for their valuable input to these design recommendations.

Furthermore, the successful delivery of the experimental programme would not have been possible without the countless hours and valuable advice of the technical staff at the University of Canterbury, most notably Dave Carney, Alan Thirlwell, Russell McConchie, Norman King, Dave MacPherson and John Maley. A special thanks to Giovanni de Francesco for his help with the development of the loading protocols. Also noteworthy is the contribution of the many students who helped with the test, namely Michael Parr, Eldhose Paulose, Max Chirapattanakorn, Trevor Garrett, Abhishek Madan, Yuxin Huang, Mohamed Mostafa and Ana Sarkis.

This project was (partially) supported by QuakeCoRE, a New Zealand Tertiary Education Commission-funded Centre. This is QuakeCoRE publication number 0712.

6 REFERENCES

ACI (American Concrete Institute). 2019. Building Code Requirements for Structural Concrete (ACI 318-19) and Commentary (ACI 318R-19). Code. Farmington Hills, Michigan, United States: ACI.

Brooke, N. J., Büker, F., Bull, D. K., Elwood,K. J., Henry, R. S. and Hogan, L. S. 2022. "Overview of Retrofit Requirements and Techniques for Precast Concrete Floors." Journal of the Structural Engineering Society New Zealand, 35 (1).

Büker, F. 2022. "Development and Experimental Validation of Hollow-core Floor Retrofits." PhD Thesis (In Production), University of Auckland, Auckland, New Zealand.

Büker, F. (In Preparation). "Development and Experimental Validation of Hollow-core Floor Retrofits." PhD Thesis. University of Auckland, New Zealand.

Büker, F., Brooke, N. J., Elwood,K. J., Bull, D. K., Hogan, L. S. and Parr, M. 2021. "Development and Validation of Retrofit Techniques for Hollow-core Floors." Proceedings of the 2021 SESOC Conference, 14. Hamilton, New Zealand: Structural Engineering Society New Zealand.

Büker, F., Hogan, L. S., Elwood,K. J., Brooke, N. J. and Bull, D. K. 2022a. "Design Recommendations for Seating Angle Retrofits." SESOC Journal, 35 (1).

Büker, F., Parr, M., De Francesco, G., Hogan, L. S., Bull, D. K., Elwood, K. J., Liu, A. and Sullivan, T. J. 2022b. "Seismic Damage Observations of Precast Hollow-Core Floors from Two Full-Scale Super-Assembly Tests." Journal of the Structural Engineering Society New Zealand, 35 (1).

Bull, D. K., and Matthews, J. 2003. Proof of Concept Tests for Hollowcore Floor Unit Connections (Research Report 2003-1). 1–84. Department of Civil Engineering, University of Canterbury.

CEN. 2018. EN 1992-4: Eurocode 2 - Design of Concrete Structures - Part 4: Design of fastenings for use in concrete. Brussels, Belgium: CEN.

Fenwick, R., Bull, D. K., and Gardiner, D. 2010. Assessment of Hollow-Core Floors for Seismic Performance (Research Report 2010-02). University of Canterbury, Christchurch, New Zealand (https://ir.canterbury.ac.nz/handle/10092/4211).

Henry, R. S., Dizhur, D., Elwood, K. J., Hare, J. and Brunsdon, D. 2017. "Damage to Concrete Buildings with Precast Floors During the 2016 Kaikoura earthquake." Bulletin of the New Zealand Society for Earthquake Engineering, 50 (2): 174–186.

Jensen, J. 2006. "The Seismic Behaviour of Existing Hollowcore Seating Connections Pre and Post Retrofitted." ME Thesis. University of Canterbury, Christchurch, New Zealand.

Liew, H. Y. 2004. "Performance of Hollow-core Floor Seating Connection Details." ME Thesis. University of Canterbury, Christchurch, New Zealand.

Matthews, J. 2003. "Hollowcore Floor Slab Performance Following a Severe Earthquake." PhD Thesis. University of Canterbury, Christchurch, New Zealand.

MBIE. 2019. Acceptable Solutions and Verification Methods - For New Zealand Building Code Clause - B1 Structure (Amendment 19). 94p. Wellington, New Zealand: Ministry of Business and Employment.

MBIE, EQC, NZSEE, SESOC, and NZGS. 2018. Technical Proposal to Revise the Engineering Assessment Guidelines - Part C5 Concrete Buildings. Wellington, New Zealand: Ministry of Business, Innovation, and Employment.

Parr, M., Elwood, K. J., Bull, D. K., Büker, F., Hogan, L. S., Puranam, A. Y., Henry, R. S. and Brooke, N. J. 2019. "Development and Testing of Retrofit Solutions for Hollow-core Floors in Existing Buildings." Proceedings of the 2019 Concrete New Zealand Conference, 12. Dunedin, New Zealand.

SESOC, NZSEE, and ENZ. 2021. "Advice on Hollow-core Floors." Accessed October 6, 2021. https://www.sesoc.org.nz/precast-flooring-resources/.

SNZ. 2009. Structural Design Actions. Part 1 : Permanent , Imposed and Other actions (Incorporating Amendments Nos. 1 and 2). NZS1170.1:2002. Wellington, New Zealand: SNZ.

SNZ. 2011. Structural Design Actions. Part 0: General Principles (Incorporating Amendments Nos 1,2,3,4 and 5). NZS1170.0:2002. Wellington, New Zealand: SNZ.

SNZ. 2017. Concrete Structures Standard (Incorporating Amendment No. 1,2 and 3). NZS 3101:2006. Wellington, New Zealand: SNZ.

Woods, L. J. 2008. "The Significance of negative bending moments in the seismic performance of hollow-core flooring." ME Thesis. University of Canterbury, Christchurch, New Zealand, 294p.

BUILDING PERFORMANCE CONSULTATION DOCUMENT

Consultation document Building Code *update 2022 Structural stability of hollow-core floors,* amending Verification method B1/VM1 (2 May 2022).

The building regulator has commenced with the 2022 building code update consultation. This includes proposing changes to the compliance pathway for hollow-core floors. The change that is being consulted on proposes the removal of a 'deemed to comply' solution for the support of hollow-core floors in new building designs. It is proposed that the design of hollow-core floor systems will still be possible via an 'alternative' solution pathway. Consultation will run until 1 July 2022.

ISSN No. 2744-7871

SEISMIC PERFORMANCE OF PRECAST HOLLOW-CORE FLOORS WITH MODERN DETAILING: A CASE STUDY

Mostafa, M.[1,*], Hogan, L.[2], Elwood, K.J.[3]

ABSTRACT

This paper describes the observed seismic performance of precast hollow-core floors from an instrumented building subjected to design-level ground shaking during the 2016 Kaikōura earthquake. The hollow-core floors in the building incorporated the detailing requirements of the current design standard, NZS3101:2006-A3, which were intended to suppress undesirable failure modes such as loss of support, negative moment failure, positive moment failure, and rupture of non-ductile topping mesh. The structural system was extensively surveyed to document the severity and distribution of the damage sustained in the flooring system. Furthermore, the building response during the earthquake was reconstructed from the acceleration records obtained from instruments installed throughout the building to estimate the demands on the floor units. While the failure modes that the NZS 3101 hollow-core detailing was designed to suppress were not observed in the building, the damage survey showed unexpected poor performance of hollow-core floor units seated within the plastic hinge regions of the supporting beams and in line with columns, which are referred to as "beta units". It was found that beta units incurred more damage than units seated outside the plastic hinge zone. The susceptibility of these beta units to sustain severe damage is neither recognised in the current design standard, NZS3101:2006-A3, nor in the technical proposal aiming to revise the Assessment Guidelines C5 (Yellow Chapter).

1 INTRODUCTION

The susceptibility of precast hollow-core floors to sustain severe damage under seismic actions has been recognised and extensively investigated since the early 2000s, as summarised in Corney et al. (2021) and Puranam et al. (2021). Through these previous investigations, improvements to the floor-to-support connection details have been developed and proof tested to address the potential failure mechanisms that have been identified in previous research (Lindsay 2004; MacPherson 2005). Although extensive laboratory tests have been undertaken to investigate the performance of these floors, the tests setups that were used represent a simplified version of real-life structures and lack the ability to replicate all of the deformation and inertial demands present in a building during an earthquake. Discrepancies between the observed building performance and laboratory specimen behaviour are attributed to many factors, such as size effects, 3D interaction between multiple structural components, and dynamic characteristics of the earthquake. Accordingly, learning from structural damage observations in previous earthquakes has played a pivotal role in enhancing the understanding of the performance of different structural components when incorporated in a structural system. These damage observations have also led to the progressive improvement of design standards and building codes. Recognising the significance and benefits of learning from the response of real buildings under earthquakes, multiple buildings have been instrumented throughout New Zealand over the years to capture the seismic demand and the response of these structures (Uma et al. 2011; Van Houtte et al. 2017).

The 2016 Kaikōura earthquake resulted in seismic demands exceeding the design level demands for buildings with periods of 1-2 s at some locations in Wellington (Henry et al. 2017). The building investigated in this paper was one of six instrumented buildings in Wellington and the Upper South Island that experienced shaking in the Kaikōura earthquake. The building sustained widespread damage after the earthquake, with extensive damage to the floors resulting in the demolition of the building. As part of the demolition programme all non-structural components were removed prior to the structure's demolition, leaving the damaged structure exposed. The structure was extensively surveyed to document the severity and distribution of damage resulting from the earthquake. Detailed damage documentation and crack mapping were undertaken to capture the structural damage sustained in the building. Furthermore, the data recorded from the instrumentation

PAPER CLASS & TYPE: GENERAL REFEREED

1 Ph.D. Candidate, University of Auckland
2 Lecturer, University of Auckland
3 Professor, University of Auckland
** mohamed.mostafa@auckland.ac.nz*

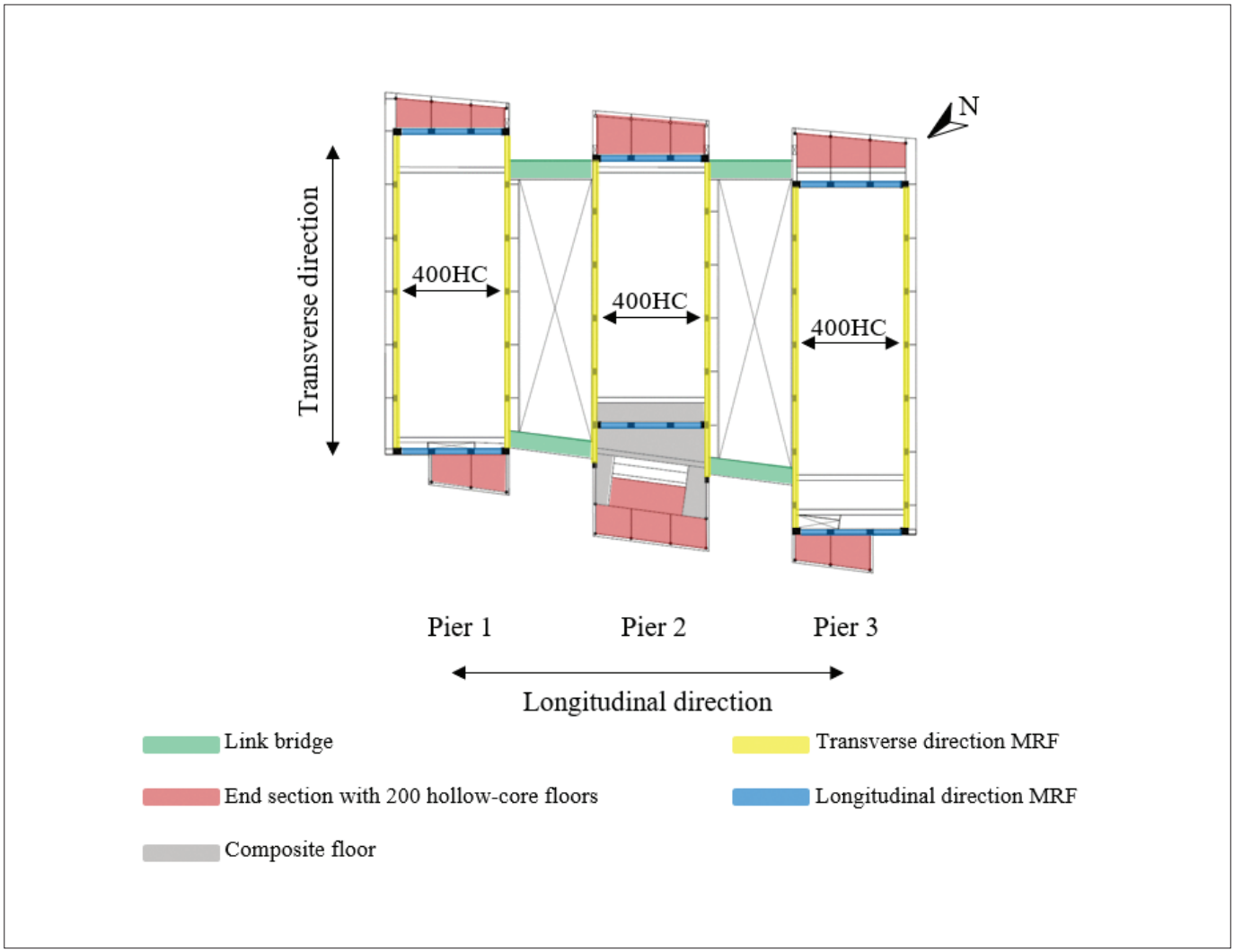

Figure 1: Schematic for building layout

installed in the building were used to provide an estimate of drift demand, which has been correlated with observed damage. This paper aims to highlight the key floor damage observations in the building and potential implications this observed damage has on the current design standard, NZS3101:2006 (Standards New Zealand 2017), as well as the technical proposal aiming to revise the Assessment Guidelines C5 (MBIE et al. 2018).

2 BUILDING DESCRIPTION

The building investigated was a commercial office building with ductile reinforced concrete moment resisting frames and a precast flooring system constructed in 2009. The building was located on the waterfront in Wellington. The layout of the building consisted of three seismically linked buildings referred to as "piers" that were connected via composite steel-concrete pedestrian 'link bridges' and separated by two atrium spaces, as is shown in Figure 1. Pier 1 and Pier 3 were five stories tall, while Pier 2 had an additional sixth storey constructed of steel to house mechanical equipment. The link bridges were designed with sufficient strength to tie the piers together in the longitudinal direction. In addition to the link bridges at each floor, Piers 2 and 3 were connected with a floor diaphragm at Level 1. Ductile reinforced concrete perimeter moment resisting frames (MRFs) were used to serve both the gravity load carrying system as well as the lateral load resisting system. The frames consisted of precast concrete beams with in-situ columns and joint elements designed and detailed for high ductility in both principal directions of the building.

The spacing between the column centrelines in the longitudinal frame varied between 5.4 to 6.0 m, whereas in the transverse frames the columns were 8.1 m apart. A precast, prestressed hollow-core floor system was used to span approximately 17 m in the longitudinal direction of the building between the perimeter frames. The typical floor system was a 400 mm thick hollow-core slab (HC) with a cast-in-situ 100 mm topping layer

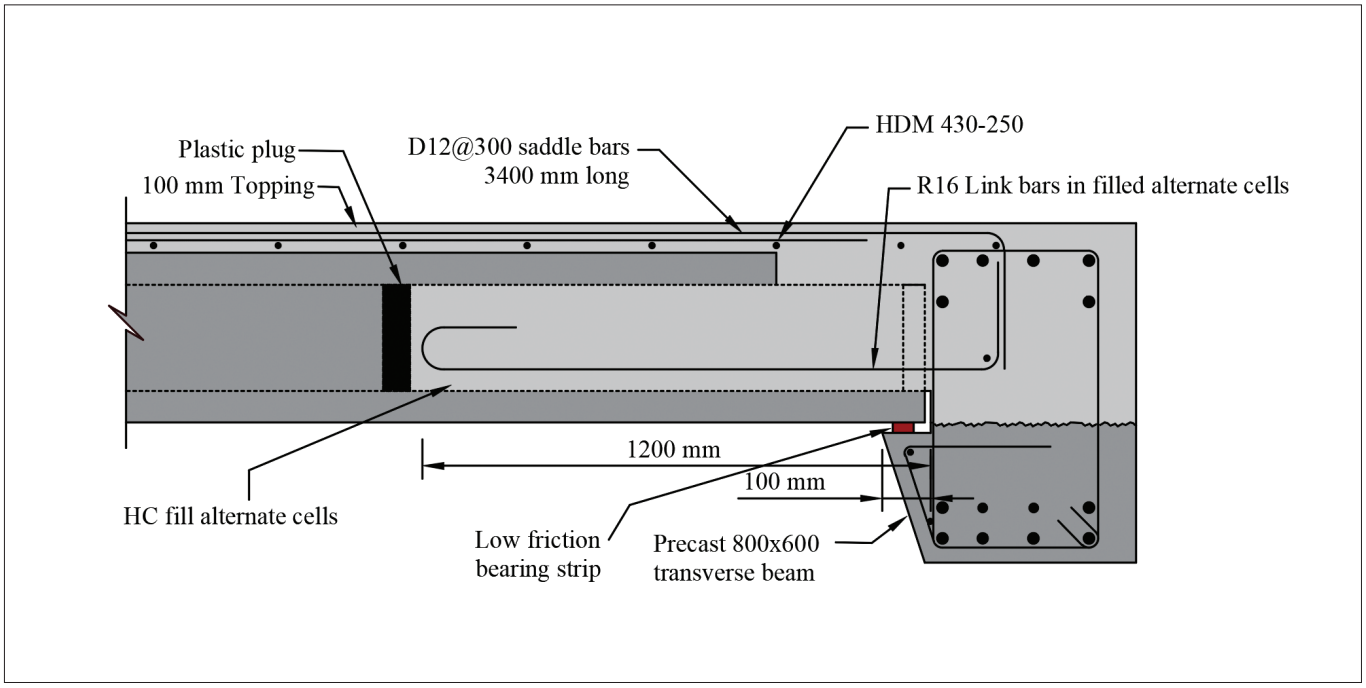

Figure 2: Schematic of floor to beam connection detail (dark grey colour indicates precast portion)

reinforced with ductile mesh (HDM-430-300). Figure 2 shows a typical floor connection detail. The connection detail used in the building was consistent with C18.6.6(e) of NZS3101:2006-A3, which is referenced within clause 3.1.1 of B1/VM1 (MBIE 2021) and hence can be considered a deemed-to-comply solution meeting the performance objectives of the Building Code. The hollow-core units had 100 mm specified seating length with a 50 mm wide low friction bearing strip. Every second cell of the unit was filled, and a 16 mm plain round bar was cast in these filled cells and tied back to the supporting beam. In-situ "link slabs" were used to accommodate deformation incompatibilities between the floor and frame in locations where hollow-core slabs run parallel to multiple-bay frames.

At the north and south ends of each pier, steel frames and 200 mm thick hollow-core slabs were used for the floor system (Figure 1). Composite flooring was used in the area around the lift shafts in Pier 2. Furthermore, 175 mm thick precast cantilever floors were used for edge walkways in the building. At roof level, cold-formed purlins were supported by structural steel portal frames. The ground level used a slab-on-grade concrete floor. NZS3101:2006 was used to design the concrete moment frames and the floors.

3 GROUND MOTION

The magnitude 7.8 Kaikoura earthquake occurred along the east coast of the upper South Island on 14 November 2016 at 12:02 a.m. local time, with an epicentre approximately 20 km south of the Hope fault, at a depth of 15 km (GeoNet 2016; Hamling et al. 2017). The event included multiple fault segment ruptures, which propagated northeast from North Canterbury with significant energy being propagated towards the Wellington region (Bradley et al. 2017; Kaiser et al. 2017). The approximate location of the source zone and rupture propagation direction are indicated in Figure 3a. Despite Wellington's distance from the source, strong shaking was experienced in some parts of the city. This shaking intensity is mainly attributed to the amplification of ground motion by the deep sediments underlying the city as well as being in the path of the focussed seismic waves propagating in the direction of rupture. For the building investigated, a free field sensor located at the building site showed local site amplification effects due to deep soil deposits, which resulted in strong energy content in the 1–2 s period range, as shown in Figure 3b. For comparison purposes, the spectral values for the Wellington CBD, soil class D based upon NZS 1170.5:2004 (Standards New Zealand 2016) was plotted for both the ultimate limit state (ULS) and serviceability limit state (SLS) against the 5% damped response spectra of the ground motion recorded with the free-field instrument located at the building site along the longitudinal and transverse axes of the building. The

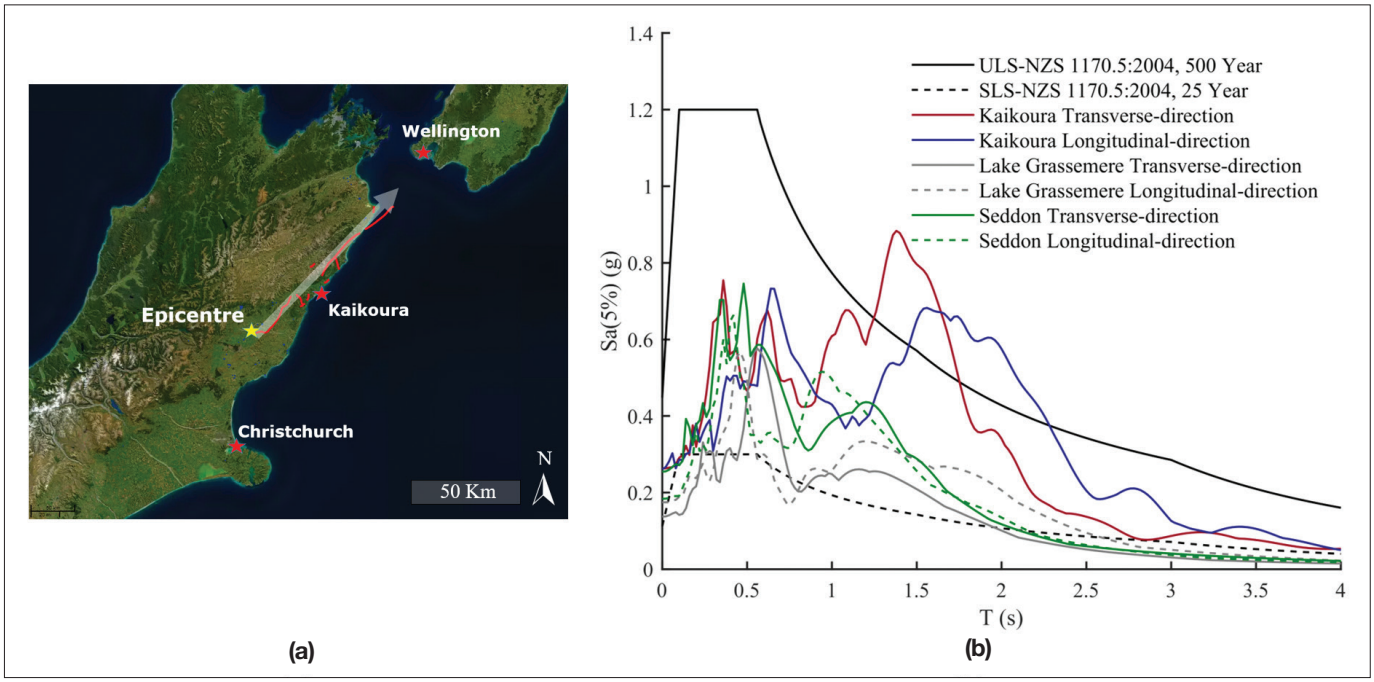

Figure 3: (a) approximate location of Kaikōura earthquake epicentre and faults ruptures according to Hamling et al., (2017) (b) 5% damped spectral accelerations of the free-field ground motions rotated to coincide with the longitudinal and transverse axes of the building and the ULS and SLS design response spectra according to NZS1170.5:2004.

moderately long duration of the ground motion alongside the high energy content in the 1-2 s period range led to floor accelerations reaching about 0.8g and inter-storey drifts reaching about 1.8%, which resulted in damage to different structural components in the building, including spalled concrete in columns and beams, cracks in beams, columns and floor slabs at the column joints. It is worth noting that the building was previously subjected to two earthquakes in 2013, the M-6.5 Cook Strait earthquake (GeoNet 2013a) and the M-6.6 Lake Grassmere earthquake (GeoNet 2013b). Following the Cook Strait earthquake (sometimes referred to as the Seddon earthquake), minor structural damage was observed and a significant amount of non-structural damage was observed (Dominion Post 2013).

4 BUILDING RESPONSE

The building response was captured using 14 tri-axial CUSP-M accelerometers (CSI Limited 2017) installed throughout the building, as shown in Figure 4, and one free-field accelerometer was used to capture the local site ground motions. Pier 3 was instrumented with at least one accelerometer in each storey. Sensors 3-11 and sensor 15 were used for levels G to 6 in Pier 3 to monitor the motion at the centre of each level. The fifth floor (ceiling of level 4) of the building was instrumented with five sensors to capture any twisting motion if present.

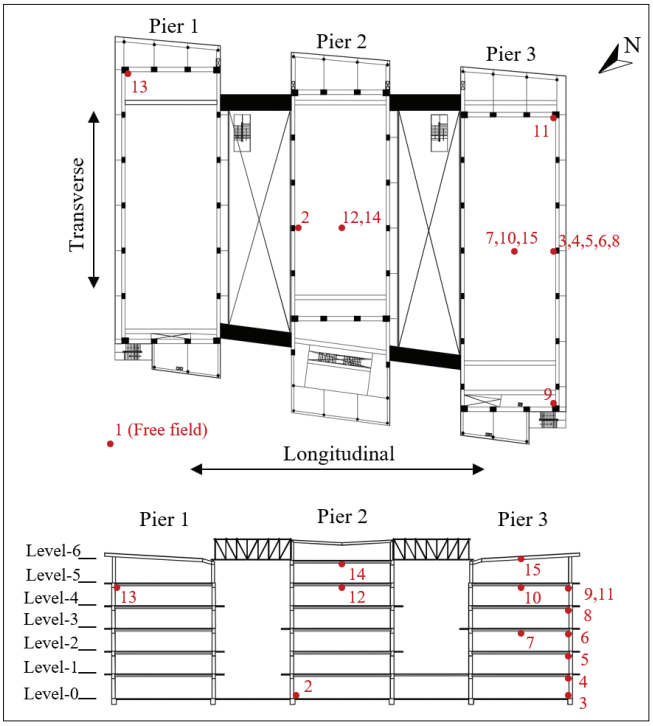

Figure 4: Locations of installed triaxial accelerometers throughout the building

The strong motion data was obtained through the GeoNet instrumentation network (GeoNet 2016) and was then processed based on recommendations from Boore and Bommer (2005) to have the two orthogonal horizontal components of each record coinciding with the longitudinal and transverse direction of the building.

Since Piers 1 and 2 of the building were too sparsely instrumented to be able to reconstruct the response of these portions of the building, only the response of Pier 3 was reconstructed and computed. For each floor level in Pier 3, sensors 3, 4, 5, 6, 8 and 10 were considered to represent the motion of the entire floor, assuming a rigid diaphragm. The peak floor acceleration (PFA) at each level for both transverse and longitudinal directions of the building was computed as the absolute maximum acceleration over the entire time series. As such, these PFA's values could have occurred at different times and directions. The PFA variation along the height of the building for both orthogonal directions of the building are plotted in Figure 5a. A maximum PFA of about 0.8 g was observed at the fifth level in the transverse direction. To compute the inter-storey drifts, the displacement time series for each level was first computed by double integrating the acceleration time series for each level using the software Seismosignal (Seismosoft 2016). Then the inter-storey drift ratio (ISD) time series of each storey was computed as the difference between the derived displacement time series of the upper and lower levels of each storey normalised by the storey height. The peak ISD for each storey was computed as the absolute maximum ISD over the entire time series. Similar to PFA, peak ISD could have also occurred at different instants of time. Figure 5b shows the variation in peak ISD over the building height.

The simplified method of response spectral ratios (McHattie 2013) was used here to estimate the fundamental modal period in each orthogonal direction of the building. The spectral ratio can be calculated as the ratio of the spectral acceleration of the seismic response recorded at a given point in the structure and the spectral acceleration recorded at the ground floor. As shown in Figure 6, the non-dimensional acceleration peaks generally take place around the same period because buildings amplify frequencies close to their modal frequencies. Hence, the period at which response spectral ratios peaks was adopted as an estimate of the fundamental period of building. The fundamental period of vibration for the transverse and longitudinal directions was estimated to be approximately 1.2 s and 1.3 s, respectively. By plotting the deduced periods for both longitudinal and transverse frames against the response spectra (Figure 7), it can be found that the estimated fundamental periods generally match the recorded peak floor acceleration. It is important to note that, although a simple method was used here to estimate the fundamental modal periods, there are more sophisticated methods available that can be used to provide a more refined approximation of the modal properties (Hasan et al. 2018; Peeters and De Roeck 1999).

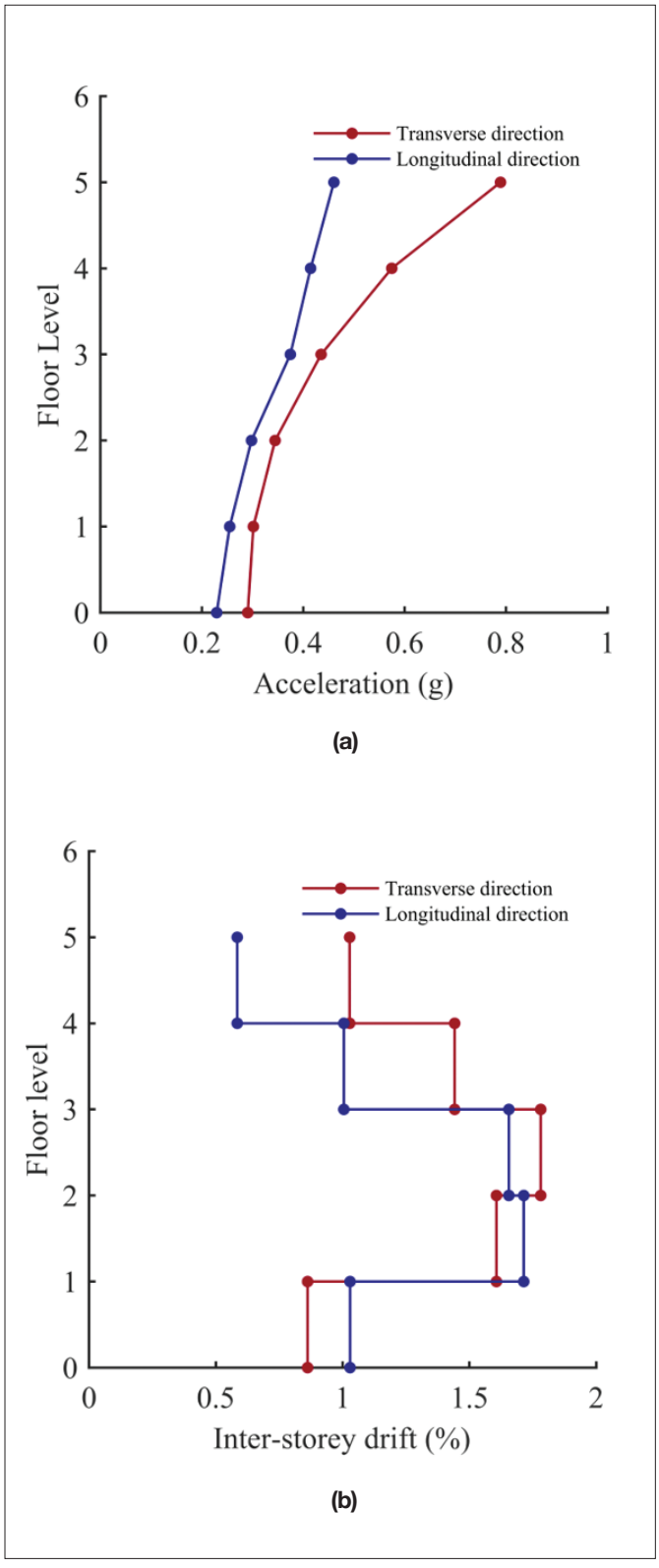

Figure 5: (a) peak floor accelerations (b) peak inter-storey drifts

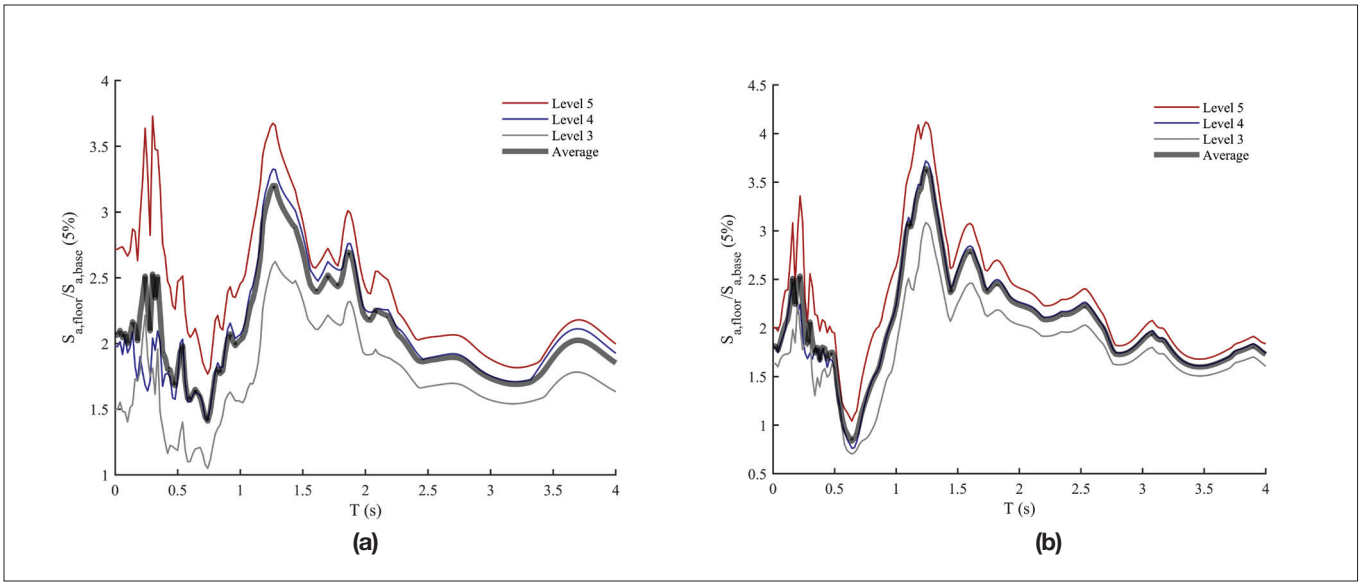

Figure 6: Spectral ratios from the top three storeys' instruments (a) transverse direction (b) longitudinal direction

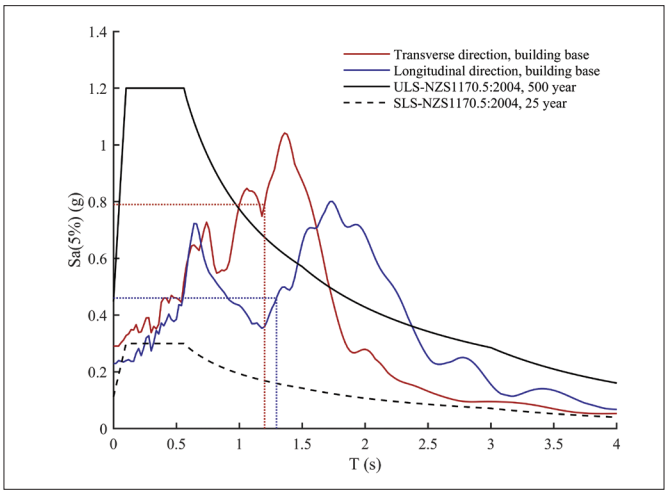

Figure 7: 5% damped response spectra of the building-base ground motions in the transverse and longitudinal directions of the building relative to the 500-year and 25-year return period (NZS 1170.5:2004) elastic design spectra with the fundamental periods inferred from response spectral ratios analysis indicated

5 OBSERVED FLOOR PERFORMANCE

This section summarises the key observations from the damage investigation of the floors. The discussion is limited to the observations of different damage states observed in the building rather than the performance of the building itself. More information regarding the building performance can be found in Siddiqui et al. (2019a) and Siddiqui et al. (2019b). Nevertheless, it is worth noting that the frame damage observed was predominantly concentrated in beam plastic hinge zones, with damage ranging from minor cracking to concrete cover spalling and residual crack widths up to 4 mm. This level of frame damage was generally considered to be repairable. More information regarding the damage sustained in the building can be found in Mostafa et al. 2022b.

The information collected and presented herein is based on extensive damage mapping of the floor units and floor diaphragm (topping). After removing the non-structural elements such as ceilings, carpets, linings and panelling, detailed damage inspections of the floors were undertaken. The extent of floor diaphragm damage was mapped and crack widths were measured. Inspection of the damage sustained in the soffit of the hollow-core floor and reduction in support length due to seating ledge spalling was also conducted.

5.1 TOPPING AND SUPPORT DAMAGE

The damage in the topping of the floors was observed throughout the building. Figure 8 shows one-floor diaphragm damage as an example of the typical damage observed and marked with red lines. The topping damage primarily consisted of longitudinal cracks between adjacent units and some longitudinal cracking within the width of units. These longitudinal cracks had residual widths ranging from 0.3 mm to 7 mm, with larger crack widths typically occurring between units. In the areas adjacent to the columns, concentrated transverse and longitudinal cracking with crack widths ranging from hairline to 4 mm wide were observed. No mesh rupture was observed in the topping as ductile mesh was used.

Support ledge spalling at the columns and plastic hinge

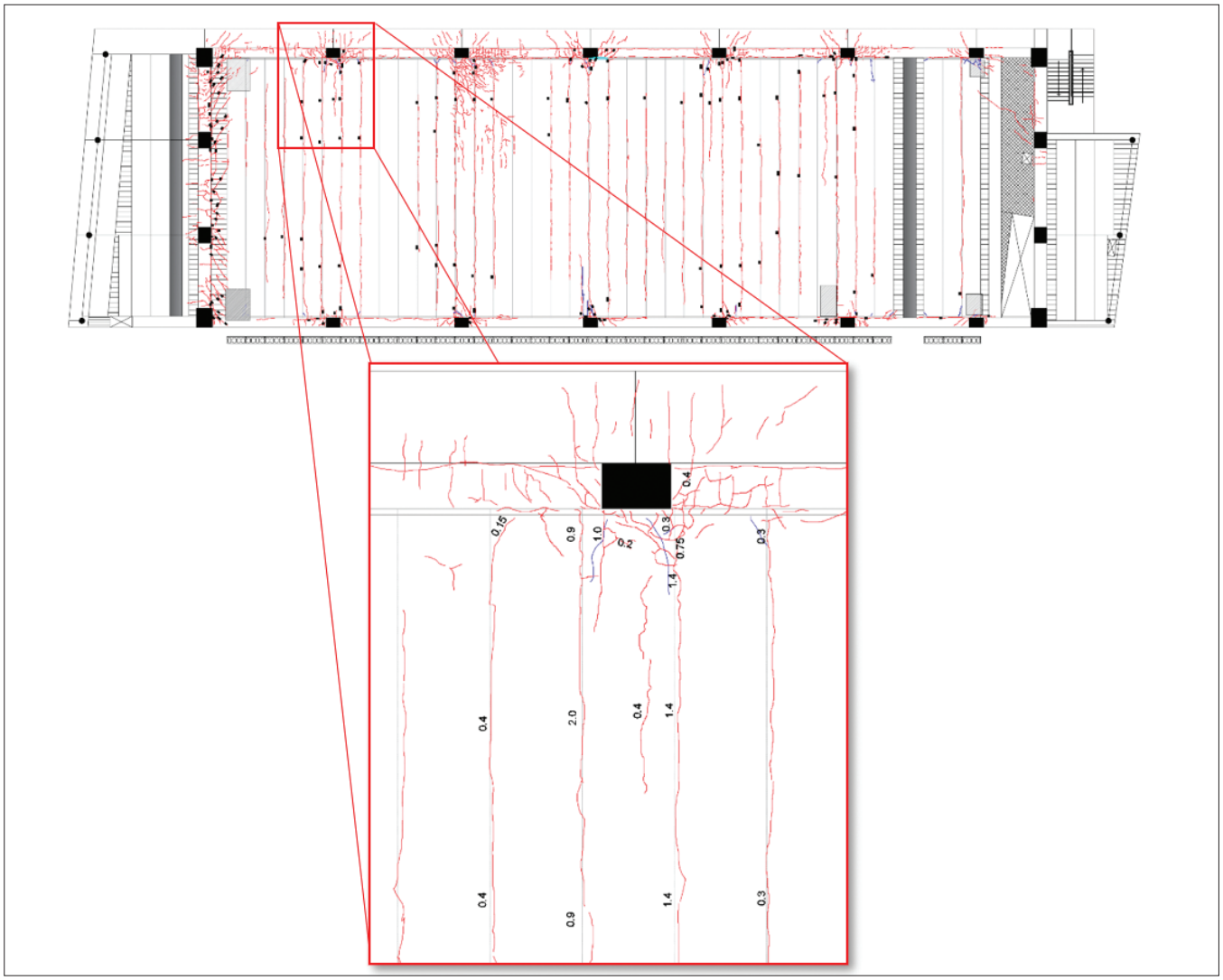

Figure 8: Crack map sample from the second floor in Pier 3 with floor top cracking marked in red, soffit cracks marked in blue,

zones was observed in multiple locations in the building (e.g. Figure 9). However, no loss of unit support was observed due to the ledge reinforcement detailing used in this building.

(a) **(b)**

Figure 9: Significant support ledge spalling observed at different locations in the building (a) Pier 3 level 1 (modified from Siddiqui et al. (2019a)) (b) Pier 2 level 1

5.2 DAMAGE TO UNIT SOFFIT

As for the hollow-core units damage observed at the soffit, a significant proportion of the hollow-core floor units in the building sustained some level of damage due to deformation incompatibilities between the hollow-core units and the supporting frames under seismic demands. The corners of the hollow-core units were found to be damaged in many units throughout the building. This corner cracking was found to occur in units regardless of their location in the building (i.e. seated over a column, within the plastic hinge zone or outside the plastic hinge zone) with various degrees of damage, as shown in Figure 10. Given the prevalence of this crack type, with evidence of grout seeping out of one unit corner crack in the building (Figure 11a), this corner cracking is also being observed in buildings located in Auckland that have not been subjected to earthquake loading (Figure 11b). These corner cracks were likely caused by non-seismic damage. Such damage could have occurred during production due to the saw-cut not being deep enough, the saw blade binding when the member cambers, or uneven handling due to pick-up devices not being level (Hoisington et al. 1983).

Another reason for this cracking could be damage initiation during construction, in which the units are usually placed on their side first while installing them in their final location. This installation method could place localized stress on the corners of the units at the supports resulting in the observed cracking. While it is likely these corner cracks were initiated during the production or construction phases, it is expected that these corner cracks opened up during the earthquake and propagated through one or two webs, reducing the shear capacity of the units. Moreover, where the side of the units was visible, it was found that the corner cracking observed from the bottom of the units propagated through the external web of the unit (Figure 10c). Corner cracking propagation through the external webs could not be confirmed for units seated within the middle of the floor (Figure 10a and Figure 10b).

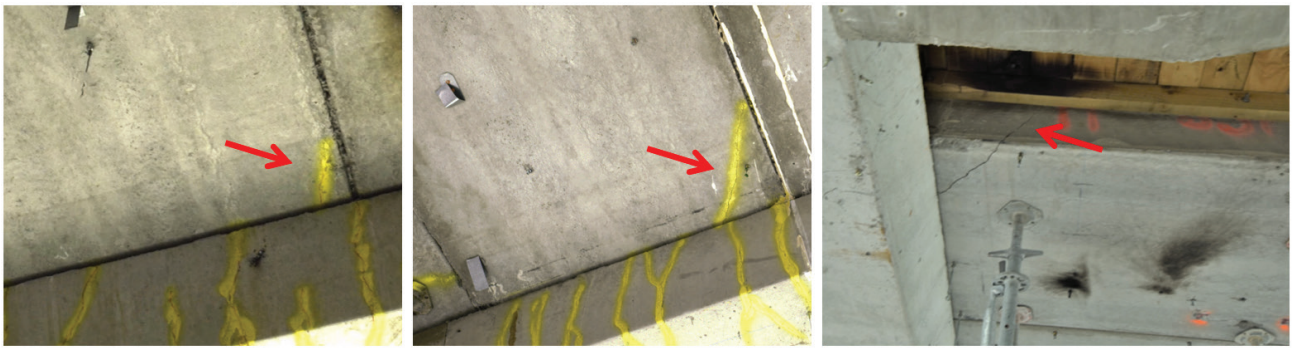

(a) (b) (c)

Figure 10:(a) minor hairline corner crack (b) Moderate corner crack (c) corner cracking propagating through exterior web when visible

(a) (b)

Figure 11: (a) corner crack with grout seeping out observed in the building investigated (b) corner crack observed in a carpark in Auckland

In addition to the corner cracking in the soffit of the units, longitudinal cracking in the bottom flange of the hollow-core units was also observed in multiple units with varying degrees of severity from hairline cracking to wide cracks that extended the full length of the unit. Longitudinal cracking might be problematic if the cracking crossed a web (Figure 12) which was typically found in units seated within the plastic hinge zone. Longitudinal cracking of units seated within the plastic hinge region occurs due to the deformation of the supporting beam under seismic demands and can be accompanied by web splitting that may result in the separation of the unit's bottom half from the unit's top half. Web splitting was identified in the units seated within the plastic hinge region via borescope.

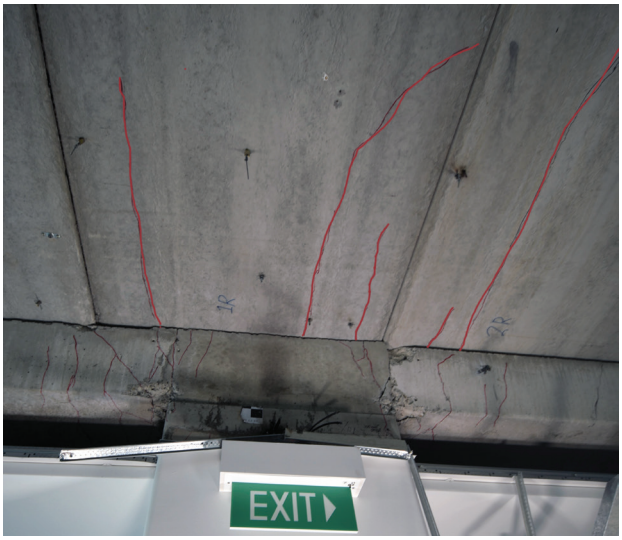

Figure 12: longitudinal cracking of HC unit soffit

Transverse cracking in the soffit of the precast hollow-core units was also observed in multiple units. Based on previous research observations (Fenwick et al. 2010), such damage indicates the propagation of cracking through the unreinforced unit webs (e.g. Figure 13a). Several floor units throughout the building were temporarily shored immediately after the earthquake as the damage observed in these units suggested that their vertical load-carrying capacity had been compromised. Moreover, web cracking was evident in units where the side of the hollow-core unit was visible, with no signs of damage observed at the unit's soffit (Figure 13b). Such observations not only reinforce the concerns regarding the risk these floors possess - given the inability to inspect these webs without invasive techniques such as using a borescope - but also raise concerns regarding the efficiency of the low friction bearing strip to suppress positive moment damage. A preliminary explanation of the web damage observed (Figure 13b) would be due to the filled cores with R16 bars trapping the unit and not allowing the unit to slide over the low friction bearing strip. Furthermore, cracking of hollow-core unit's external webs was observed in multiple units where the side of the unit was visible (Figure 14). In one of these units with exposed sides, severe web cracking of approximately 30 mm was observed (Figure 14b).

(a)

(b)

Figure 13: (a) positive moment failure in test conducted by Bull & Matthews (2003) (b) web cracking observed from unit side

(a) (b)

Figure 14: (a) transverse cracking observed at the soffit of the HC unit away from the support propagating through the web (b) HC unit corner severely damaged and unit dropping with severe web cracking (about 30 mm) propagating through the web

In addition to the units' corner, longitudinal, and transverse cracking, a damage pattern that has not been previously observed in either test specimens or other hollow-core building damage reports was observed repeatedly throughout the building. The damage pattern primarily consists of the two corners of the unit ends being cracked accompanied by a curved transverse cracking about 300 mm away from the support (Figure 15). This "transverse hoop" damage pattern was found in units seated on a column, where these units have been subjected to a combination of rotational and bending demands in both transverse and longitudinal directions of the units during the earthquake shaking. Units exhibiting this transverse hoop damage pattern were located on different floors that were subjected to different drift demands.

Finally, transverse cracking at a unit soffit accompanied by web cracking (Figure 16c) was observed at the top storey where the imposed storey drift demand was as low as 0.6% in the longitudinal direction of the unit and 1.0% in the transverse direction. Preliminary analysis suggests that diaphragm demands (Figure 16) due to higher floor accelerations may have influenced the occurrence of such damage at such low drift demands. Almost half of the floor inertial load in the longitudinal direction needs to be transferred to the moment-resisting frame through a tension tie due to the presence of a floor opening in the shown location. Although a tie beam was present, the tensile forces from the inertial loads, in addition to the relatively small deformation demands imposed on the unit from the supporting frame, was sufficient to cause the damage pattern shown in Figure 16c. Such damage highlights the challenges of ensuring good performance of hollow-core floors even when incorporated in regular floor diaphragms.

(a) (b) (c)

Figure 15: Previously unidentified repeated damage pattern highlighted in red (a) Pier 2 level 4 (b) Pier 3 level 2 (c) Pier 2 level 3

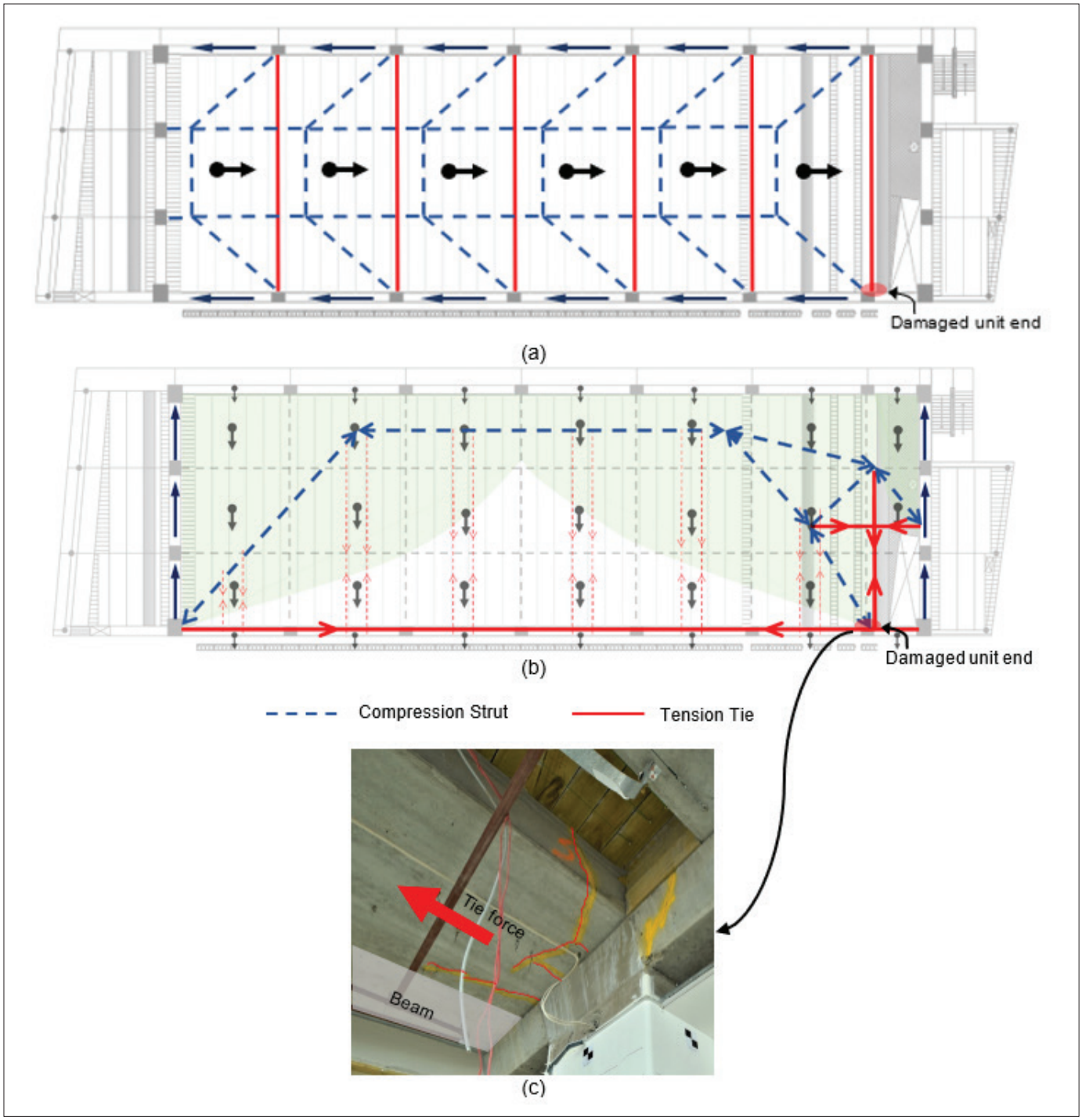

Figure 16: Simplified Strut and Tie (S-T) model for diaphragm inertial forces and damage observed at top storey with low drift demands highlighted in red, (a) S-T model for inertial loads in the transverse direction (b) S-T model for inertial loads in the longitudinal direction (c) damage observed in hollow-core unit at top storey

5.3 FLOOR DAMAGE CLASSIFICATION

Various degrees of hollow-core units damage were observed throughout the building, from insignificant hairline cracking to very wide cracking reaching approximately 30 mm. To quantify the extent of damage sustained in the floors, a qualitative framework was developed to classify different observed damage states. Table 1 summarises the approach used to quantify observed floor damage. Using the defined framework, the observed damage state at each floor unit was qualitatively assessed, and a damage state was assigned to each hollow-core unit.

The inspection of the floor units was only possible from the soffit. Hence the categorisations of the damage sustained in the hollow-core units primarily relied on the inspection of the floor unit's soffit. There was a degree

of engineering judgement involved in interpreting the significance of different damage states, and as such, some potential variance in evaluations can result. However, the interpretation of damage severity was based on available research information on the seismic performance of these floors (Bull et al., 2009; Fenwick et al., 2010). According to the classification criteria defined herein, the damage severity for each end of the hollow-core units was mapped for each floor. An example is shown in Figure 17. Then the damage severity for each end of the hollow-core units was plotted against each unit location relative to the nearest column for 684 unit-ends (i.e. 342 units) (Figure 18). It was noted that there was a trend for the damage severity, where the closer the unit was to a column, the higher the degree of damage. More severe damage was found in units seated either fully or partially on a column (referred to as 'beta units'), where the precast floor units were subjected to localised deformation to accommodate the deformation of the supporting seismic and gravity systems. These observations highlighted the susceptibility of hollow-core floor units to sustain a higher degree of damage when seated within the plastic hinge regions. The plastic hinge length was taken as half of the supporting beam depth (effective plastic hinge length ~0.5h_b, according to the yellow chapter-C5).

Table 1: Summary of damage quantification framework used to assess different floor damage states

Damage State	Damage Index	Description	Possible damage patterns
No Damage	0	No visible damage	-
Light Damage	1 2	Damage that is expected to have generally not compromised the units' gravity load carrying capacity	• Hairline longitudinal cracking. • Corner crack crossing the external web only. • Minor local support ledge spalling.
Moderate Damage	3	Damage that has potentially compromised the gravity load carrying capacity	• Visible longitudinal cracking of units. • Large corner cracking crossing more than one web. • Hairline web cracking (no risk of losing load path), visible in units beside link slabs. • Moderate support ledge spalling.
Heavy Damage	4	Damage that has compromised the units' capacity and a reliable load path is lost and/or possesses the risk of collapse in an aftershock	• Soffit transverse cracking. • Soffit diagonal cracking (not corner crack). • Web cracking. • Reduced floor support (significant support ledge spalling).

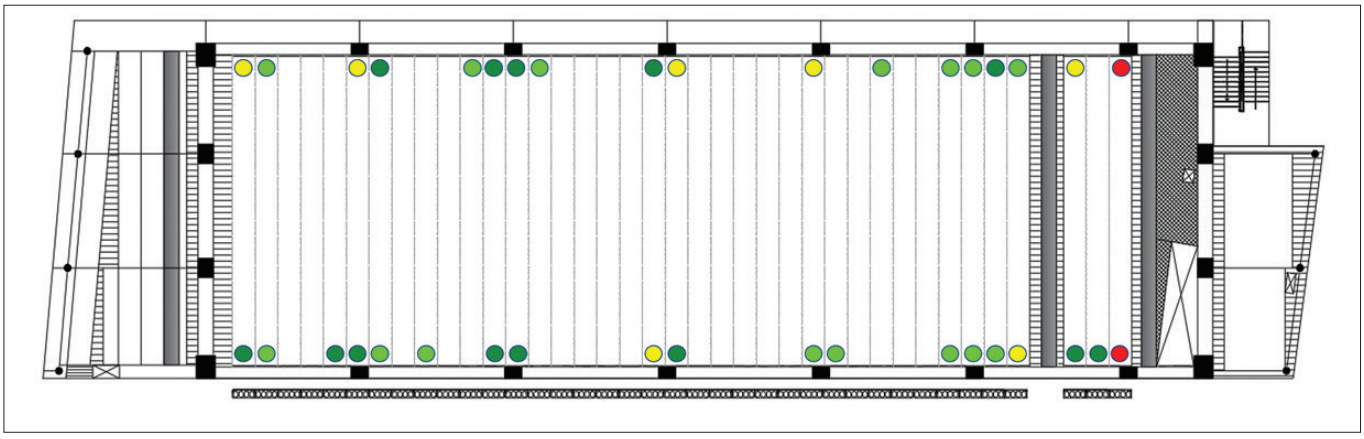

Figure 17: Floor damage distribution example, Pier 3 - level 2

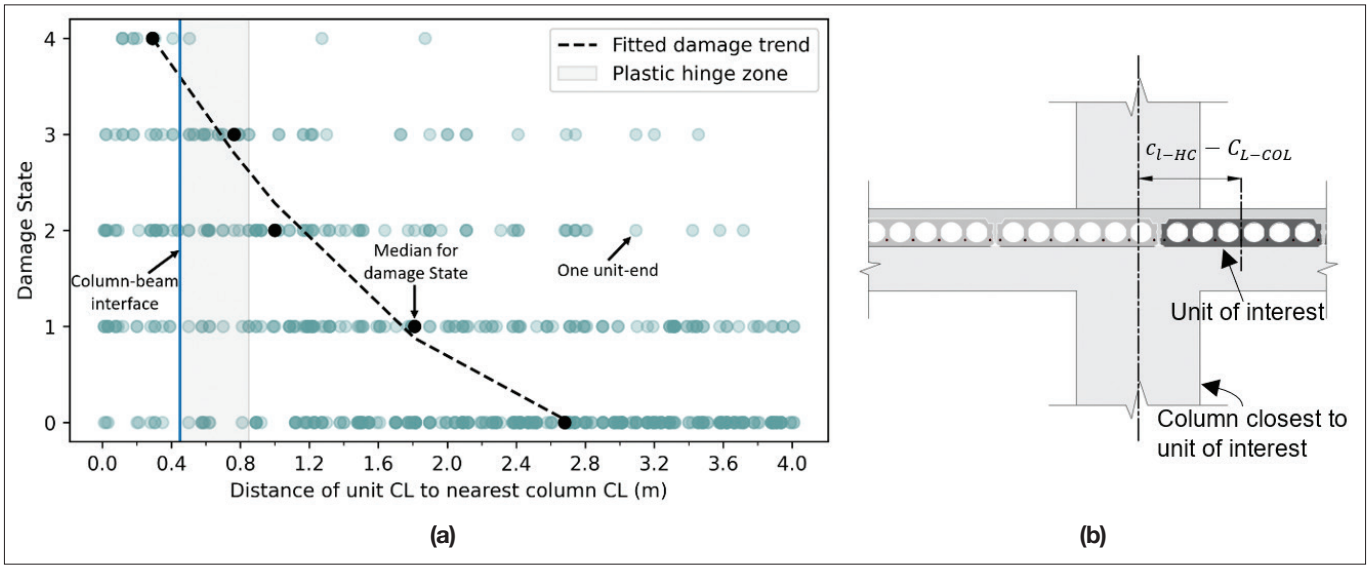

Figure 18: (a) Damage severity trend relative to unit location (centreline of unit relative to centreline of nearest column) (b) illustrative schematic of the units' location used

6 CONCERNS

The observations discussed above raise the following concerns regarding the expected seismic performance of hollow-core floors in future earthquakes:

- The susceptibility of hollow-core floor units to sustain a higher degree of damage when seated within the plastic hinge regions of the supporting beam or within the column depth ('beta' units) is neither recognised in the current design standard, NZS3101:2006-A3 (Standards New Zealand 2017), nor in the Yellow Chapter of the Assessment Guidelines C5 (MBIE et al. 2018).
- The seating detail (Figure 2) is consistent with C18.6.7(e) of NZS3101:2006-A3, which is referenced within clause 3.1.1 of B1/VM1, and hence, can be considered a deemed-to-comply solution meeting the performance objectives of the Building Code. However, the damage reported above suggests that this detail does not result in performance consistent with the life safety and amenity performance objectives of the Building Code.
- Inertial forces in the diaphragm can cause additional unintended tensile forces in hollow-core units which can lead to unit damage at lower-than-expected drifts.
- The assessment guidelines do not treat beta units differently from any other units and consequently an engineer may miss identifying the vulnerability of these units, potentially leading to a retrofit design which does not fully address the higher risks posed by such units (Mostafa et al. 2022a).

7 CONCLUSION

The major floors damage observations of a case study building with hollow-core floors subjected to design-level ground shaking during the 2016 Kaikoura Earthquake have been presented in this paper. Poor and unexpected performance of precast hollow-core floor units designed according to the current design standard, NZS 3101:2006-A3, was observed. Heavy damage was primarily found in hollow-core units seated either fully or partially on a column, where the precast floor units were subjected to localised deformations to accommodate the deformation of the supporting seismic and gravity systems. A hollow-core unit with transverse soffit cracking and web cracking was observed at the top floor with storey drift levels of approximately 0.6% and 1% longitudinal and transverse to the unit direction, respectively. Preliminary analysis suggests that diaphragm demands due to higher upper-storey floor accelerations may have influenced the occurrence of such damage at such low drift demands. A previously unidentified damage pattern, including both soffit and web cracking, was also repeatedly observed. The observed damage patterns are not directly accounted for in the assessment procedures of the Yellow Chapter of the Assessment Guidelines (MBIE et al. 2018).

Despite the above concerns, the seating detail did suppress the classical hollow-core seismic failure modes (i.e. loss of seating, positive moment failure, and negative moment failure). While significant support ledge spalling was observed, the ledge reinforcement detailing used in this building provided sufficient support length after

spalling. Negative moment failure was not observed. Classical positive moment failure was not observed, albeit transverse cracking at the soffit was observed in association with other forms of damage reported above. No ductile mesh rupture was observed, despite the diaphragm sustaining residual crack widths of approximately 7 mm. The frame damage observed was moderate and generally considered to be repairable.

Based on the observations discussed herein, SESOC, NZSEE, and Engineering NZ have recently advised that "the use of hollow-core floors in new buildings is not considered to represent good structural engineering practice and therefore we do not recommend its use" (SESOC et al. 2021). Furthermore, MBIE is currently initiating public consultation on changes to B1/VM1 such that the seating detail in Figure C18.4 NZS 3101:2006-A3 will not be considered a deemed-to-comply solution.

8 ACKNOWLEDGEMENT

This investigation is supported by the Building Research Association of New Zealand (BRANZ) under Grant No. LR13069 and ReCast project. Thanks goes to Dr. Andrew Stolte and Dr. Max Stephens for their help collecting the data and the Natural Hazards Engineering Research Infrastructure (NHERI) RAPID Facility for providing the BLK360 scanners. The authors would like to thank Prof. Des Bull for his feedback and review of this paper and Will Parker for reviewing this paper.

9 REFERENCES

Boore, D. M., and Bommer, J. J. 2005. "Processing of Strong-Motion Accelerograms: needs, options and consequences." Soil Dynamics and Earthquake Engineering, 25 (2): 93–115. https://doi.org/10.1016/j.soildyn.2004.10.007.

Bradley, B. A., Razafindrakoto, H. N. T. and Polak, V. 2017. "Ground-Motion Observations from the 14 November 2016 M_w 7.8 Kaikoura, New Zealand, Earthquake and Insights from Broadband Simulations." Seismological Research Letters, 88 (3): 740–756. https://doi.org/10.1785/0220160225.

Bull, D. K., Fenwick, R., Fulford, R., Jury, R., Hopkins, D., Lawrance, G., McSaveney, L., Pampanin, S., Smith, A. and Smith, P. 2009. Seismic Performance of Hollow Core Floor Systems Guidelines for Design Assessment and Retrofit.

Bull, D., and Matthews, J. 2003. Proof of Concept Tests for Hollowcore Floor Unit Connections. 84. Research Report. New Zealand: University of Canterbury.

Corney, S., Puranam, A., Elwood, K. J., Henry, R. S. and Bull, D. 2021. "Seismic Performance of Precast Hollow-Core Floors: Part 1—Experimental Data." SJ, 118 (5). https://doi.org/10.14359//51732821.

CSI Limited. 2017. "CUSP-Ms RS422 Structural Monitoring System Technical Manual."

Dominion Post. 2013. "BNZ Harbour Quays building Closed After Quake." 2013.

Fenwick, R., Bull, D. and Gardiner, D. 2010. Assessment of Hollow-Core Floors for Seismic Performance. 152P. Research Report. New Zealand: University of Canterbury.

GeoNet. 2013a. "M_w 6.5 Cook Strait Sun, Jul 21 2013." Accessed June 22, 2021. https://www.geonet.org.nz/earthquake/technical/2013p543824.

GeoNet. 2013b. "M_w 6.6 Lake Grassmere Fri, Aug 16 2013." Accessed June 22, 2021. https://www.geonet.org.nz/earthquake/technical/2013p613797.

GeoNet. 2016. "M_w 7.8 Kaikōura Mon, Nov 14 2016." Accessed June 22, 2021. https://www.geonet.org.nz/earthquake/technical/2016p858000.

Hamling, I. J., Hreinsdóttir, S., Clark, K., Elliott, J., Liang, C., Fielding, E., Litchfield, N., Villamor, P., Wallace, L., Wright, T. J., D'Anastasio, E., Bannister, S., Burbidge, D., Denys, P., Gentle, P., Howarth, J., Mueller, C., Palmer, N., Pearson, C., Power, W., Barnes, P., Barrell, D. J. A., Van Dissen, R., Langridge, R., Little,T., Nicol, A., Pettinga, J., Rowland, J. and Stirling, M. 2017. "Complex Multifault Rupture During the 2016 M_w 7.8 Kaikōura Earthquake, New Zealand." Science, 356 (6334): eaam7194. https://doi.org/10.1126/science.aam7194.

Hasan, M. D., Ahmad, Z. A. B., Leong, M. S. and Hee, L. M. 2018. "Enhanced Frequency Domain Decomposition Algorithm: A Review of a Recent Development for Unbiased Damping Ratio Estimates." Journal of Vibroengineering, 20 (5): 1919–1936.

Henry, R. S.,Dizhur, D., Elwood, K. J.,Hare, J. and Brunsdon, D. 2017. "Damage to Concrete Buildings With Precast Floors During The 2016 Kaikoura Earthquake." BNZSEE, 50 (No.2): 174–186.

Hoisington, R. W., Rabbat, B. G., Clark,T. H., Nijhawan, J. C., Coenen, V., Patel, I. C., Stephen, D. D., Scalia, D., Henry, J. B., Snow, J. D. and Sturm, E. R. 1983. "Fabrication and Shipment Cracks in Prestressed Hollow-Core Slabs and Double Tees." PCI journal, 28 (1).

Kaiser, A., Balfour, N., Fry, B., Holden, C., Litchfield, N., Gerstenberger, M., D'Anastasio, E., Horspool, N., McVerry, G., Ristau, J., Bannister, S., Christophersen, A.,Clark, K., Power, W., Rhoades, D.,Massey, C., Hamling, I., Wallace, Mountjoy, L. J., Kaneko Y., Benites, R., Van Houtte, C., Dellow, S., Wotherspoon, L., Elwood, K. and Gledhill, K. 2017. "The 2016 Kaikōura, New Zealand, Earthquake: Preliminary Seismological Report." Seismological Research Letters, 88 (3): 727–739. https://doi.org/10.1785/0220170018.

Lindsay, R. 2004. "Experiments On The Seismic Performance Of Hollow-core Floor Systems In Precast Concrete Buildings." Masters of Engineering. Christchurch, New Zealand: University of Canterbury.

MacPherson, C. 2005. “Seismic Performance And Forensic Analysis Of a Precast Concrete Hollow-core Floor Super-assemblage.” Masters of Engineering. Christchurch, New Zealand: University of Canterbury.

MBIE. 2021. Acceptable Solutions and Verification Methods For New Zealand Building Code Clause: B1 Structure. New Zealand: Ministry of Business, Innovation and Employment.

MBIE, EQC, NZSEE, SESOC, and NZGS. 2018. “Technical Proposal to Revise the Engineering Assessment Guidelines- PART C5 -Concrete buildings.” The Seismic Assessment of Existing Buildings. New Zealand.

McHattie, S. A. 2013. “Seismic Response of The UC Physics Building in The Canterbury Earthquakes.” New Zealand: University of Canterbury.

Mostafa, M., Büker, F., Hogan, L. S., Elwood, K. J. and Bull, D. 2022a. “Seismic Performance of Precast Hollow-core Units Seated Within the Plastic Hinge Region.” New Zealand Society for Earthquake Engineering. New Zealand: Proceedings of the 2022 NZSEE Annual Technical Conference.

Mostafa, M., Hogan, L. S., Stephens, M., Olsen, M. J. and Elwood, K. J. 2022b. “A Detailed Damage Investigation of an Instrumented Building Damaged During the M_w 7.8 Kaikoura Earthquake (In development).” Earthquake Spectra.

Peeters, B., and De Roeck, G. 1999. “Reference-Based Stochastic Subspace Identification for Output-Only Modal Analysis.” Mechanical Systems and Signal Processing, 13 (6): 855–878.

Puranam, A., S. Corney, Elwood, K. J., Henry, R. S., and Bull, D. 2021. “Seismic Performance of Precast Hollow-Core Floors: Part 2—Assessment of Existing Buildings.” SJ, 118 (5). https://doi.org/10.14359/51732822.

Seismosoft. 2016. SeismoSignal - A computer program for signal processing of time-histories.

SESOC, NZSEE, and ENZ. 2021. “Advice on Hollow-core Floors.” Accessed January 22, 2022. https://www.sesoc.org.nz/precast-flooring-resources/.

Siddiqui, U., Parker, W., Davey, R. and Therkleson. S. 2019a. “Seismic Response of BNZ Building in Wellington Following The 2016 Kaikoura Earthquake.” Auckland, New Zealand.

Siddiqui, U., Parker, W., Davey, R., Therkleson, S. and Ma., Q. 2019b. “Methodologies to Assess and Quantify Earthquake Damage: A Damage Assessment Case Study of The BNZ Building in Wellington Following The 2016 Kaikoura Earthquake.” Auckland, New Zealand.

Standards New Zealand. 2016. Structural design actions. New Zealand Part 5, Part 5. (NZS 1170.5).

Standards New Zealand. 2017. Concrete structures standard. Part 1: The Design of Concrete Structures. Part 2: Commentary on the Design of Concrete Structures. (NZS 3101.1:2006 & NZS 3101.2:2006).

Uma, S. R., King, A.,Cousins, J. and Gledhill,K. 2011. “The Geonet Building Instrumentation Programme.” NZSEE, 44 (1): 53–63.

Van Houtte, C., Bannister, S., Holden, C., Bourguignon, S. and McVerry, G. 2017. “The New Zealand Strong Motion Database.” NZSEE, 50 (1): 1–20.

SESOC SOFTWARE

Software can be found on the SESOC Webpage: sesoc.org.nz/software/.

MemDes NEW UPDATE

MemDes – Version v4.0 is now available on the SESOC website. Improvements include:

- Customised properties for standard sections
- User and project libraries of saved custom sections
- User-specified fy for custom welded beams
- Output calculations to PDF; improved calculation formatting
- Batch mode allowing multiple analyses in a single run
- Various technical and UI improvements.

SOFTWARE LICENSE ACTIVATION

- The SESOC License Key can now be found on the SESOC webpage. Details on how to activate software can be found at https://www.sesoc.org.nz/software/licensing-support/
- Please note that SESOC allows members two activations each, eg one in the office, and one at home.
- However, when upgrading a PC the user is advised to uninstall each of the SESOC software programs from off the old PC – this will release the activation back to the pool, otherwise contact software@SESOC.org.nz to remedy the problem.

ISSN No. 2744-7871

REAL WORLD EXPERIENCE OF SEISMIC PERFORMANCE AND RETROFITS USED IN BUILDINGS WITH HOLLOW-CORE FLOORS

Liu, A.[1], Hogan, L. S.[2], Henry, R. S.[2], Brooke, N. J.[3]

ABSTRACT

Hollow-core floors have been recognised to have a potentially poor seismic performance since the 1994 Northridge earthquake, with subsequent research leading to significant developments in design and detailing requirements. Damage evaluations after the 2016 Kaikōura earthquake confirmed the expected seismic vulnerabilities in existing precast hollow-core floors and also revealed some previously unknown behaviour types. The Kaikōura earthquake provided significant impetus to advance our understanding of seismic performance of existing buildings with hollow-core floors and suitable retrofit solutions. Subsequently, the ReCast floors research programme was initiated. The reported work is one component of the ReCast floors programme in which investigations of the real-world performance of buildings with hollow-core floors was conducted. The objective was to collate information on damage patterns observed in buildings following the Kaikōura earthquake, the engineering characteristics of existing Wellington buildings with hollow-core floors, current strengthening status and the retrofit solutions implemented to help inform the ReCast research activities.

1 INTRODUCTION

Floors are integral parts of a building structure, and they play a significant role to meet life-safety objectives when subjected to different loading conditions. When considering gravity loads, the floors transfer vertical floor loads to the supporting members and also act to provide lateral restraint to ensure stability of vertical members, such as columns and walls. During earthquakes the floors also act as diaphragms to transfer the seismic actions across the buildings to lateral load resisting systems. As such, floors can be subjected to significant direct and indirect seismic actions. Direct actions result from the loads on floors, and indirect actions result from deformation compatibility between the supporting systems and the floors. The latter presents a great challenge for buildings with precast hollow-core floors that are stiff and brittle.

Hollow-core floors consist of precast hollow-core floor units and thin in-situ reinforced concrete topping. Although precast hollow-core floor units are one-way spanning elements between supporting members, the floor acts as a diaphragm in all directions to transfer seismic actions across the building in an earthquake. The diaphragm action of the floors is achieved by a thin in-situ reinforced concrete topping slab, where short starter bars are usually provided from the topping to the supporting members along the edges of the floors, thus creating some degree of continuity along the slab edges.

There are many potential issues for hollow-core floor systems. Firstly, there are significant deformation incompatibility issues between one-way spanning hollow-core units and the two-way functioning in-situ topping slabs. This deformation incompatibility will induce shear actions between hollow-core units as well as between hollow-core units and in-situ slabs. The actions introduced to the floors could cause damage or failure to the precast hollow-core units. The local damage/failure of the floor systems could result in a localised collapse of the floor in addition to the loss of the lateral restraints to gravity supporting systems, leading to the instability of the primary supporting systems. Such damage could lead to progressive failure/collapse of the entire building. Therefore the vulnerabilities of hollow-core floors need to be addressed when assessing the seismic response and implementing retrofit or strengthening measures.

Concerns about the seismic integrity of precast concrete hollow-core floors constructed in New Zealand were raised following damage to similar floors during the Northridge earthquake in 1994. As a result, a research programme was funded to investigate the seismic behaviour of buildings with hollow-core floors constructed at that time (Matthews 2004, Lindsay 2004, Macpherson 2005, Jensen 2006, Wood 2008). One project of this research programme was the simulated cyclic loading

PAPER CLASS & TYPE: GENERAL REFEREED

1 Building Research Association of New Zealand
2 Dept. of Civil and Environmental Engineering, University of Auckland
3 Compusoft Engineering Limited, Auckland

test on a full-scale super-assembly of hollow-core floors supported by reinforced concrete frames, undertaken at the University of Canterbury (Matthews, 2004). The supporting details used in the test simulated the common practice in buildings constructed prior to 2003 using a 300 mm deep hollow-core floor. The test confirmed that hollow-core floors detailed at that time could be vulnerable in earthquakes and the observed evidence indicated serious gaps between assumed and actual behaviour of hollow-core floors of ductile frame buildings during strong earthquakes.

The Kaikōura earthquake in 2016 provided a reality check of existing buildings with precast floors. Partial collapse of precast concrete floors in the Statistics Building caused serious concerns about seismic resilience of buildings with precast floors (MBIE 2017, 2018), especially when the primary lateral load resisting systems are ductile frames. In response to these concerns, Wellington City Council established a Targeted Assessment Programme and a total of 64 mid-rise (5 to 15 storey high) reinforced concrete frame buildings with precast floors were assessed (Brunsdon et al., 2017).

An earthquake damage survey from the Targeted Assessment Programme revealed that hollow-core floors were more vulnerable to earthquake damage compared with other precast floor systems. The observed damage patterns confirmed the seismic vulnerabilities of older precast hollow-core floors as revealed in Matthews's test, and also revealed some previously unknown behaviour types (Henry et al., 2017). This brought about the realisation that reasonably modern buildings with hollow-core floors constructed before the mid 2000s may still experience significant damage and/or suffer collapse of the floors during a design level earthquake and potentially become the new class of vulnerable buildings in earthquakes.

Assessing the likely performance of precast floors presented a significant challenge for engineers. MBIE established a working group after the Kaikōura earthquake to revise and improve the available guidance for assessing precast floors. This guidance relied heavily on previous guidelines developed from research at the University of Canterbury (Fenwick 2010) as well as findings from the Canterbury and Kaikōura earthquakes. The guidance was included as an appendix to the technical proposal to revise Section C5 (Concrete Buildings) of the "Guidelines for Detailed Seismic Assessment of Buildings" (MBIE et al., 2018). Despite improved seismic assessment guidance, engineers also required urgent direction on appropriate retrofit approaches to address the identified vulnerabilities with precast floors. As a result the ReCast research programme was initiated (Brooke et al., 2019). As part of the programme, there was a need to understand the existing retrofits being implemented by the industry to help inform the research direction. This paper details the investigation into the retrofits installed in hollow-core buildings in Wellington at the initiation of the ReCast floors project and included three objectives:

- To use the real-world experience from damage during the Kaikōura earthquake to help characterise the failure modes of hollow-core floors that require further investigation;
- To gain insights into the engineering characteristics of existing buildings with hollow-core floors to help inform the lab-based research and theoretical simulations; and
- To gain insights into currently implemented retrofit solutions associated with hollow-core floors.

2 CHARACTERISTICS OF EARTHQUAKE DAMAGE

2.1 GENERAL

A huge engineering effort was made during the Targeted Assessment Programme to assess seismic damage of the existing buildings with precast concrete floors in Wellington. The work within the Targeted Assessment Programme provided a large amount of valuable information. However much of the information collected remains confidential with only high level statistical information reported (Brunsdon et al., 2017). Surveying earthquake damage in buildings of interest was extremely difficult because of many concerns including health and safety. Consequently the intended effort for conducting the real-world investigations into Wellington buildings with hollow-core floors had many challenges.

To characterise the earthquake damage patterns observed in hollow-core floors at component level and global performance level, input was sought after the Kaikōura earthquake from engineers who had real-world experience in evaluating buildings with hollow-core floors. Input was also sought from contractors who were involved in demolishing or strengthening buildings with hollow-core floors. The engineering professionals provided insights into damage patterns in hollow-core floors and insights into the effects of global structural characteristics of a building on seismic damage in hollow-core floors, these insights not being easy to obtain from lab testing.

2.2 CHARACTERISTICS OF DAMAGE OBSERVATION IN HOLLOW-CORE FLOORS

Many of the damage patterns discussed with the engineers were covered previously in the report by Henry et al (2017). However, engineers and contractors also

highlighted other damage characteristics that were not previously reported, as follows:

- **Hidden web cracking and/or splitting of hollow-core floors**

Web cracking and web splitting is typically not visible from an external inspection. In a few buildings with no visible damage to hollow-core units, engineers confirmed the presence of web cracking/splitting by conducting investigations using borescope cameras.

- **Web cracking/splitting associated with incompatibility of the supporting systems**

A commonly reported phenomenon was that web cracking/web splitting was often associated with incompatible supporting systems at two ends of hollow-core units. For instance, hollow-core units that were supported by concrete frames at one end and block walls at the other end, or seismic resisting frames at one end and gravity frames at the other end. Incompatible supporting systems at the two support ends of hollow-core units may introduce torsion to the units, contributing to the damage to hollow-core webs.

- **Units supported on concrete masonry wall**

It was observed that there was severe damage to reinforced concrete masonry walls in buildings with reinforced concrete frame as the primary load resisting system. The damage included spalling/crushing of the reinforced concrete masonry walls in the areas supporting the precast floor units and severe diagonal shear cracking to the masonry walls.

The observed spalling or crushing in the areas supporting precast floor units occurred because concrete masonry units have much lower bearing strength than normal concrete members. Although not directly addressed in existing guidance, testing of precast ribs supported on masonry walls has confirmed increased spalling (Corney 2018). This suggests that seismic retrofit solutions designed to enhance the masonry wall supports to hollow-core floor units may need to be different from the solutions developed with concrete supporting members.

- **Irregularity effects**

The structural irregularity in buildings with hollow-core floors often caused significantly amplified seismic damage in some parts of the buildings and exacerbated damage not only in the lateral load resisting systems but also in the precast floors. In comparison, engineers commented that regular arrangements of lateral seismic resisting frames often resulted in much less damage to frames, although the damage to hollow-core floors sometimes was still significant because of the large building deflections caused by the high ductility used in design.

3 STRUCTURAL CHARACTERISTICS OF PRE-2006 CONCRETE BUILDINGS

To help inform the wider ReCast research programme, the structural characteristics of pre-2006 concrete buildings with hollow-core floors were categorised by searching and studying consent documents of buildings with hollow-core floors in Wellington. In total 165 existing concrete buildings with hollow-core floors were collated with the help from Wellington City Council (WCC) staff. The findings are summarised as follows:

- **Precast hollow-core floor systems and their support details**

The most common precast hollow-core floor systems used 200 series hollow-core units and had 50 mm to 70 mm concrete topping reinforced with cold-drawn mesh. Specified seating lengths of the hollow-core floor units varied greatly and they could be as small as 30 mm.

Starter bars were commonly grade 300 reinforcing bars of 12 mm in diameter, spaced at between 300 mm to 600 mm centre to centre. At the support ends of the hollow-core floor units, starter bars often stopped at a distance of 300 mm to 600 mm from the support edge.

Of significant concern is the uncertainty associated with hollow-core floors supported by concrete masonry walls as shown in Figure 1, which was observed in ~10% of the buildings surveyed. Masonry walls have significantly lower bearing capacities and lower stiffness and premature spalling of the masonry face shell supporting the hollow-core floor could easily occur.

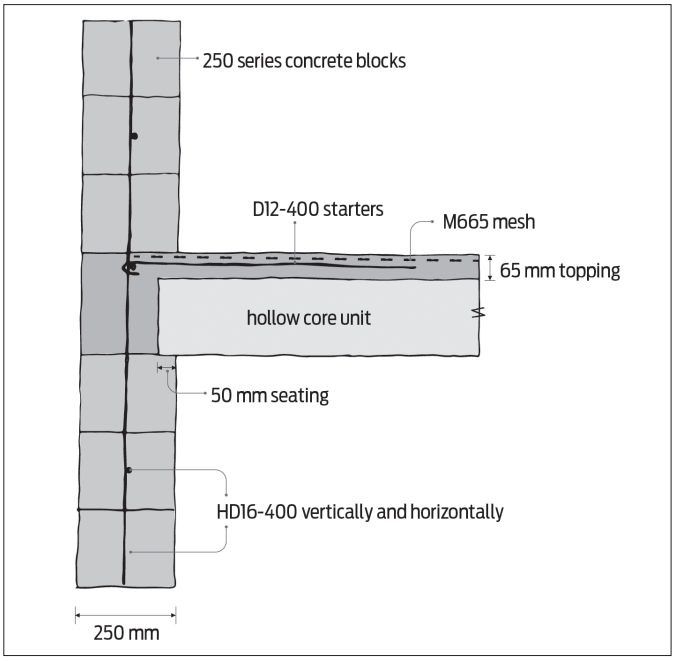

Figure 1: Concrete masonry walls supporting hollow-core floors

- **Pre-2006 concrete frame buildings**

For most pre-2006 reinforced concrete frame buildings, perimeter frames were seismic resisting systems and designed to a high ductility while internal frames were gravity load resisting systems, as shown in Figures 2 and 3. The different bay spacing between the gravity and seismic frames means that the two ends of a hollowcore unit supported at mid-span of a gravity frame and the plastic hinge zone of a perimeter seismic frame would experience differential rotations/movements. Such differential twisting in earthquakes would induce torsional responses, causing damage within individual hollowcore units or in the toppings.

In the case of a long narrow building subjected to shaking along the short direction, floor diaphragms need to bring the seismic actions from the floors to the lateral resisting systems spaced at a large distance. In such cases the floor diaphragms could be expected to have severe cracking in the floors, leading to large in-plane deflections as demonstrated in some earthquake damaged buildings in Wellington.

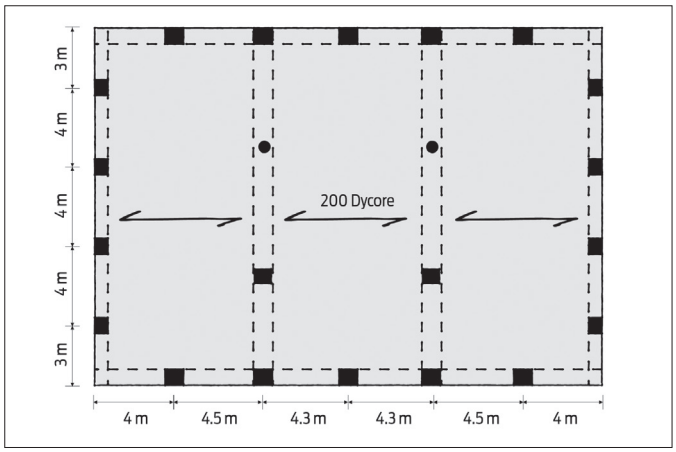

Figure 2: A typical floor plan of a 10-level building

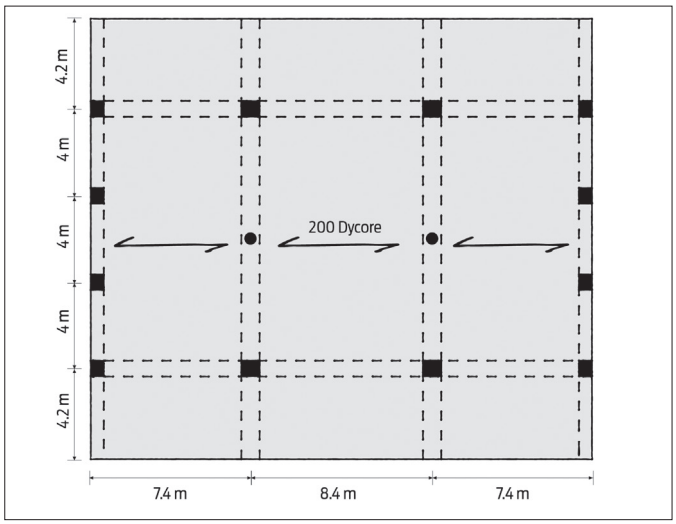

Figure 3: A typical floor plan of a 16-level building

- **Precast hollow-core units spanning multiple bays of moment resisting frames**

It was common in pre-2006 construction for hollow-core units to span parallel to two spans of moment resisting frames. This happens because the frame bay widths of seismic resisting frames along the perimeters are often much smaller than the spacing of internal gravity frames, as illustrated in Figure 2. The consequence is that hollow-core units need to accommodate the beam elongations from all the plastic hinges in the two frame spans. This significantly increases the deformation demands and risk of support loss in earthquakes and also exacerbates deformation incompatibility with the alpha slab adjacent to the frames (Fenwick et al. 2010).

- **No corner columns and structural irregularities**

It was not uncommon to find existing buildings that were designed as a ductile frame system with no corner columns, as shown in Figures 2 to 3. Such an arrangement potentially could substantially amplify the damage to the floors around the corners in earthquakes. If the building also has an irregular floor plan, for example, as shown in Figure 4, extra precautions need to be taken. This is because one end of the hollow-core units needs to be cut at an oblique angle to fit into the floor shape and, therefore, the construction tolerance at that end could compromise the seating length significantly. In other words, this structural irregularity would further increase the chance for support loss failure of some units adjacent to the corners.

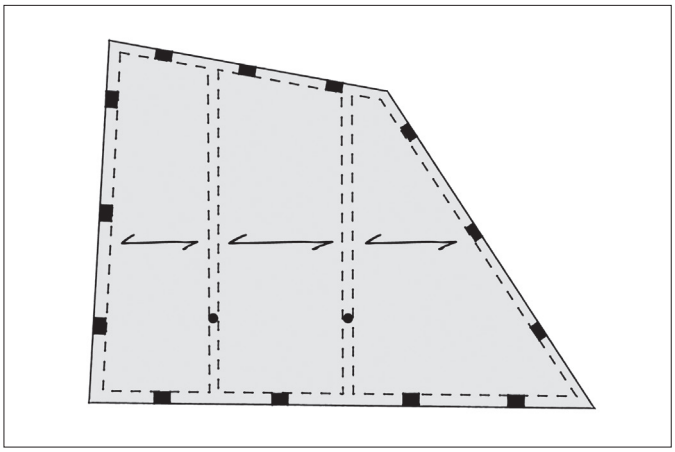

Figure 4: An irregular floor plan with no corner

4 SEISMIC RETROFIT OF EXISTING BUILDINGS WITH HOLLOW-CORE FLOORS

4.1 RETROFIT STATUS

Among the 165 existing buildings included in this study, 15 buildings had floor strengthening completed at the start of the ReCast program (2019), this representing less than 10% of them. Most of the floor strengthening was only in the form of providing supplementary floor unit seating by adding steel members (steel angles or steel hollow sections) 10 mm to 20 mm below the hollow-core floor soffit.

Clearly only a small portion of existing concrete buildings with hollow-core floors had been strengthened as of 2019 and concerningly there were many examples where seismic strengthening had been undertaken for the primary lateral load resisting systems without making effort to retrofit the hollow-core floors. For instance, many buildings with precast floors have undergone seismic strengthening by adding braced frames or walls but with no retrofits to address the floor vulnerabilities. The reason for the low strengthening efforts for the floors could be due to either of two reasons:

- Prior to 2010, no credible guidance documents for assessing and strengthening buildings with hollow-core floors were available, or
- After 2010, when relevant assessment guidance (Fenwick et al. 2010) was published, industry uptake of this guidance was slow.

4.2 RETROFIT METHODS

In general, currently used seismic retrofit solutions implemented in existing buildings with hollow-core floors could be classified into two broad categories: local behaviour improvement and global behaviour improvement.

Local behaviour improvement measures included enhancement of hollow-core floor seating by adding steel angles or steel hollow members either hard against floors or with a gap (10 mm to 20 mm) to the floors, as shown in Figure 5. It should be noted that testing by Liew (2004) and Parr (2019) showed that when stiffened angles or steel hollow members (e.g. SHS or RHS) are installed hard up against the soffit of the unit, that these retrofits can inadvertently trigger a negative moment failure in some cases. Additionally, it is acknowledged that many of the older seating retrofits do not provide an effective retrofit against positive moment failure (Brooke et al. 2022).

Additional local behaviour retrofits included adding catch frames for hollow-core alpha units (see Figure 6) and enhancing composite action for hollow-core alpha units by adding dowels (see Figure 7). In isolated cases seismic strengthening was undertaken after the Kaikōura earthquake due to the observed transverse cracks at

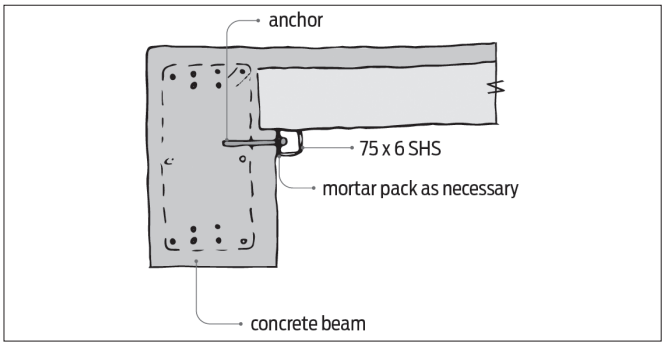

Figure 5: Supplementary seating

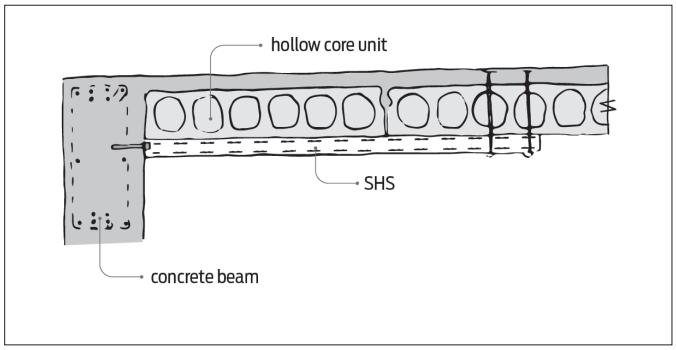

Figure 6: Catch frames to alpha units columns

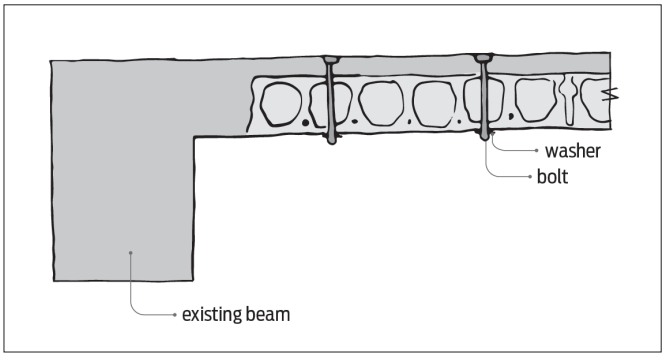

Figure 7: Ties through topping and units

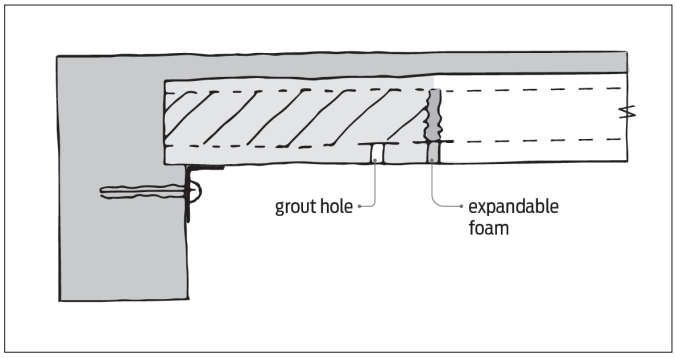

Figure 8: Grouting of hollow-core at supports

the bottom of the hollow-core floor units close to the supports. An example strengthening method is shown in Figure 8, where the hollow-core cells at their supports were grouted with no added reinforcement. The filling of cores has been recommended against since the publication of the document by Bull et al (Bull et al. 2009). Further discussion on the issues of filling cores as a retrofit or repair technique are described in the companion paper by Brooke et al. (2022).

Global behaviour improvement measures were designed to address the undesirable global performance issues such as unpredictable torsional issues in irregular structures, progressive failures caused by instabilities of corner columns or non-ductile gravity columns as well as inadequate diaphragm capacity of the floors. Examples of the global behaviour improvements included:

- Provision of new seismic resisting systems to reduce the lateral drifts or reduce torsional responses in irregular buildings;
- Addition of ties which restrain the perimeter columns into the floors;
- Provision of linkage from the internal gravity columns to the floor;
- Wrapping the non-ductile gravity columns using FRP (fibre-reinforced polymer);
- Provision of extra floor frame members in the cases of no corner columns;
- Enhancement of floor diaphragms by providing extra capacity based on analysis.

5 CONCLUSIONS

The real-world investigations formed an important research area of the ReCast project and the objective was to use real-world experience to help inform other research activities. The work reported in this paper was one element of the real-world investigations conducted to gain insights into the critical issues affecting the seismic performance of hollow-core floors. The issues studied included

(1) Earthquake damage to existing buildings with hollow-core floors in the Kaikōura earthquake;

(2) Engineering characteristics of pre-2006 buildings with hollow-core floors; and

(3) Current strengthening status and retrofit solutions implemented for hollow-core floors.

With regard to earthquake damage vulnerabilities of hollow-core floors, the findings are that:

- Web cracking or splitting of hollow-core floor units may not be visible and different supporting systems at the two support ends of the hollow-core units may increase the likelihood of inducing web cracking/ splitting.
- Spalling and loss of support would be more likely to occur if hollow-core floors are supported by reinforced concrete masonry walls. As such, retrofit solutions for hollow-core floors supported by block walls may need to be different from the solutions for reinforced concrete supporting members.
- Structural irregularities could significantly exacerbate earthquake damage around building corners.

As for engineering characteristics of pre-2006 frame buildings with hollow-core floors, the findings are that:

- It is common that perimeter frames of a concrete frame building were the lateral seismic resisting systems while internal frames were gravity resisting systems. As a result, the two ends of precast hollow-core floor units were supported by the structural systems of very different stiffness, potentially causing significant torsional response of the units in earthquakes.
- Hollow-core floor units often span parallel to two bays of lateral seismic resisting frames, thus increasing the deformation demands due to beam elongation and risk of support loss.
- Perimeter seismic resisting frames have no corner columns in many concrete frame structures.

As for the retrofit solutions used for hollow-core floors, the findings are that:

- Only a limited number of buildings in Wellington have received seismic strengthening due to the lack of technical retrofit guidance at the time of the investigation.
- The seismic retrofit methods used in strengthening the existing buildings with hollow-core floors have two broad categories: local behaviour improvement and global behaviour improvement.
- Local behaviour improvement solutions were primarily designed to address support loss of hollow-core units and prevent alpha units from collapsing. Retrofits for other failure modes had not been confirmed.
- Global behaviour improvement solutions varied significantly, including mitigating adverse effects related to some well-known structural behaviour at global performance level, such as high drift demands, torsional responses and progressive failures caused by column instability.

6 ACKNOWLEDGEMENTS

This research project was funded by the Building Research Levy. The authors would like to acknowledge the support from Wellington City Council and the wider engineering community.

7 REFERENCES

Matthews, J. 2004. Hollow-Core Floor Slab Performance Following a Severe Earthquake, PhD Thesis, Dept. of Civil Engineering, University of Canterbury, Christchurch, New Zealand.

Lindsay, R., Mander, J.B. & Bull, D.K. (2004). Experiments on the Performance of Hollow-core Floor Systems in Precast Concrete Buildings. Proceedings 13th World Conference on Earthquake Engineering, Vancouuver, Canada

MacPherson, C. 2005. Seismic Performance and Forensic Analysis of Precast Concrete Hollow-Core Floor Super-Assemblage, ME thesis, Dept. of Civil Engineering, University of Canterbury, Christchurch, New Zealand.

Jensen, J. 2006. The Seismic Behaviour of Existing Hollow-Core Seating Connections Pre and Post Retrofit, ME thesis, Dept. of Civil Engineering, University of Canterbury, Christchurch, New Zealand.

Woods, L. 2008. The Significance of Negative Bending Moments in the Seismic Performance of Hollow-Core Flooring, ME thesis, Dept. of Civil Engineering, University of Canterbury, Christchurch, New Zealand.

MBIE (2017) Investigation into the Performance of Statistics House in the 14 November 2016 Kaikoura Earthquake. Ministry of Business, Innovation, and Employment, Wellington, New Zealand. 36p.

MBIE (2018) Addendum: Investigation into the Performance of Statistics House in the 14 November 2016 Kaikoura Earthquake. Ministry of Business, Innovation, and Employment, Wellington, New Zealand. 25p.

Brunsdon, D., Elwood, K. J., and Henry, R. S. (2017) Wellington City Council Targeted Assessment Programme following the Kaikoura Earthquake of 14 November 2016 Technical Report (Kestrel WCC TAP Technical Report 20170507). Kestrel Group, Wellington, New Zealand. 60p.

Henry, R.S., Dizhur, D., Elwood, K.J., Hare, J. & Brunsdon, D. 2017. Damage to Concrete Buildings with Precast Floors During the 2016 Kaikoura Earthquake, Bulletin of the New Zealand Society for Earthquake Engineering, Vol 50(2) 174-186.

Fenwick, R., Bull, D., & Gardiner, D. (2010). Assessment of Hollow-Core Floors for Seismic Performance (Research Report No. 2010–02; p. 152). University of Canterbury. https://ir.canterbury.ac.nz/handle/10092/4211

MBIE, EQC, NZSEE, SESOC, and NZGS. 2018. Technical Proposal to Revise the Engineering Assessment Guidelines - Part C5 Concrete Buildings. Wellington, New Zealand. http://www.eq-assess.org.nz/

Brooke, N, J., Elwood, K. J. Bull, D.K., Liu, A., Henry, R.S., Sullivan, T., Hogan, L. S., del Rey Castillo, E. (2019), ReCast Floors - Seismic assessment and improvement of existing precast concrete floors, SESOC Journal, Volume 32 Issue 1.

Corney, S. (2018). Seismic Performance of Precast Concrete Flooring Systems, PhD thesis, Dept. of Civil and Environmental Engineering, University of Auckland.

Liew, H. Y. (2004). Performance of Hollow-core Floor Seating Connection Details (Master's Thesis). The University of Canterbury, Christchurch, New Zealand, 278p.

Parr, M., Bueker, F., Elwood, K. J., Hogan, L. S., Henry, R. S., Puranam, A., Bull, D. K. and Brooke, N. J. (2019). Development and Testing of Retrofit Solutions for Hollow-core Floors in Existing Buildings. Proc. Concrete New Zealand Conference, Concrete New Zealand Learned Society, Dunedin, New Zealand.

Brooke, N.J., Büker, F., Bull, D. K., Elwood, K. J., Henry, R. S., Hogan, L. (2022), Overview of Retrofit Requirements and Methods for Precast Concrete Floors, SESOC Journal, Volume 35 Issue 1.

Bull, D. K., Fenwick, R., Fulford, R., Jury, R., Hopkins, D., Lawrance, G., McSaveney, L., Pampanin, S., Smith, A. & Smith, P. (2009). Seismic Performance of Hollow-core Floor Systems Guidelines for Design Assessment and Retrofit. https://www.nzsee.org.nz/db/PUBS/HollowCoreFloorSystems.pdf

MEMBERS TIPS AND TRICKS

SESOC are seeking members' Tip and Tricks for inclusion in the SESOC Journal. If you have any invaluable tip, tricks or 'traps for young players' that you've encountered over the years and would like to share these with members, please email them to Journal Editor, Stewart Hobbs, at journal@sesoc.org.nz

ISSN No. 2744-7871

TORSIONAL CAPACITY ASSESSMENT OF PRECAST HOLLOW-CORE FLOORS

Mostafa, M.[1,*], Hogan, L.[2], Elwood, K.J.[3]

ABSTRACT

Estimation of the torsional capacity of precast hollow-core floor units is required as a step for assessing the expected seismic performance of these floors according to the seismic assessment procedure followed in New Zealand. Due to limited research on the torsional behaviour of hollow-core units, there are multiple uncertainties regarding the accuracy of the procedure currently used to assess the torsional capacity of hollow-core floors. This paper discusses the basis and limitations of the procedure adopted in the New Zealand assessment guidelines (C5) for quantifying the torsional capacity of hollow-core floor units, describes potential implications of the limitations of the available methodology on the assessed torsional capacity accuracy and potential impact on other hollow-core seismic failure modes, and provides a twist-limits chart as a simple tool to assess the torsional deformation capacity of typical hollow-core unit depths based on the methodology available in the current assessment guidelines. The twist-limits chart provides a useful assessment tool for engineers, but must be used with due consideration of the limitations of the torsional capacity assessment methodology discussed herein. Informing the judgement of how and when to use this twist-limit information in the assessment process, given the limitations and uncertainty of conditions in the field, remains a key challenge for future research on the seismic assessment of precast floors.

1 INTRODUCTION

The lack of shear reinforcement in precast hollow-core floor units due to the extrusion process is the primary reason for the susceptibility of these floors to sustaining severe damage under seismic demands, as described in Fenwick et al. (2010). This lack of shear reinforcement makes hollow-core floor units inherently vulnerable to brittle failure due to the application of torsional demands. Consequently, the torsional capacity of hollow-core units depends significantly on the relatively low angles of twist they can resist before torsional cracking occurs, as once torsional cracking is initiated the flexural and shear strength of the hollow-core floor unit are compromised.

Various studies have been conducted on hollow-core floor units subjected to flexural and shear actions (Walraven and Mercx 1983; Yang 1994; El-Sayed et al. 2019; Michelini et al. 2020). However, little research has been conducted on the behaviour of hollow-core floor units undergoing torsion or shear-torsion actions. Previous research regarding the torsional performance of hollow-core floor units included experimental testing of bare hollow-core units (i.e. without topping) subjected to pure torsion (Pajari 2004a) and shear-torsion demands (Pajari 2004b). The experiment results were then used to validate and calibrate a finite element model (Broo et al. 2007), which was then used in a parametric study where the capacity of 200 mm and 400 mm hollow-core units with different shear and torsion demands were investigated. Then both the experimental and numerical results were compared with the analytical methodology available in the European standard for hollow-core design EN-1168 (British Standards Institution (BSI) 2005) by Broo et al. (2005).

Although previous work has provided some basis for understanding the torsional performance of hollow-core floors, it does not provide enough information regarding the torsional behaviour of hollow-core units in a seismic event in which the torsional demands are induced to the units from the supporting structure through the connection rather than an eccentric gravity load. There is considerable uncertainty about the torsional performance of hollow-core units in floors under seismic demands. This uncertainty is primarily due to limited research and a general lack of information regarding the torsional response of these floor units and lack of information on how different floor to support connections affect the torsional demand induced to the units. Due to the current limited state of knowledge, the current structural concrete design standard, NZS3101:2006, simply contains a caution on using these units where appreciable twisting may occur (clause C9.4.3.6) (Standards New Zealand 2017).

Moreover, many buildings incorporating hollow-core floors, especially those constructed in areas of high seismicity, need to be assessed for their seismic capacity. The torsional capacity of these floor units has to be assessed as part of the seismic assessment procedure (MBIE et al. 2018; Puranam et al. 2021).

PAPER CLASS & TYPE: GENERAL REFEREED

1 Ph.D. Candidate, University of Auckland
2 Lecturer, University of Auckland
3 Professor, University of Auckland
** mohamed.mostafa@auckland.ac.nz*

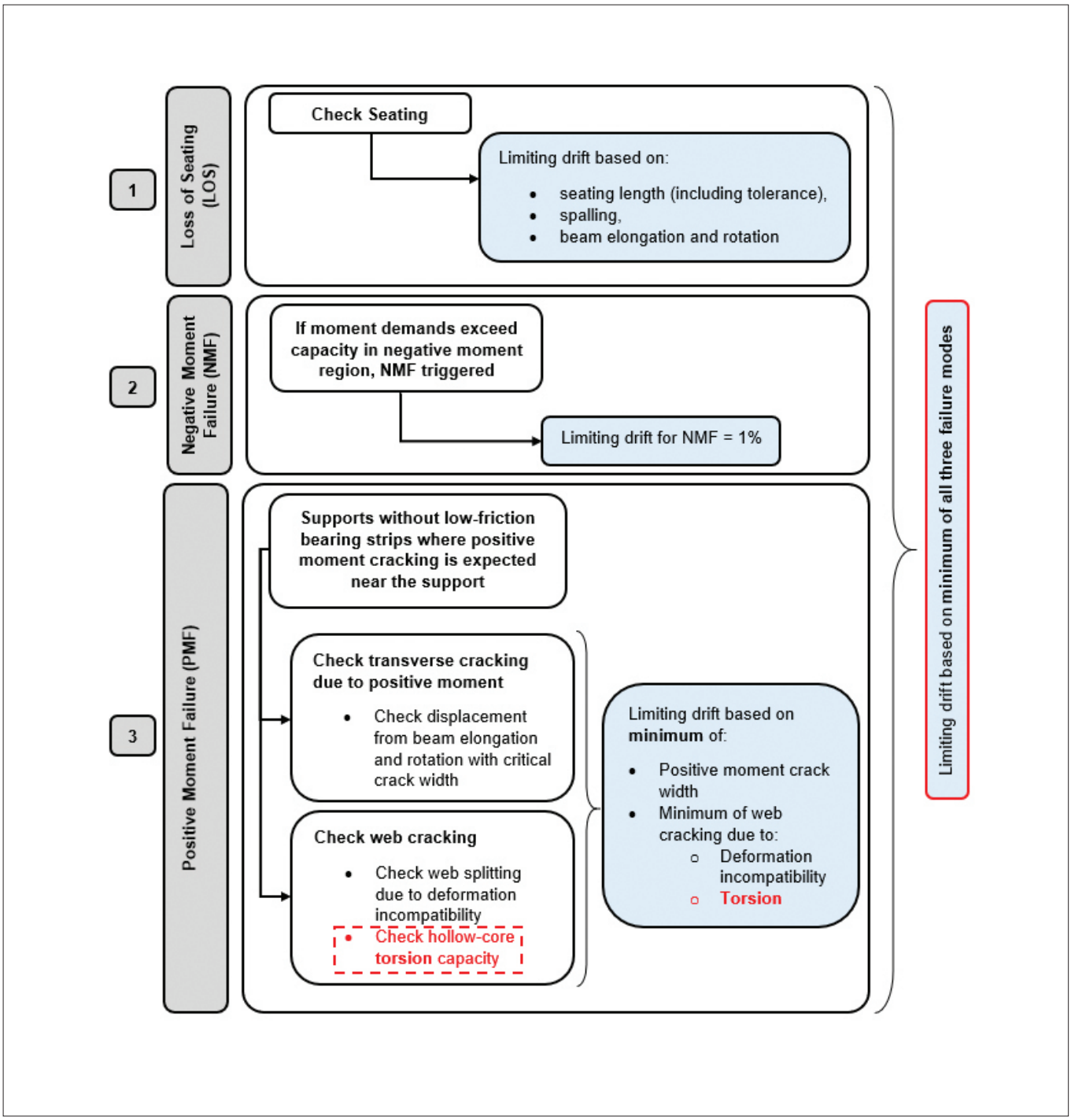

Figure 1: Summary of hollow-core floors assessment procedure according to the New Zealand Seismic Assessment Guidelines (C5) modified from MBIE et al. (2018)

Furthermore, it was noted that hollow-core torsional capacity can result in a low seismic rating of the floor in areas of low seismicity, which can lead to consideration of retrofit. This realisation highlights the importance of better understanding the torsional behaviour of hollow-core floor units as it affects rated performance in low seismic zones, possibly triggering retrofit when the remaining hollow-core failure modes scores were satisfactory.

Currently, the New Zealand seismic assessment guidelines (C5) consider the susceptibility of hollow-core floor units to sustain torsional damage only when web cracking due to torsion is accompanied by transverse cracking through the bottom flange of the hollow-core unit. Hence, torsion is only considered under the positive moment failure check, as shown in Figure 1, instead of treating torsional damage as a potential failure mode itself. It is worth noting

that, currently, checking if a low-friction bearing strip was incorporated in the connection detail is considered a binary check that decides whether or not a unit is deemed susceptible to Positive Moment Failure (PMF) and consequently torsion as well. This binary check is due to the assumption that a low-friction bearing strip suppresses transverse cracking of the bottom flange of the unit.

Torsional demands can be imposed on one or more hollow-core units in floors in multiple situations, more relevantly, where the seismic response of a building could cause twisting (torsion) of these units about their longitudinal axes due to differential rotations of the supporting structure at each end of the unit. Some examples of when significant twisting of the units might occur include but are not limited to:

- One end of a unit supported on a link of an eccentrically braced frame.
- One end of a unit supported on a cantilever beam in buildings with moment resisting frames that do not have corner columns (a and d in Figure 2).
- One end of a unit supported on a coupling beam.
- One end of a unit supported on a shear wall and the other end supported on a frame (b in Figure 2).
- One end of a unit is slanted or supported on a skewed supporting element (c in Figure 2).
- Units supported within the plastic hinge zone of frames with staggered columns, where one end is supported on a column and the other on a beam's plastic hinge (e in Figure 2).
- One end of a unit is supported within the plastic hinge region of a seismic frame, and the other end of the unit is seated intra-span of a gravity frame resulting in different end rotation demands.

This paper provides a twist-limits chart and table as a simple tool for assessing the torsional deformation capacity of different hollow-core unit depths according to the available assessment procedure described in the seismic assessment guidelines C5 (referred to as the 'Yellow Chapter' within the Structural Engineering community in New Zealand) (MBIE et al. 2018). Furthermore, the basis of the assessment methodology adopted in assessment guideline C5 and the assumptions used to determine the torsional capacity are described in this paper. Limitations of the torsional assessment procedure and how these limitations might impact the torsional capacity assessment of the floor are highlighted so that prudence can be practised as necessary when assessing the torsional capacity of these floors.

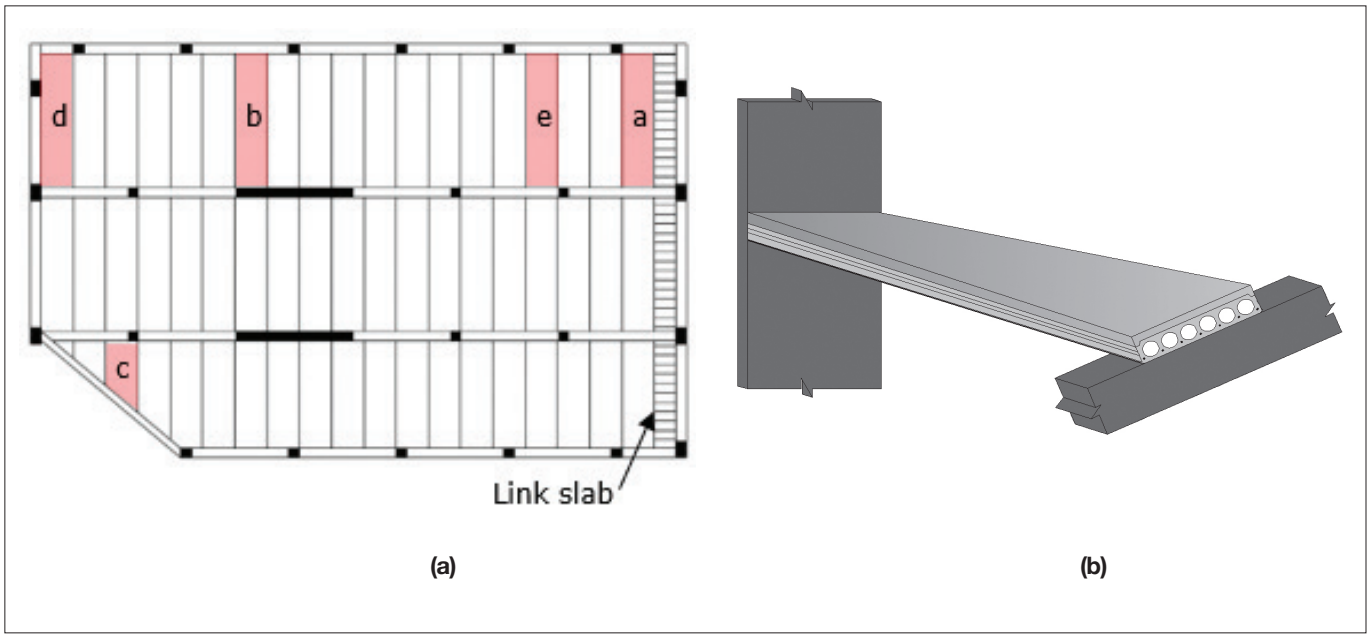

Figure 2: (a) examples of when torsional demands can be induced into a floor unit under due to the seismic response of the building (b) illustrative example

2 HOLLOW-CORE TORSIONAL CAPACITY ASSESSMENT

2.1 BACKGROUND

The torsional limit state for hollow-core units is governed by the twisting angle of the unit about its longitudinal axis, where the critical twisting angle (capacity) should be used to calculate a maximum allowed inter-storey drift at which that critical twist is reached in the unit. The approach adopted in the assessment guidelines C5 uses the principle of stationary total potential energy to relate the unit torsional stiffness to the applied torque, where the limiting twist angle is deduced by equating the work done by the external forces (Equation 1) and the internal strain energy due to the shear force generated in the unit (Equation 2).

$$W = \frac{1}{2} * T * \theta \quad (1)$$

$$U = \frac{1}{2} * F * \gamma \quad (2)$$

Where,

U Strain energy (due to shear)

W Potential energy of the load (work done by torque)

T Torque

θ Angle of rotation of the hollow-core unit about its longitudinal axis

F Shear force due to the shear flow generated in the unit as a result of the unit twisting/torsion

γ Shear strain

Whilst shear demands from gravity loads are assumed to be uniformly distributed along the hollow-core unit webs as shown in Figure 3a, when a unit is subjected to torsion the shear stresses are primarily generated in the perimeter of the section. Hence it is reasonable to analyse the section as a thin-walled tube in which torsion is resisted by a shear flow as shown in Figure 3b. Bredt's thin tube theory, as explained in Collins & Mitchell (1997), is used to theoretically estimate the hollow-core torsional cracking moments. The expression used in the assessment guidelines C5 is given by (Equation 3).

$$q = \frac{T}{2A_o} = \tau * t \quad (3)$$

Where,

τ Shear stress

q Shear flow

A_o Area enclosed by the centreline of the tube cross section

T Torque

t Tube wall thickness

Using thin tube theory includes multiple simplifications and assumptions, which are summarised below:

- All calculations assume an uncracked section.
- Assume that the hollow-core unit is subjected to pure torsion (i.e. not accounting for the interaction of gravity shear forces).
- Use of thin tube theory implicitly implies ignoring the section distortions (i.e. shear deformation perpendicular to the torsional twisting).
- The intensity of the shear stresses varies across the thickness of the assumed tube. Since the tube is thin, it can be assumed that the shear stress is constant across the thickness of the tube.

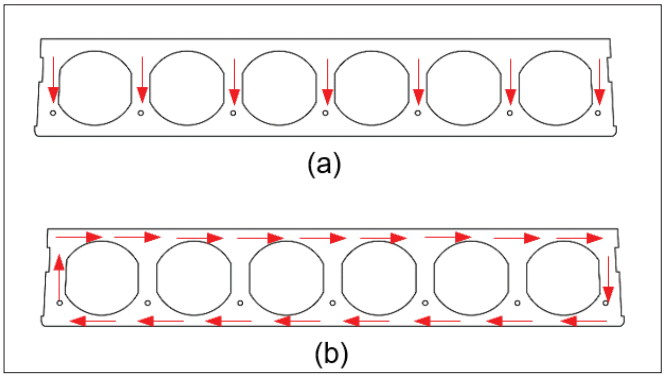

Figure 3: (a) sketch showing uniform shear stress distribution among hollow-core webs due to gravity shear (b) sketch showing shear distribution in hollow-core due to torsion

Under the assumption of pure torsion, torsional cracking is assumed to occur when the principal tensile stress at the critical point reaches the tensile strength of concrete. Therefore, using Mohr's Circle, the maximum shear stress the section can withstand before cracking is defined by (Equation 4).

$$\tau_{cr} = f_{ct}\sqrt{1 + \frac{f_{pc}}{f_{ct}}} \quad (4)$$

Where,

f_{ct} Concrete tensile strength

f_{pc} Precompression stress at the at the neutral axis in the critical section

τ_{cr} Cracking shear stress

The cracking torque, τ_{cr}, is calculated by substituting the cracking shear stress obtained from Equation 4 into Equation 3.

$$\tau_{cr} = 2 * q * t * A_o \qquad (5)$$

The external work done (Equation 1) should be a function of the cracking angle of twist, θ_{cr}, where it will be equated with the internal shear strain energy to obtain the cracking angle of twist, as shown in (Equation 6). Appendix B discusses the derivation of the equations used herein for elaboration.

$$\theta_{cr} = \frac{2*U}{T_{cr}} \qquad (6)$$

The critical section for assessing the torsional capacity of the unit will be within the transfer length of the prestressing strands. It is difficult to exactly calculate the value of longitudinal stress applied to the critical section as the longitudinal stress will depend on the strands' prestress and on the bending moment, which varies continuously during an earthquake. Consequently, for practical purposes, the conditions leading to torsional cracking can only be assessed to be in a likely range of structural actions (Bull et al. 2009). Therefore, the longitudinal stress at the critical section is assumed to be equivalent to the precompression stress applied on the section due to one-third of the effective prestressing force from all the prestressing strands after long term losses have occurred as a best estimate.

Torsional cracking in a concrete member without torsion reinforcement can result in the collapse of the member. However, as shown in Figure 4, two out of four pure torsion tests conducted by Pajari (2004a) showed that the hollow-core units sustained between two and four times the twist corresponding to torsional cracking before an abrupt and severe drop in torsional resistance (torsional strength capacity) took place. Based on these test results, Fenwick et al. (2010) recommends that the twist at torsional failure, θ_f, which is deemed to be accompanied by loss of gravity carrying capacity be taken as:

$$\theta_f = 2.5\theta_{cr} \qquad (7)$$

It should be noted that the limited tests available focused on torsional failure or loss in torsional strength capacity, whereas assessing the torsional capacity of a hollow-core unit when subjected to seismic demands is in fact a compatibility torsion issue where we are ultimately interested in the potential loss of gravity support, not loss in torsional strength capacity. Furthermore, it is worth mentioning that all four tests failed by cracking the top flange at an angle of 45° with the longitudinal axis of the unit. This failure mode is not expected to occur in typical building applications due to the presence of gravity loads and the presence of a continuous concrete topping. Instead, a brittle shear-tension or strand anchorage failure would be expected. Brittle shear failure would be expected as the floor bending moment decreases the tensile stresses in the top flange, and prestressing strands reduce the tensile stresses in the bottom flange. At the same time, one of the outermost webs will be subjected to shear stresses due to the combination of gravity shear and torsion shear (Figure 3). These stresses, in combination with the thickness of the outermost webs relative to the top flange with concrete topping, indicate that a web shear failure should be expected to occur.

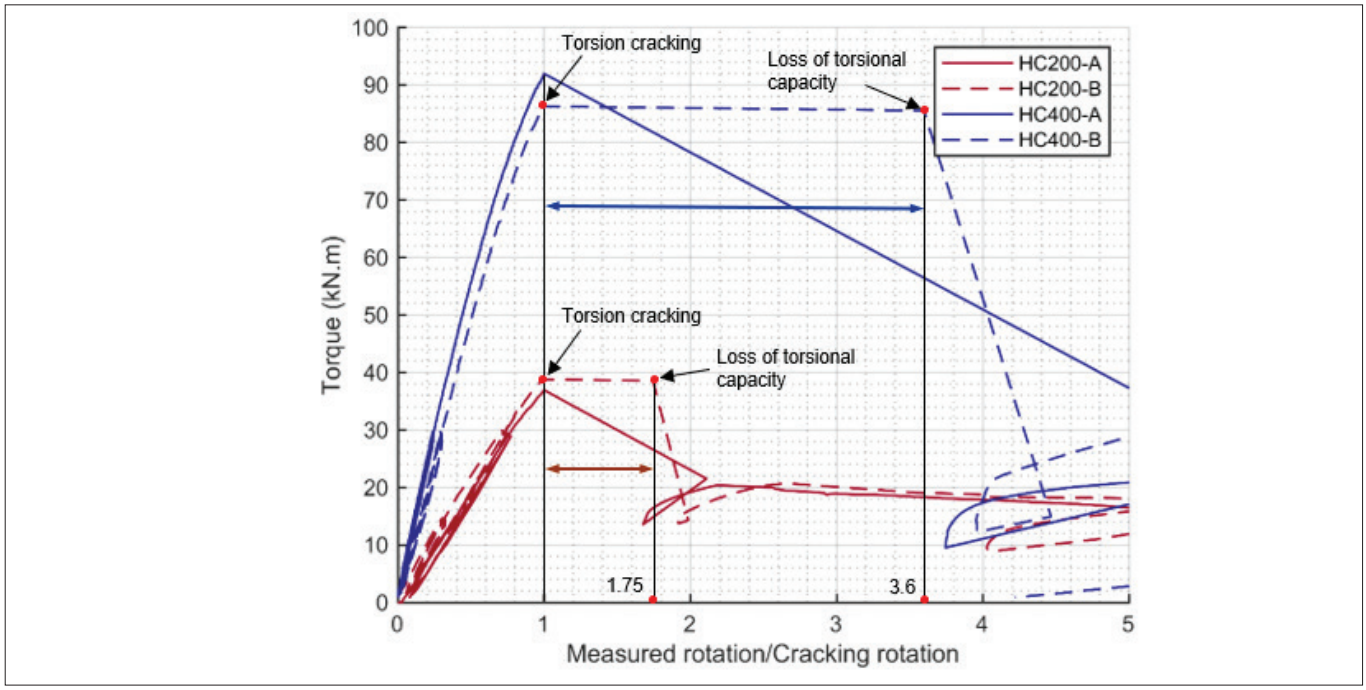

Figure 4: Pure torsion tests results modified from Pajari (2004a) showing two HC200 tests and two HC400 tests results

2.2 SUMMARY OF ASSESSMENT APPROACH

The current analytical assessment methodology considers two potential scenarios of how a hollow-core unit might resist torsional demands due to deformation compatibility under seismic actions. The first scenario assumes that a torsional shear flow can develop in the outside perimeter of the unit, as illustrated in Figure 5a. For this "equivalent tube" scenario, the torsional deformation capacity can be taken as 2.5 times the twist corresponding to the nominal cracking torque, θ_{cr}, (eq. 7). The second scenario assumes wide longitudinal cracks under the voids of the hollow-core unit due to bending of the supporting beam, as illustrated in Figure 5b, and the unit is assumed to be effectively separated into a series of I-beams linked by the concrete topping. The assessment guidelines (C5) assume the maximum torsional rotation (twist) sustained by the "top flange only" scenario, is determined based on design limits for a beam without torsional reinforcement as specified in cl. 7.6.1.2 - NZS 3101:2006-A3. For the top flange only case, the thickness where shear flow due to torsion is generated, t_w, should be calculated according to eq. 8 (Collins & Mitchell (1997)):

$$t_w = \frac{3A_c}{4p_c} \qquad (8)$$

Where,

p_c Section circumference (external perimeter) of the assumed tube cross section

A_c Area enclosed by the external perimeter of the assumed tube cross section

The calculations for the limiting twist for both scenarios are summarised below (Figure 6 and Figure 7). The assessment guidelines (C5) and Fenwick et al (2010) indicate that the controlling scenario is the case with the larger limiting twist, which may seem illogical to most engineers. Below we challenge the validity of the top flange only scenario, and recommend that engineers can focus on the equivalent tube scenario.

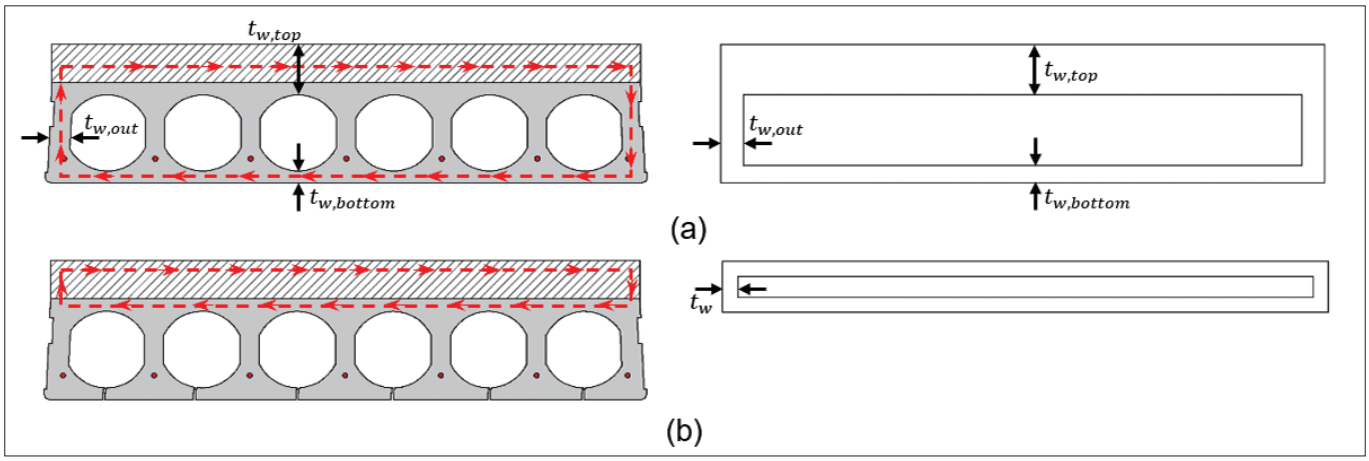

Figure 5: (a) equivalent tube section for assessing scenario one, (b) top flange only for assessing scenario two

SEISMIC PERFORMANCE OF NON-STRUCTURAL ELEMENTS: DISCUSSION BETWEEN AND SEAOC

The Structural Engineering Society of New Zealand (SESOC) and Structural Engineers Association of California (SEAOC) have been collaborating for the past seven years, in an effort to share knowledge between the two organizations. This has included publishing paired articles in both organizations' newsletters on topics of shared interest. Jan Stanway, Principal Structural Engineer at WSP, New Zealand, and SESOC member has recently led writing of an article regarding the current state of design practice for non-structural elements in New Zealand. To get feedback from the SEAOC community and provide a snapshot of California practice compared to New Zealand, SEAOC members active in non-structural component seismic performance and functional recovery were asked to provide their thoughts and reactions to the article. Part 1 of this paired article set is the article by Jan Stanway et. al. Part 2 presents excerpts from the responses provided by SEAOC members.

A copy of the article can be downloaded here: https://www.sesoc.org.nz/wp-content/uploads/2022/04/2022-02-22-SESOC-SEAOC-Paired-Article-Nonstructural.pdf

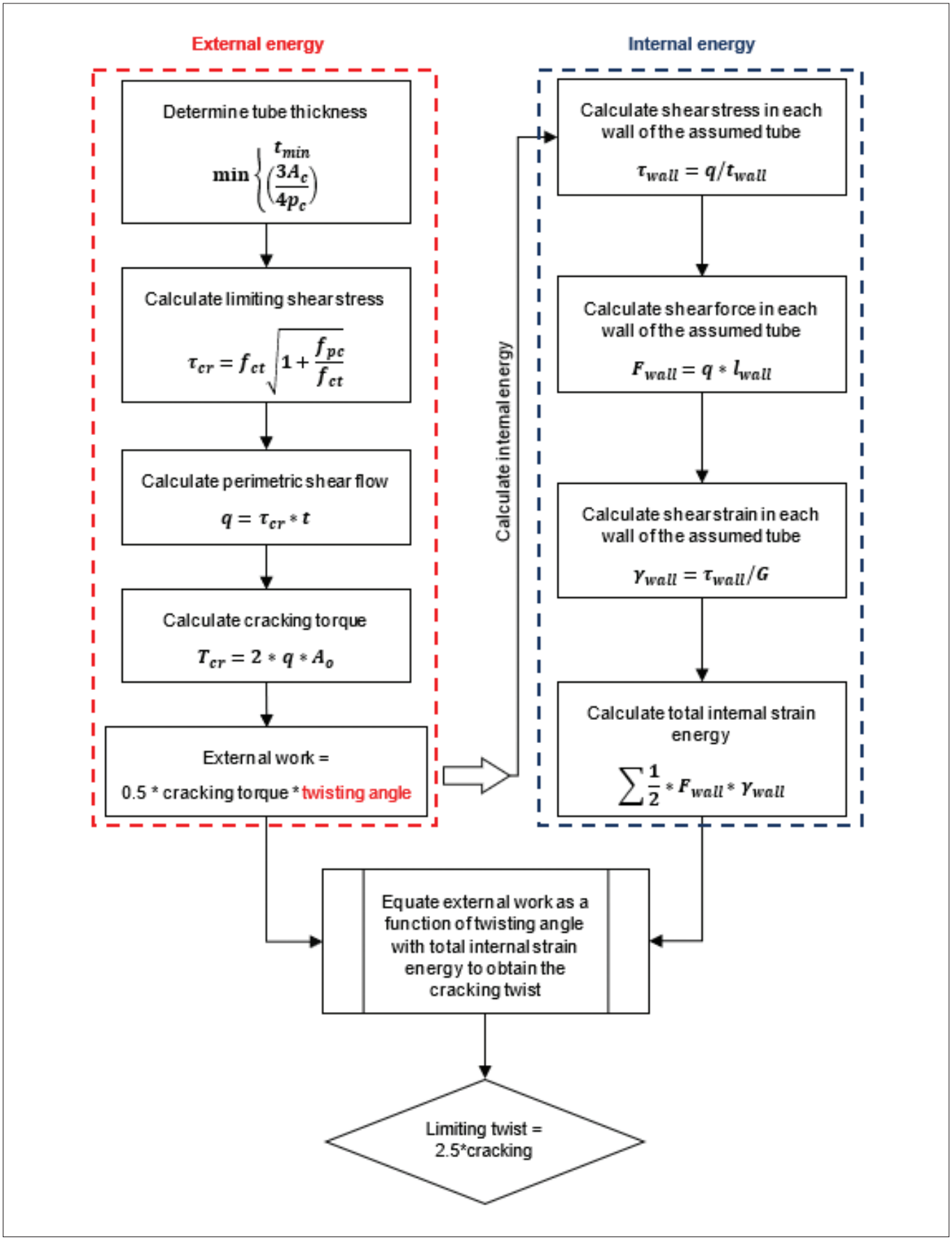

Figure 6: Flow chart summarising the torsional capacity assessment procedure for the equivalent tube case

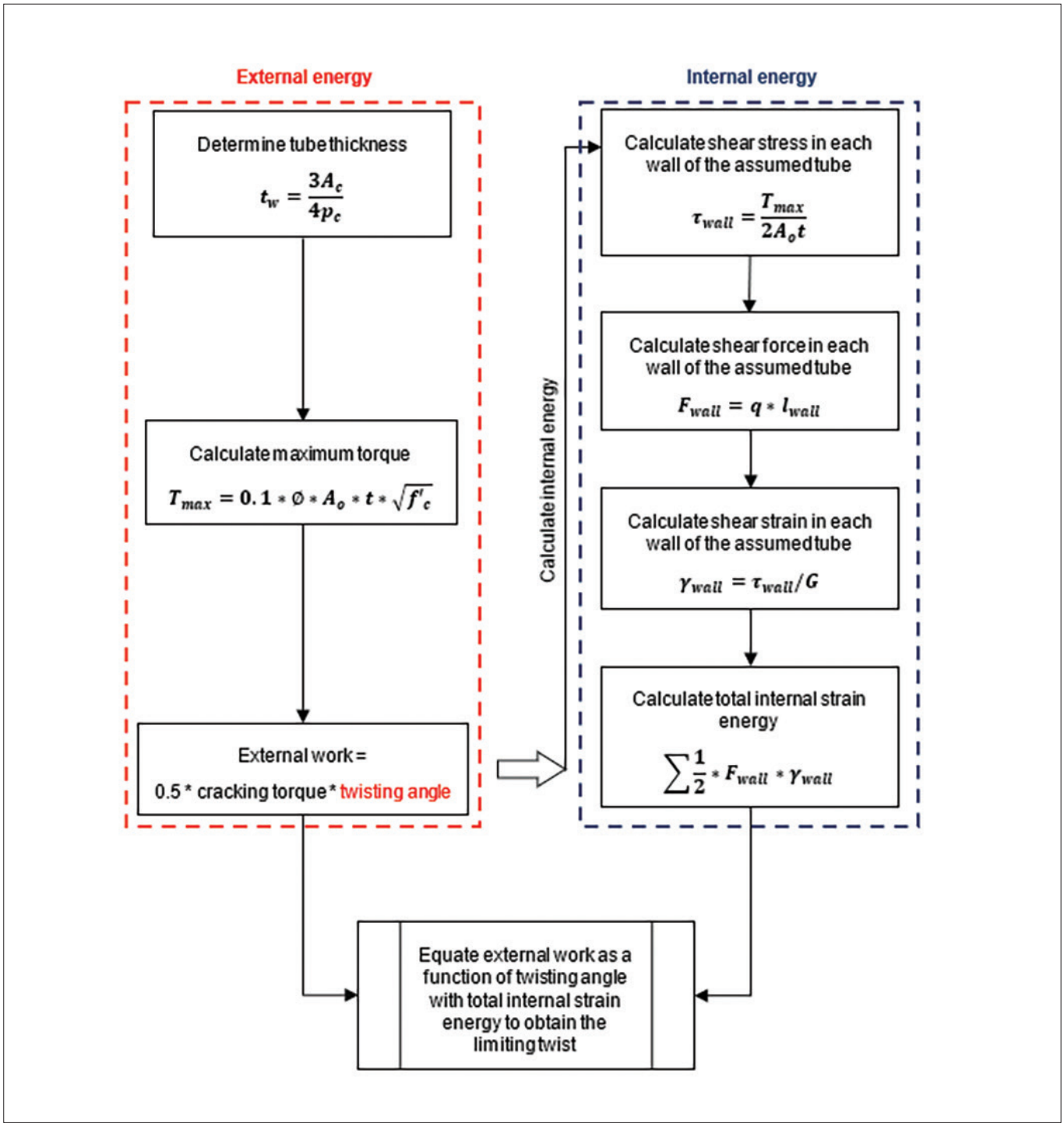

Figure 7: Flow chart summarising the torsional capacity assessment procedure for the flange only case

2.3 TORSION DEFORMATION CAPACITY ESTIMATES AND TWIST-LIMITS CHARTS

The torsional capacity of hollow-core units is sensitive to the actual material properties and geometry of the units, which varies with different manufacturers. Differences in parameters, such as floor depth, number of strands, strand height or web width can significantly affect the torsional capacity.

To facilitate the assessment of the torsional capacity of hollow-core units under the current methodology, the torsional capacities for different hollow-core depths and span lengths are plotted following the procedures described above. The plot produced herein is based on the average probable capacity from all the different manufacturers cross-sections found in Bull et al. (2009).

Probable material properties were used in assessing the expected hollow-core floor unit torsional capacity, as design values would not reflect the likely performance. Probable values for concrete strength are deemed to be significantly higher than the specified 28-day strength (MBIE et al. 2018). It is recommended to increase the specified compressive strength by a factor of 1.5 for a specified strength smaller or equal to 40 MPa and by a factor of 1.4 for a specified strength greater than 40 MPa (MBIE et al. 2018).

The concrete used in hollow-core units requires a high early strength (typically 30 MPa after 24 hours) to resist the prestressing force when releasing the prestressing strands and cutting the units to their specified lengths. Usually, the 28-day strength significantly exceeds the specified concrete strength and ranges between 50 MPa and 60 MPa (MBIE et al. 2018). Furthermore, the probable tensile strength of concrete was based on the equation $f_{ct} = 0.55\sqrt{f'c}$ found in C5.4.2.4 in the assessment guideline C5 (MBIE et al. 2018).

The probable effective prestress, f_{se}, was taken as 80% of the probable initial prestress, accounting for losses. The prestressing strands are typically pretensioned to 65% of the ultimate strength of the strands. The ultimate strength of the strands used to produce the plot below was obtained from AS/NZS 4672.1:2007, where 12.7 mm-7 wire strands were assumed to be used. Finally, the shear modulus, G, was used to obtain the shear strain at each wall of the assumed tube section and was assumed to be 40% of the concrete using Young's modulus ($G = 0.4E$).

The equivalent tube case was found to always produce a larger limiting twist compared with the top flange only case. The top flange only case assumes a thin unreinforced section (topping and top flange of the unit) and uses the torsional limit of an unreinforced section (i.e. torque upon which torsion reinforcement is required) based on requirements for design. Such design provisions are used to identify when it is prudent in new design to include torsion reinforcement; they are naturally conservative and should not be used as a forensic tool to predict failure.

The indicative limits for different unit depths were calculated based on the analytical method currently available in the assessment guidelines C5. The length and depth of the unit are the only required information to use the indicative limits in Table 1 and the twist-limits chart in Figure 8.

It is worth noting that the principal stress at the critical point in the critical section depends on the longitudinal compression stress and on the bending moment at that location, which varies continuously during an earthquake. Consequently, for practical purposes, the conditions leading to torsional cracking can only be assessed to be in a likely range of structural actions (Bull et al. 2009). Calculated capacities for each hollow-core type (different manufacturers) with varying prestressing forces at the critical sections can be found in the table provided in Appendix C, and a detailed worked example can be found in the worked example by Büker et al. (2020).

The following assumptions were used in calculating the limits provided herein:

- In-situ topping was 75mm (charts are conservative for thinner toppings; thinner toppings allow slightly higher torsional deformation)
- Probable hollow-core concrete compressive strength was 58.8 MPa (1.4*42 MPa)
- Probable topping concrete compressive strength was 37.5 MPa (1.5*25 MPa)

Table 1: Indicative twisting limits for different hollow-core depths

Probable limiting vertical displacement per span length of unit (mm/m)			
	Cracking twist	**Equivalent tube case**	**Top flange only case**
200HC	1.2	3.0	0.2
300HC	1.0	2.4	0.2
400HC	0.8	2.0	0.2

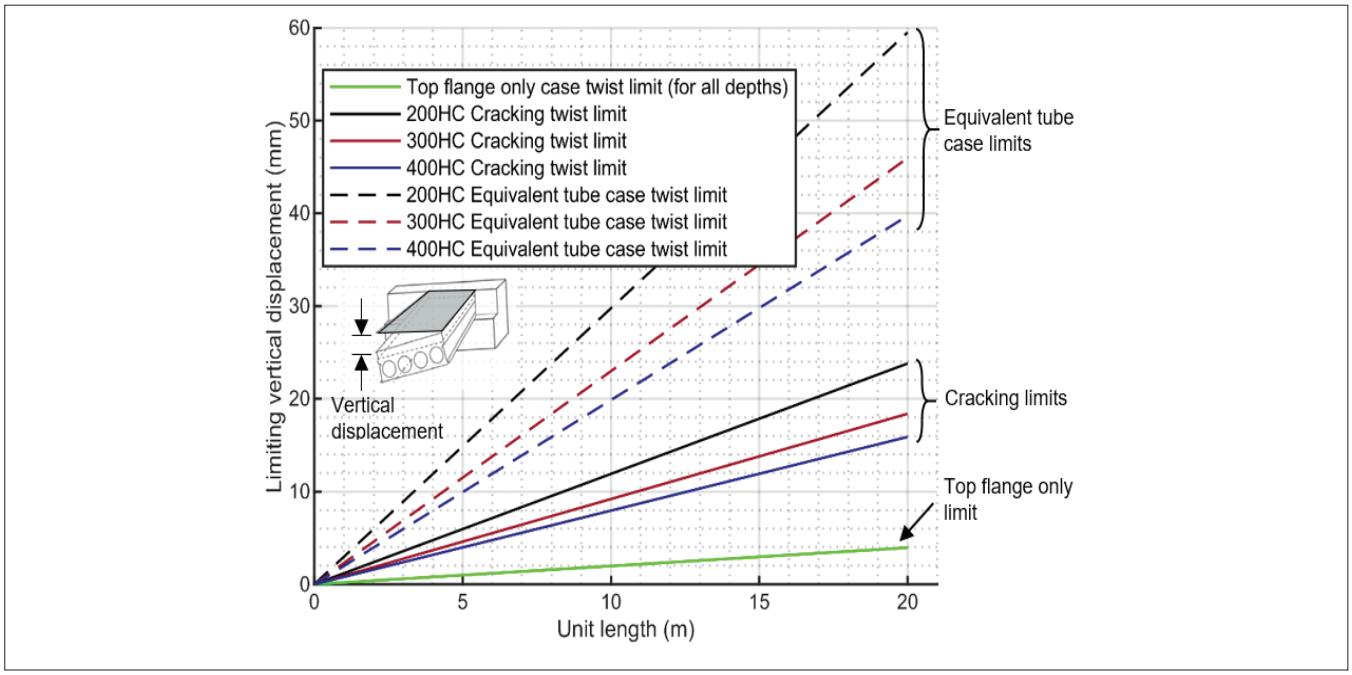

Figure 8: Torsion vertical displacement limits (deformation required to crack the unit due to torsion and deformation capacity of the unit according to both cases adopted in C5-equivalent tube case and top flange only case)

3 LIMITATIONS AND CONSIDERATIONS OF THE ADOPTED ASSESSMENT APPROACH

Most of the available information and existing research conducted on the seismic performance of hollow-core floors mainly focused on the effect of the supporting system rotation and elongation relative to the hollow-core units in the longitudinal direction (i.e. parallel to the unit direction). There has been very limited research investigating the effect of the deformations of the supporting system relative to the transverse direction of the units (i.e. perpendicular to the unit direction). Deformations in the transverse direction of the hollow-core units can cause potential problems in cases where lateral sway of a building can induce significant twist into hollow-core units. Furthermore, transverse deformations also play an important role in damage to units supported within the plastic hinge regions of intermediate columns (Beta units), as described in Mostafa et al. (2022a).

There is significant uncertainty in the available torsion methodology described herein; Broo et al. (2005) indicate that the torsional capacity of a unit subject to pure torsion might be overestimated (Figure 9) using the analytical methodology adopted in EN-1168, which is also adopted in the assessment guideline C5. Also shown in Figure 9, the shear-torsion interaction impact on the torsional capacity is not directly accounted for in the assessment guidelines methodology, potentially leading to an overestimation of torsional capacity.

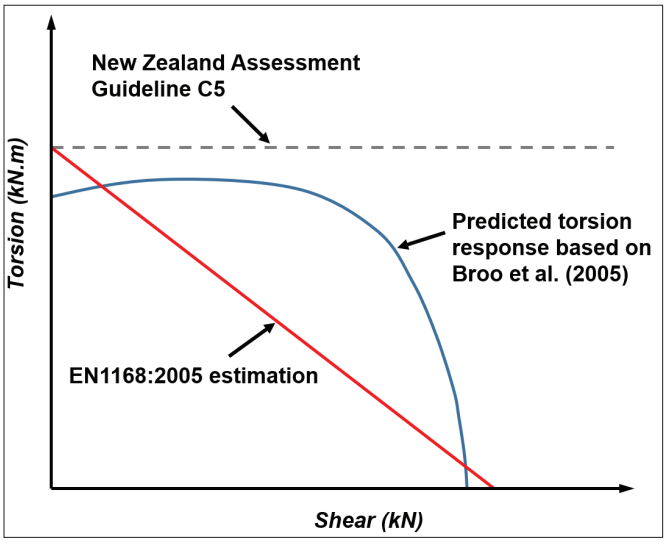

Figure 9: Schematic of shear torsion interaction estimation (Modified from (Broo et al. 2005))

On the other hand, the assessed torsional demand on the unit could also be overestimated, as the connection flexibility is not accounted for in the calculations. As twisting of the units due to the seismic response of the building is induced into the units through the connection, the connection generally acts as a fuse. The more flexible the connection is, the less twist (torsion) induced in the unit. Therefore, higher drift levels can be sustained by

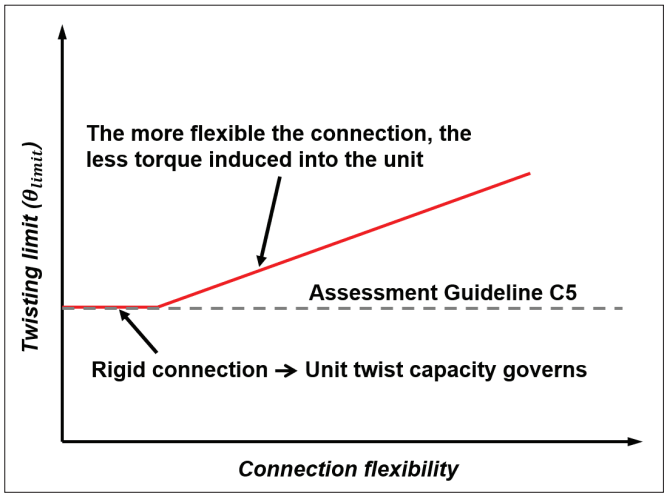

Figure 10: Schematic of the expected twist limit when accounting for different connections flexibilities

the units prior to torsional cracking. If the connection is considered rigid (e.g. filled and reinforced cores), then the connection will not dissipate deformations and the full torsional demand may be induced into the unit (Figure 10).

Table 2: Summary of current torsion assessment limitations

Limitation	Effect
• Based on the work done by Broo et al. (2005), the analytical method is unconservative for pure torsion. • Not accounting for shear-torsion interaction.	Overestimate torsional capacity
• The 2.5 factor for limiting twist is based on only two of the four tests used to develop the torsion assessment. More data points are required to verify this 2.5 factor.	Either underestimate or overestimate torsional capacity
• Not accounting for different connection flexibility on the torsional response of a hollow-core unit.	Overestimate torsional demand

Another limitation of the current torsion assessment methodology used in C5 is that only individual units are assessed. By not accounting for the contribution of neighbouring units to the hollow-core unit capacity, the potential risk of premature cracking of the webs of a unit subjected to torsion due to a compression strut that is generated in the unit from restraint by the neighbouring units, as described by Fenwick et al. (2010) and illustrated in Figure 11, is obscured.

The primary concern regarding the torsional response of hollow-core floor units is not that a unit will collapse due to torsion damage alone – this has not been observed in post-earthquake reconnaissance (Mostafa et al. 2022b; Henry et al. 2017). Instead, the concern is any potential impact torsional damage may have on other failure modes (e.g. negative moment failure (NMF) and positive moment failure (PMF)). Torsional damage will cause web cracking that, when combined with positive moment cracking or negative moment cracking, may reduce the drift capacity estimated for each individual potential failure mode.

Such impact is not well understood, and further large-scale testing of super-assembly systems incorporating units subject to high torsional demands are required to assess if there should be a reduction in the assessed drift at NMF or PMF due to damage caused by torsion. In the absence of such tests and given the generally conservative assessment of NMF and PMF using the assessment guidelines, it is not currently considered necessary to reduce the assessed drift capacity of units due to torsion damage beyond that provided by C5.

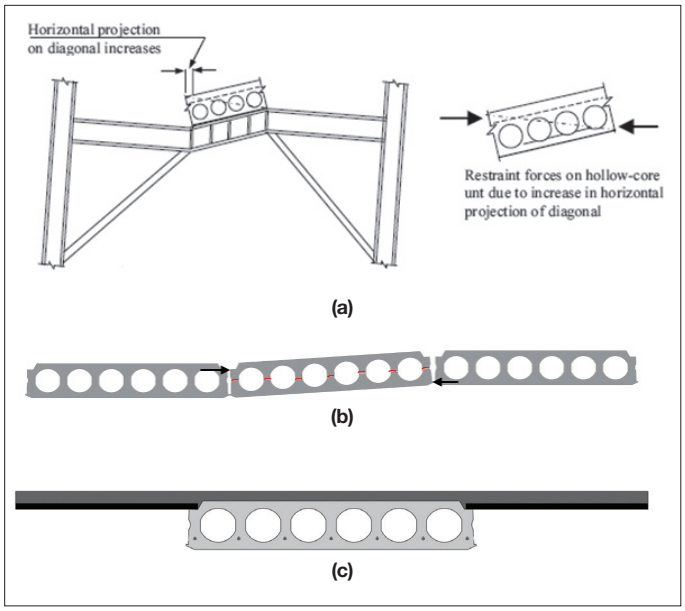

Figure 11: Example of where neighbouring units might affect unit capacity (a) twist of unit increases length of diagonal in plane of floor and restrain forces from neighbouring unit act on hollow-core (Fenwick et al. 2010) (b) schematic of potential contribution of neighbouring units when subjected to torsion (c) spaced unit will not have such contribution

Given the uncertainties listed in Table 2 and illustrated in Figures 9-11 regarding the ability of the assessment procedure to predict the torsional cracking of hollow-core units and the impact of this cracking on performance, it is recommended that in the case of a unit susceptible to high torsion demands due to its location or loading, as described in Figure 2, a conservative approach be taken when devising retrofit scope (i.e. for any units expected to undergo significant torsional demands, a retrofit be used which can provide gravity support even if a torsional crack were to form away from the support).

4 CONCLUSION

This paper provides a twist-limit chart and table as a simple tool for assessing the torsional deformation capacity of precast hollow-core floor units with varying depths according to the New Zealand seismic assessment guideline C5. It is recommended to only consider the equivalent tube case for assessing the torsional capacity of hollow-core floor units and not consider the flange only case for the following reasons:

- The equivalent tube case is stiffer and hence more likely to attract torsional demands leading to cracking.
- Based on post-earthquake reconnaissance observations, a hollow-core unit is unlikely to reach a damage state assumed by the top flange only scenario where longitudinal cracking between all the hollow-core unit webs completely loses interaction even due to aggregate interlock between webs leaving only the top flange and topping to provide torsional resistance.
- Selecting a limiting twist based on a design trigger for torsion reinforcement, as is suggested in C5 for the top flange only scenario is overly conservative.

Moreover, an extensive literature review was conducted to trace back the basis of the analytical methodology adopted in the seismic assessment guidelines C5 for assessing the torsional capacity of hollow-core floor units. Limited research on the torsional behaviour of precast hollow-core floor units was found to serve as the foundation of the methodology adopted in the assessment guidelines C5.

The lack of research data led to multiple uncertainties regarding the accuracy of the procedures currently in use. The primary limitations of the current torsion assessment procedure include the following:

- Not accounting for different connection flexibilities on the torsional response of a hollow-core unit can lead to an underestimation of the total drift at which a hollow-core unit will experience torsional cracking.
- The 2.5 factor used for the limiting twist (Equation 7) is based on only two test results that primarily focused on loss of torsional strength rather than the damage state leading to loss of gravity support. More tests are required to verify this number.
- The analytical method adopted in the assessment guidelines C5 to calculate the cracking torque can be unconservative according to Broo et al. (2005).
- Exclusion of any units with low-friction bearing strips from torsion assessment.

Despite these limitations, the guidance in C5 (modified by the above recommendation to ignore the top flange only scenario) is the best and simplest available approach to estimate the twist at torsional cracking and failure. But given the uncertainties and limitations described above, regardless of the assessed twist capacity, it is recommended that if a building with hollow-core floor units is being retrofitted, then, for any units expected to undergo significant torsional demands (even if support details have a low-friction bearing strip), a retrofit should be used which can provide gravity support even if a torsional crack were to form away from the support.

5 ACKNOWLEDGEMENT

This investigation is supported by Building Research Association of New Zealand (BRANZ) under Grant No. LR13069 and the ReCast project. The authors would like to acknowledge Dr. Matti Pajari for sharing the pure torsion tests data, Andrew Thompson and John Wood for reviewing this paper. This is QuakeCoRE publication number 0753.

6 REFERENCES

British Standards Institution (BSI). 2005. BS EN 1168:2005+A3:2011. Precast concrete products - Hollow core slabs. London: BSI.

Broo, H., Lundgren, K. and Engstrom, B. 2005. “Shear and Torsion Interaction in Prestressed Hollow Core Units.” Mag. Concr. Res., November 2005.

Broo, H., Lundgren, K. and Engstrom, B. 2007. “Shear and Torsion in Prestressed Hollow Core Units: Finite Element Analyses of Full-Scale Tests.” Struct. Concr., 8 (2): 87–100.

Büker, F., Poland, C. and Brooke, N. 2020. “Assessment of Existing Precast Concrete Floors: Hollow-core Worked Example-Revision 1.” Struct. Eng. Soc. N. Z. SESOC, 33 (2): 44–86.

Bull, D. K., R. Fenwick, R. Fulford, R. Jury, D. Hopkins, G. Lawrance, L. McSaveney, S. Pampanin, A. Smith, and P. Smith. 2009. Seismic Performance of Hollow Core Floor Systems Guidelines for Design Assessment and Retrofit.

Collins, M. P., and Mitchell, D. 1997. Prestressed Concrete Structures. Toronto: Response Publications.

El-Sayed, A. K., Al-Negheimish, A. I. and Alhozaimy, A. M. 2019. “Web Shear Resistance of Prestressed Precast Deep Hollow Core Slabs.” ACI Struct. J., 116 (1): 139–150.

Fenwick, R., Bull, D. and Gardiner, D. 2010. Assessment of Hollow-Core Floors for Seismic Performance. 152p. Research Report. New Zealand: University of Canterbury.

Henry, R. S., Dizhur, D., Elwood, K. J., Hare, J. and Brunsdon, D. 2017. “Damage to Concrete Buildings With Precast Floors During the 2016 Kaikoura Earthquake.” Bull. N. Z. Soc. Earthq. Eng., 50 (No.2): 174–186.

MBIE, EQC, NZSEE, SESOC, and NZGS. 2018. “Technical Proposal to Revise the Engineering Assessment Guidelines PART C5 - Concrete Buildings.” Seism. Assess. Exist. Build. New Zealand.

Michelini, E., Bernardi,P., Cerioni, R. and Belletti, B. 2020. “Experimental and Numerical Assessment of Flexural and Shear Behavior of Precast Prestressed Deep Hollow-Core Slabs.” Int. J. Concr. Struct. Mater., 14 (1): 14–31.

Mostafa, M., Büker, F., Hogan, L. S., Elwood, K. J. and Bull, D. 2022a. “Seismic Performance of Precast Hollow-core Units Seated Within the Plastic Hinge Region.” N. Z. Soc. Earthq. Eng. New Zealand: Proceedings of the 2022 NZSEE Annual Technical Conference.

Mostafa, M., Hogan, L. S. and Elwood, K. J. 2022b. “Seismic Performance of Hollow-core Floors with Modern Detailing: A Case Study ‘submitted for review.’” J. Struct. Eng. Soc. N. Z.

Pajari, M. 2004a. Pure Torsion Tests on Single Hollow Core Slabs. 64. Research Report. Finland: Technical Research Centre of Finland, VTT Building and Transport.

Pajari, M. 2004b. Shear-Torsion Interaction Tests on Single Hollow Core Slabs. 204. Research Report. Finland: Technical Research Centre of Finland, VTT Building and Transport.

Puranam, A., Corney, S. R., Elwood, K. J. and Bull, D. 2021. “Seismic Performance of Precast Hollow-Core Floors: Part 2—Assessment of Existing Buildings.” ACI Struct. J., 118 (5). https://doi.org/10.14359/51732822.

Standards New Zealand. 2017. Concrete structures standard. Part 1: The Design of Concrete Structures. Part 2: Commentary on the design of Concrete Structures. (NZS 3101.1:2006 & NZS 3101.2:2006).

Walraven, J. C. and Mercx, W. P. M. 1983. “The Bearing Capacity of Prestressed Hollow Core Slabs.” HERON, 28 (3).

Yang, L. 1994. “Design of Prestressed Hollow Core Slabs with Reference to Web Shear Failure.” J. Struct. Eng., 120 (9): 2675–2696.

Appendix A – Notations

π	Total potential energy
U	Strain energy (due to shear)
W	Potential energy of the load (Work done by torque)
T	Torque
θ	Angle of rotation of the hollow-core unit about its longitudinal axis
F	Shear force due to the shear flow generated in the unit as a result of the unit twisting/torsion
γ	Shear strain
τ	Shear stress
q	Shear flow
G	Shear modulus
E	Young's modulus
A_o	Area enclosed by the centreline of the tube cross section
A_c	Area enclosed by the external perimeter of the assumed tube cross section
p_c	Section circumference (external perimeter) of the assumed tube cross section
t_w	Thickness of the assumed tube cross section
f_{ct}	Concrete tensile strength
f_{pc}	Precompression stress at the neutral axis in the critical section
T_{cr}	Cracking torque
θ_{cr}	Cracking angle of twist
θ_f	Estimated failure angle of twist
F_{se}	Effective prestressing force on the section
f'_c	Probable concrete strength
Ø	Strength reduction factor, taken as 0.75 for torsion

Appendix B – Derivations and basis of the current assessment approach

The torsional capacity assessment methodology for hollow-core floor units adopted in the assessment guidelines C5 is based on the principle of stationary total potential energy (π), which is defined as the sum of the stored strain energy (U) and the potential energy of the load (W) where the potential energy of the external load is due to the torque induced into the unit (T) and the corresponding angle of rotation of the hollow-core unit about its longitudinal axis (θ), and the internal stored strain energy is due to the shear forces generated in the unit (F) and the corresponding shear strain (γ).

To be in equilibrium the total potential energy should be zero. Therefore, the energy from the work done by external forces should be equal to the internal strain energy.

$$\pi = W - U \qquad (9)$$

$$W = \frac{1}{2} * T * \theta \qquad (10)$$

$$U = \frac{1}{2} * F * \gamma \qquad (11)$$

$$W = U \qquad (12)$$

All the calculations used to satisfy equilibrium are based on Bredt's thin tube theory as explained in Collins & Mitchell (1997). As the wall of the tube is assumed to be thin, the shear stresses are considered to be constant across the wall thickness. If we consider the equilibrium in the longitudinal direction of the small element shown in Figure 12d, we conclude that the shear flow has to remain constant along the total perimeter of the section, Equation 13.

To relate the torsional demands applied on the element, T, to the shear flow, q, an element of area of length ds is considered, where ds is measured along the centreline of the tube. The total shear force acting on the element is the sum of $q.ds$ along the entire tube length, and the moment of this shear force about any point 'O' is the multiplication of the shear force by its lever arm, r_p. The torque produced by shear is obtained by integrating the shear flow along the entire length of centreline of the cross section as shown in Equation 14. The quantity $r_p * ds$ is equivalent to twice the area of the shade triangle shown in Figure 12c. Therefore, the integral $\int r_p * ds$ represents double the area enclosed by the centreline of the cross section, A_o.

$$q = \tau * t = constant \qquad (13)$$

$$T = q \int r_p * ds \qquad (14)$$

$$\int r_p * ds = 2A_o \qquad (15)$$

$$T = 2 * q * A_o \qquad (16)$$

$$q = \frac{T}{2A_o} = \tau * t \qquad (17)$$

Under the assumption of pure torsion, torsional cracking is assumed to occur when the principal tensile stress reaches the tensile strength of concrete, f_{ct}. Therefore, the maximum shear stress the section can withstand before cracking, (Equation 25), is obtained using the stress Mohr-circle. Once cracking torque, T_{cr}, is calculated by substituting the cracking shear stress obtained from Equation 25 into Equation 17, internal shear energy, U, should be calculated and equated to external work done, W, as a function of the cracking angle of twist, θ_{cr}.

$$Origin\ of\ Mohr's\ circle = \frac{-f_{pc}}{2} \tag{18}$$

$$Radius\ of\ Mohr's\ circle = \sqrt{\left(\frac{-f_{pc}}{2}\right)^2 + (\tau)^2} \tag{19}$$

$$f_{ct} = Origin + Radius \tag{20}$$

$$f_{ct} = \frac{-f_{pc}}{2} + \sqrt{\left(\frac{-f_{pc}}{2}\right)^2 + (\tau)^2} \tag{21}$$

$$(\tau)^2 = \left(f_{ct} + \frac{f_{pc}}{2}\right)^2 - \left(\frac{-f_{pc}}{2}\right)^2 \tag{22}$$

$$(\tau)^2 = {f_{ct}}^2 + \left(\frac{f_{pc}}{2}\right)^2 + f_{ct}.f_{pc} - \left(\frac{-f_{pc}}{2}\right)^2 \tag{23}$$

$$(\tau)^2 = {f_{ct}}^2 + f_{ct}.f_{pc} \tag{24}$$

$$\tau_{cr} = f_{ct}\sqrt{1 + \frac{f_{pc}}{f_{ct}}} \tag{25}$$

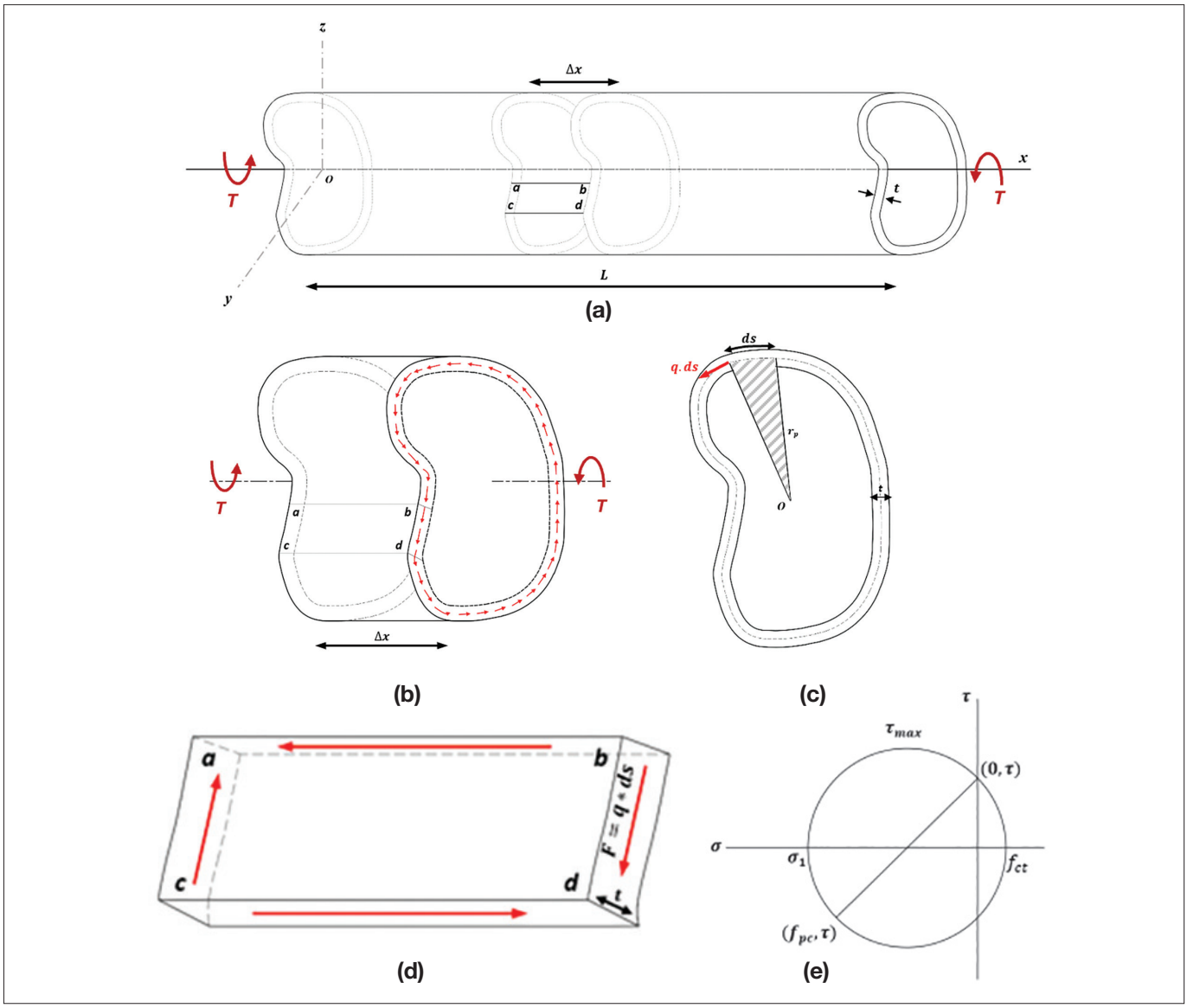

Figure 12: (a) Arbitrary thin tube element (b) Elemental section subjected to torsion with shear flow (c) Element section (d) Shear forces on an infinitesimal section (e) Stress state at the critical section

Appendix C – Torsion limits of different manufacturers

	HC - Type		Prestressing Stress (Mpa)	Limiting rotaion per meter run (rad./m)			Limiting vertical disp. per meter run (mm/m)		
				Cracking twist	Scenario 1	Scenario 2	Cracking twist	Scenario 1	Scenario 2
Stahlton	Echo	200HC	0	0.0009	0.0019	0.0002	1.11	2.22	0.23
			3.5	0.0010	0.0021	0.0002	1.26	2.51	0.23
			7	0.0012	0.0023	0.0002	1.38	2.77	0.23
			3.50 (probable)	0.0010	0.0021	0.0002	1.26	2.51	0.23
		300HC	0	0.0007	0.0014	0.0002	0.86	1.72	0.22
			3.5	0.0008	0.0016	0.0002	0.97	1.94	0.22
			7	0.0009	0.0018	0.0002	1.07	2.14	0.22
			4.78 (probable)	0.0008	0.0017	0.0002	1.01	2.02	0.22
		400HC	0	0.0006	0.0011	0.0002	0.68	1.35	0.22
			3.5	0.0006	0.0013	0.0002	0.76	1.53	0.22
			7	0.0007	0.0014	0.0002	0.84	1.68	0.22
			4.11 (probable)	0.0006	0.0013	0.0002	0.78	1.56	0.22
	Elematic	200HC	0	0.0009	0.0019	0.0002	1.11	2.23	0.23
			3.5	0.0010	0.0021	0.0002	1.26	2.52	0.23
			7	0.0012	0.0023	0.0002	1.39	2.78	0.23
			3.56 (probable)	0.0011	0.0021	0.0002	1.26	2.52	0.23
		300HC	0	0.0007	0.0013	0.0002	0.80	1.59	0.20
			3.5	0.0007	0.0015	0.0002	0.90	1.80	0.20
			7	0.0008	0.0017	0.0002	0.99	1.98	0.20
			5.72 (probable)	0.0008	0.0016	0.0002	0.96	1.92	0.20
		400HC	0	0.0006	0.0012	0.0001	0.69	1.39	0.18
			3.5	0.0007	0.0013	0.0001	0.78	1.57	0.18
			7	0.0007	0.0014	0.0001	0.86	1.73	0.18
			4.69 (probable)	0.0007	0.0014	0.0001	0.81	1.62	0.18
	Spirol	200HC	0	0.0008	0.0017	0.0002	0.99	1.98	0.25
			3.5	0.0009	0.0019	0.0002	1.12	2.24	0.25
			7	0.0010	0.0021	0.0002	1.24	2.47	0.25
			5.44 (probable)	0.0010	0.0020	0.0002	1.19	2.37	0.25
		300HC	0	0.0006	0.0013	0.0002	0.76	1.53	0.23
			3.5	0.0007	0.0014	0.0002	0.86	1.73	0.23
			7	0.0008	0.0016	0.0002	0.95	1.91	0.23
			8.22 (probable)	0.0008	0.0016	0.0002	0.98	1.96	0.23
Stresscrete	Dycore	200HC	0	0.0008	0.0016	0.0002	0.95	1.89	0.24
			3.5	0.0009	0.0018	0.0002	1.07	2.14	0.24
			7	0.0010	0.0020	0.0002	1.18	2.36	0.24
			5.76 (probable)	0.0010	0.0019	0.0002	1.14	2.28	0.24
		300HC	0	0.0006	0.0012	0.0002	0.71	1.43	0.23
			3.5	0.0007	0.0013	0.0002	0.81	1.61	0.23
			7	0.0007	0.0015	0.0002	0.89	1.78	0.23
			6.72 (probable)	0.0007	0.0015	0.0002	0.88	1.77	0.25

ISSN No. 2744-7871

SEISMIC DAMAGE OBSERVATIONS OF PRECAST HOLLOW-CORE FLOORS FROM TWO FULL-SCALE SUPER-ASSEMBLY TESTS

Büker, F.[1,*], Parr, M.[2], De Francesco, G.[3], Hogan, L.S.[4], Bull, D.K.[5], Elwood, K.J.[6], Liu, A.[7], Sullivan, T.J.[8]

ABSTRACT

Serious concerns about the life safety risk of hollow-core floors during earthquakes were raised following the collapse of hollow-core units during the 1994 Northridge earthquake and in subsequent laboratory tests. To enhance the understanding of the seismic performance of existing hollow-core floors, a substantial experimental programme of two large-scale super-assembly tests with hollow-core floors was carried out. Each test specimen consisted of a two-bay by one-bay concrete frame with full-scale hollow-core floors, which were constructed using typical 1980s floor detailing. The specimens were loaded with a simulated earthquake record applied quasi-statically.

This paper discusses the progression of hollow-core floor damage observed in both super-assembly experiments. The main findings include the early onset of cracks in the unreinforced webs of the hollow-core units at 0.5% interstorey drift. The tests also demonstrated the detrimental effect of web cracking on the gravity load-carrying capacity of hollow-core floors. Additionally, hollow-core units that are seated at intermediate columns (so-called 'beta units') were found to get damaged more heavily than those supported away from the columns. Moreover, several transverse cracks were observed in the floor soffit away from the support and beyond the provided seating retrofits. Lastly, the extent of floor damage was found to be sensitive to the ground motion, with pulse-type motions (pushing the structure in one direction) tending to cause more severe floor damage than far-field motions with multiple cycles. The paper also outlines key challenges and recommendations for web crack inspections.

1 BACKGROUND

The collapse of precast hollow-core floor units during the 1994 Northridge earthquake raised serious concerns about the seismic resilience of such floors. Subsequent earthquake reconnaissance (Norton et al. 1994) concluded that the failure had initiated at the support connection. This hollow-core floor collapse in the USA raised serious concerns in New Zealand, where hollow-core floors had been widely used since the late 1970s (PCFOG 2009). A series of component tests (Herlihy 1999; Mejia-McMaster 1994; Oliver 1998) furthered the understanding of the seismic performance of hollow-core floor connections, but it was not until the early 2000s that the critical shortcomings of these floors were exposed in a large-scale three-dimensional laboratory experiment (Matthews 2003).

Matthews (2003) tested a segment of a typical precast concrete frame building with hollow-core floors (super-assembly test). As shown in Figure 1, the super-assembly specimen comprised topped 300 mm hollow-core units spanning 12 m over two bays. While the nominal seating of the floors was specified as 50 mm, typical of field conditions, the achieved actual seating length measured 20 mm (east) and 40 mm (west) due to construction tolerances.

PAPER CLASS & TYPE: GENERAL REFEREED

1 PhD Candidate, University of Auckland
2 PhD Candidate, University of Canterbury
3 Research Engineer, University of Canterbury
4 Lecturer, University of Auckland
5 Technical Director, Holmes Consulting
6 Professor, University of Auckland
7 Senior Structural Engineer, BRANZ
8 Professor, University of Canterbury
** frank.bueker@auckland.ac.nz*

(a) Super-assembly specimen with loading rig

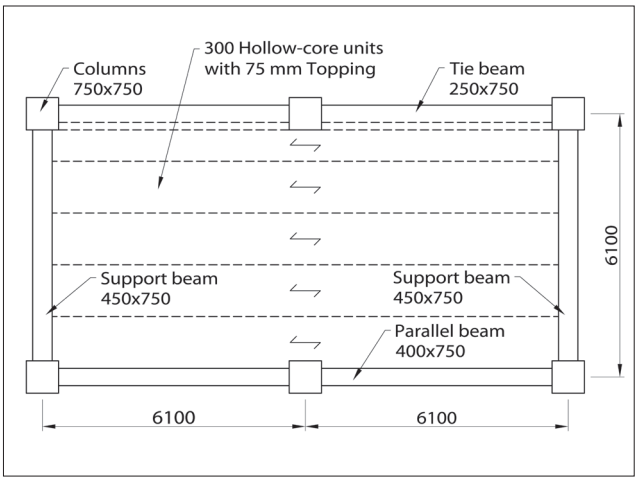

(b) Plan view of the super-assembly specimen

Figure 1: Super-assembly test with 300 mm hollow-core floors (adapted from Matthews (2003))

During Matthews' experiment the hollow-core floors performed in a brittle manner and exhibited critical damage such as:

- A longitudinal tear forming between the first and second unit at 1.9% drift,
- Collapse of the bottom flange of the first unit at 2.0% drift and
- Complete floor collapse after 2.5% drift while loading the floor with design live load.

One of the critical observations was that the damage occurred within the hollow-core units themselves (see Figure 2), disproving previous assumptions that all the deformation and damage manifests at the beam-to-floor interface.

Improved hollow-core floor detailing, which was developed based on the findings from Matthews' test and further testing (Lindsay 2004; MacPherson 2005; Trowsdale 2004), was subsequently introduced into the New Zealand Concrete Structures Standard with the third amendment to NZS3101:1995 (SNZ 2004). These provisions were refined and maintained in NZS3101:2006-A1, A2&A3 (SNZ 2017)). In addition, further investigation into the seismic performance of the pre-2000s hollow-core floor detailing was conducted through several sub-assembly connection tests (Bull and Matthews 2003; Jensen 2006; Liew 2004; Woods 2008). These single hollow-core unit to beam specimens largely contributed to the development of seismic assessment procedures for hollow-core floors published by Fenwick et al. (2010). Three primary modes of failure, namely loss of support (LOS), negative moment failure (NMF) and positive moment failure (PMF), were identified in these assessment procedures.

Hollow-core floor damage found after the 2016 Kaikōura earthquake was of a nature that emphasised the need to

(a) Photo of the support connection after floor collapse

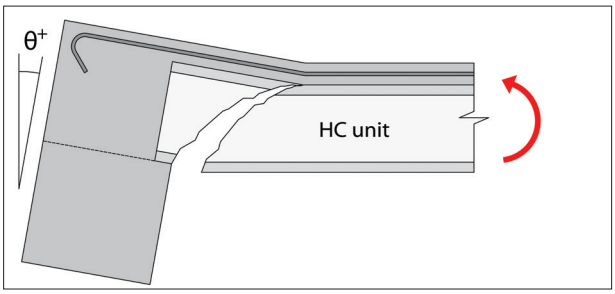

(b) Cross section showing the positive moment cracking generated by relative rotation demands as observed in Matthews' experiment

Figure 2: Cracking within the hollow-core units (adapted from Matthews (2003))

assess and retrofit the many existing pre-2000 hollow-core floor buildings (Henry et al. 2017). The earthquake damage observations and subsequent research (Corney et al. 2018) led to refinements of the seismic assessment methods for precast floors, which were incorporated in the technical proposal to revise Section C5 (Concrete Buildings) of the "Guidelines for Detailed Seismic Assessment of Buildings" (MBIE et al. 2018), from hereon referred to as Assessment Guidelines C5.

Whilst consideration has been given to assessment of the hollow-core floor performance, guidance on hollow-core floor retrofits has been more limited with some options presented in a draft document prepared by the Precast Concrete Floors Overview Group (PCFOG 2009); however, those presented retrofit solutions have remained largely unvalidated.

1.1 RECAST FLOORS PROJECT

The 'ReCast Floors' research project was established with the primary objective of validating existing and developing new precast floor retrofits as well as improving the understanding of the seismic performance of precast floors. As part of the ReCast Floors project, two super-assembly tests were conducted in the laboratory facilities at the University of Canterbury. These tests were primarily carried out to experimentally validate proposed hollow-core floor retrofit solutions but also to address some further questions on the seismic behaviour of existing hollow-core floors, such as:

- What is the seismic performance of a hollow-core floor with common detailing features found in existing pre-2000s buildings? Selected detailing features included:
  - 200 mm hollow-core units spanning a single bay,
  - Units that are seated at intermediate columns (beta β units) and related,
  - Notches in the units to fit the units around columns.
- How does NMF in hollow-core floors progress on a system level?
- At what inter-storey drifts do web cracks form and how do they progress relative to the imposed peak drifts?
- How does floor damage affect the diaphragm performance?

The last of these topics is discussed in detail by Parr et al. (2022a; b).

This paper discusses the floor damage observations from the two ReCast Floors super-assembly tests, addressing the above questions and informing what earthquake damage can be expected in existing hollow-core floor buildings. These damage observations are then compared to demonstrate the effect of different floor detailing and the ground motion sensitivity. The damage observations are further compared to the assessed limiting drifts based on the Assessment Guidelines C5. Lastly, recommendations are made on effective inspection techniques for the detection of web cracks.

2 SUPER-ASSEMBLY SPECIMENS AND SETUP

Two super-assembly specimens were tested in the laboratory facilities at the University of Canterbury, Christchurch, New Zealand. Both test specimens represented a segment of a reinforced concrete frame building with retrofitted hollow-core floors and were each subjected to quasi-static simulated earthquake loading. Whilst the frame components were nominally the same for both test specimens, there were distinct differences in floor detailing, retrofit solutions and loading protocol between the two tests.

2.1 TEST SPECIMENS

The test specimens consisted of two-bay by one-bay reinforced concrete frames with precast hollow-core floor units, as shown in Figure 3. The general frame configuration incorporated typical 1980s Wellington building features, such as the eccentric alignment between beam centreline and column centreline and the resulting protrusion of the columns into the floor plate. The structural design and detailing of the frame components satisfied the latest ductile design provisions in accordance with NZS3101:2006-A3 (SNZ 2017) to ensure that these components had deformation capacity that was sufficient not to influence the experiment. Non-critical parts of the frame structure test specimens (i.e. columns, longitudinal beam reinforcement and the lower middle of the parallel beams) from the first test specimen were re-used for the construction of the second test specimen.

The floor was formed with eight 200 mm deep precast hollow-core floor units spanning 7.1 m in the one-bay direction and a 75 mm deep topping layer reinforced with non-ductile cold-drawn 665 mesh. Each hollow-core floor unit contained five 12.5 mm prestressing strands. The support connections to the frame, shown in Figure 4, replicated 1980s Wellington construction practice. The actual seating length varied for each unit end ranging from 15 to 55 mm.

Four of the eight hollow-core units (U1, U4, U5 and U8 in Figure 3a) were seated on the plastic hinges of the support beams. The hollow-core units U1 and U8, located adjacent to the parallel beams, can be classified as 'alpha (α) units' (Brooke et al. 2022; PCFOG 2009). Previous research has identified that alpha units can be subjected to displacement incompatibilities with the adjacent parallel beam deforming in double curvature while the hollow-core units attempt to remain flat (Fenwick et al. 2010; Matthews 2003; MBIE et al. 2018). Conversely, units U4 and U5 were seated on the plastic hinges at the intermediate columns and classified as 'beta units' (Brooke et al. 2022). The unique boundary conditions of beta units can lead to complex local demands in their support regions. Because previous super-assembly tests (Lindsay 2004; MacPherson 2005; Matthews 2003) did not include beta units, the super-assembly tests described in this paper were designed to gain insights into the seismic behaviour and damage patterns of beta units, particularly when subjected to bi-directional interstorey drift demands, as expected in real buildings.

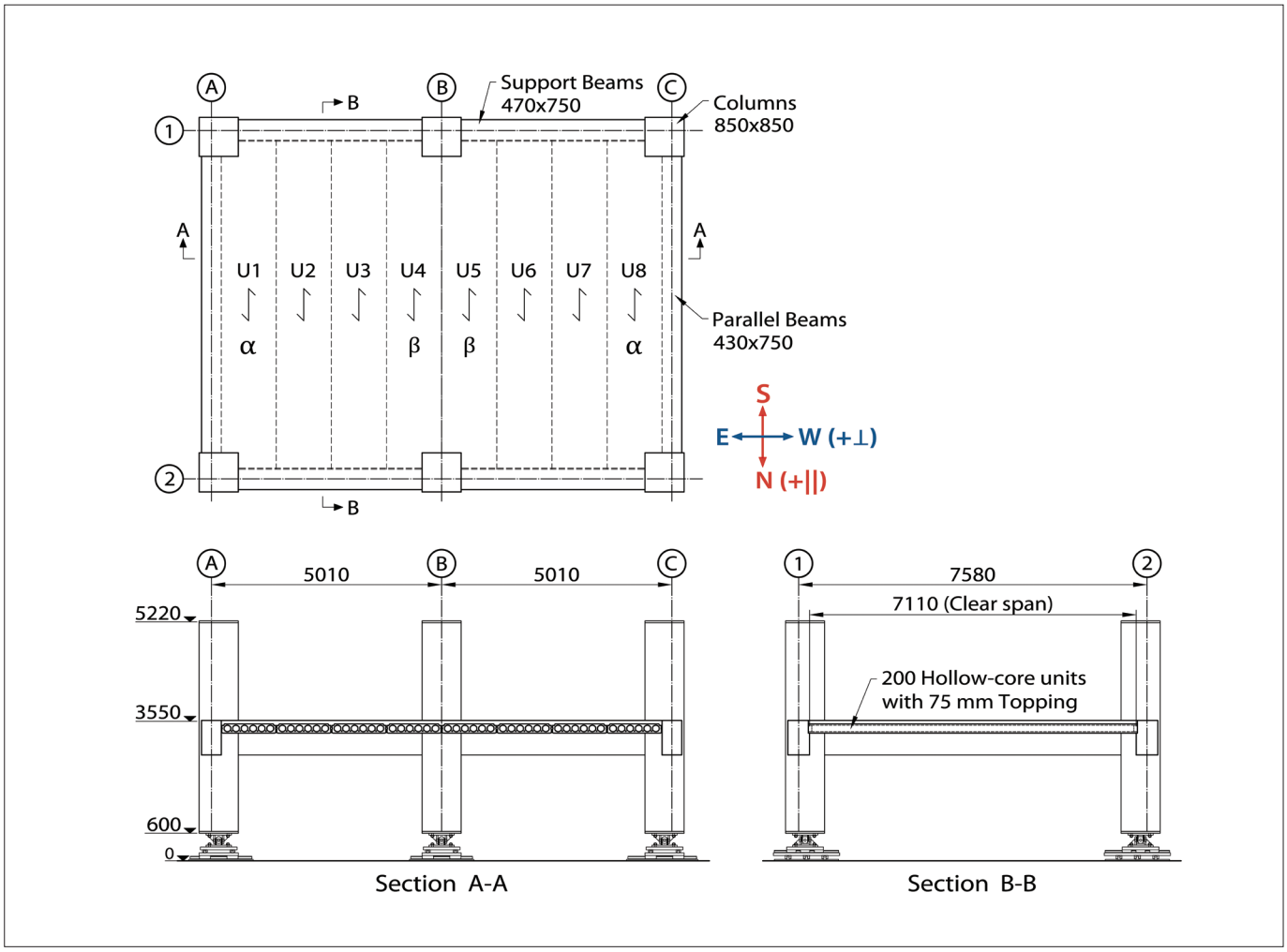

Figure 3: Super-assembly specimen with nominal dimensions.

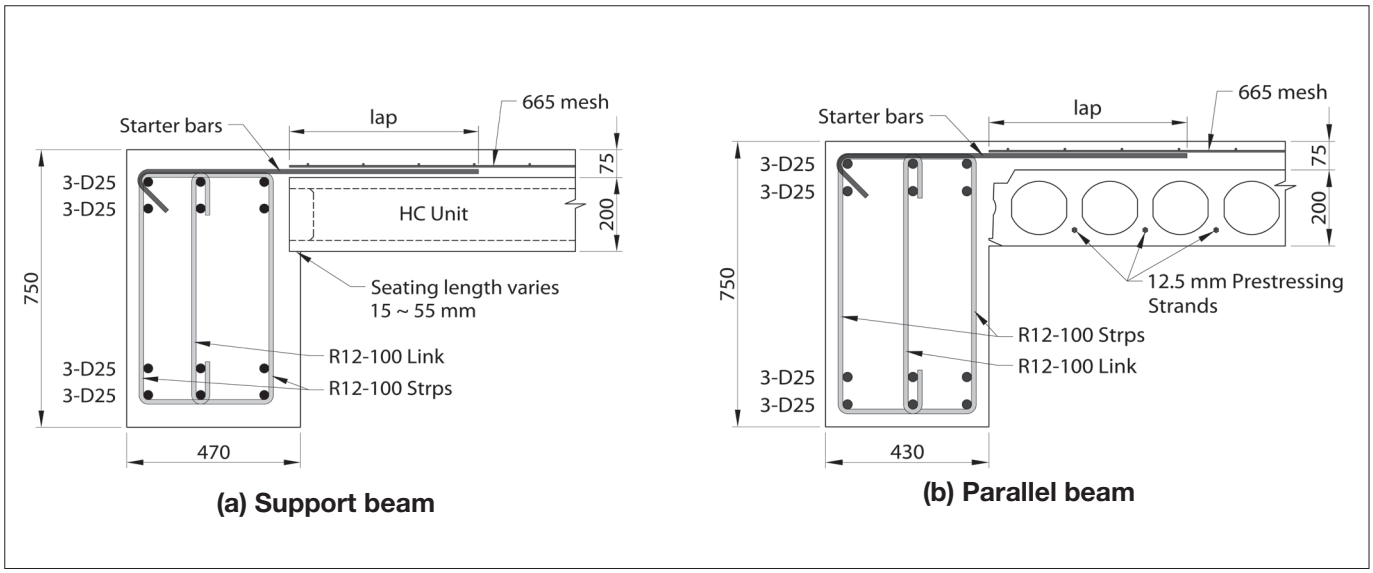

Figure 4: Cross-section view showing the floor-to-beam connections.

2.2 SETUP

The setup for the super-assembly tests, shown in Figure 5, allowed simultaneous bi-directional earthquake loading with 14 actuators installed along an L-shaped strongwall. The actuators were connected to the top and bottom of the columns along the south and east side of the test specimens. Load transfer between the columns was achieved through internal loading frames that acted as pantographs. The bottom of the columns rested on bi-directional sliders with universal hinges. The combination of internal loading frames and sliders ensured that the columns remained parallel while allowing the frame to dilate due to beam elongation. Loading of the test specimens was quasi-static and thus horizontal and vertical accelerations could not be simulated.

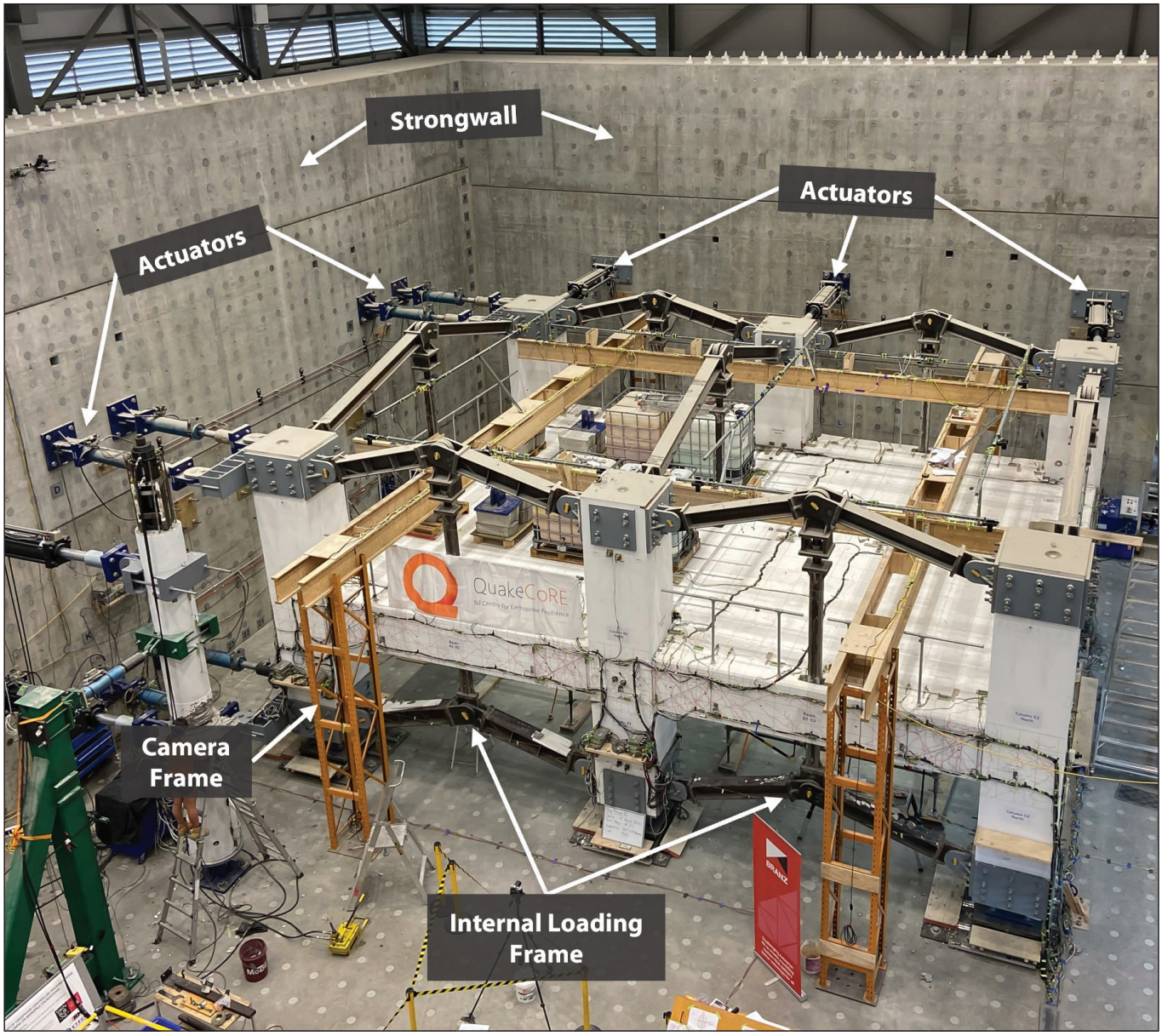

Figure 5: Super-assembly test setup in University of Canterbury laboratory

2.3 TEST CONFIGURATIONS AND LOADING PROTOCOLS

While the frame and setup of the two test specimens were generally similar, there were distinct differences in terms of floor detailing, floor retrofits and loading protocols. These differences are outlined for each of the two tests in Table 1 and elaborated in the following sub-sections. Table 1 also contains references to companion papers with more detail on the retrofits.

Table 1: Summary of floor detailing, retrofits and loading protocols for Tests 1 and 2

	Test 1	Test 2
Starter bar configuration (see Figure 6)	**Beam A1-B1 & A2-B2:** HD12 @400 mm centres with 600 mm lap **Beam B1-C1 & B2-C2:** HD12 @400 mm centres with 600 mm lap and mesh extending into top of the beam	**Beam A1-B1 & B2-C2:** HD12 @400 mm centres with 600 mm lap **Beam B1-C1:** HD12 @300 mm centres with 450 mm lap and mesh extending into top of the beam **Beam A2-B2:** 665 mesh extending into top of the beam (no starter bars)
Retrofits	**Unit U1 & U4:** Catch beams **Unit U2 & U3:** Supplementary seating **Unit U5:** Catch beams + supplementary transverse reinforcement **Unit U6 & U7:** Supplementary seating + supplementary negative moment reinforcement **Unit U8:** Supplementary transverse reinforcement (For conceptual retrofit details, refer to companion paper by Brooke et al. (2022))	**Units U1-U4:** Cable-catch retrofit (Brooke et al. 2022; Büker et al. 2021) **Units U5-U8:** Strongback retrofit (Büker et al. 2022)
Column ties (see Figure 6)	2x HD20 column tie bars (installed prior to casting the topping)	2x HD20 column tie bars (post-installed after casting the topping.) D12 'stitching bars' in transverse direction (reinstating the load path across cut mesh between units U4 and U5.)
Additional gravity weights on floor	No additional loads (only self-weight of the floor)	Additional weights on units U1-U4 in accordance with: $E_d = G + \psi_E Q + E_u$ (SNZ 2011)
Loading protocol (see Figure 7)	**Phase 1:** 2016 Kaikoura Earthquake (far-field) **Phase 2:** Standard Loading Protocol (Bi-directional circular loading pattern)	**Phase 1:** 1994 Northridge Earthquake (pulse-type) **Phase 2:** Standard Loading Protocol (Bi-directional elliptical loading pattern with 1 (‖) to 0.5 (⊥) ratio)

2.3.1 Starter bar configurations

The starter bar configurations at the supports were varied between the two test specimens to investigate the effect of different reinforcement arrangements on the floor performance. For the first specimen, the starter bar configuration was generally kept consistent with slight variations between the two bays (refer to Table 1 and Figure 6a).

Test specimen 2 comprised several different starter bar configurations, as shown in Figure 6b (also refer to Table 1). Most notably, the detailing along B1-C1 was designed to be particularly critical for negative moment failure, firstly to investigate how a negative moment failure evolves on a system level and secondly to test the retrofit solutions for this failure mode. A 30 mm-deep saw cut was made at the end of the starter bars along beam B1-C1 prior to testing to ensure that a negative moment crack formed in this for NMF critical location (Figure 6b). The detailing along beam A2-B2 was in contrast to this highly reinforced connection, with only mesh extending from the topping into the top of the beam. Although the 'mesh only' configuration is not typically encountered along seismic frames, it is more commonly found at internal supports.

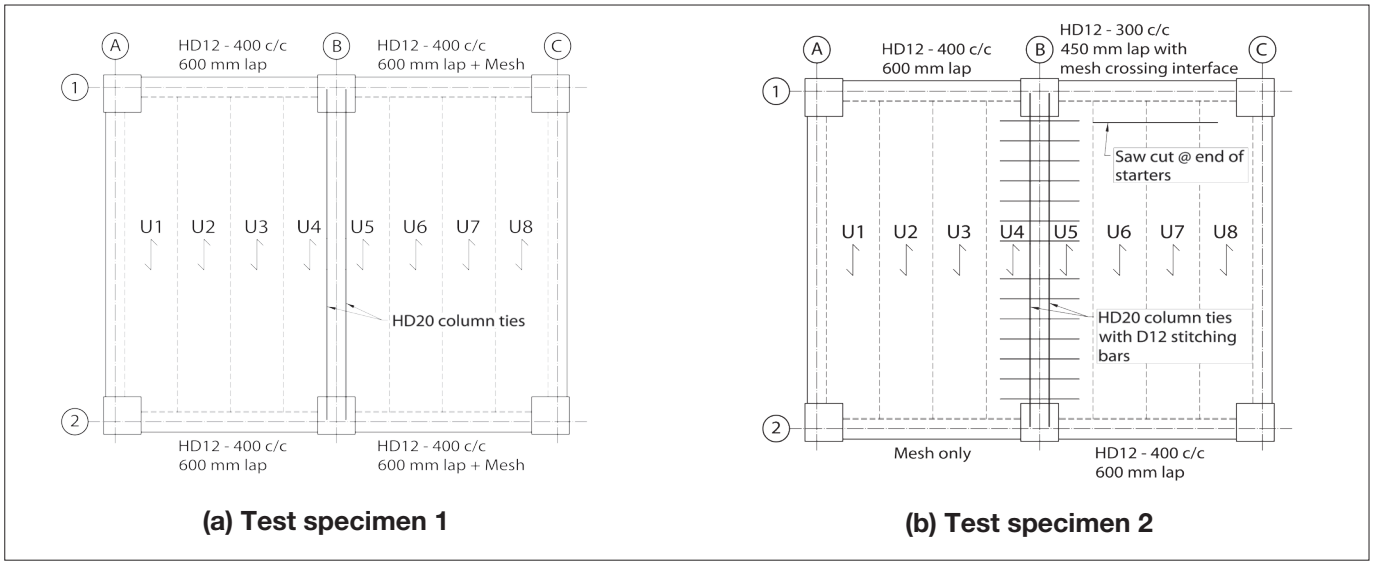

(a) Test specimen 1 **(b) Test specimen 2**

Figure 6: Starter bar configuration and column tie detailing.

2.3.2 Retrofits

Both test specimens comprised a variety of floor retrofits that primarily aimed to prevent the collapse of the flooring units and ensure life safety performance. The retrofits were designed to only actively engage when the floor underwent vertical dislocation relative to the support structure. For this reason, the damage observed at low-to-medium drift levels was not significantly affected by the presence of the floor retrofits. A list of the retrofit solutions that were installed in each test specimen can be found in Table 1. However, it should be noted that this paper does not discuss the performance of the retrofit solutions but only focuses on the floor performance. For more detail on the retrofit solutions refer to the companion papers by Brooke et al. (2022) and Büker et al. (2022).

That notwithstanding, the column tie retrofits, which tie the intermediate columns into the topping layer, warrant further elaboration within this paper because these tie bars actively affected the floor performance. Column tie reinforcement was required for the intermediate columns B1 and B2 as per NZS3101:2006-A3 (SNZ 2017) to prevent the columns from translating outwards. As column ties were typically not installed in existing 1980s precast floor buildings, they were considered a retrofit solution for these tests. For the first test specimen, the column tie bars were epoxied into the inner face of the intermediate columns and placed under the mesh reinforcement before casting the topping concrete. For the second test specimen the column ties were post-installed after the topping concrete had been laid. Grooves were cut into the topping layer, which required cutting the mesh reinforcement to achieve sufficient depth for reinforcement coverage. For this reason 'stitching bars' were needed to be installed across where the mesh had been cut. The grooves for both the column ties and stitching bars were roughened and subsequently filled with high-strength cementitious grout.

2.3.3 Loading Protocols

Two different series of loading protocols were adopted for the two experiments. The loading protocols were developed aiming to represent realistic earthquake loading scenarios for hollow-core floor buildings in Wellington. During the 2016 Kaikōura earthquake a significant number of Wellington buildings incurred damage to hollow-core flooring (Henry et

al. 2017), and consequently the displacement demands in the first test were aimed to simulate shaking from this earthquake. To evaluate the interstorey drift demands imposed by this earthquake, De Francesco and Sullivan (2022) developed a three-dimensional finite element model of a thirteen-storey reinforced-concrete frame building with hollow-core floors featuring typical characteristics of 1980s construction practice in Wellington. Nonlinear time-history analyses were conducted for both horizontal components of the 2016 Kaikōura earthquake record from the CPLB station (Chandramohan et al. 2017). The inter-storey drift response was identified to be largest at the third storey. The response at the third storey was extracted, simplified and converted into a circular bi-directional cloverleaf loading pattern, which is schematically illustrated in Figure 7c. For a clear differentiation of the loading direction, the inter-storey drift demands applied in the direction parallel to the hollow-core unit span (North-South direction) are marked with a '||' symbol and inter-storey drift demands transverse to the unit span (East-West direction) are marked with a '⊥' symbol. After the simulation of the 2016 Kaikōura earthquake, loading was continued with progressively increasing drift levels following the same circular cloverleaf pattern. The entire loading sequence for Test 1 is shown in Figure 7a and is listed numerically in Table 2.

The experimental observations during Test 1 (refer to Section 3.1) highlighted that torsional softening of the frame structure, due to the many bi-directional cycles of the far-field 2016 Kaikōura earthquake motion, can significantly decrease the floor demands. To contrast these findings, the second test simulated a near-fault, pulse-type motion from the 1994 Northridge earthquake recorded at the Rinaldi Receiving Station. The inter-storey drift response was derived using the same procedure as for Test 1. The derived simplified earthquake demand consisted of an initial pulse to -2.0% (||) inter-storey drift, followed by loading to +1.0% (||) and ±1.0% (⊥) as shown in Figure 7b. The directionality from the 1994 Northridge earthquake motion was further continued in the standard loading protocol phase by using an elliptically shaped cloverleaf loading pattern (Figure 7d). The aspect ratio between the parallel (||) and transverse (⊥) direction was 1:0.5. The entire loading sequence for Test 2 is shown in Figure 7b and is listed numerically in Table 3.

Figure 7: Loading protocols with low-intensity cycles to 0.125% drift omitted for clarity. (Note: ROM# refers to the application of Rhomboid loading as shown in Figure 8.)

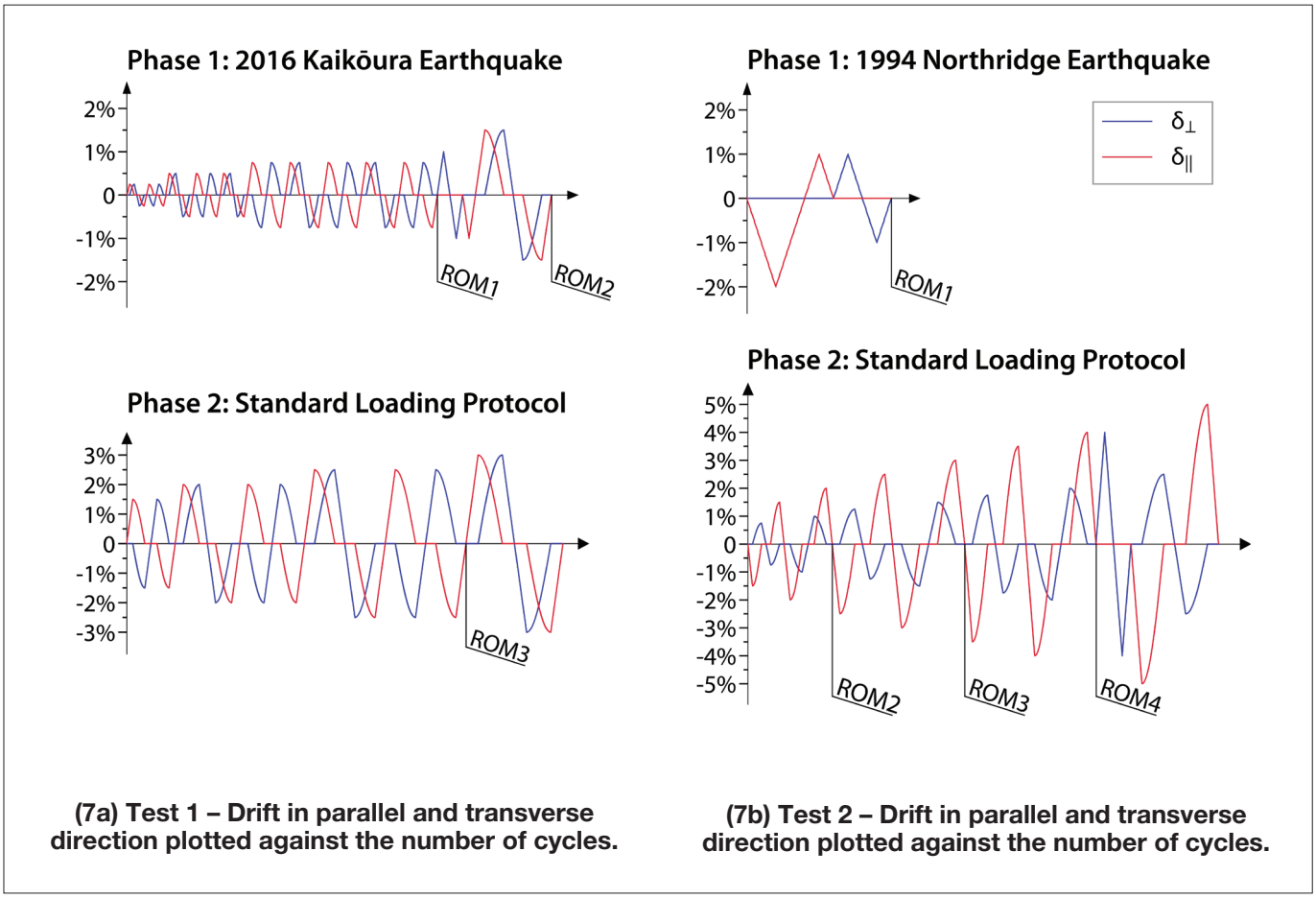

(7a) Test 1 – Drift in parallel and transverse direction plotted against the number of cycles.

(7b) Test 2 – Drift in parallel and transverse direction plotted against the number of cycles.

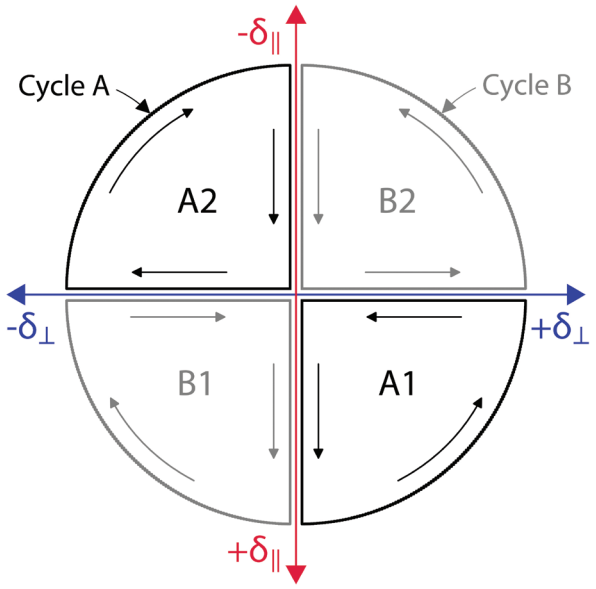

(7c) Test 1 – Circular loading pattern

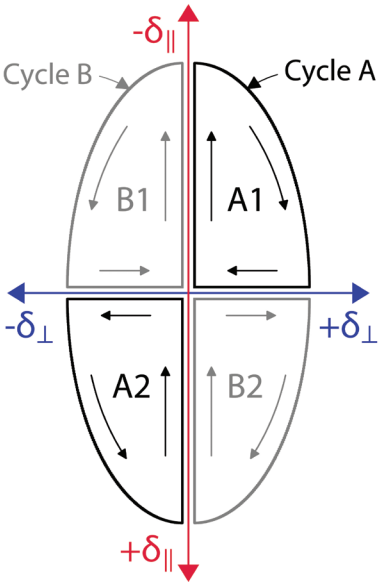

(7d) Test 2 – Elliptical loading pattern with an aspect ratio of 1:0.5

Table 2: Numerical loading sequence of Test 1

Loading Phase	No. of Cycles	Inter-storey drift
Low intensity cycles	2	0.125%
2016 Kaikōura EQ	2	0.25%
	3	0.5%
	5	0.75%
	-	ROM1
	1	1.0%
	1	1.5%
	-	ROM2
Standard Loading Protocol	1	1.5%
	2	2.0%
	2	2.5%
	-	ROM3
	1	3.0%

Table 3: Numerical loading sequence of Test 2

Loading Phase	No. of Cycles	Inter-storey drift
Low intensity cycles	2	0.125%
1994 Northridge EQ	-	-2.0% (‖), +1.0% (‖), +1.0% (⊥), -1.0% (⊥)
	-	ROM1
Standard Loading Protocol	1	1.5%[1]
	1	2.0%[1]
	-	ROM2
	1	2.5%[1]
	1	3.0%[1]
	-	ROM3
	1	3.5%[1]
	1	4.0%[1]
	-	ROM4
	-	+4.0% (⊥),
		-4.0% (⊥),
	1	5.0%[1]

[1] Reflects peak-drift value in (‖) direction. Drift in (⊥) is 50% of the stated (‖) value due to the elliptical loading pattern (Figure 7d).

Because of the quasi-static application of loading, no inertial forces were applied to the specimen and consequently the in-plane diaphragm demands could not be simulated. Nonetheless, to investigate the effect of progressive floor damage on the diaphragm capacity, a deformation pattern referred to as 'rhomboid' loading (ROM) was imposed at different points throughout the earthquake loading phases. The rhomboid loading was applied by horizontally translating the frame at gridline 2 in the positive and negative transverse direction while holding the frame at gridline 1 in place, as schematically shown in Figure 8. For further details on the rhomboid loading, as well as an analysis of the diaphragm performance at different floor damage stages, refer to Parr et al. (2022a; b).

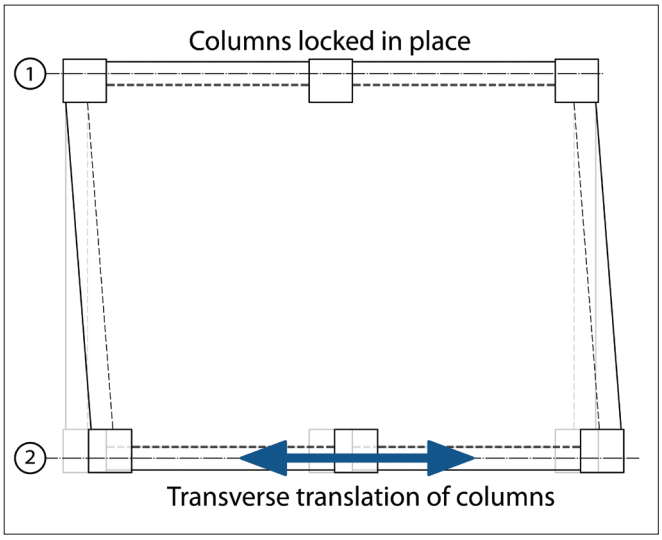

Figure 8: Rhomboid loading

2.4 ASSESSED DRIFT CAPACITY OF THE FLOOR SYSTEM

The drift capacity of the precast floor components in the super-assemblies can be assessed for the three potential failure modes (LOS, NMF and PMF) using the Assessment Guidelines C5 (MBIE et al. 2018). This assessment identifies the drift level at which a flooring unit is expected to lose its reliable gravity load path. This point is unlikely to coincide with the collapse of the flooring unit because precast concrete floors, particularly hollow-core floors, may have unreliable load paths that cannot reliably be quantified and depended on (MBIE et al. 2018).

The assessed drift capacities of the tested flooring units are listed in Table 4. The drift capacities are provided for each failure mode under consideration of the different demands based on the flooring unit's location relative to the parallel beams. All listed drift capacities exclude the factor of 2, which is used in the Assessment Guidelines C5 to account for the uncertainties in estimating the drift demands and capacities and the step-change nature of the floor performance when the demands exceed these capacities. For simplicity, the LOS assessment was conducted assuming a specified seating length of 50 mm and construction tolerances of 20 mm. The assessment of the floor diaphragm is omitted in this paper.

Table 4: Assessed drift capacities based on the Assessment Guidelines C5 (excluding factor 2)

Failure mode	Units affected	Limiting drift
LOS1*	U1,U2,U7,U8	1.2%
LOS2*	All	1.3%
NMF	All**	1.0%
PMF1*	U1,U2,U7,U8	2.0%
PMF2*	All	3.1%
PMF3*	U1,U8	1.4%

Footnote:

* Drift capacities depend on the displacement demands, which are defined as follows:

PMF1 – Demands due to support rotation and elongation of the parallel beam (within elongation zone)

PMF2 – Demands due to support rotation and unit movement due to plastic elongation of the starter bars (outside elongation zone)

PMF3 – Demands due to displacement incompatibility between floor and parallel beam (alpha units only)

** NMF is precluded for the mesh only configuration (U1-U4 at North support of test specimen 2) and where supplemental negative moment reinforcement was installed (U6-U7 of test specimen 1)

3 QUALITATIVE DAMAGE OBSERVATIONS

The qualitative observations of floor damage relative to the imposed inter-storey drift demands are outlined in this section. A more detailed description and forensic analysis of this damage is not addressed in this paper but will form part of a PhD thesis (Büker (In Preparation)).

3.1 FLOOR DAMAGE IN TEST 1

This section outlines the observed floor damage from Test 1 chronologically. The progression of damage in the floor is also summarised in Figure 11, where the key damage states are plotted against the imposed peak drifts. Visualisations of the floor damage in the form of photos and crack maps are presented sequentially in Figure 12.

As described above, the first test simulated the 2016 Kaikōura earthquake followed by a standard loading protocol with progressively increasing inter-storey drifts.

2016 Kaikōura Earthquake (KEQ)

During loading the first sign of floor damage occurred at +0.25% (⊥) inter-storey drift when a longitudinal split (0.4 mm wide) formed between the beta units U4 and

U5 (Figure 12a). This split was initiated by the transverse displacement demands that arise from the rotation and elongation of the beams connecting into the intermediate columns, as schematically demonstrated in Figure 9.

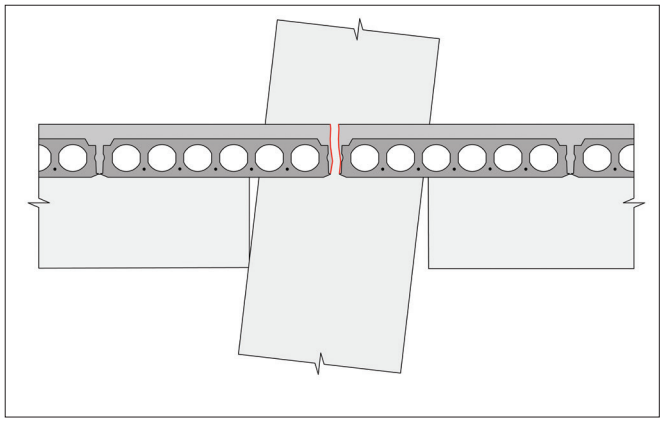

Figure 9: Transverse displacement demands generating split (shown in red) between beta units (deformation exaggerated for clarity)

During the load cycles to 0.5% drift, a substantial amount of new cracking occurred with three main locations of cracking. Firstly, longitudinal splits formed down the first cell of the alpha units U1 and U8 while loading to ±0.5% (⊥) drifts. Secondly, transverse soffit cracks along the seating ledge of the support beams in alpha and beta units occurred when loading to ±0.5% (||) drift. Lastly, the warping deformations due to the simultaneous bi-directional loading generated cracks around the columns in the soffit and top of the floor (refer to Figure 12b).

Although, at this stage, there was only minor cracking visible on the exterior of alpha unit U8, a web crack was suspected of having formed at the south support during the 0.5% drift cycles. This web crack was detected through simple acoustic testing by tapping a hammer on the underside of the floor lengthways along the webs. A distinct difference in the pitch of the sound response could be heard where the crack was suspected. Nonetheless, visual confirmation of the crack was not possible with a borescope camera at this stage. The web crack at this previously identified location became clearly visible at +1.0% (||) drift, as indicated in Figure 12c.

At +1.5% (||) the transverse soffit cracks along the south support of the units had widened substantially. Most notably, the transverse soffit crack in beta unit U4 measured 4 mm with a vertical offset of 2.7 mm and the soffit corner crack in alpha unit U1 measured 3.8 mm in width with a vertical offset of 2.5 mm. These observations are of particular significance because a vertical dislocation in excess of 2 mm is considered an indicator that the reliable gravity load paths between the floor and the support have been lost (Corney et al. 2021).

With further progression of loading, the elongation from the plastic hinges at the intermediate columns B1 and B2 concentrated in the split between the two beta units U4 and U5. As a result, the non-ductile 665 mesh wires across the split fractured while loading to +1.5% (⊥) drift (Figure 12d).

At this point in the test, the beams had sustained extensive cracking in the plastic hinges, resulting in a significant reduction in the torsional stiffness of the damaged beam hinges. Furthermore, dilation of the frame due to beam elongation induced tension in the starter bars which extend from the top of the beam into the floor topping. This eccentrically acting tension force in the starter bars combined with the eccentrically acting floor weight with respect to the centre of the beam caused the beam to sustain a permanent positive rotation relative to the floor. This behaviour had three critical effects on the floor performance:

1. As the beams were no longer fully constrained to twist as drift was imposed on the columns, the relative rotations between the floor and the beams decreased, particularly for the units closer to the midspan of the beam, as indicated in Figure 10.
2. A permanent relative positive rotation between the support beam and the floor meant an increase in seating demands or widening of the positive moment cracks.
3. The behaviour described in above points (1) and (2) also resulted in the relative negative rotations between the floor and the support (remaining small after the beams lost torsional stiffness). Thus, the negative moment demands at the end of the starter bars, which is the critical section for negative moment failure, were relieved to some extent thus decreasing the potential for negative moment failure.

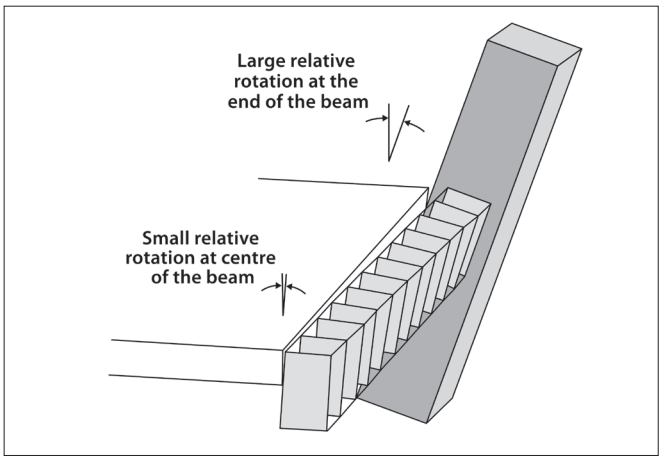

Figure 10: Schematic demonstrating the effect of reduced torsional stiffness in the support beam on the relative rotation between the floor and beam (adapted from Matthews (2003))

Standard Loading Protocol (SLP)

Despite the reduced relative rotation demand on the floor, additional damage was observed during the standard loading protocol phase particularly in locations already damaged during the 2016 Kaikōura earthquake simulation.

Throughout the seismic loading, splitting cracks along the column ties had developed in the vicinity of the intermediate columns. During the cycles to 2.0% and 2.5% the topping concrete over the column ties at the face of the columns spalled off, exposing the reinforcement (Figure 12e).

From the borescope inspections conducted during the 2.5% drift cycles it was concluded that web cracking was present in multiple locations, as indicated in Figure 12f. Only alpha and beta units exhibited web cracking in this first test. The majority of detected web cracks were an extension of the soffit cracks and propagated at an angle of 45° or steeper in the direction of the gravity shear, which is consistent with the positive moment crack propagation observations from Matthews' super-assembly experiment (2003, see Figure 2).

The first experiment was terminated after finishing the 3% drift cycles due to an actuator control error.

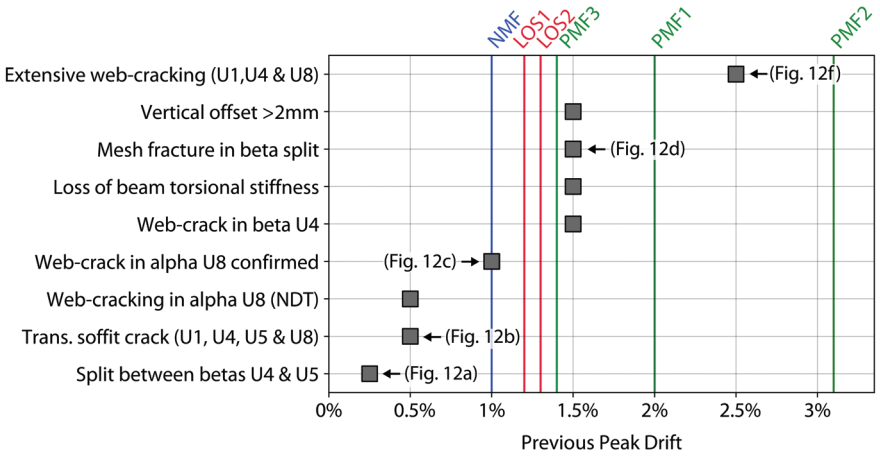

Figure 11: Summary of damage observed in first experiment (refer to Section 2.4 for the definition of failure modes)

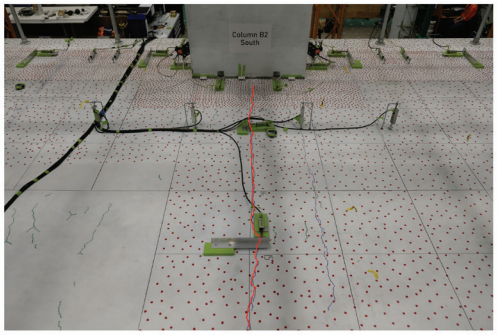

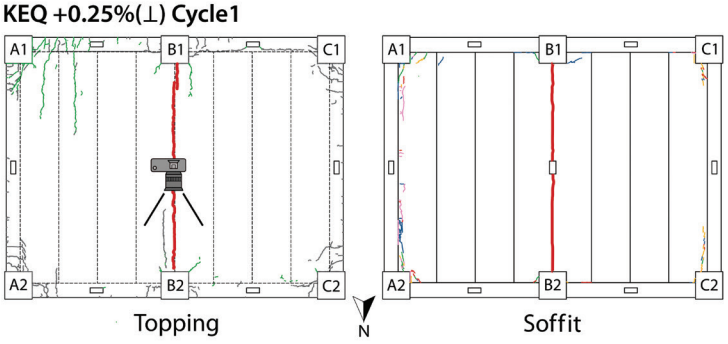

12(a) Full-length longitudinal split between the two beta units shown after 0.25% drift cycles.

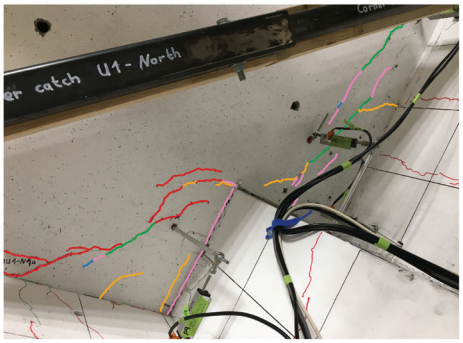

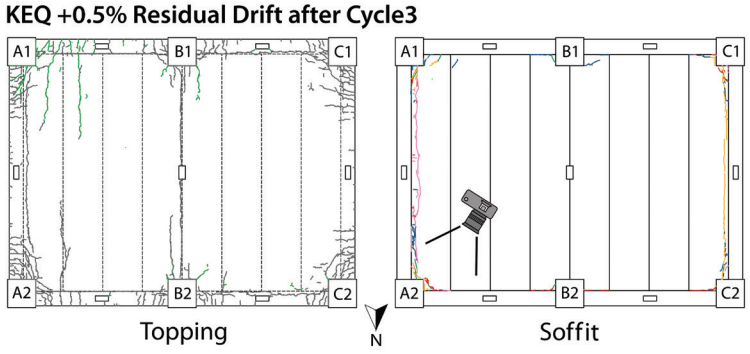

12(b) Transverse soffit cracking in alpha and beta units, longitudinal splits through the first cell of alpha units U1 and U8, and increased cracking around the corners during the 0.5% cycles.

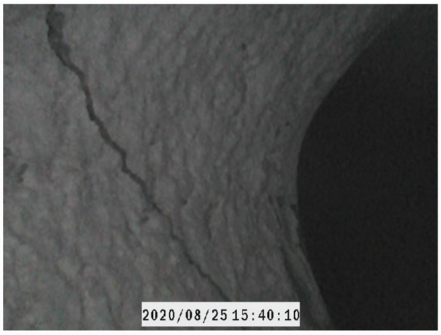

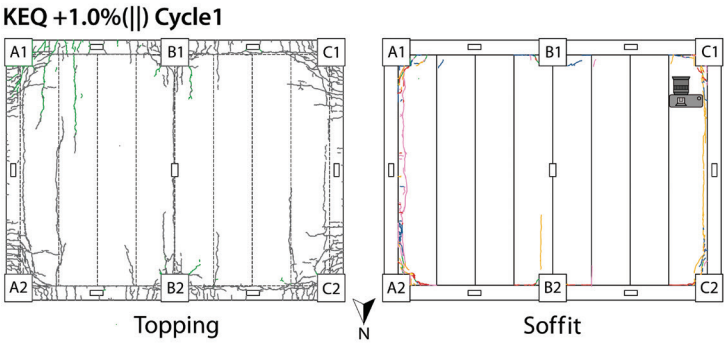

(12c) Web crack in alpha unit U8 at +1.0% (||) (where at 0.5% drift a web crack was detected via acoustic testing)

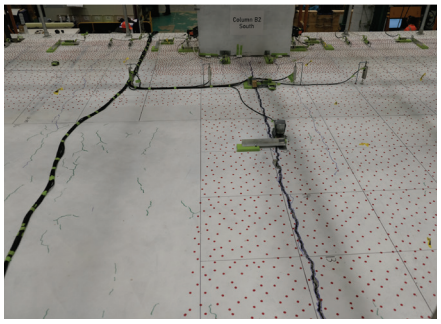

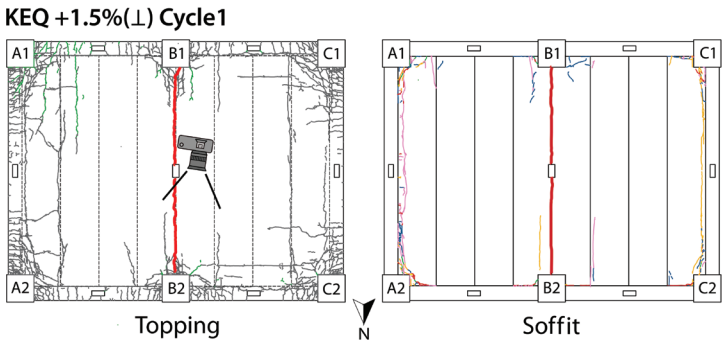

(12d) Widened longitudinal split between beta units after rupture of mesh reinforcement shown after 1.5% drift cycles

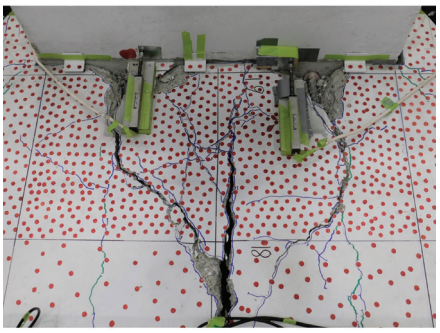

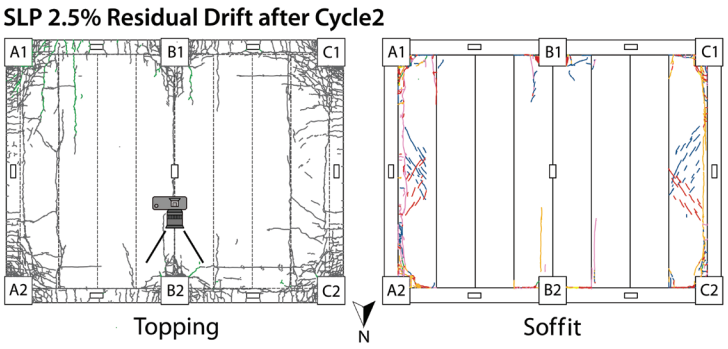

(12e) Extensive spalling and splitting cracks at 2.5%

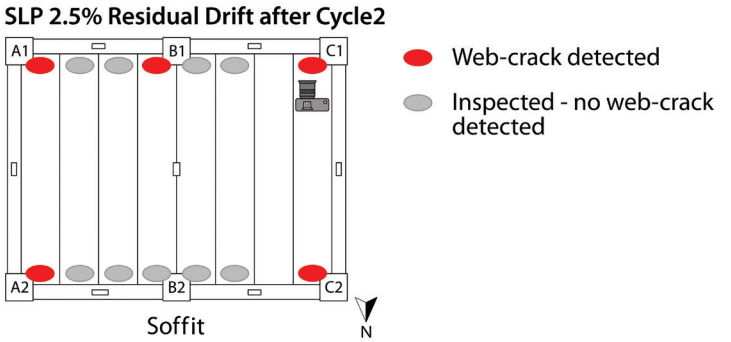

(12f) Extensive web cracking in multiple hollow-core unit ends at 2.5%

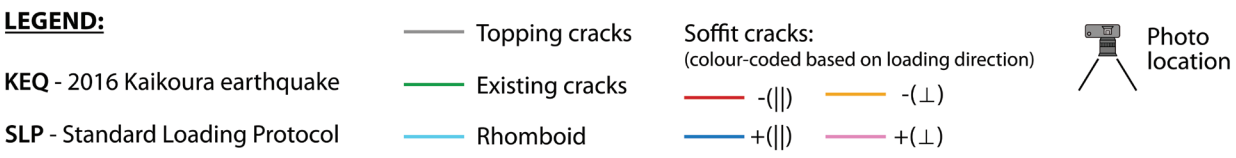

Figure 12: Floor damage observed in Test 1

Gravity test of earthquake damaged hollow-core units

Following the seismic loading, a gravity test was conducted on beta unit U4. The objective of this gravity test was to investigate the residual gravity load-carrying capacity of an earthquake-damaged hollow-core unit. Prior to testing the hollow-core unit of interest was isolated by removing the adjacent flooring units to avoid load sharing between units and allow for a clear view of the sides. The gravity load was applied by placing 1000-litre water tanks on the hollow-core unit and slowly filling the tanks with water.

The actuator control error at the end of the first test mainly affected beta unit U4 at the south support because column B1 was accidentally pulled outwards by 29 mm when the specimen was at -1.5% (||). Before the gravity test the loading error was partially corrected by pushing the column back inwards by 8.3 mm and bringing the specimen into the upright position (0% (||) drift). This correction reinstated the initial conditions to a satisfactory extent because the displacements imposed by the loading error concentrated at the back face of the unit and did not cause noticeable additional damage to the hollow-core unit itself. The web cracking and delamination that beta unit U4 sustained during the earthquake loading are illustrated in Figures 13 a - d. As shown in Figure 13b, the floor was only partially seated.

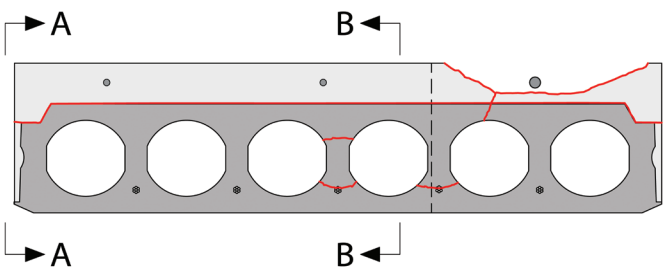

(a) Existing web cracking before the gravity test (Note: This figure only shows the web cracks that were detected by borescope)

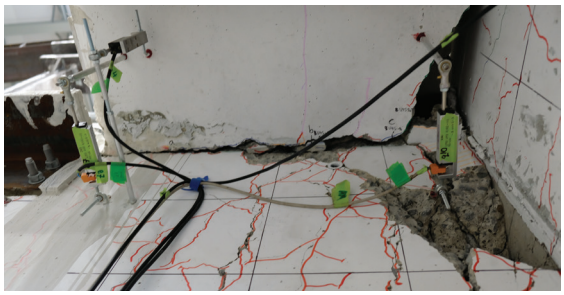

(b) Bottom-view

(c) Side-view from the East (Section A-A in Figure 13a)

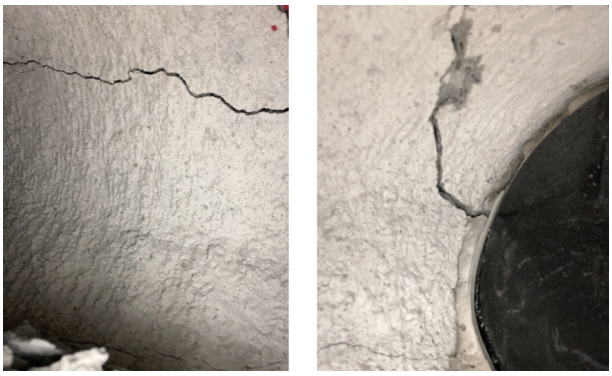

(d) Web cracks in central web (Section B-B in Figure 13a)

Figure 13: Condition of beta unit U4 (south support) after seismic demands and before gravity test

During the gravity test, beta unit U4 could sustain shear loads of up to 38.7 kN and sudden brittle failure occurred when this load was reached, as shown in Figure 14a. Further drop was prevented by the SHS that was installed as a seismic 'catch beam' retrofit underneath this hollow-core unit as part of the overall retrofit solutions (Table 1). Extraction of the failed beta unit U4 gave further insights into the failure mechanism. While the outer web failed in a shallow web-shear crack (Figure 14a), the three interior webs sheared off at a much steeper angle (Figure 14b).

(a) Side-view after failure

(b) Photo of failed end after the extraction

Figure 14: Gravity Test of a damaged beta unit U4.

The shear load of 38.7 kN at which the hollow-core unit failed corresponds to 91% of the design gravity shear demand (1.2G+1.5Q with Q = 3.0 kPa). When comparing the measured shear loads to the design web-shear capacity, they correspond with 52% of the design web shear capacity per NZS3101:2006-A3 (SNZ 2017) when accounting for the reduced section due to the notches and omitting the strength reduction factor of 0.75. While only indicative, given the wide variability in web damage expected in beta units due to earthquake damage and potential effect from the actuator control issue, the test results give a sense of how much web cracking may compromise the residual gravity capacity of hollow-core floors.

The finding that web damage reduces the strength of hollow-core units is consistent with the fact that the shear design of hollow-core floors is done under the presumption that the unreinforced webs remain uncracked. El-Sayed et al. (2019) and Sarkis et al. (2022) conducted experimental component tests on the web-shear cracking behaviour of hollow-core floors, including the post-cracking behaviour. The experiments showed that the load-carrying capacity of the hollow-core units is compromised and reduces substantially once a web-shear crack through the webs has formed. These observations, along with the findings from the gravity test presented in this study, validate concerns regarding how much earthquake-induced damage (in particular, web cracking) compromises the gravity load-carrying capacity of hollow-core units. Further research is required to investigate this matter, given that it was observed in this test that web cracks can form at drifts as low as 0.5% and that many buildings with hollow-core floors in Wellington likely experienced drift demands larger than 0.5% during the 2016 Kaikōura earthquake.

3.2 FLOOR DAMAGE IN TEST 2

The second specimen was loaded with a pulse-type motion from the 1994 Northridge Earthquake, followed by progressively increasing drifts (Figure 7b). The progression of damage is described below and summarised in Figure 15.

1994 Northridge Earthquake (NEQ)

The first pulse to -2.0% (||) drift, as part of the 1994 Northridge earthquake loading, caused extensive damage to the floor. When the pulse reached -0.35% (||) drift, a negative moment crack formed in the saw-cut at the end of the starters along beam B1 C1. The detailing along this support beam (Figure 6b) was intentionally designed to be particularly critical for negative moment failure.

Subsequently the first web cracking was detected at -0.5% (||) drift in units U7 and U8 (North end), as shown in Figure 16a. Although the detected web cracks were an extension of the aforementioned negative moment crack, the low drift at which these web cracks formed highlighted the fragility of the unreinforced webs. The detection of such narrow web cracks with a borescope camera was difficult due to the challenging navigation of the borescopes and poor lighting conditions in the voids. Furthermore there was no indication of the web crack through damage on the underside of the floor because the web crack was an extension of the negative moment cracking that initiated at the top of the floor.

The first transverse soffit cracking occurred along the north support at -0.5% (||) and additional soffit cracks formed while loading to -0.75% (||) drift. Most notably a transverse soffit crack formed 200-350 mm away from the support in alpha unit U1 (Figure 16b). Although the soffit crack only measured 0.3 mm in width, it propagated internally as a diagonal web crack in the direction of the gravity shear towards the top of the unit. This soffit crack had initiated at

the corner of the notch that was cut into the unit to fit the alpha unit around the precast columns. Thereby, this crack demonstrated how the notches acted as a stress raiser that promoted soffit and web cracking away from the support. Similarly the presence of the stitching bars that were installed transversely along the column ties acted as a stress raiser, promoting a negative moment crack near the end of the starter bars along support A1-B1 (see topping crack map in Figure 16b).

At -1.0% (||) drift a vertical offset of 1.3 mm across the soffit crack at the north support of beta unit U5 was measured. During the loading to -1.5% (||) drift the vertical offset across the now 3 mm wide soffit crack increased to 2.6 mm and thus exceeded the vertical offset benchmark of 2 mm, which indicates a loss of reliable load path (Corney et al. 2021). The vertical offset measured across the soffit crack in beta unit U4 (north end) was even more pronounced, measuring 3.7 mm. This soffit crack formed approximately 100 mm from the support beam ledge and propagated internally as a shallow web crack approximately 400-500 mm towards mid-span, as shown in Figure 16c.

With further loading the negative moment crack at the end of the starter bars along beam B1-C1 continued to widen. From -1.6% (||) onwards, the 665 mesh at the end of the starter bars fractured starting at column C1 and progressing to column B1. When -2.0% (||) drift was reached the width of the negative moment crack ranged from 3.5 mm (at beta unit U5 – Figure 16d) to 5.0 mm (at alpha unit U8) and a substantial vertical offset of up to 3.2 mm (at beta unit U5) was measured across this crack.

The presence of web cracking in every hollow-core unit was confirmed at the peak of the first pulse (-2.0% (||) drift) as indicated in Figure 16e. Furthermore additional vertical offsets across the transverse cracks in the soffit of beta units U4 and U5 were recorded, with a magnitude of 6 mm and 4.5 mm respectively. Figure 16f illustrates the extent of the vertical offset in beta unit U5. It should be noted that further vertical offset of beta unit U5 was prevented by the strongback retrofits, but the cable-catch retrofit under beta unit U4 allowed for additional vertical offset.

During drift demands in the transverse direction (±1.0% (⊥)) it became evident that the stitching bars (see Figure 6b) prevented the formation of a single dominating longitudinal split between the beta units as was previously observed in the first test. Instead the transverse deformation demands distributed to several longitudinal splits that had predominantly formed beyond the stitching bars.

Standard Loading Protocol (SLP)

Further significant damage to the hollow-core floor was observed during the standard loading protocol phase (Figure 7b). At +1.6% (||) drift the mesh at the floor perimeter along beam A2-B2 fractured during loading to +2.0% (||) drift. This particular support comprised no starter bars but only 665 mesh that extended from the topping into the top of the beam. Following the fracture of the mesh, the previously distributed negative moment cracking in the floor topping closed up and deformations started to concentrate in the crack where the mesh ruptured, subsequently behaving as a pinned support.

With increased peak displacements the web cracks widened substantially, as demonstrated by the borescope photo depicted in Figure 16g at -2.5% (||) drift. Despite the significant width of web cracks at peak drift the web cracks were found to close up when the test specimen was moved to residual displacement. This observation has two key implications for a post-earthquake inspection. Firstly, the inspection for web cracks in real buildings can be challenging with the web cracks having closed. Secondly, the width of the web crack after the earthquake cannot directly be correlated to the length and extent of the web crack.

With the progression of loading the gravity load paths at the end supports of the flooring units became heavily compromised. The strongback retrofits that were installed under units U5-U8 successfully limited the vertical offset, whereas the cable-catch retrofits that were installed under units U1-U4 required the floor to drop before the cables engaged. During the 3% drift cycles units U3 and U4 had sustained a large vertical offset while units U1 and U2 experienced comparatively little vertical offset. This limited offset could be attributed to load sharing between the parallel beam A1-A2, unit U1 and unit U2. Although this load path is structurally unreliable it evidently helped prevent the units from sustaining excessive vertical drop at this stage of the test.

During loading to 3.5% (||) drift the mesh along beam A1 B1 fractured in a negative moment crack at the end of the starter bars. This negative moment crack propagated from the stitching bars across the units U1-U4 and merged with a flexural crack in the top of the beam A1-A2. At this support the starter bar configuration was assessed to be on the verge of being prone to negative moment failure using the Assessment Guidelines C5 (MBIE et al. 2018). A possible interpretation is that the yield force of the starter bars acting in tension was not sufficient to fracture the mesh at the end of the starter bars, but the strain hardening of the starter bars was sufficient to trigger the negative moment failure. Following this failure the floor sustained a

significant vertical displacement, leading to all hollow-core floor units being at least partially supported by the retrofits.

During the fourth rhomboid (ROM4) the northern frame was displaced transversely by +34 mm and -32 mm. At +34 mm transverse displacement the mesh along the west end of the stitching bars fractured, resulting in a wide longitudinal split running through beta unit U5 (Figure 16h).

At -4.0% (⊥) drift a secondary crack in the bottom part of beta unit U4 along the edge of the seating angle formed when the floor engaged with the angle, which was intentionally set down by 40 mm (Figure 16i). The collapse of the hollow-core unit was prevented by the cable-catch system that was anchored back to the seating angle. Nonetheless, this crack highlights the fragility of hollow-core units that have sustained shallow web cracking and indicates that seating angle retrofits may not be suitable solutions to address this damage (Brooke et al. 2022; SESOC et al. 2021).

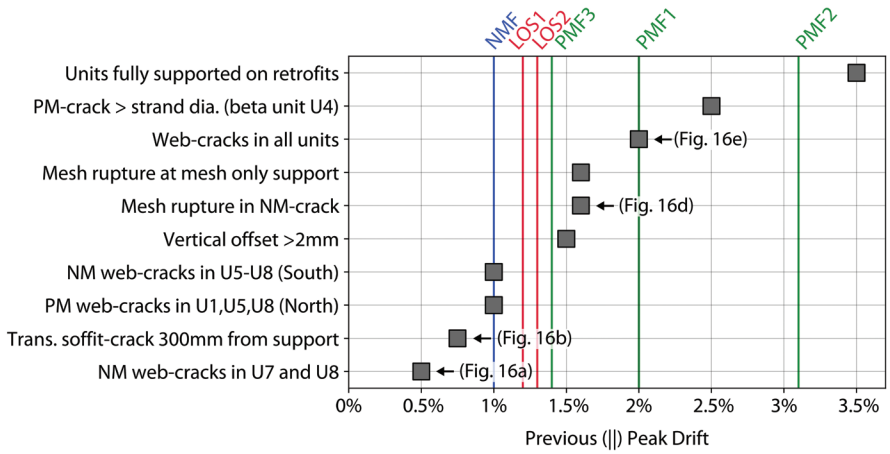

Figure 15: Summary of damage progression of Test 2 (refer to Section 2.4 for the definition of failure modes)

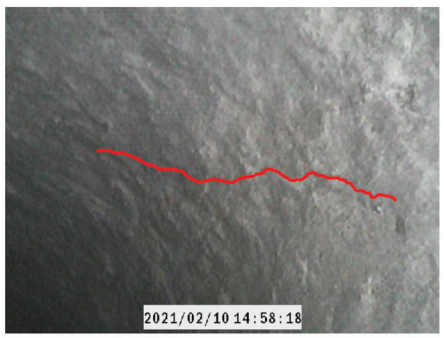

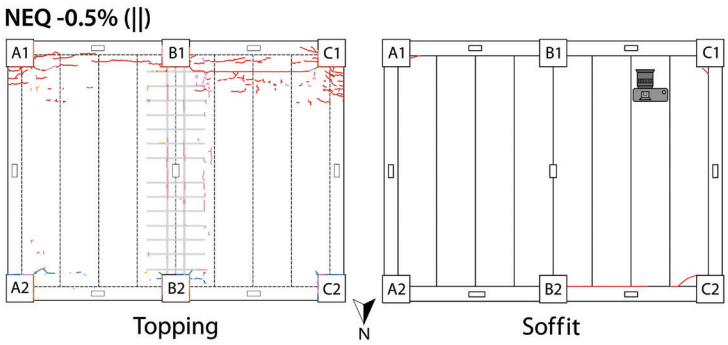

(a) First web crack in Unit U7 (illustrated in the photo) and alpha unit U8 – crack is highlighted in red

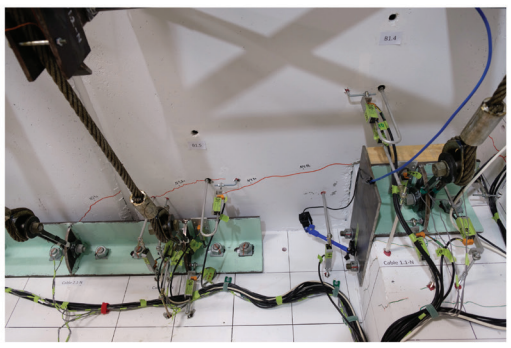

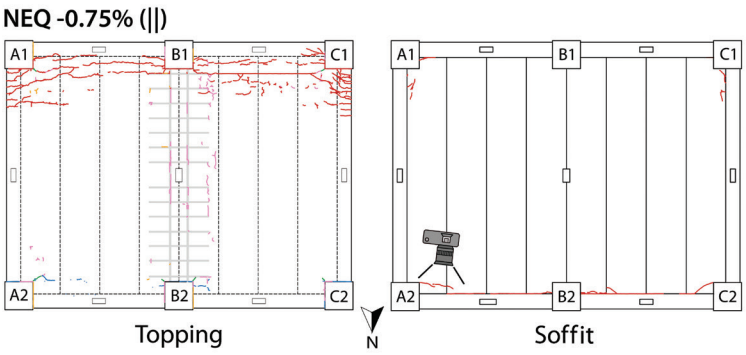

(b) Transverse soffit crack approx. 200-350 mm away from the support ledge (Alpha U1 – North)

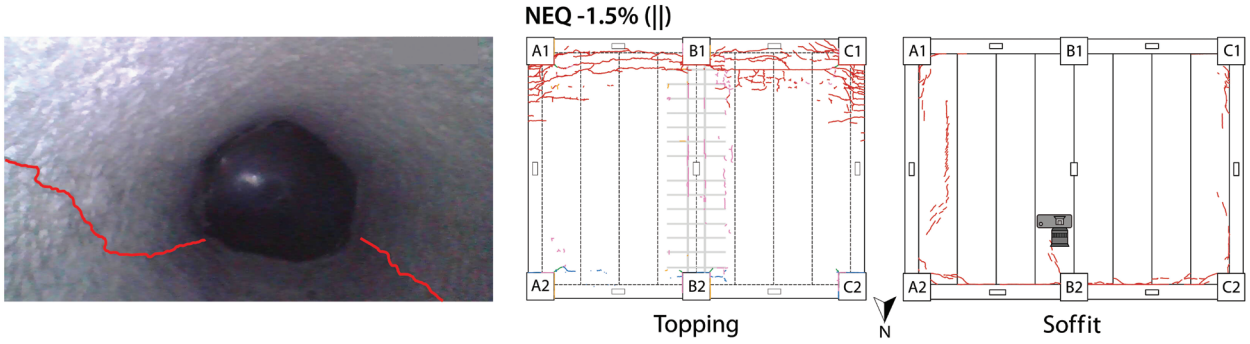

(c) Web cracking in beta unit U4 (North support)

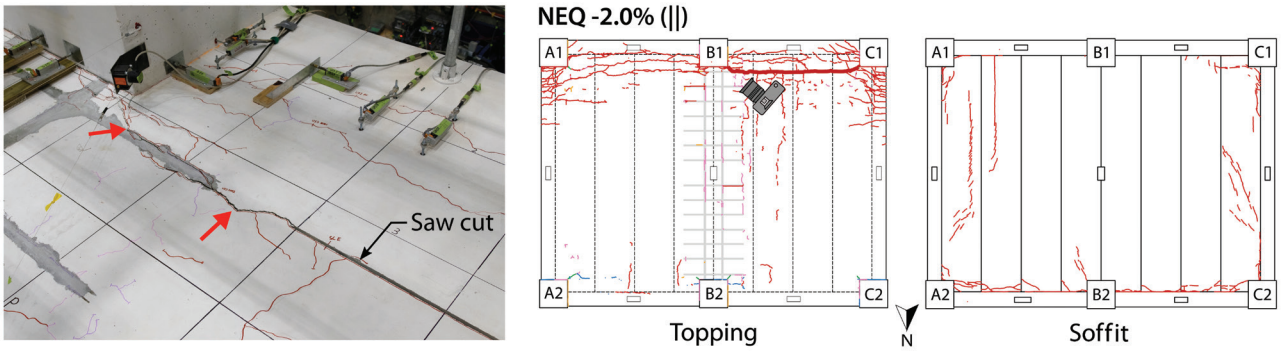

(d) Negative moment crack shown at -2.0% (||) after mesh rupture at -1.6% (||)

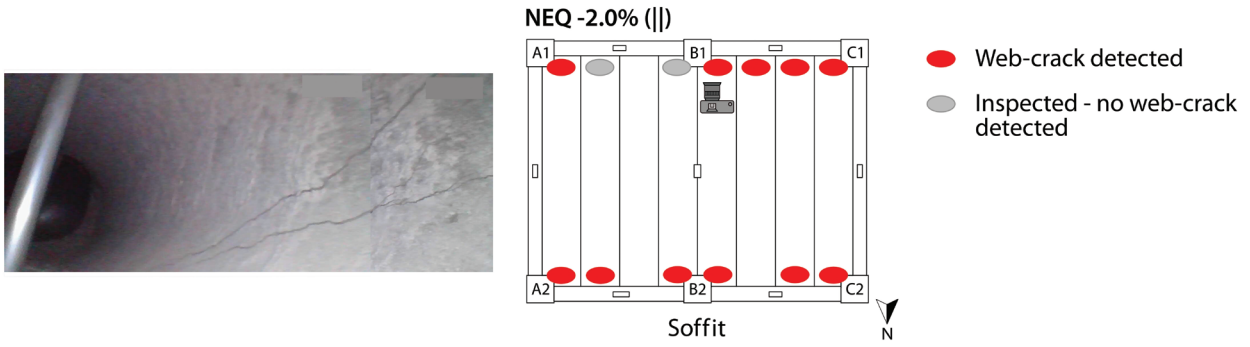

(e) Web cracking at -2.0% (||). The photo shows a web crack that is an extension of the negative moment crack in unit U5.

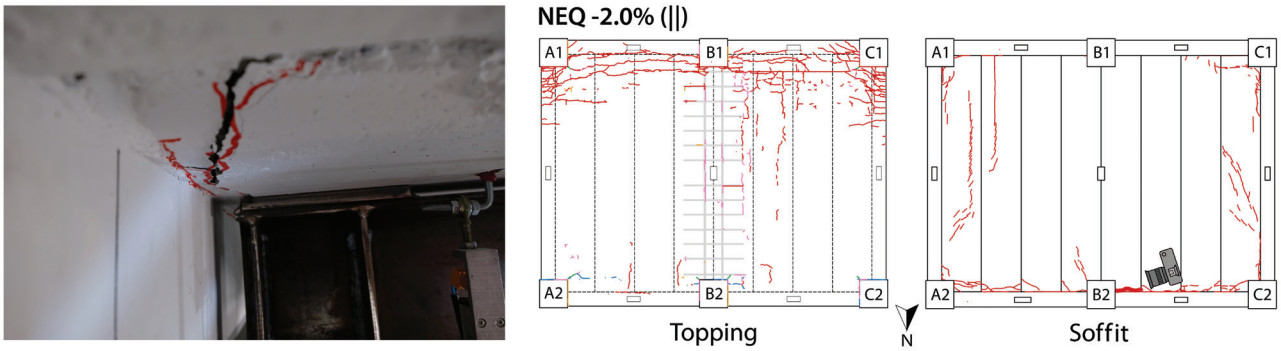

(f) Vertical offset in beta unit at -2.0% (||)

(g) Shallow diagonal web crack in unit 2 at -2.5% (||)

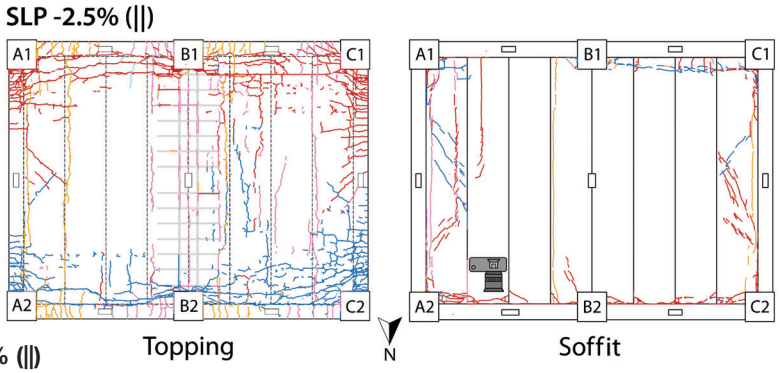

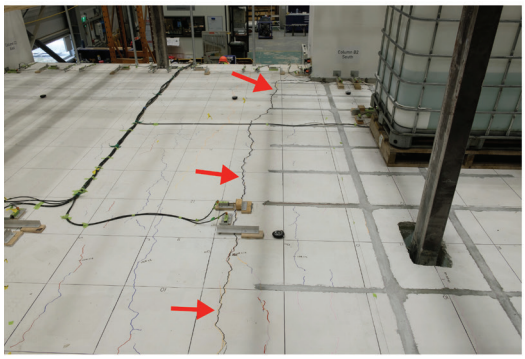

(h) Mesh rupture in a longitudinal split running through the last cell of beta unit U5

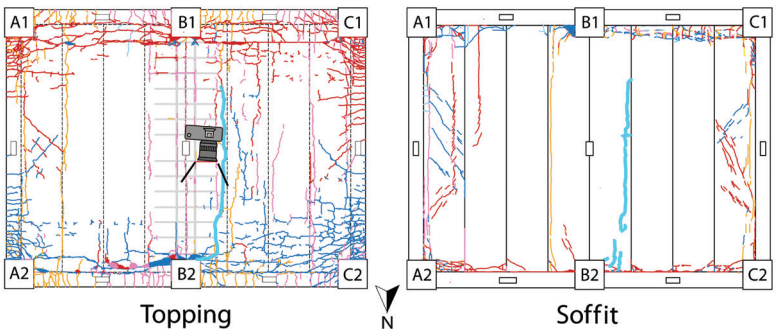

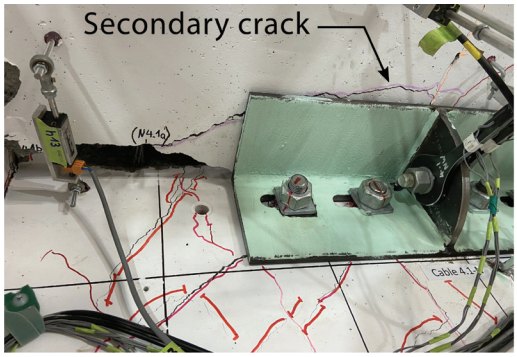

i) Secondary cracking in the bottom flange of unit formed when floor drops on set-down angle.

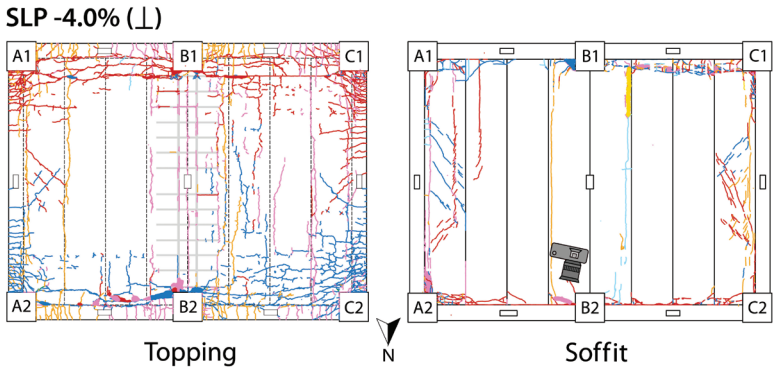

LEGEND:

NEQ - 1994 Northridge earthquake

SLP - Standard Loading Protocol

Existing cracks

Rhomboid

Topping and soffit cracks:
(colour-coded based on loading direction)

-(||)

-(⊥)

+(||)

+(⊥)

Photo location

Figure 16: Floor damage observed in Test 2

3.3 COMPARISON OF FLOOR DAMAGE PROGRESSION OF TESTS 1 AND 2

When comparing the extent of floor damage observed in the two super-assembly tests, it can be summarised that the second test exhibited more severe damage to the floor than the first test. The difference in damage levels can primarily be attributed to the early loss of torsional stiffness in the supporting beams during the first test. As described in Section 3.1 the loss of torsional stiffness in the beams decreases the relative rotation between the floor and the beam which leads to a reduction in demands and, consequently, less damage to the floor. This effect has also been observed in previous super-assembly tests (Lindsay 2004; MacPherson 2005; Matthews 2003; Peng 2009).

A further contributing factor to the limited amount of floor damage in the first test was the softening of the floor perimeter through a large number of cycles at relatively low inter-storey drifts (e.g. 1% drift) in the 2016 Kaikōura earthquake input motion. With the softened perimeter, additional deformations concentrated in the damage at the floor-to-beam interface in the first test. This observation contrasts with the damage observed in the second test, where the pulse-type nature of the 1994 Northridge earthquake with the initial monotonic pulses to -2% (||) and +1% (||) in the direction of the floor span caused significantly more transverse cracking and associated web cracking within the hollow-core units.

In addition, the shallow nature of the web cracks and the presence of soffit cracks forming away from the support observed in the second test stood out. These damage patterns draw into question the efficacy of seating retrofits, such as seating angles, to address positive moment failures. (Brooke et al. 2022; Büker et al. 2021; SESOC et al. 2021).

In both tests beta units were found to sustain a higher degree of damage than units seated outside the plastic hinge region. This statement is based on test observations indicating a concentration of damage in beta units with (1) earlier onset of web cracking, (2) more extensive web cracking, (3) larger vertical offsets and (4) susceptibility to large longitudinal splits. Mostafa et al. (2022) further elaborate on the vulnerabilities of beta units and emphasise that the damageability of these units is neither considered in the current New Zealand Concrete Structures Standard NZS3101:2006-A3 (SNZ 2017) nor in the Assessment Guidelines C5 (MBIE et al. 2018).

These two super-assembly tests also showed that the detailing of the column ties can have an influence on the location of cracking. In the first test the transverse displacement demands on the floor that arise from rotation and elongation of the beams at the intermediate column (Figure 9) caused a longitudinal split between the two beta units. With the mesh rupturing during the 1.5% drift cycle the floor diaphragm completely separated in this location. For the second test ductile D12 stitching bars were installed transversely across the interface between the beta units U4 and U5 to reinstate the load path across the portion of the mesh that needed to be cut during post-installation of the column ties (Figure 6b). The presence of these stitching bars resulted in the displacements manifesting in a split that formed beyond the stitching bars and through beta unit U5, as shown in Figure 16h. While the stitching bars successfully prevented significant longitudinal splitting along the column ties where the mesh was cut, the splitting shifted beyond the stitching bars, where there was only mesh reinforcing the topping layer (Figure 16h). These observations emphasise the brittleness of floor diaphragms reinforced with non-ductile mesh reinforcement (665 mesh in this case). As a consequence of mesh rupture in these splits, the ability for tension ties to develop as part of the diaphragm strut-and-tie load path is removed, which is further discussed in the companion papers by Parr et al. (2022a; b).

3.4 COMPARISON OF FLOOR PERFORMANCE TO ASSESSED CAPACITY

The seismic assessment of the flooring units (Section 2.4) can be compared to the floor damage observed in the super-assembly tests. Generally, the floor damage in the two experiments was highly variable and it was found that the observed failure pattern does not necessarily reflect the predicted governing failure mode based on the assessment (i.e. failure mode with the lowest assessed drift capacity). For instance, in the second test much of the deformation along the north support between columns A2 and B2 concentrated at the positive moment soffit cracks, while a LOS failure was expected to be the governing failure mechanism as per assessment. This finding underlines the importance of installing floor retrofits that address all failure modes (not only the governing failure mode) with drift capacities lower than the expected demand.

Although the actual failure mechanism sometimes differed from the predicted governing failure mechanism, the assessed drift capacities gave a good indication as to when the floor would lose the reliable load path. Similar to previous work (Corney et al. 2021) the load path of the floor was considered to be unreliable once a vertical drop of 2 mm was reached. In both tests this vertical drop benchmark was exceeded when the peak drifts were increased from 1.0% to 1.5%. These drift levels lie in the range of the typical drift limits for LOS and NMF, as illustrated in the damage summary plots (Figure 11 for Test 1 and Figure 15 for Test 2).

3.5 DETECTION OF WEB CRACKING

Precast hollow-core floors in New Zealand have no vertical shear reinforcement and, thus, rely solely on the capacity of the prestressed concrete to resist shear demands. The shear stresses are highest in the hollow-core floor webs, which are optimised to resist the shear stresses as an uncracked section. However the observed damage from the super-assembly tests shows that the earthquake-induced deformations can result in various degrees of web cracking, initiating at drift levels as low as 0.5%. Web cracks may reduce the gravity load-carrying capacity for both gravity loading and future earthquake loading, as indicated by the results of the gravity test described in Section 3.1. Nonetheless further research is required to reliably quantify the residual gravity load capacity of web-cracked hollow-core units.

Based on the experience gained from the many web crack inspections performed during the super-assembly tests, the following recommendations can be made:

- Web crack inspections should commence on floors/levels which likely experienced the largest interstorey drift in a previous earthquake(s). Additionally, the Assessment Guidelines C5 (MBIE et al. 2018 - Section C5E.2) provide recommendations on where to conduct inspections for precast concrete floors.
- Alpha and beta units are particularly (but not exclusively) vulnerable to web cracking and should be prioritised when conducting an inspection for web cracks.
- Significant cracking in the topping at the end of the starter bars may indicate a negative moment failure, which involves shallow web cracking. Negative moment failure cracks typically run vertically through the topping and top flange of the hollow-core unit but then propagate as shallow web cracks, branching towards the support and usually also towards mid-span. This type of cracking can lead to a sudden collapse even when the mesh is still intact (see Woods (2008) for background information on negative moment failure in hollow-core floors).
- Transverse and diagonal soffit cracks that cross underneath one or multiple webs of the hollow-core unit likely have propagated into the above webs. If there is a vertical offset across the soffit crack, this offset likely reflects the width of the web crack.
- While web cracking associated with positive moment cracking is typically accompanied by soffit cracking, this soffit cracking may not be visible as it may occur behind the support ledge or can be covered by existing retrofits. Beta units can experience web cracks that initiate at the end of the unit. Hence some units without visible soffit or topping cracks may still have experienced web cracking and thus should not be ignored in an inspection protocol.
- When inspecting the interior of a hollow-core unit it is recommended to actively check for potential web cracking during the inspection. Trying to identify web cracks after the inspection from recorded photos and videos is challenging and may require additional inspections to confirm the presence and location of a web crack.
- Web cracks will be challenging to identify after an earthquake when the building has returned to plumb as the cracks will have closed. Not identifying web cracks in the inspection does not necessarily guarantee there are no web cracks present.
- Acoustic testing, such as hammer tapping or more sophisticated non-destructive testing methods, may be helpful to identify web cracks.

4 SUMMARY

This paper presents the progression of hollow-core floor damage from two super-assembly tests. The tested hollow-core floors were constructed using common floor details in New Zealand during the 1980s. The most relevant floor damage observations are as follows:

- Cracking in the unreinforced webs of the hollow-core units initiated at 0.5% drift in both tests. Based on this early onset it may be concluded that many existing hollow-core floor buildings in Wellington that were affected by the 2016 Kaikōura Earthquake and were subjected to drifts equal to or exceeding 0.5% drift contain hollow-core units with cracked webs.
- The detection of the early narrow web cracks in the test specimens was difficult due to poor light conditions and navigation challenges with the borescope camera, even in ideal laboratory conditions. Additionally, web cracks that were of substantial width and length at peak drifts tended to close up at residual displacement. Therefore, inspecting units for web cracks and not identifying any cracks during the inspection does not guarantee that none exist in a building that has experienced drift demands beyond 0.5%. Recommendations are presented on how to identify the hollow-core units that likely sustained web cracks and how to effectively inspect the interior of those flooring units.
- Earthquake damage, particularly web cracking near the support, can decrease the gravity load-carrying capacity of hollow-core floors, as demonstrated by loading an earthquake-damaged unit with gravity weights. The damaged unit only withstood 91% of the gravity design load (1.2G+1.5Q) and 52% of the design capacity according to NZS3101:2006-A3 (SNZ 2017), excluding the strength reduction factor.

- Transverse soffit cracking can occur away from the support and beyond the typical seating retrofits (i.e. seating angles). Hollow-core units with notches are particularly prone to such cracking because the notches act as a stress raiser. Furthermore the web cracks extending from the transverse soffit cracks were found in these tests to propagate at very shallow angles. These findings raise concerns about the ability of seating retrofits to address positive moment failure (Brooke et al. 2022; SESOC et al. 2021).
- Pulse-type ground motions tend to cause more severe damage to the hollow-core floors than far-field ground motions, which involve many smaller cycles leading up to the peak response.
- Hollow-core units seated at the intermediate columns (beta units) are more susceptible to damage than units that are supported closer to the mid-span of the support beam. Whilst alpha units are addressed, the heightened fragility of these beta units is not recognised in the current seismic assessment procedures in the Assessment Guidelines C5 (MBIE et al. 2018) and requires further research.
- The Assessment Guidelines C5 (MBIE et al. 2018) have been found to provide a good indication of the drift capacity of the tested hollow-core floors. However in many instances the observed damage patterns did not reflect the predicted governing failure modes.

5 ACKNOWLEDGEMENT

The authors would like to thank the funders who made the super-assembly tests described in this paper possible. The main funders were BRANZ (from the Building Research Levy), QuakeCoRE, the Earthquake Commission (EQC), Concrete NZ and the University of Canterbury. Blacks Fasteners, Fischer and Hilti kindly sponsored the material for fasteners. Thanks are also extended to the Advisory Group of the 'ReCast Floors' project for the valuable input for developing the tests. The successful delivery of the experimental programme would not have been possible without the countless hours and valuable advice of the technical staff at the University of Canterbury, most notably Dave Carney, Alan Thirlwell, Russell McConchie, Norman King, Dave MacPherson and John Maley. Also noteworthy is the contribution of the many students who helped with the test, namely Eldhose Paulose, Max Chirapattanakorn, Trevor Garrett, Abhishek Madan, Yuxin Huang, Claire Dong, Mohamed Mostafa, Ana Sarkis, Justin Brown, Jacob Nicholls and Alex Kirby.

This project was (partially) supported by QuakeCoRE, a New Zealand Tertiary Education Commission-funded Centre. This is QuakeCoRE publication number 0749.

6 REFERENCES

Brooke, N. J., Büker, F., Bull, D. K., Elwood, K. J., Henry, R. S. and Hogan, L. S. 2022. "Overview of Retrofit Requirements and Techniques for Precast Concrete Floors." Journal of the Structural Engineering Society New Zealand, 35 (1).

Büker, F. (In Preparation). "Development and Experimental Validation of Hollow-core Floor Retrofits." PhD Thesis. University of Auckland, New Zealand.

Büker, F., Brooke, N. J., Elwood, K. J., Bull, D. K., Hogan, L. S. and Parr, M. 2021. "Development and Validation of Retrofit Techniques for Hollow-core Floors." Proceedings of the 2021 SESOC Conference, 14. Hamilton, New Zealand: Structural Engineering Society New Zealand.

Büker, F., Brooke, N. J., Hogan, L. S., Elwood, K. J., Bull, D. K. and Sullivan, T. J. 2022. "Design Recommendations for Strongback Retrofits." Journal of the Structural Engineering Society New Zealand, 35 (1).

Bull, D. K., and Matthews, J. 2003. Proof of Concept Tests for Hollowcore Floor Unit Connections (Research Report 2003-1). 1–84. Department of Civil Engineering, University of Canterbury.

Chandramohan, R., Ma, Q., Wotherspoon, L. M., Bradley, B. A., Nayyerloo, M., Uma, S. R. and Stephens, M. T. 2017. "Response of instrumented Buildings Under the 2016 Kaikoura Earthquake." BNZSEE, 50 (2): 237–252. https://doi.org/10.5459/bnzsee.50.2.237-252.

Corney, S. R., Elwood, K. J., Henry, R. S. and Nims, D. K. 2018. Assessment of Existing Concrete Buildings in Wellington with Precast Floors. Kaikoura Earthquake Research Programme (2017-18). Lower Hutt, New Zealand: Natural Hazards Research Platform.

Corney, S. R., Puranam, A. Y., Elwood, K. J., Henry, R. S. and Bull, D. K. 2021. "Seismic Performance of Precast Hollow-Core Floors: Part 1—Experimental Data." ACI Structural Journal, 118 (5): 49–64. https://doi.org/10.14359/51732821.

De Francesco, G., Sullivan,T. J. and Nievas, C. I. 2022. "Highlighting the Need for Multiple Loading Protocols in Bi-Directional Testing (In Production)." Bulletin of the New Zealand Society for Earthquake Engineering, 15.

El-Sayed, A. K., Al-Negheimish, A. I. and Brennan, A. M. 2019. "Web Shear Resistance of Prestressed Precast Deep Hollow Core Slabs." ACI Structural Journal, 116 (1): 139–150. https://doi.org/10.14359/51706919.

Fenwick, R., Bull, D. K., and Gardiner, D. 2010. Assessment of Hollow-Core Floors for Seismic Performance (Research Report 2010-02). University of Canterbury, Christchurch, New Zealand (https://ir.canterbury.ac.nz/handle/10092/4211).

Henry, R. S., D. Dizhur, K. J. Elwood, J. Hare, and D. Brunsdon. 2017. “Damage to Concrete Buildings with Precast Floors During the 2016 Kaikoura earthquake.” Bulletin of the New Zealand Society for Earthquake Engineering, 50 (2): 174–186.

Herlihy, M. D. 1999. “Precast Concrete Floor Support and Diaphragm Action.” PhD Thesis. University of Canterbury, Christchurch, New Zealand.

Jensen, J. 2006. “The Seismic Behaviour of Existing Hollowcore Seating Connections Pre and Post Retrofitted.” ME Thesis. University of Canterbury, Christchurch, New Zealand.

Liew, H. Y. 2004. “Performance of Hollow-core Floor Seating Connection Details.” ME Thesis. University of Canterbury, Christchurch, New Zealand.

Lindsay, R. 2004. “Experiments on the Seismic Performance of Hollow-core Floor Systems in Precast Concrete Buildings.” ME Thesis. University of Canterbury, Christchurch, New Zealand.

MacPherson, C. 2005. “Seismic Performance and Forensic Analysis of a Precast Concrete Hollow-Core Floor Super-Assemblage.” ME Thesis. University of Canterbury, Christchurch, New Zealand.

Matthews, J. 2003. “Hollowcore Floor Slab Performance Following a Severe Earthquake.” PhD Thesis. University of Canterbury, Christchurch, New Zealand.

MBIE, EQC, NZSEE, SESOC, and NZGS. 2018. Technical Proposal to Revise the Engineering Assessment Guidelines - Part C5 Concrete Buildings. Wellington, New Zealand: Ministry of Business, Innovation, and Employment.

Mejia-McMaster, J. C. 1994. “Precast Concrete Hollow-core Floor Unit Support and Continuity.” ME Thesis. University of Canterbury, Christchurch, New Zealand.

Mostafa, M. T., Büker, F., Hogan, L. S., Elwood, K. J., Bull, D. K. and Parr, M. 2022. “Seismic Performance of Precast Hollow-core Units Seated Within the Plastic Hinge Region.” Proceedings of the 2022 NZSEE Annual Technical Conference, 12. Wellington, New Zealand: New Zealand Society for Earthquake Engineering.

Norton, J. A., King, A. B., Bull, D. K., Chapman, H. E., McVerry, G. H., Larkin, T. J. and Spring, K. C. . 1994. “Northridge Earthquake Reconnaissance Report.” Bulletin of the New Zealand National Society for Earthquake Engineering, 27 (4): 235–344. Bulletin of the New Zealand National Society for Earthquake Engineering, December, Vol. 27, No.4.

Oliver, S. J. 1998. “The Performance of Concrete Topped Precast Hollowcore Flooring Systems Reinforced with and Without Dramix Steel Fibres Under Simulated Seismic Loading.” ME Thesis. University of Canterbury, Christchurch, New Zealand.

Parr, M., Büker, F., De Francesco, G., Bull, D. K., Brooke, N. J., Elwood, K. J., Hogan, L. S., Liu, A. and Sullivan, T. J. 2022a. “Load-Path and Stiffness Degradation of Floor Diaphragms in Reinforced Concrete Buildings Subjected to Lateral Loading - Part I, Experimental Observations.” Journal of the Structural Engineering Society New Zealand, 35 (1).

Parr, M., Bull, D. K., Brooke, N. J., De Francesco, G., Elwood, K. J., Hogan, L. S., Liu, A. and Sullivan. 2022b. “Load-Path and Stiffness Degradation of Floor Diaphragms in Reinforced Concrete Buildings Subjected to Lateral Loading - Part II, Data Analysis.” Journal of the Structural Engineering Society New Zealand, 35 (1).

PCFOG. 2009. Seismic Performance of Hollow Core Floor Systems - Guidelines for Design Assessment and Retrofit (Preliminary Draft). Precast Concrete Floors Overview Group (SESOC, NZSEE, and NZCS), Wellington, New Zealand. http://www.nzsee.org.nz/db/PUBS/HollowCoreFloorSystems.pdf.

Peng, B. H. 2009. “Seismic Performance Assessment of Reinforced Concrete Buildings with Precast Concrete Floor Systems.” PhD Thesis. University of Canterbury, Christchurch, New Zealand.

Sarkis, A. I., Büker, F., Sullivan, T., Elwood, K. J., Brunesi, E. and Hogan, L. 2022. “Aspects Affecting the Nonlinear Behaviour of Precast Pre-stressed Hollow-core Units Failing in Shear (Accepted and in Production).” Structural Concrete. https://doi.org/10.1002/suco.202100579.

SESOC, NZSEE, and ENZ. 2021. “Advice on Hollow-core Floors.” Accessed October 6, 2021. https://www.sesoc.org.nz/precast-flooring-resources/.

SNZ. 2004. Amendment 3 to the Concrete Structures Standard. NZS 3101:1995-A3. Wellington, New Zealand: SNZ.

SNZ. 2011. Structural Design Actions. Part 0: General Principles (Incorporating Amendments Nos 1,2,3,4 and 5). NZS1170.0:2002. Wellington, New Zealand: SNZ.

SNZ. 2017. Concrete Structures Standard (Incorporating Amendment No. 1,2 and 3). NZS 3101:2006. Wellington, New Zealand: SNZ.

Trowsdale, J. 2004. “Seismic Performance of Hollowcore Seating Detail Specified by Amendment No 3 NZS 3101:1995.” Bachelors (Honours) - Final year project report. University of Canterbury, Christchurch, New Zealand.

Woods, L. J. 2008. “The Significance of Negative Bending Moments in the Seismic Performance of Hollow-Core Flooring.” ME Thesis. University of Canterbury, Christchurch, New Zealand, 294p.

ISSN No. 2744-7871

LOAD-PATH AND STIFFNESS DEGRADATION OF FLOOR DIAPHRAGMS IN REINFORCED CONCRETE BUILDINGS SUBJECTED TO LATERAL LOADING

PART I: EXPERIMENTAL OBSERVATIONS

Parr, M.[1], Büker, F.[2], De Francesco, G.[1], Bull, D. K.[3], Brooke, N.[4], Elwood, K. J. [2], Hogan, L.[2], Liu, A.[5], Sullivan,T. [1]

ABSTRACT

An experimental investigation into the degradation of load-paths in damaged diaphragms was conducted to provide answers to the New Zealand structural engineering community following concerns that strut-and-tie load-paths could not cross wide cracks that develop around the floor perimeter during earthquake loading demands. A full-scale super-assembly concrete moment frame specimen with a hollow-core flooring system installed was subjected to realistic drift deformations to induce damage in the floor, followed by in-plane shear deformation demands to assess the ability of the diaphragm to transfer load between frames at different floor damage levels. It was found that compression struts could form across much wider cracks in floors than previously anticipated. This was due to contact compressive stresses forming via loose aggregate that lodged within rugged sinusoidal wide floor cracks. Additionally, it was found that diaphragm compression struts can only transfer to the primary lateral load resisting frame through beam plastic hinges acting in minor axis shear following gaps opening between the floor and columns at moderate drift demands. Smooth floor to column interfaces did not provide the same residual rubble aggregate binding compressive load path observed in cracks within the floor. The primary driver of diaphragm shear stiffness degradation was found to be torsional softening of the perimeter beams of the floor. This was caused by simultaneous bi-directional demands applied to longitudinal beam bars and a phenomenon known as the bowstring effect applying large torsional demands through the beam-floor continuity reinforcement. The diaphragm strength and rate of shear stiffness degradation was found to be highly reliant on earthquake directionality. A set of generalised equations was developed to describe the rate of diaphragm shear stiffness degradation with respect to magnitude and directionality of drift demands.

Part I of II in this journal series details the full-scale super-assembly experiment conducted on a floor diaphragm at different damage states and the observed behaviour during testing.

1 INTRODUCTION AND OBJECTIVES

The purpose of a floor diaphragm is to link frame and lateral load resisting elements to stiffen a structure subjected to lateral loading, such as earthquake demands. In design a rigid diaphragm assumption is typically used, meaning it is assumed the frames are perfectly linked through the floor for the entirety of lateral loading. The strut-and-tie method is generally used to identify and design load-paths for floor diaphragms (SNZ 2017). This method is used to understand the flow of internal forces for many aspects of reinforced concrete design and assumes that all compression forces are borne through the concrete in compression “struts” and all tension forces are transferred through steel reinforcing acting as tension “ties”. Concrete is assumed to carry no tension and steel is assumed to carry no compression. Examples of typical strut-and-tie solutions are displayed in Figure 1.

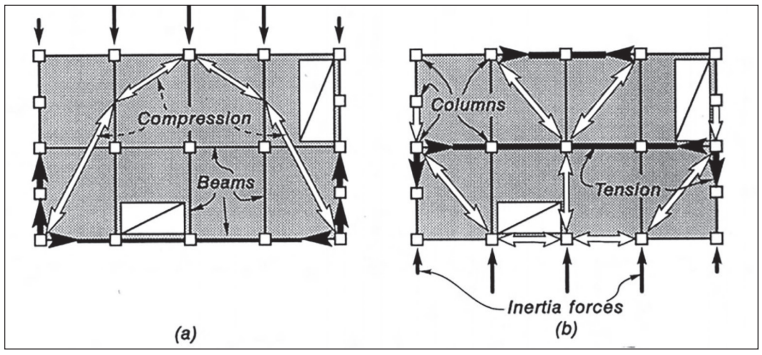

Figure 1: Strut-and-tie load-paths, using diagonal compression fields, for different directions of seismic forces (Paulay 1996)

PAPER CLASS & TYPE: GENERAL REFEREED

1 *University of Canterbury*
2 *University of Auckland*
3 *Holmes Consulting LP*
4 *Compusoft Engineering*
5 *BRANZ*

(a) Significant floor perimeter cracking following the 2011 Christchurch earthquakes (Kam et al. 2011)

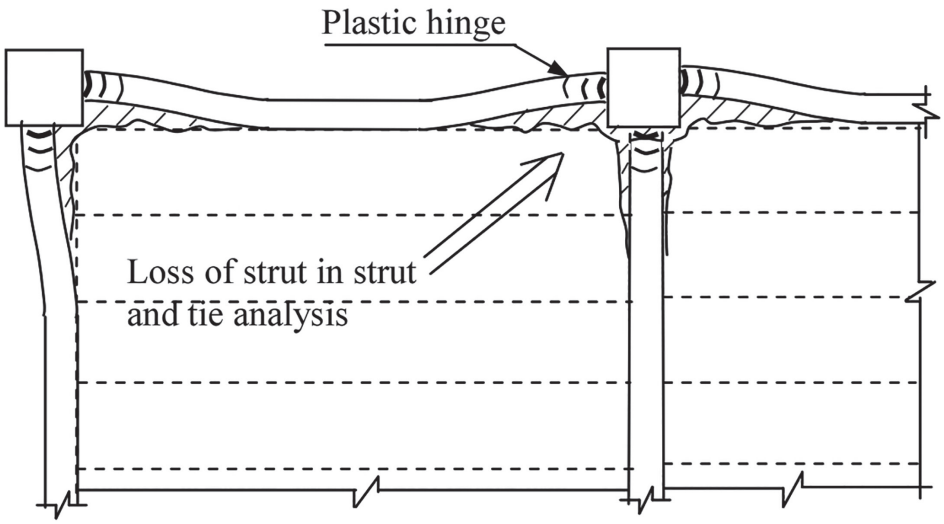

(b) Loss of strut landing points due to significant perimeter cracking (Fenwick et al2010)

Figure 2: Examples of significant floor perimeter cracking and loss of compression strut load paths

Evidence of possible deficiencies with current diaphragm design assumptions for buildings with reinforced concrete frame structures with precast concrete floors was observed in the aftermath of the 2011 Christchurch earthquake. Floors were found with large cracks and openings around their perimeter where they connect to supporting beam and column elements as shown in Figure 2a. This confirmed previous concerns, for example as shown in Figure 2b.

The extensive perimeter floor cracking seen in concrete frame buildings with precast floors is primarily due to beam elongation in the frame. This creates deformation incompatibility between the frame and floor, leading to cracking at weak sections, which tends to be at the interface between the beam and floor. In addition, cracks were observed between individual precast flooring units, providing evidence of diaphragm degradation out in the floor span. Across these cracks it was commonly observed that the floor reinforcing mesh had ruptured, leading to the loss of the tension tie component of the diaphragm load path. Examples of this form of diaphragm damage are displayed in Figure 3.

Figure 3: Cracking between individual precast concrete flooring units and mesh rupture observed following the 2011 Christchurch earthquakes (Henry and Ingham 2012)

These are some of the most recent findings that support concerns that the assumptions justifying the use of the strut and-tie method could be at least partially invalid. This is because the compression strut portion of the load-path cannot cross an air gap (in other words, it is impossible to push on air) and loss of tension ties through mesh rupture also eliminates the viability of the designed load-path.

This research seeks to experimentally investigate diaphragm load-paths throughout different stages of earthquake-induced damage. Based on previous research and post-earthquake observations it is assumed that the designed strut-and-tie load-path for floor diaphragms degrades and (at least partially) fails under sufficient earthquake loading. Leading from this initial assumption, the following questions arise:

- How does the designed load-path degrade with respect to drift demand?
- What is the alternative load-path that develops as the designed load-path degrades?
- What is the residual load sharing capacity of the degraded diaphragm load-path relative to the stiff idealised load-path?

The main useful outcome made clear from previous literature was the necessity of creating a full-scale experimental rig for the floor that included the structural frame of a reinforced concrete building. This was due to multiple observations that the main driver for the development of perimeter cracking is beam elongation in the frame. It would not be possible to create a representative model of diaphragm degradation without realistic frame inelastic response driving the floor damage.

The challenge encountered after these starting decisions was in finding how to load a diaphragm frame specimen in a way that could form a residual diaphragm load path while being representative of a real structure. Previous experimental studies related to earthquake performance of precast flooring units in frame specimens have captured degradation of the floor but did not capture the development of a residual load-path.

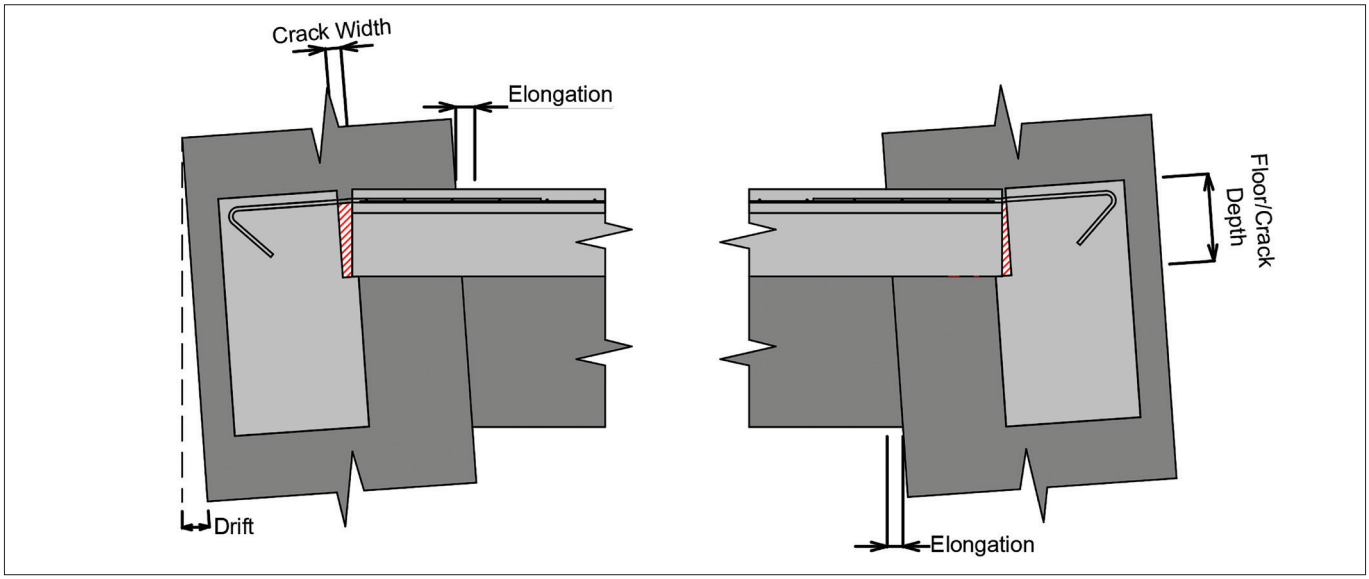

Figure 4: Loss of diaphragm load-path under uni-directional loading

The reason degradation and development of floor load-paths has not been captured in previous literature is because it was not the purpose of previous testing to try and capture these effects. Design of a test that could capture these effects required two core assumptions to be made at the planning phase.

The first of these assumptions is that realistic diaphragm degradation and formation of a residual load path can only develop under simultaneous bi-directional loading conditions with the associated three-dimensional effects. Simple geometry can show that a unidirectional push in either of a frame's primary axes would not lead to suitable binding for load transfer in a floor with wide cracks around the entire perimeter, as shown by the red hatched areas in Figure 4. Additionally, the damage state of the corner of a floor plate would not be realistic under unidirectional loading and this is the most likely zone for a residual load path to form.

As a simple example using rough geometry, for a 275 mm total floor depth (200 mm hollowcore + 75 mm topping) at 3% drift it would require a crack width of approximately 275 mm * 0.03 = 8.25 mm at the beam to floor interface to prevent the possibility of any binding between the floor and frame. Beam elongation for a single plastic hinge can reach to approximately 30 mm, therefore forcing a crack width well above what is required to remove the load-path even under extreme drift demands.

This illuminates the need for simultaneous bidirectional loading to engage a residual diaphragm load-path (or at least "set the stage" for one to develop through the imposed damage state). This is likely a major cause for the lack of available literature on this topic because most pseudo-static earthquake structural experimental studies focus on unidirectional pushes to simplify the results. However real earthquakes do not take into consideration the cardinal directions so simultaneous bidirectional loading is highly appropriate for capturing true diaphragm behaviour.

The second assumption is that the frame does not maintain its shape as the diaphragm degrades, but instead warps in plan. As perimeter cracks become very wide it is likely that simultaneous bidirectional loading would not cause binding of the diaphragm and load transfer between frame elements. However, at this stage of damage the frames would not be linked and therefore would be deforming independently of one another. This would create torsional and warping deformation of the entire structure in plan. Evidence of this kind of structural behaviour was provided in recent shake table testing in Taiwan (Suzuki et al. 2020). If the surrounding frame elements of the floor were to warp into a rhomboidal shape in plan, this could create an intermittent strut from the floor wedging across the diagonals between columns of the warped frame as displayed in Figure 5.

In other words, if the frame undergoes shear deformation in plan, this could wedge the floor and instate a residual load transfer mechanism to link the frames. For pseudo-static testing this would require manually enforcing the shear deformation in plan by moving one frame with hydraulic actuators while keeping the other fixed in the manner shown in Figure 5.

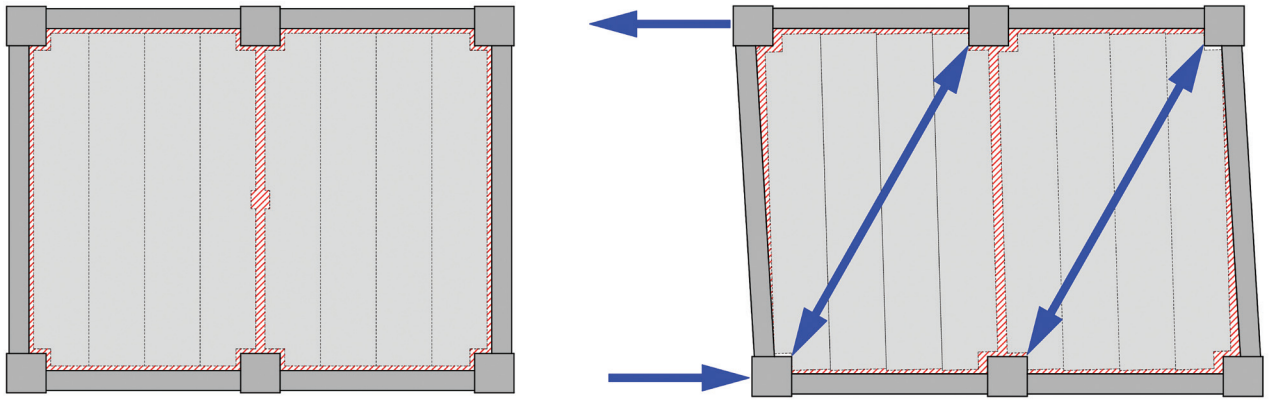

(a) Damaged diaphragm with no viable strut-and-tie load path at perimeter

(b) Shear deformation in plan creating the proposed residual load-path

Figure 5: Proposed residual diaphragm load path – shear deformation in plan creating the "picture frame effect"

This has not been attempted in previous experimental studies on realistically damaged floor specimens, which means it presents a research gap that will be covered by this report. The proposed diaphragm shear distortion residual load path has been compared to a picture sitting within a rectangular frame that is too large for it, meaning it is free to jostle within the frame until it either twists diagonally or the frame warps diagonally into a rhomboid. For simplicity, the effect will commonly be referred to as the "picture-frame effect".

Part I of this journal series explains the design and rationale of the full-scale super-assembly experiment for capturing residual floor diaphragm load-paths and explores the observations made during testing. Analysis of instrument data from the test can be found in Part II (Parr et al. 2022). Further detailed discussion of the experimental layout and loading justification can be found in the thesis (Parr 2022).

2 SPECIMEN DETAILS AND LOADING

As detailed in a companion paper (Büker et al. 2022) the two super-assembly experiments conducted at the University of Canterbury (UFC) during 2020 and 2021 (Fig 8) were designed to provide realistic deformation incompatibility demands under lateral loading into a hollow core floor system via a support frame based on a subsection of a typical ductile reinforced concrete moment frame building. The two experiments used the same frame and hollow-core layout shown in Figure 6.

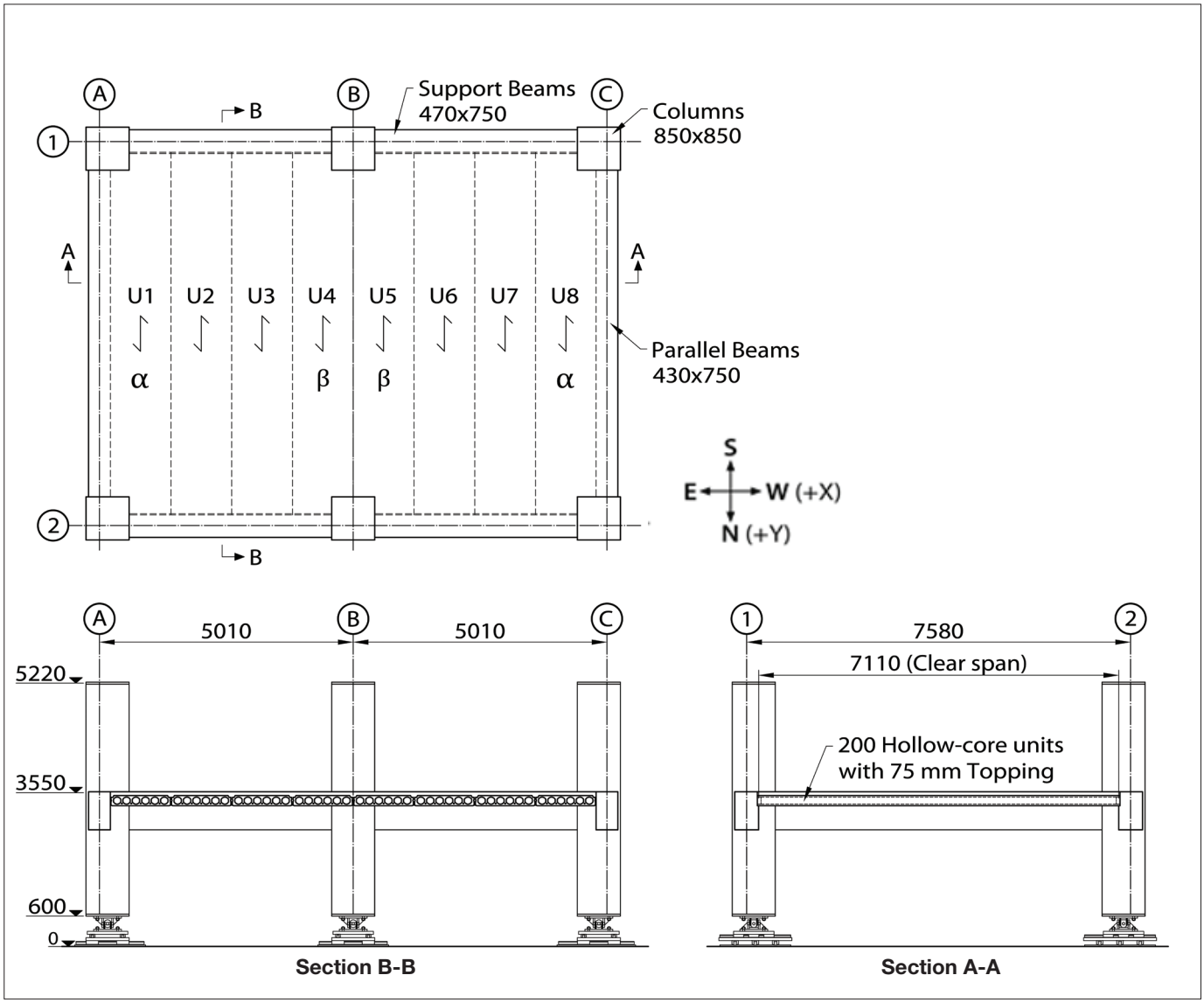

Figure 6: 2020 UC super-assembly experiment frame layout and nominal dimensions (Büker et al. 2022)

When referring to columns or beams their location on the gridlines will be used. For example the south-eastern column would be referred to as column A1 and the beam spanning between column A1 and column B1 would be referred to as beam A1B1.

Hollow-core units in different positions within the floor system are commonly referred to by different names. The units at the end of the floorplate seated on plastic hinge zones of supporting beams next to longitudinal beams are referred to as alpha units (units 1 and 8 in the 2020 UC super-assembly experiment). This is because they have historically been the units of primary concern due to deformation incompatibility with the surrounding frame elements increasing likelihood of catastrophic failure. Interior units seated on beam plastic hinges are referred to as beta units (units 4 and 5 in the 2020 UC super-assembly experiment). This is because they are the units of secondary concern with considerable deformation incompatibility demands with the surrounding frame but were not focussed on as heavily in early research. In this paper units not seated on plastic hinges of the beams (units 2, 3, 6 and 7 in the 2020 UC super-assembly experiment) will be referred to as intra-span units, as they are seated within the span of the supporting beam. Further explanation of terminology related to hollow-core units can be found in a companion paper (Brooke 2022).

The two super-assembly experiments used different floor detailing and loading protocols. The first experiment used a standard starter bar configuration around the entire floor perimeter, cast-in-place tie bars linking the intermediate beams and a linearized circular loading protocol with 1:1 directionality of loading for the standard loading protocol. The first bay of the specimen had no mesh crossing the beam-floor interface. The second bay did have mesh crossing the beam-floor interface to observe the effects of a stronger connection on the hollow-core units, which had been retrofitted against negative moment failure. The layout of this experiment is displayed in Figure 7 (a) and will be referred to in this report as TEST 1.

The second super-assembly experiment used different starter bar configurations at the four support ends of the two bays to encourage targeted local hollow-core failure modes to initiate at the critical end. In the first (eastern) bay, the northern end of the hollow-core units was designed as critical end for failure, targeting loss of seating with a weak mesh-only beam-floor interface. In the second (western) bay, the southern end of the hollow-core units was designed as the critical end for failure, targeting negative and positive moment failures at the end of the starter bars with high strength beam-floor continuity reinforcement. The targeted critical failure ends of each bay were installed on the diagonals opposite each other to minimise interaction of failure modes that could affect results. Additionally, D12 “stitching” bars were installed linking the two beta units (unit 4 and unit 5) to strengthen the connection after results from the TEST 1 experiment determined that this was a critical weak point for both the gravity carrying and diaphragm functions of the floor. The layout of this experiment is displayed in Figure 7 (b) and will be referred to in this report as TEST 2.

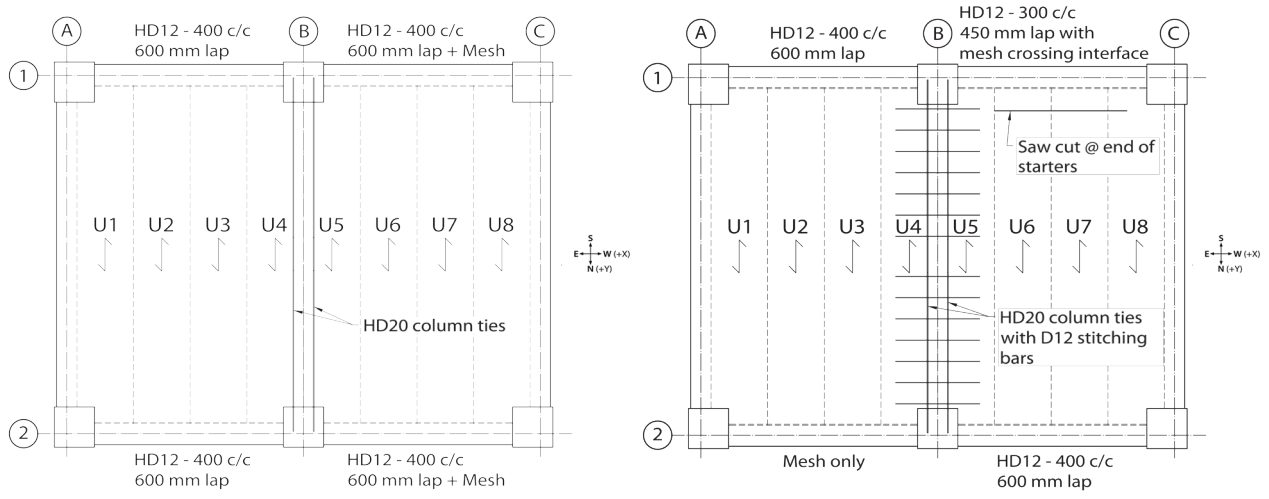

(a) TEST 1 Continuity Reinforcement

(b) TEST 2 Continuity Reinforcement

Figure 7: Floor continuity reinforcement arrangements for TEST 1 and TEST 2 (Büker et al. 2022)

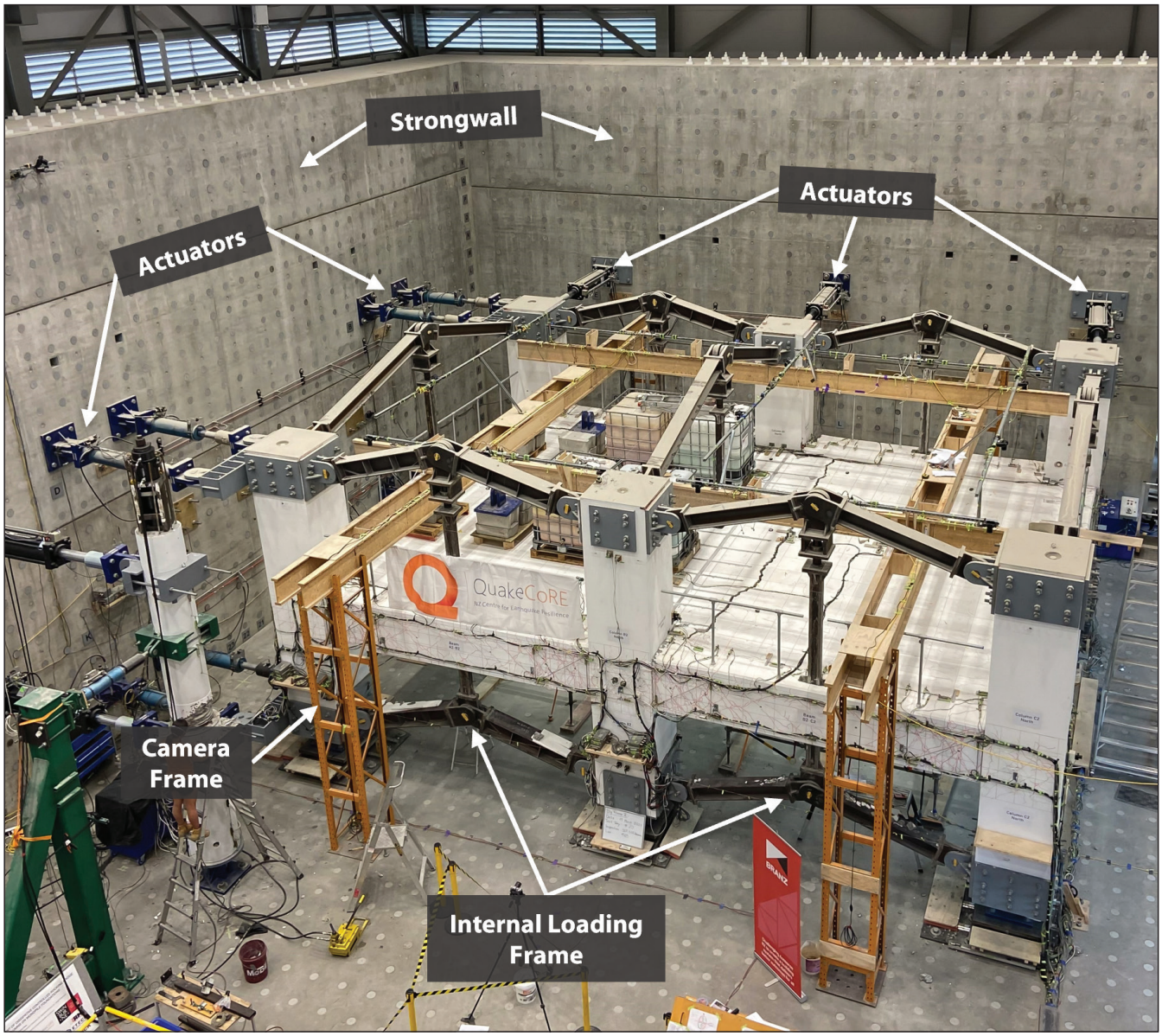

Figure 8: Experimental layout of the 2020 University of Canterbury super-assembly experiments (Büker et al. 2022)

Displacement demands were applied to the specimen using an arrangement of fourteen hydraulic actuators pushing and pulling from a strong-wall as shown in Figure 8.

Internal loading frames consisting of arrow-frames and bi-directional frictionless sliders were used to enforce realistic demands between individual columns. The objective was to keep the columns parallel during loading while avoiding restriction or promotion of beam-elongation. This was done to ensure the forces and deformation incompatibility applied to the floor was representative of a real structure subjected to lateral loading.

The control software for the actuators was programmed to allow the structure to grow from beam-elongation outward from the origin at column A1 depicted in Figure 9. The concept of how the arrow-frame and bi-directional sliders also facilitated this structural growth is shown in Figure 10. Further details on the design philosophy of the experiment can be found in the thesis (Parr 2022).

The beam-column casting interfaces of TEST 1 and TEST 2 were different. The bottom half of the longitudinal beams in TEST 1 were cast with the pre-cast columns, meaning there was no cold-joint. The top half of the longitudinal

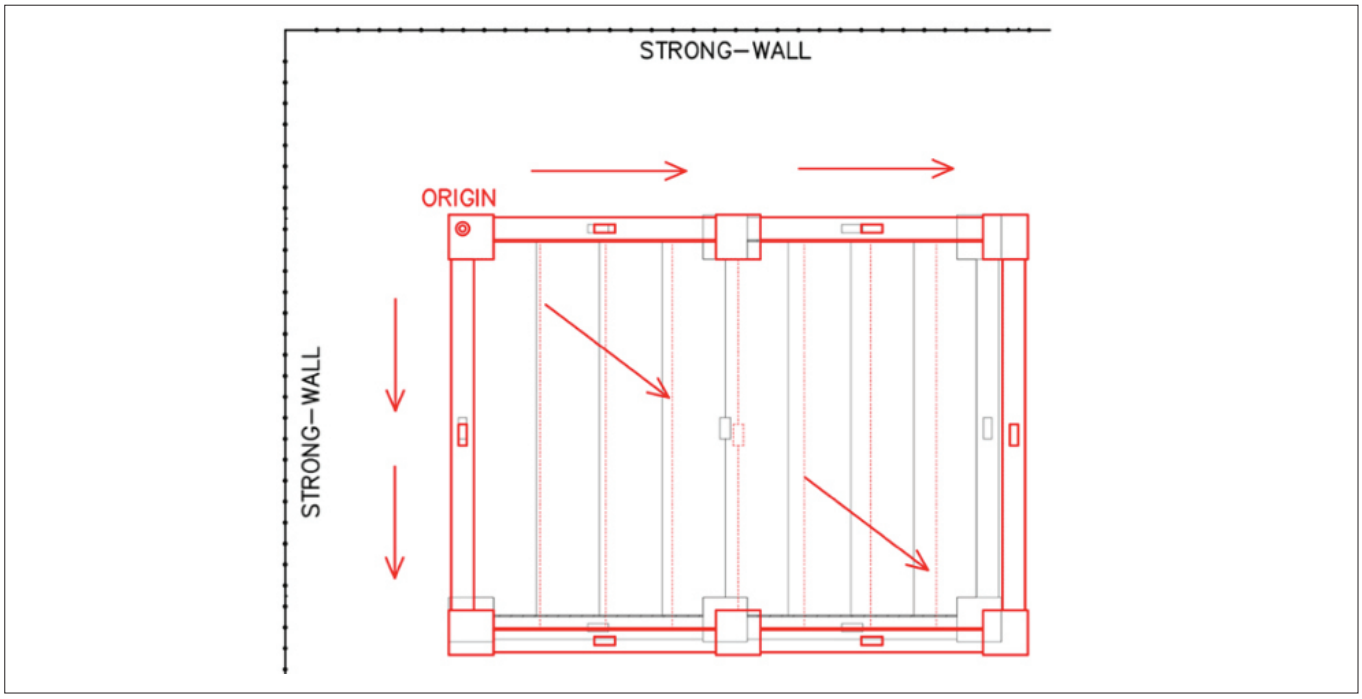

Figure 9: Specimen growth from the origin at column A1 due to beam elongation

beams were cast in-situ and had a smooth casting surface against the pre-cast column interface. The support beams of TEST 1 were cast in-situ and had an array of slightly roughened and smooth casting interfaces with the pre-cast columns.

After observations in TEST 1 of beams losing torsional stiffness (as discussed in Section 3), all beams in TEST 2 were cast in situ against purposely roughened column interface surfaces to provide better interlock across the cold joint.

TEST 1 and TEST 2 also used different standard loading protocols. TEST 1 used a linearised circular loading protocol with directionality 1:1 to enforce the widest range of possible deformations on the specimen and floor as shown in Figure 11 (c). This was considered as the upper bound of directionality expected from an earthquake. After the findings detailed in Section 3 and Part II (Parr et al. 2022) related to TEST 1, it was decided that TEST 2 would have a more targeted directionality typical of a pulse or near-fault earthquake shaking.

This led to the use of a 2:1 directionality linearised oval protocol as shown in Figure 11 (d). This was considered as the lower bound of likely realistic earthquake directionalities based on research conducted by Nievas and Sullivan (2017). This meant TEST 1 and TEST 2 would provide an upper and lower bound of simultaneous bi-directional actions imparted into a floor system respectively.

TEST 1 began with an approximation of the 2016 Kaikoura Earthquake drift cycles for the prototype Wellington building the specimen was based on to allow comparisons to damage modes observed in real buildings. A standard circular loading protocol of increasing drift demands was then applied as shown in Figure 11 (a). TEST 2 started with an approximation of the 1994 Northridge Earthquake to simulate a pulse style loading followed by a standard oval loading protocol of increasing drift demands as displayed in Figure 11 (d).

At selected locations within the TEST 1 and TEST 2 loading protocols, the loading was switched to a rhomboid loading protocol to enforce plan shear distortion into the floor diaphragm and assess the diaphragm load paths. The locations where the standard loading protocols (SLP's) were stopped for rhomboid loading in TEST 1 and TEST 2 are displayed in Figure 11 (a) and (b).

The locations for stopping the standard loading protocol to perform a rhomboid loading protocol were chosen based on the desire to compare the stiffness and load path changes from a relatively undamaged floor diaphragm to

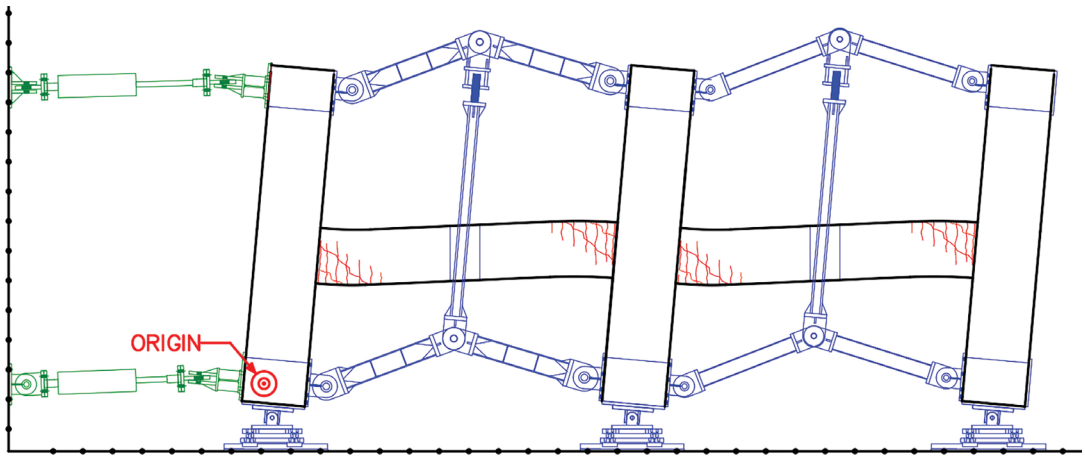

(a) Super-assembly specimen when subjected to positive east-west drift demands

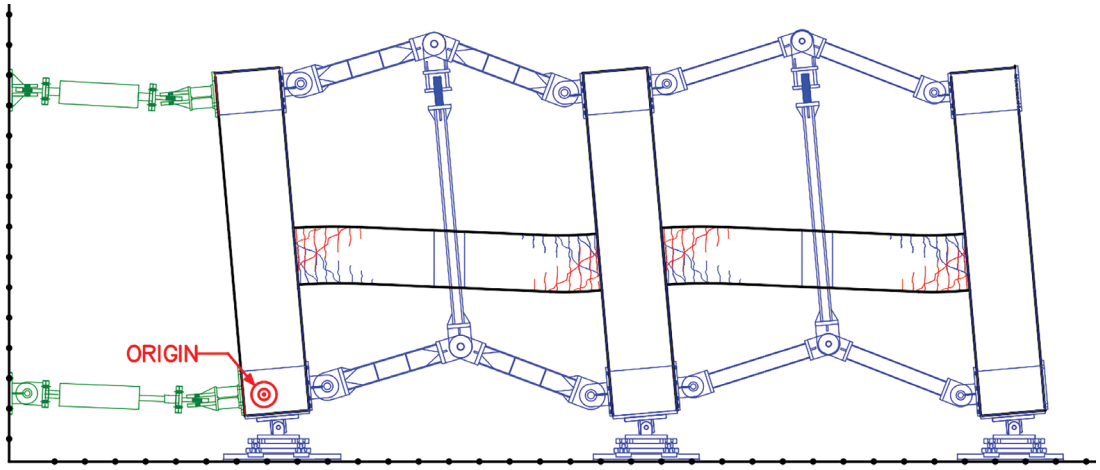

(b) Super-assembly specimen when subjected to negative east-west drift demands

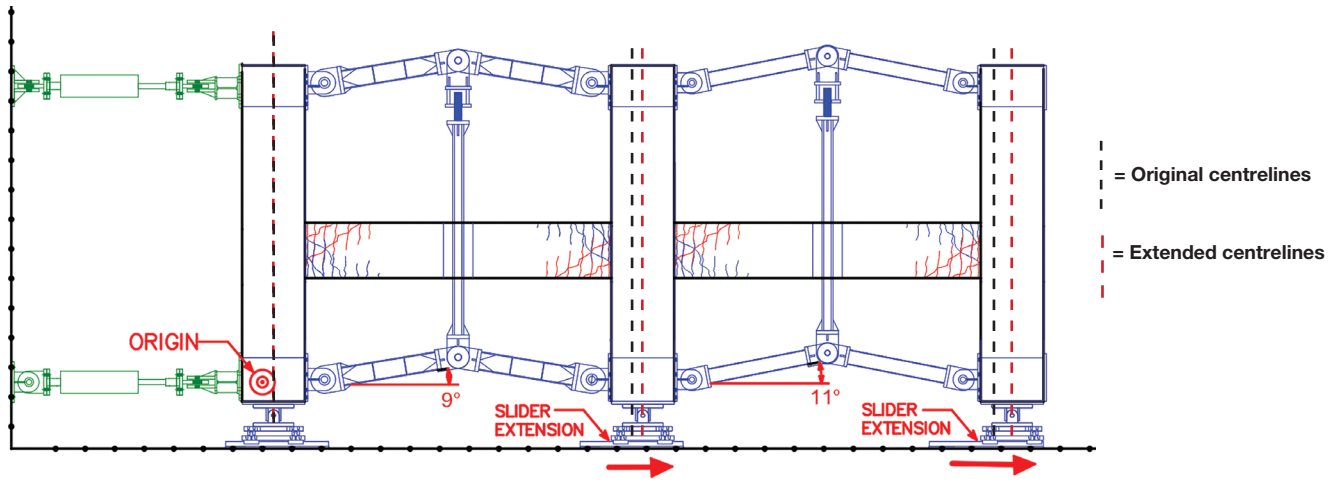

(c) Super-assembly specimen after growth due to beam elongation following reverse cyclic demands

Figure 10: Loading frame system allowing for specimen growth without restraining or promoting beam elongation in the 2020 UC super assembly experiments

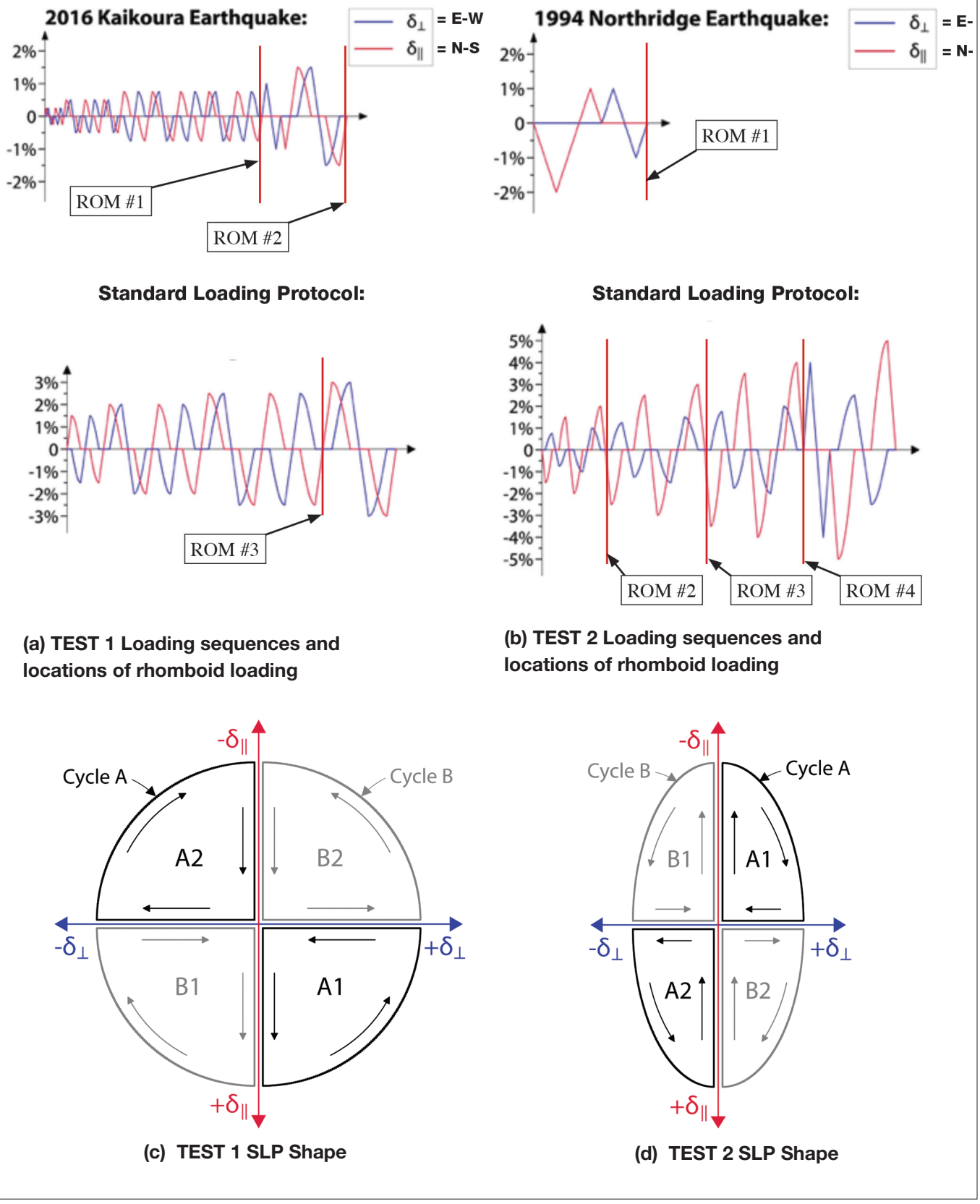

Figure 11: Standard loading protocols and locations of rhomboid loading protocols for the TEST 1 and TEST 2 experiments (Büker et al. 2022)

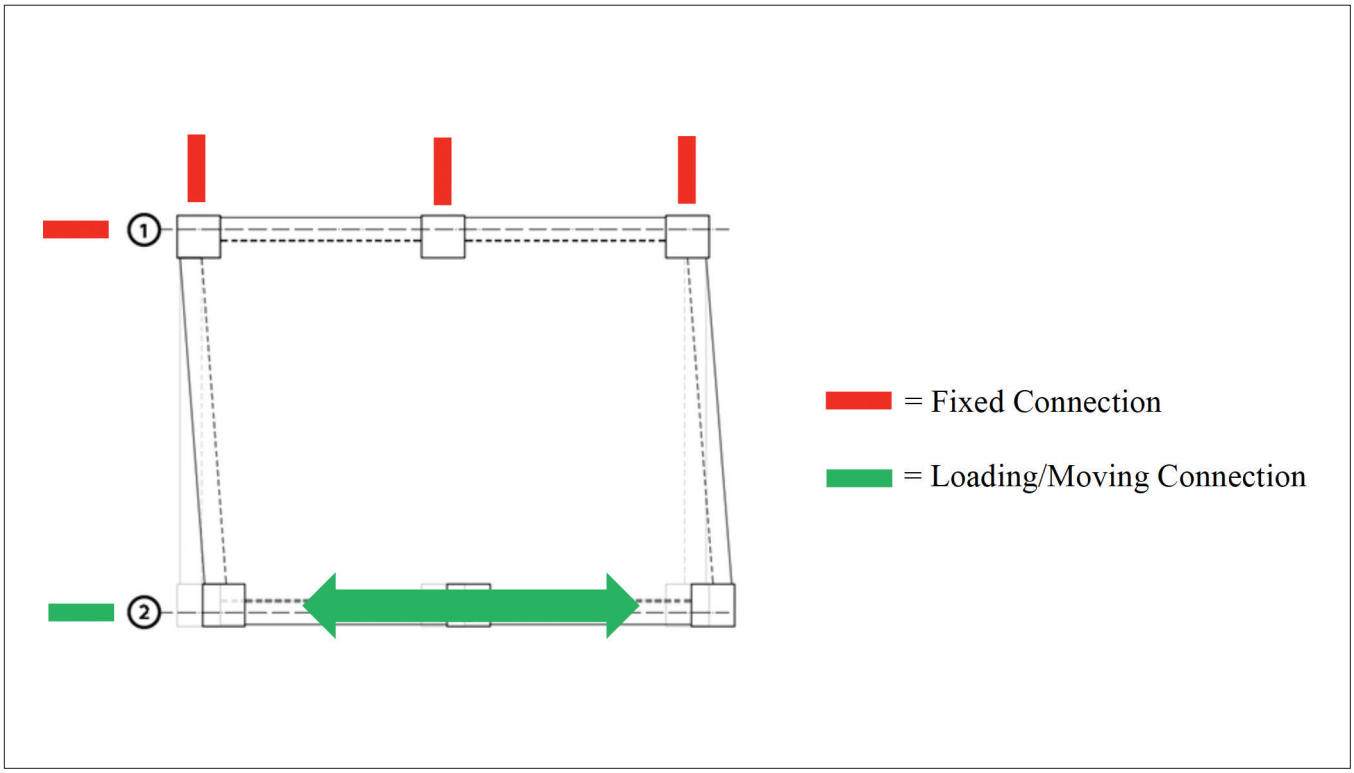

Figure 12: Fixity and loading of the specimen during rhomboid loading (positive shear distortion shown)

the same diaphragm when it was partially damaged and heavily damaged. This would allow for observation of the degradation of the designed load-path and formation of true residual load-paths.

Each rhomboid loading protocol was undertaken once the specimen was brought back to the closest approximation of residual drift that could be achieved after the previous standard loading cycle. The fixities of the loading system for the rhomboid loading protocol are displayed in Figure 12.

As shown in Figure 12 the south frame (frame 1) was held stationary by all actuators attached to columns A1, B1 and C1. The north frame (frame 2) was driven with positive and negative displacements in the east-west direction via the double actuator configuration attached to column A2 to enforce shear distortion on the specimen floorplate in plan. No drift was applied during the rhomboid loading protocols as it was desired to isolate the effects of shear distortion for determining diaphragm load-paths.

The magnitude of each rhomboid loading protocol was different depending on the level of damage the specimen had sustained in previous standard linearised circular loading cycles. Early rhomboid loading protocols within each test (TEST 1 and TEST 2) were force controlled and had small maximum displacements, with each subsequent rhomboid protocol within a test increasing the displacement demand. This was done to avoid prematurely damaging the specimen before it had softened from the standard loading protocol. Higher deformation was imposed for the final TEST 2 rhomboid compared to TEST 1 as it was the specimen's end-of-life with no further refurbishment planned.

Table 1: TEST 1 and TEST 2 Rhomboid applied displacement and shear distortion demands

Rhomboid #	+- Plan Shear Distortion, γ (%)				Targeted state of the diaphragm for testing
	Test 1		Test 2		
	± Shear Distortion, γ (%)	± Force (kN)	± Shear Distortion, γ (%)	± Force (kN)	
1	0.01	250	0.005	250	No/low damage to designed load-paths
2	0.05	500	0.02	500	Intermediate damage to design load-paths
3	0.11	450	0.06	600	High damage to designed load-paths
4	n/a	n/a	0.25	700	Extreme damage to designed load paths

3 EXPERIMENTAL OBSERVATIONS

The critical observations relating to the diaphragm behaviour for both TEST 1 and TEST 2 are described in this section.

3.1 DIAPHRAGM DAMAGE OBSERVED FROM STANDARD LOADING PROTOCOLS

By 0.25% drift, the damage modes and crack patterns observed in the TEST 1 and TEST 2 diaphragms had diverged significantly. This was due to the difference in directionality of the standard loading protocols as well as the beta-beta unit stitching retrofit installed in the TEST 2 specimen.

The TEST 1 specimen developed a full-length split between the beta-beta unit interface at 0.25% drift. Further damage concentrated at this split in later cycles with mesh rupture along the interface occurring in the first arc loading at 1.5% drift. From this point on, the two bays of the specimen acted as separate floor plates. There were early signs of cracks developing in the floorplate at the ends of starter bars up to approximately 1.5% drift, but in future cycles, these cracks were observed closing compared to previous cycles. The closing up of inner floor cracks coincided with observations that the beams were beginning to rotate torsionally into the structure. Development of additional significant cracking relevant to diaphragm performance from this stage was limited to the topping located near plastic hinge zones of the beams, particularly in the corners of the overall floorplate where seating of the alpha units was located. An example of significant beam torsion observed at the end of the TEST 1 test in a support beam is displayed in Figure 13. Note that the black lines drawn near the bottom corners of the beam aligned with the original location of the beam face.

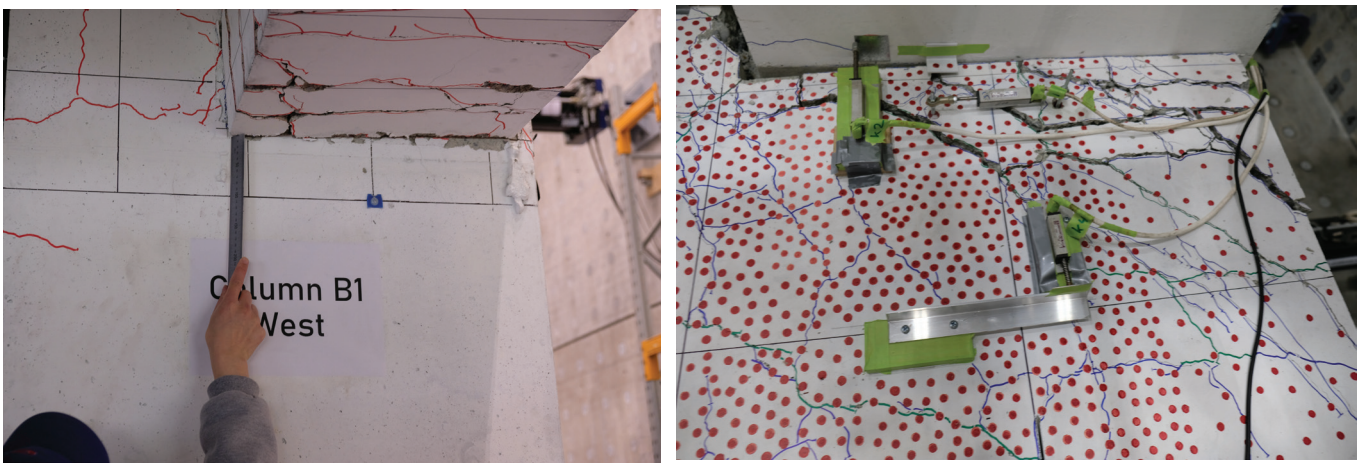

Figure 13: Significant beam torsion visible at the conclusion of the TEST 1

The TEST 2 specimen developed wide cracks at the end of the starter bars on the south end of the floor and at the beam-unit interface on the north end of the floor, with mesh rupture occurring at approximately 1.5% as discussed in (Büker et al. 2022). Cracking occurred between most units, but these cracks were small and distributed compared to the major beta-beta unit crack observed in the TEST 1 test. Other than the improved performance between the beta-beta unit interface, the visible damage in the floor was significantly more severe in TEST 2, with end of starter bar and beam-unit interface cracks with widths of approximately 30-40 mm and 30 mm vertical offset by the end of the test. These extremely wide cracks were useful to compare against those observed in real buildings, where there have been concerns that compression struts could not form across perimeter cracks, destroying the diaphragm load-path.

The crack patterns recorded at the end of TEST 1 and TEST 2 are displayed in Figure 14, depicting the different damage modes observed between them. Hairline cracks and cracks that closed following primary damage modes forming are removed in Figure 15 to allow for easier comparison of the primary damage modes.

Note that the primary floor cracking damage in TEST 1 ran in the north-south direction, the primary example being the split between the two beta units which caused the two bays to act independently from 1.5% drift onwards. Other than this major crack most damage was contained to areas near the beam plastic hinge zones. In TEST 2 the primary floor cracking damage ran in the east-west direction, at the end of the starter bars on the south end and at the beam-floor interface on the north end. This was due to the stitching bar retrofit strengthening the beta-beta unit interface and the directionality of loading being more critical in the north-south direction compared to TEST 1.

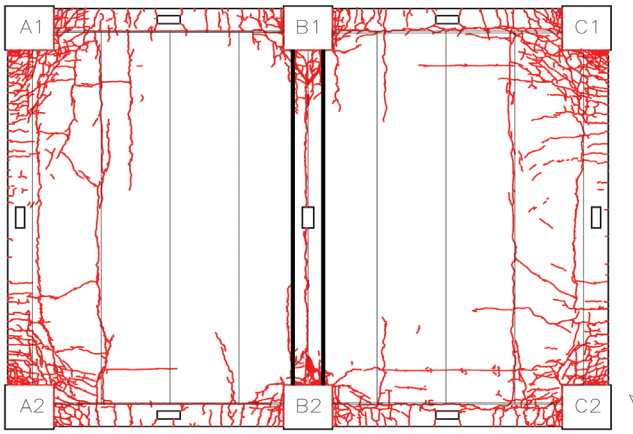

(a) TEST 1 Topping crack map after 3.0% drift

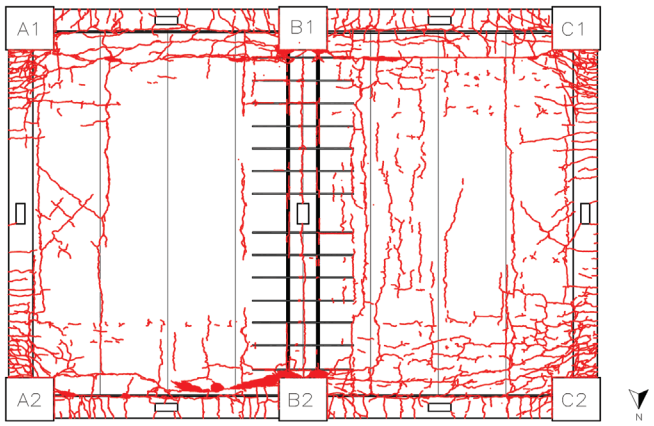

(b) TEST 2 Topping crack map after 5.0% drift

Figure 14: Topping crack maps for TEST 1 and TEST 2 at conclusion of experiments

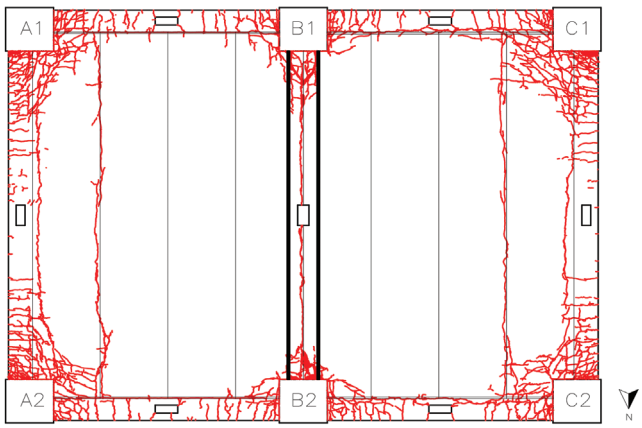

(a) TEST 1 Topping crack map showing only wide/important cracks demonstrating the observed load-paths

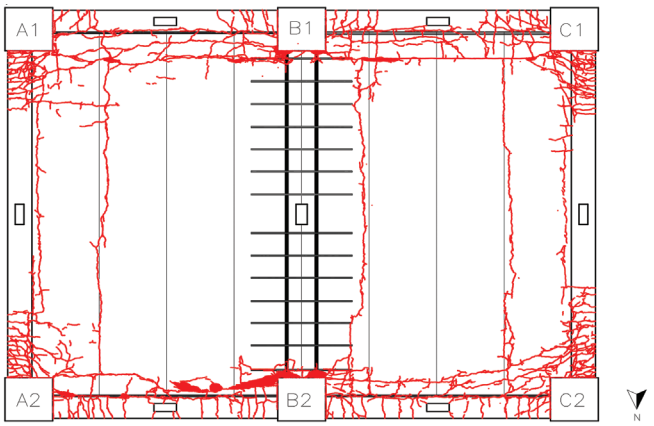

(b) TEST 2 Topping crack map showing only wide/important cracks demonstrating the observed load-paths

Figure 15: Topping crack maps for TEST 1 and TEST 2 at conclusion of tests with only critical wide cracks impacting load-paths visible

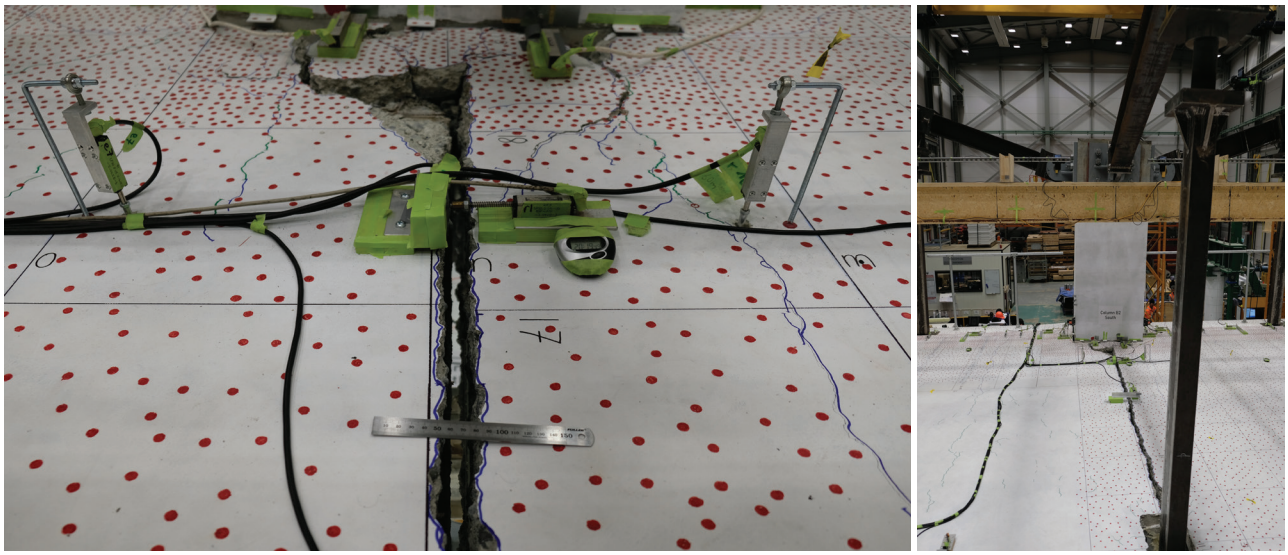

(a) TEST 1 Beta-beta unit interface crack following 3.0% drift demands

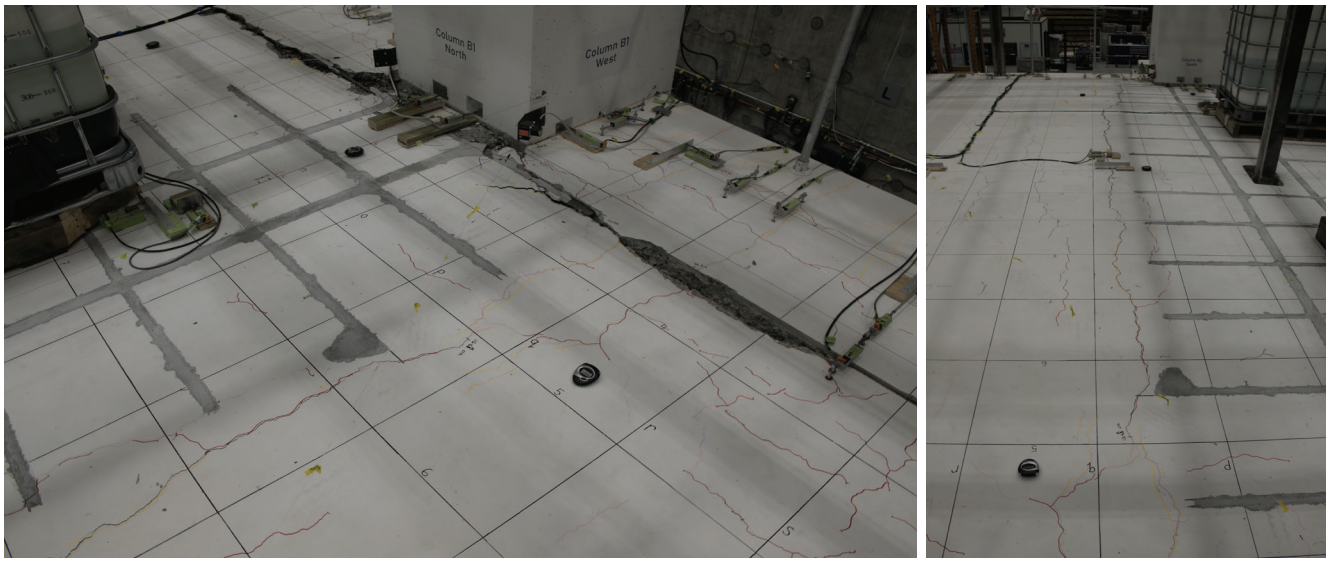

(b) TEST 2 Unit 5 – Unit 6 crack (only developed under large shear distortion demands after 4.0% drift)

Figure 16: Comparison of inter-unit cracking near the beta units between the TEST 1 and TEST 2 experiments

A comparison between TEST 1 and TEST 2 of the beta-beta unit interfaces near the end of both tests is displayed in Figure 16.

The stitching bars succeeded in preventing significant cracking developing between the two beta units, with a maximum beta-beta unit crack width recorded of approximately 0.2 mm. Instead multiple smaller cracks developed along and between units. As there was no mesh rupture or wide cracks this meant diaphragm actions could develop across both bays. This was the case until the 4th rhomboid when significant shear distortion in the positive direction (at a γ value between 0.23% and 0.25%) caused a large split to occur between unit 5 and unit 6 near the end of the stitching bar retrofit.

A comparison between the TEST 1 and TEST 2 experiments of cracking at the end of the starter bars at the south end of the floor near the end of both tests is displayed in Figure 17.

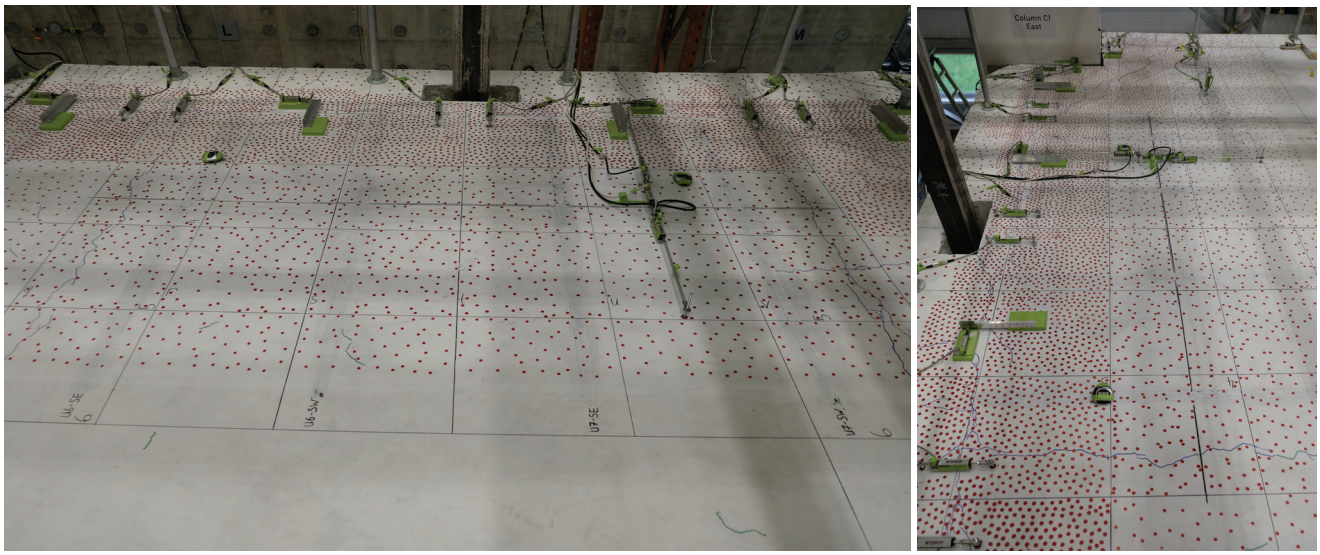

(a) TEST 1 End of starter bar cracks following 3.0% drift demand

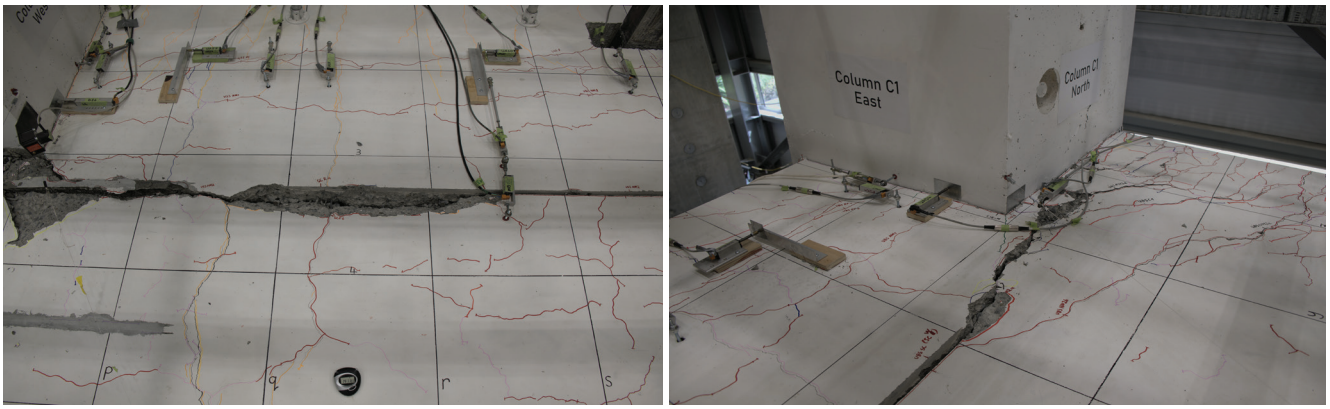

(a) TEST 2 End of starter bar cracks following 4.0% drift demand

Figure 17: Comparison of cracking at the end of starter bars on the south end of the floor between the TEST 1 and TEST 2 experiments

The TEST 2 specimen sustained much greater damage at the end of the starter bars compared to the TEST 1 specimen. This was primarily due to the change in directionality of loading protocols with less beam torsional softening observed in TEST 2 due to the reduction of simultaneous demands. An additional factor altering the strength hierarchy of the beam torsional capacity vs floor strength between the two tests was the additional roughening of the cold joint between the column concrete element and beam concrete elements in TEST 2 as described in Section 2. These factors meant the beams remained stiff enough to impart large deformation incompatibility demands into the floor units, leading to significant early cracking.

By approximately 1%-1.5% drift in both tests, openings were observed around the entire perimeter of the floor-to-column interfaces, removing any possibility of diaphragm compression struts landing directly into the columns including into the intermediate columns B1 and B2. These openings grew wider with subsequent drift cycles. This means that early in the earthquake record the only remaining diaphragm load path to link the frame elements was through the beams. The only caveat to this general rule was where the tie-bars were anchored into the intermediate columns, though these would not have provided a significant stiff load-path as they were only two D20s acting in compression and dowel action for the purposes of landing compression struts into the columns.

(a) Gaps at column A1 (Alpha unit-column)

(b) Gaps at column B1 (Beta unit-column)

Figure 18: Gaps between the floor and columns at 1% drift in TEST 1

In both experiments significant cracking and spalling of the topping occurred around the tie-bar connections into the column interface. This made the tie-bars visible at higher drift levels, which were clearly plastically deformed by deformation incompatibility between the beta units and columns. The cone shaped spalling failures this caused in the nearby concrete through bond stresses are displayed in Figure 19.

After significant cracking of the topping and hollow-core units in TEST 2 (at >2.5% drift) light could commonly

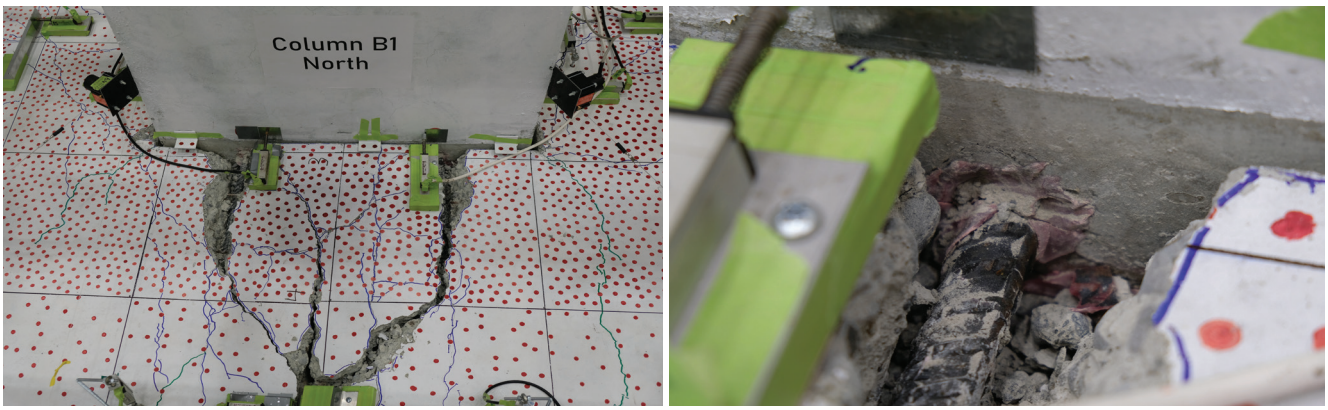

(a) TEST 1 Tie-bar anchorage rubble formation at 3.0% drift

(b) TEST 2 Tie-bar anchorage rubble formation at 4.0% drift

Figure 19: Tie-bar anchorage rubble formation observed in the super-assembly experiments

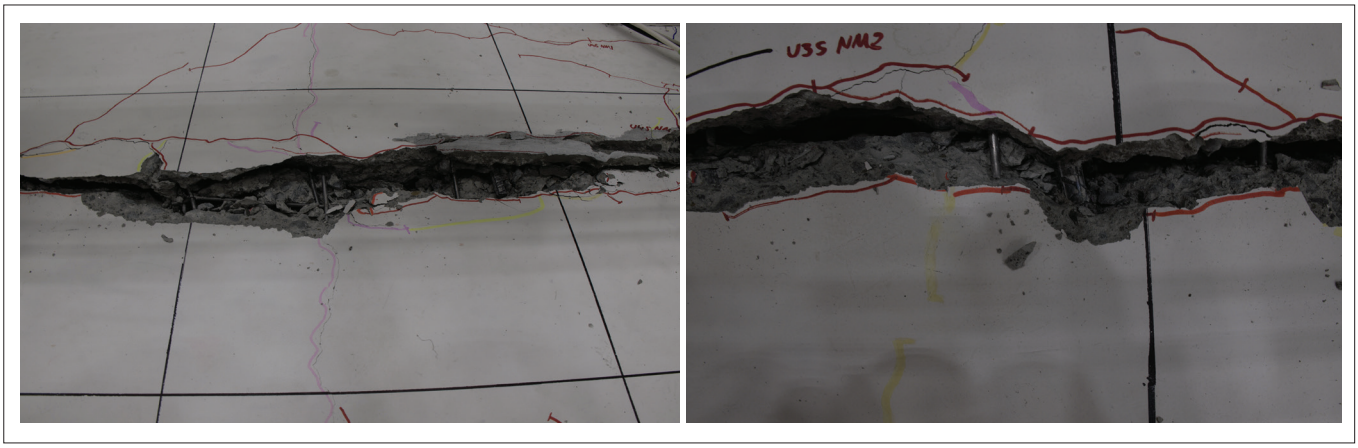

Figure 20: Starter bars and mesh initiating rubble formation within floor cracks

be observed through the wide cracks at the end of the southern starter bars, indicating small gaps where no compression struts could cross. However, these gaps were intermittent with small pieces of rubble falling into the gaps clogging the view through the crack.

The dislodgement of rubble was particularly noticeable near starter bars. The ends of the starter bar would scrape against the other side of the crack, dislodging pieces of aggregate and dropping them into the crack as shown in Figure 20. In these areas it was not possible to see through the crack and it could be reasonably assumed that rubble became lodged, forming small pathways for compression to be transferred across the crack through contact stresses.

While starter bars appeared to be primary initiators of rubble formation it also was also formed in spaces between starter bars, possibly assisted by bond with mesh. Contact stresses under cyclic loading between the two sides of cracks (and with previously formed pieces of aggregate rubble) sheared off protruding pieces of aggregate from the crack face, generating more rubble. The process appeared to be a self-replenishing system creating contact stresses across the crack provided initial rubble was generated to start the process (and a sufficient gravity load-path existed, which was provided in TEST 2 by the cable catch frame system and cantilever seating retrofits described in (Büker et al. 2022)).

The most obvious case of rubble formation providing a contact stress load-path across a crack occurred on the east side of column B2. A large wedge of concrete became detached from the topping and hollow-core at approximately 2.0% drift as shown in Figure 21.

However it was not possible to remove the detached wedge at any stage of the load protocol until approximately 5.0% drift. Between these drift demands the concrete wedge was under compression, with the wedge slowly being pushed up by the formation of rubble on either side.

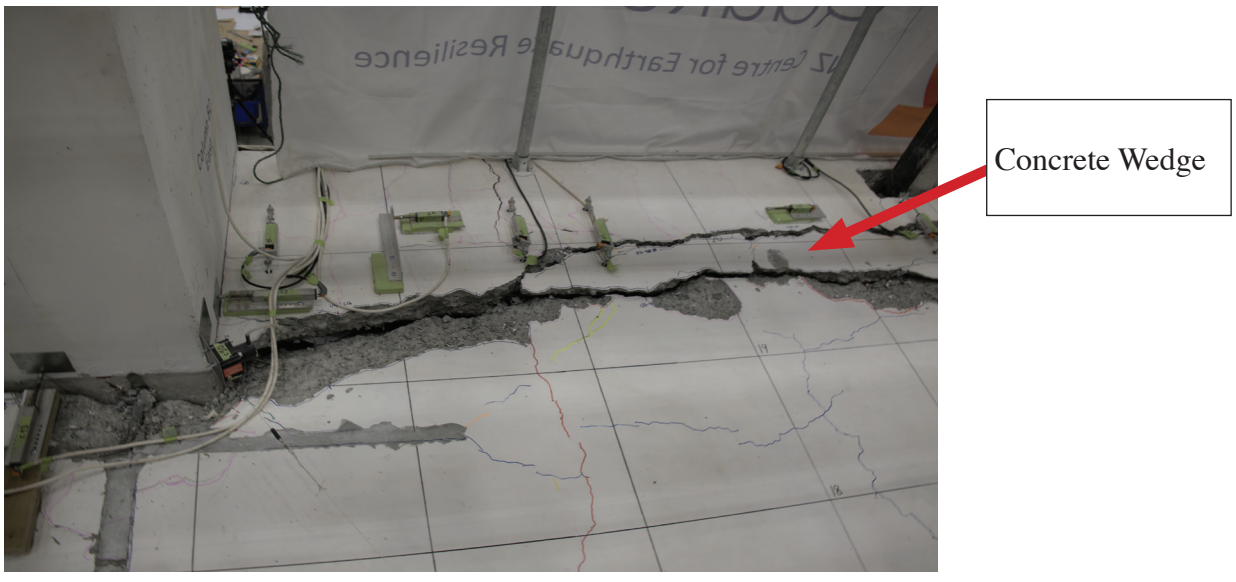

Figure 21: Beam-unit crack interface concrete wedge on east side of column B2 at 4.0% drift

3.2 DIAPHRAGM DAMAGE OBSERVED FROM RHOMBOID LOADING

The three rhomboid loading protocols conducted in TEST 1 did not display any obvious visual signs of damage other than for the third and largest rhomboid loading. This was by design, as it was undesirable to push the specimen to damage inducing deformations in the rhomboids as this could adversely affect the reliability of subsequent results for the hollow-core and future rhomboid results. The obvious impact of standard testing on the diaphragm load-path was the splitting of the two bays causing them to act as individual floorplates. In the third rhomboid a loud crack was heard at a shear distortion of approximately 0.11%. On observation of the topping it was found that a piece of cover concrete on the top of the B2C2 beam western plastic hinge had spalled off the beam and been propelled onto the floor. Another loud crack was heard at a shear distortion of approximately -0.11%. A similar observation was made of cover concrete being disturbed and left loose on the top of the western end of beam B1C1.

These observations provided evidence that the diaphragm compression struts were being transferred to the C1 and C2 columns via the support beam plastic hinges. They also provided evidence that the beam plastic hinges were deforming under the diaphragm loads and were the weak point of the system. The plastic hinges following crushing of the cover concrete are displayed in Figure 22.

The four rhomboid loading protocols conducted in TEST 2 displayed interesting behaviour related to residual compression load-paths across wide cracks. In the 2nd rhomboid, diagonal cracking was observed on the side of a wide crack as shown in Figure 23. This cracking provides evidence of significant local compression across the crack leading to landing of the strut into beam A1B1 towards column B2.

In the 4th rhomboid of the TEST 2 experiment, the diaphragm was pushed to a much greater shear distortion compared to other rhomboids, allowing for significant damage modes to form for observation. The most notable

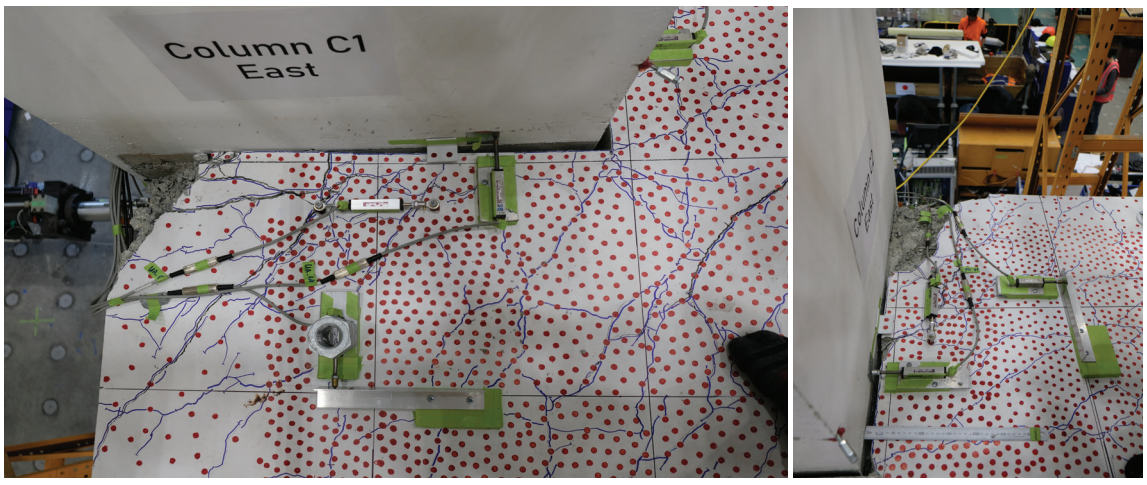

Figure 22: Beam plastic hinge spalling about weak axis from plan shear distortion demands

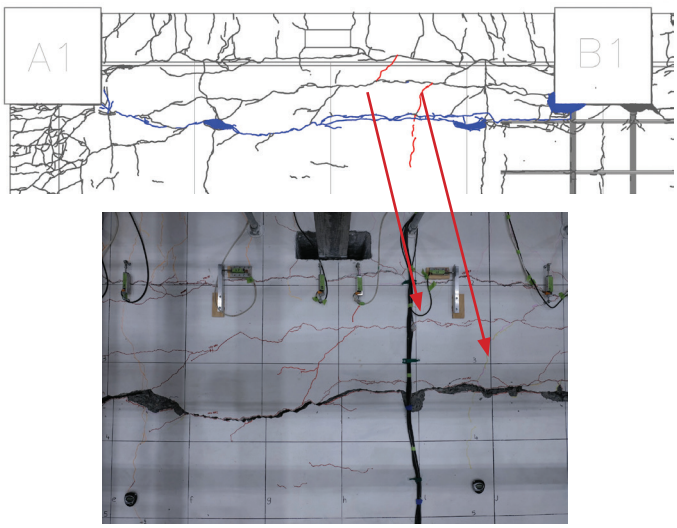

Figure 23: Diagonal cracking displaying local compression strut across wide crack at southern end of units 1-4

Figure 24: Significant split between Unit 5 and Unit 6 that developed in the TEST 2 4th Rhomboid

damage that developed from this loading was mesh rupture and splitting between unit 5 – unit 6 near the end of the stitching bar retrofit as shown in Figure 24.

This rupture occurred at a shear distortion γ in the positive direction between 0.23% and 0.25%. Mesh rupture was observed along approximately 2/3rds of the length from the north end. The crack was much wider at the north end with a width of approximately 7 mm and 4.5 mm vertical offset (with the beta units dropping). At the south end this reduced to approximately 3 mm with no vertical offset. This shows that at the northern end there were significant tensile forces across the crack due to the diaphragm internal strut-and-tie load-path. This is discussed further in Part II (Parr et al. 2022).

Additionally in the 4th rhomboid of TEST 2 a residual load-path was observed landing compression struts directly into the column faces of the intermediate columns (B1 and B2). As shown in Figure 25, as a result of loading in the positive direction, a section of the topping near the eastern tie-bar in column B1 spalled due to crushing failure. Upon observation of the gap between the column and beta unit it was not possible to see through the gap near the tie-bar. This was due to the significant spalling of the topping caused by bond stresses with the deformed tie-bars. The spalled concrete rubble had fallen and wedged between the beta units and interior column face of the intermediate columns. This formed a residual diagonal contact stress compression strut load-path directly from the diaphragm into the column face. Under negative loading similar damage was observed from struts landing into the western tie-bar anchored in column B1. The topping spalling from compression struts landing directly into column B1 is displayed in Figure 25 (b) and (c)

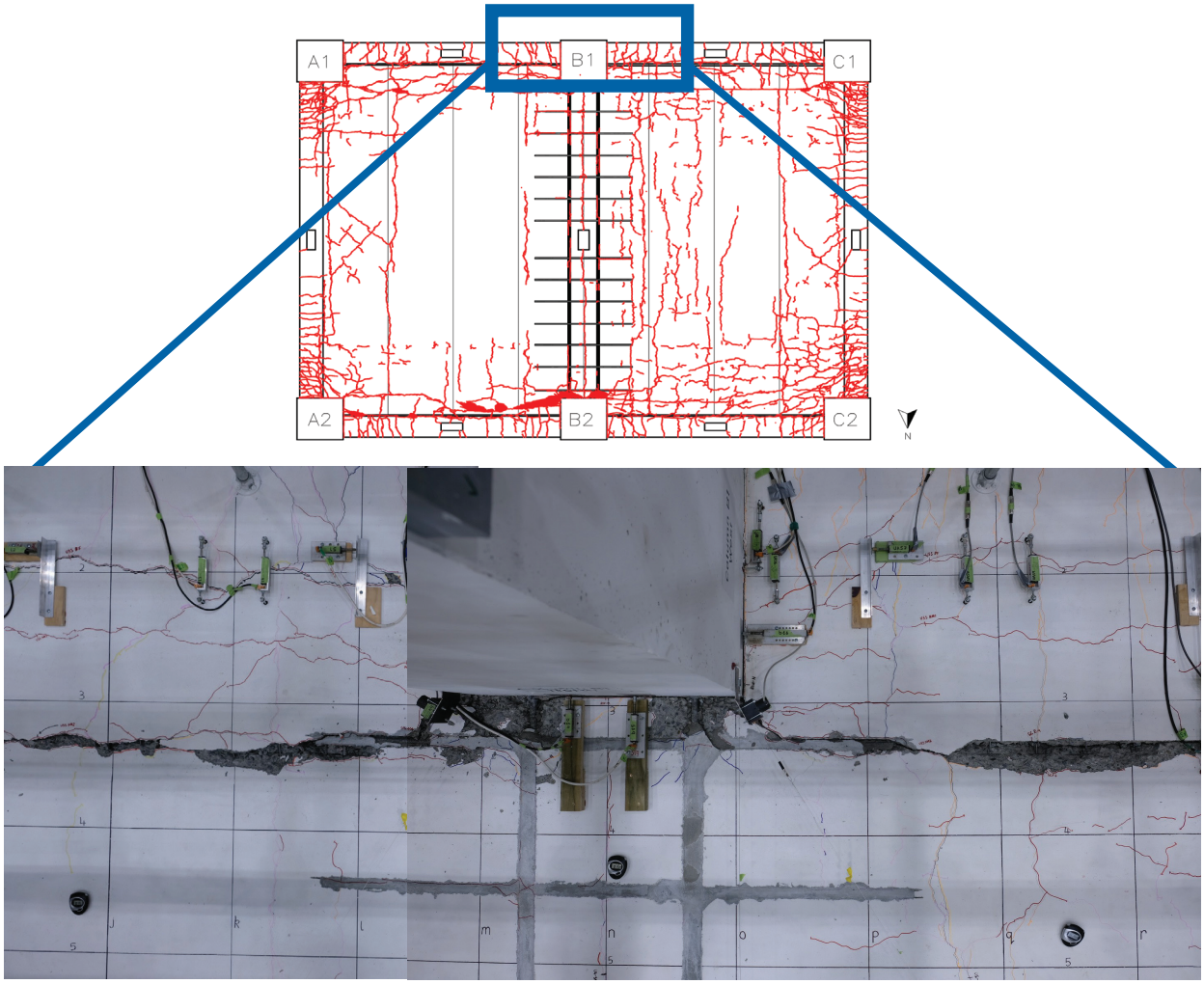

(a) Location on specimen and floor-column interface prior to rhomboid 4 loading

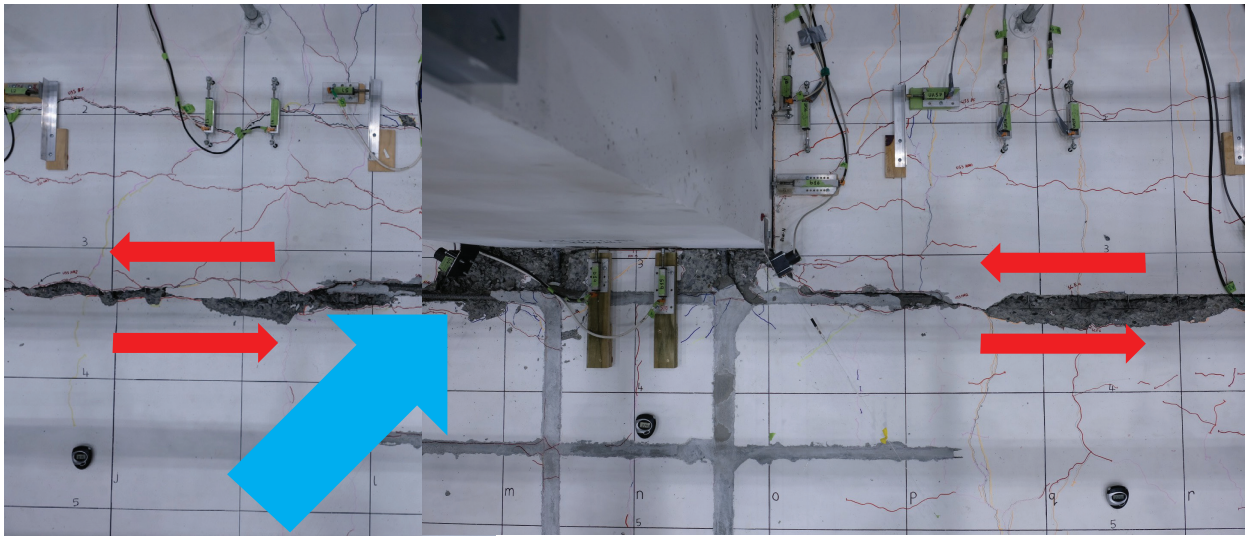

(b) Floor-Column interface with topping spalling at +0.25% floor plan shear distortion

The damage from these struts was likely more significant than for struts landing in the beams because it was the stiffest load-path. The compression strut load-path landing into beams was softened from needing to be transferred through the damaged beam plastic hinges.

Topping spalling from compression struts lands directly into column B2 was not observed. This was due to the split that developed between unit 5 and unit 6 in the positive direction removing and softening the diaphragm load-path directly into column B2.

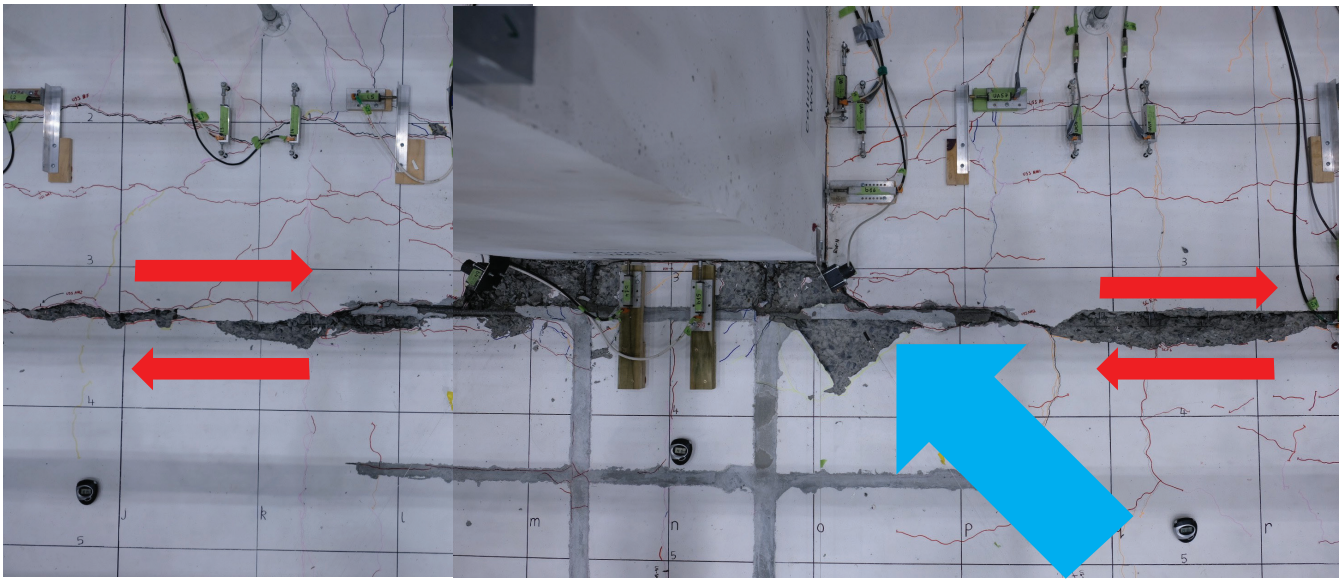

(c) Floor-column interface with topping spalling at -0.25% floor plan shear distortion

Figure 25: Evidence of compression struts landing directly into the B1 intermediate column at a high damage state due to contact stresses formed by tie-bar anchorage rubble

In both the TEST 1 and TEST 2 experiments, similar behaviour was observed with unit-unit interactions. As seen by the crack patterns displayed in Figure 14 and Figure 15, the intra-span units (units within the span, i.e. not alpha or beta units) and beta units acted as a single block rather than in a shear "racking" fashion that would have created significant cracking between each individual unit. Significant inter-unit cracking triggered in weak points within or adjacent to the alpha units and between or adjacent to the beta units. Once significant cracking was triggered at these weak points, additional damage concentrated at them instead of distributing between other unit interfaces. A likely cause for the ability of the intra-span units to act as a single element without significant damage was the relative flexibility of the beams once they began to twist. Warping and rotation of the beam plastic hinges was where deformation incompatibility demands between the intra-span units and support beams concentrated.

4 CONCLUSIONS

The previously described experimental observations have led to the following conclusions and recommendations related to precast floor units and floor diaphragms for practicing engineers:

- Residual floor diaphragm load-paths will exist even at high damage states with very wide cracks if there is a viable gravity load path for the floor and there is adequate continuity reinforcement. However there is high potential for designed strut-and-tie load-paths to break down across beta-unit-to-beta-unit interfaces where precast flooring systems are used due to local deformation incompatibility leading to mesh rupture. This is a particular concern where non-ductile mesh has been installed. Further research would be beneficial to determine if this issue still exists where ductile mesh has been installed. Based on the significant simultaneous tensile demands from the bowstring effect (described in Part II (Parr et al. 2022)) and vertical dislocation across the beta-beta unit interface, it is likely that significant strength improvement from the beta-unit-to-beta-unit stitching bars is required to prevent concentration of damage across this interface. Additionally, struts and ties can only reliably land in beams of the support frame and must be transferred into columns via the beam plastic hinge rather than landing directly into columns. For column faces of intermediate columns where tie-bars were anchored, struts were observed landing into the column face only after large amounts of damage had occurred to the floor topping.
- Contact stresses appear to form across wide concrete cracks in floors due to rubble replenishment. These contact stresses provide a rigid connection resistant to in-plane shear deformation that can allow diaphragm compressive struts to land on beams. Formation of aggregate rubble from local concrete crushing appears to be improved near steel reinforcing, particularly deformed rebar (but also mesh) as depicted in Figure 20 and Figure 26.

  This is likely due to bond with the bar causing substantial local cone-type cracking in the concrete when the steel bar deforms. Based on limited available test data presented herein, starter bar spacing of

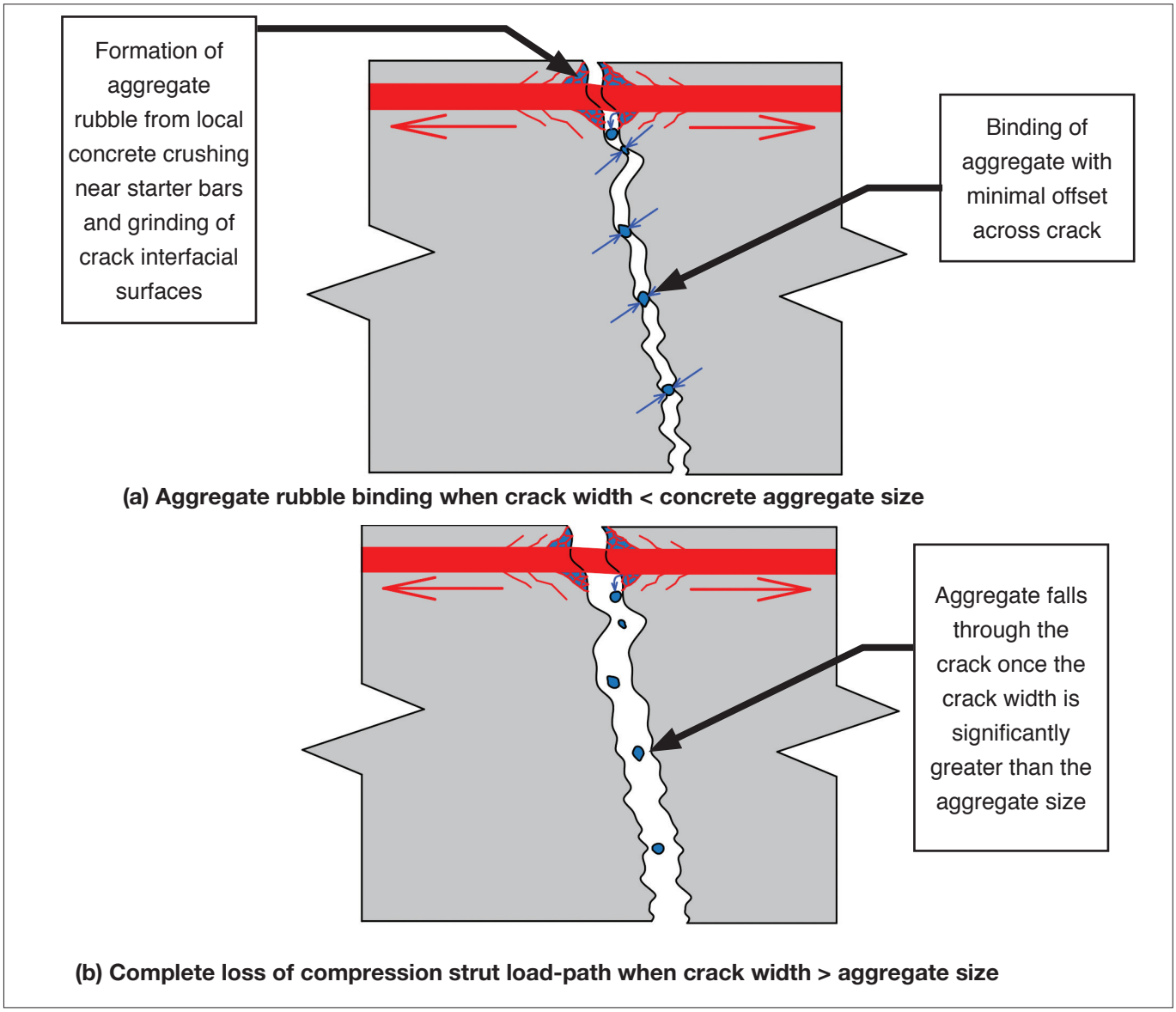

Figure 26: Residual compression strut load-paths forming across wide cracks due to aggregate rubble binding

400mm centre-to-centre crossing the crack interface appears to provide adequate rubble formation to transfer load across wide cracks. Smaller starter bar spacing should increase rubble formation, further ensuring a residual load-path develops. It is proposed that the maximum reliable crack width a compression strut can form across is dependent on the aggregate size used in the topping concrete mix. This is because aggregate rubble wedges itself between the crack interfaces and individual pieces of aggregate are unlikely to crush under compressive demands.

- Tie-bars are currently required between intermediate columns (with tie capacity to exceed 5% of maximum total axial compression force acting on the linked column or exceed 20% of the shear force from seismic actions in the column: Cl. 10.3.6 of NZS 3101:2006) to prevent them from bowing out of the structure which can lead to catastrophic floor failure. A secondary benefit of tie bars was observed during testing; that rubble is generated near the tie-bar anchor locations under earthquake loading due to bond stresses between the tie-bar and floor topping. However, this residual contact stress load path associated with the concrete around the column tie bars appears to require extensive damage and is only likely to develop after the building has experienced high peak drifts.
- For further analysis of the diaphragm performance observed in the super-assembly experiments conducted at the University of Canterbury in 2020 and 2021 refer to Part II (Parr et al. 2022)

5 REFERENCES

Brooke, N. (2022). "Overview of Retrofit Requirements and Techniques for Precast Concrete Floors." SESOC Journal, 35(1).

Büker, F., Brooke, N., Hogan, L., Elwood, K., Bull, D. and Sullivan, T. (2022). "Design Recommendations for Strongbacks Retrofits." SESOC Journal, 35(1).

Büker, F., Parr, M., De Francesco, G., Hogan, L., Bull, D., Elwood, K., Liu, A. and Sullivan, T. (2022). "Seismic Damage Observations of Precast Hollow-Core Floors From Two Full-Scale Super-Assembly Tests." SESOC Journal, 35(1).

Fenwick, R., Bull, D. and Gardiner, D. (2010). "Assessment of Hollow-core Floors for Seismic Performance (Research Report No. 2020-02; p. 152)."University of Canterbury, Christchurch, New Zealand.

Henry, R. and Ingham, J. (2012). "Performance of Precast Concrete Floor Systems During the 2010/2011 Canterbury Earthquakes." The New Zealand Concrete Industry Conference 2012 Hamilton.

Kam, W., Pampanin, S. and Elwood, K. (2011). "Seismic Performance of Reinforced Concrete Buildings in the 22 February Christchurch (Lyttelton) Earthquake." New Zealand Society for Earthquake Engineering (NZSEE).

Nievas, C. and Sullivan, T. (2017). "Accounting for Directionality as a Function of Structural Typology in Performance-Based Earthquake Engineering Design." Earthquake Engineering and Structural Dynamics, 46, 791-809.

Parr, M. (2022). "Retrofit Solutions for New Zealand Hollow-Core Floors and Investigation of True Floor Diaphragm Load Paths in Earthquakes." PhD, University of Canterbury, Christchurch, New Zealand - Currently in preparation.

Parr, M., Büker, F., De Francesco, G., Bull, D., Elwood, K., Hogan, L., Brooke, N., Liu, A. and Sullivan, T. (2022). "Load-Path and Stiffness Degradation of Floor Diaphragms in Reinforced Concrete Buildings Subjected to Lateral Loading – Part II, Data Analysis." SESOC Journal, 35(1).

Paulay, T. (1996). "Seismic Design of Concrete Structures - The Present Needs of Societies." Eleventh World Conference on Earthquake EngineeringAcapulco, Mexico.

SNZ (2017). "Concrete Structures Standard (Incorporating Amendment No. 1, 2 and 3). NZS3101.1:2006." Standards New Zealand (SNZ), Wellington, New Zealand.

Suzuki, T., Elwood, K., Puranam, A., Lee, H., Hsaio, F. and Hwang, S. (2020). "Seismic Response of Half-Scale Seven-Storey RC Systems with Torsional Irregularities: Blind Prediction." NZSEE 2020 Annual Conference, New Zealand Society for Earthquake Engineering (NZSEE).

EARTHQUAKE RESPONSE UNCERTAINTREE

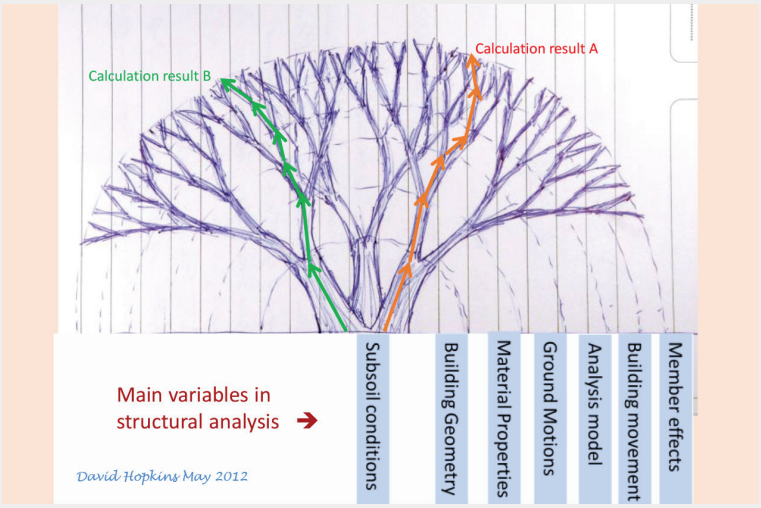

These and other examples, together with the challenges faced in the forensic time-history analyses of the CTV Building, led me to produce this ***Earthquake Response Uncertaintree***. This diagram reinforces the message that calculations, regardless of their sophistication, provide only estimates - not precise predictions. Analyses involve many assumptions, many of which are hidden from engineers' view within software. The implications of these assumptions need to be fully understood when making design decisions.

It is ***real structures, as designed and built***, that have to resist earthquake actions – not the theoretical models we analyse.

David Hopkins

ISSN No. 2744-7871

LOAD-PATH AND STIFFNESS DEGRADATION OF FLOOR DIAPHRAGMS IN REINFORCED CONCRETE BUILDINGS SUBJECTED TO LATERAL LOADING

PART II: DATA ANALYSIS

Parr, M.[1], Bull, D.[2], Brooke, N.[3], De Francesco, G.[1], Elwood, K. J.[2], Hogan, L.[2], Liu, A.[4], Sullivan, T.[1]

ABSTRACT

An experimental investigation into the degradation of load-paths in damaged diaphragms was conducted to provide answers to the New Zealand structural engineering community following concerns that strut-and-tie load-paths could not cross wide cracks that develop around the floor perimeter during earthquake loading demands. A full-scale super-assembly concrete moment frame specimen with a hollow-core flooring system installed was subjected to realistic drift deformations to induce damage in the floor, followed by in-plane shear deformation demands to assess the ability of the diaphragm to transfer load between frames at different floor damage levels. It was found that compression struts could form across much wider cracks in floors than previously anticipated. This was due to contact compressive stresses forming via loose aggregate that lodged within rugged sinusoidal wide floor cracks. Additionally it was found that diaphragm compression struts can only transfer to the primary lateral load resisting frame through beam plastic hinges acting in minor axis shear following gaps opening between the floor and columns at moderate drift demands. Smooth floor-to-column interfaces did not provide the same residual rubble aggregate binding compressive load path observed in cracks within the floor. The primary driver of diaphragm shear stiffness degradation was found to be torsional softening of the perimeter beams of the floor. This was caused by simultaneous bi-directional demands applied to longitudinal beam bars and a phenomenon known as the bowstring effect applying large torsional demands through the beam-floor continuity reinforcement. The diaphragm strength and rate of shear stiffness degradation was found to be highly reliant on earthquake directionality. A set of generalised equations was developed to describe the rate of diaphragm shear stiffness degradation with respect to magnitude and directionality of drift demands.

Part II of II in this journal series provides analysis of the cause and rate of diaphragm stiffness degradation based on instrument data and visual observations as described in Part I (Parr et al. 2022). Analysis of the formation of residual diaphragm load-paths and the relationship between torsional softening of beams with simultaneous bi-directional demands is also investigated.

1 INTRODUCTION AND OBJECTIVES

Observations of wide cracking around the perimeter of floor diaphragms in concrete moment frame buildings following earthquake shaking have led to concerns that the standard strut-and-tie design method for diaphragms does not accurately represent realistic load-paths in floors after they are damaged. This is because the compressive strut components of these load-paths cannot cross air gaps. This could also invalidate the commonly used rigid diaphragm assumption used in structural models for diaphragm elements linking beam and column elements. A residual load-path was proposed for damaged floors describing the floorplate being wedged with large compressive struts linking columns across the short diagonal once the support frame warped into a rhomboidal shape in plan due to failure of the designed load-path. This effect has been compared to a small picture sitting within a larger picture frame, so it is free to move and twist until the picture frame warps, leading to the term “picture frame effect”. A comparison between classic strut-and-tie load-path and the proposed picture frame effect is displayed in Figure 1.

In Part I of this journal series, experimental observations from two full-scale super-assembly frame experiments of crack patterns and floor damage under lateral loading and plan shear demands provided evidence that compressive struts could cross wider cracks than anticipated. It was proposed that residual contact stress load-paths could develop across wide cracks until the crack width reached approximately the aggregate size used in the concrete mix. This was because aggregate rubble was falling between the rugged interfaces of the cracks leading to binding of the two sides of the crack.

PAPER CLASS & TYPE: GENERAL REFEREED

1 University of Canterbury
2 Holmes Consulting LP
3 Compusoft Engineering
4 BRANZ

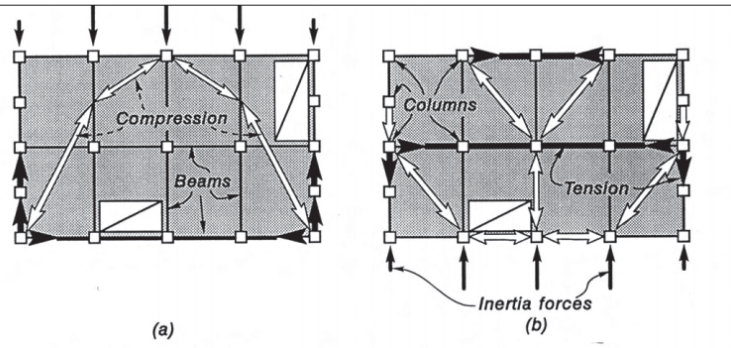

(a) Classic strut-and-tie load-paths (Paulay 1996)

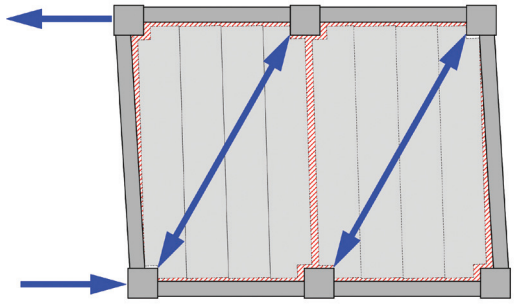

(b) Proposed "Picture Frame effect" (Parr et al. 2022)

Figure 1: Classic strut-and-tie load-paths compared to proposed residual load-path following cracking at floor perimeter

In addition it was found that gaps between the floor and columns developed relatively early (at approximately 1% to 1.5% drift). This meant diaphragm compressive struts could only land within beams from this point on, meaning the proposed "picture frame effect" required some alteration (Parr et al. 2022).

In Part II, analysis of instrumental data from the two super-assembly experiments along with the experimental observations presented in Part I will be used to quantify the degradation rate of the diaphragm plan shear stiffness and identify the primary mechanisms driving diaphragm stiffness degradation.

The layout of the two super assembly experiments is displayed in Figure 2 (a). For simplicity, the first super-assembly experiment will be referred to as TEST 1 and the second will be referred to as TEST 2 as displayed in Figure 2.

When referring to columns or beams, their location on the gridlines will be used. For example, the south-eastern column would be referred to as column A1 and the beam spanning between column A1 and column B1 would be referred to as beam A1B1 (Parr et al. 2022).

Hollow-core units in different positions within the floor system are commonly referred to by different names. The units at the end of the floorplate seated on plastic hinge zones of supporting beams next to longitudinal beams are referred to as alpha units (units 1 and 8 in the 2020 UC super-assembly experiment). Interior units seated on beam plastic hinges are referred to as beta units (units 4 and 5 in the 2020 UC super-assembly experiment). In this paper, units not seated on plastic hinges of the beams (units 2, 3, 6 and 7 in the 2020 UC super-assembly experiment) will be referred to as intra-span units, as they are seated within the span of the supporting beam. Further explanation of terminology related to hollow-core units can be found in (Brooke 2022) (Parr et al. 2022).

TEST 1 used a standard starter bar configuration around the entire floor perimeter, cast-in-place tie bars linking the intermediate beams and a linearised circular loading protocol with 1:1 directionality of loading for the standard loading protocol. The first bay of the specimen had no mesh crossing the beam-floor interface. The second bay did have mesh crossing the beam-floor interface to observe the effects of a stronger connection on the hollow-core units, which had been retrofitted against negative moment failure (Parr et al. 2022).

TEST 2 used different starter bar configurations at the four support ends of the two bays to encourage targeted local hollow-core failure modes to initiate at the critical end. In the first (eastern) bay the northern end of the hollow-core units was designed as the critical end for failure, targeting loss of seating with a weak mesh-only beam-floor interface. In the second (western) bay the southern end of the hollow-core units was designed as the critical end for failure, targeting negative and positive moment failures at the end of the starter bars with high strength beam-floor continuity reinforcement. The targeted critical failure ends of each bay were installed on the diagonals opposite each other to minimise interaction of failure modes that could affect results. Additionally, D12 "stitching" bars were installed linking the two beta units (unit 4 and unit 5) to strengthen the connection after the results from the TEST 1 experiment determined that this was a critical weak point for both the gravity-carrying and diaphragm functions of the floor (Parr et al. 2022).

After the findings detailed in Part I (Parr et al. 2022) and Section 2 related to TEST 1, it was decided that TEST 2 would have a more targeted directionality typical of a pulse or near-fault earthquake shaking. This led to the use of a 1:2 directionality linearised oval protocol as shown in Figure 2 (d). This was considered as the lower bound of likely realistic earthquake directionalities based on research conducted by (Nievas and Sullivan 2017).

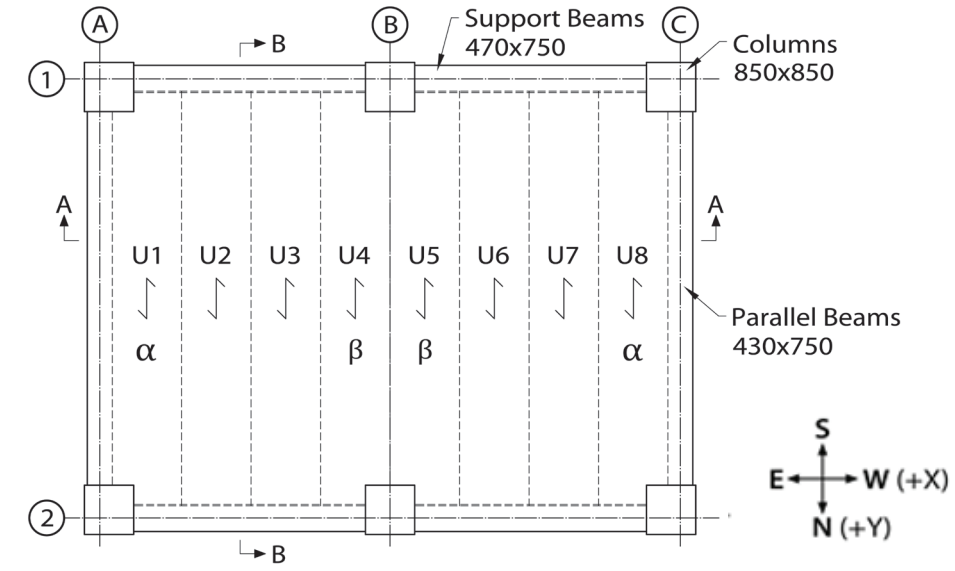

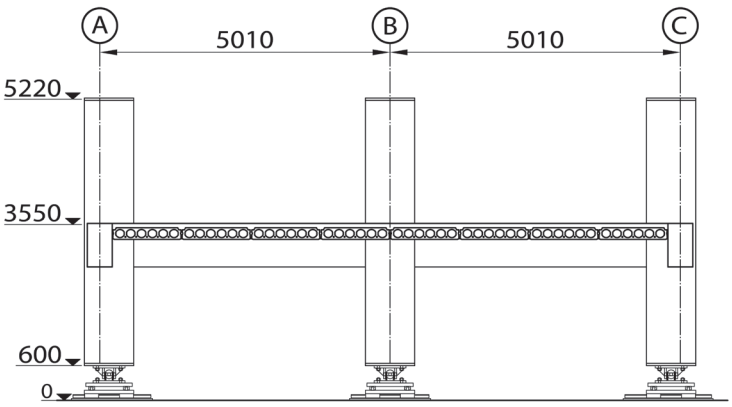

Section B-B

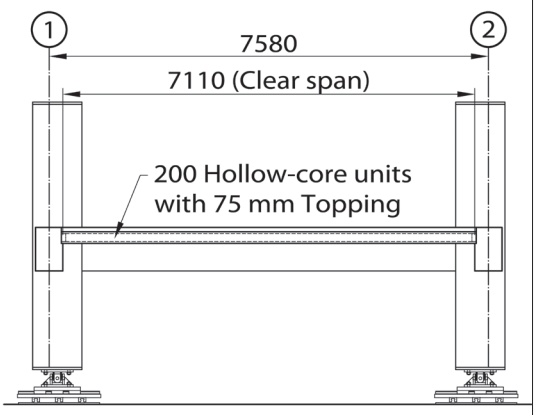

Section A-A

(a) 2020 UC Super-assembly experiment frame layout and nominal dimensions (Büker et al. 2022)

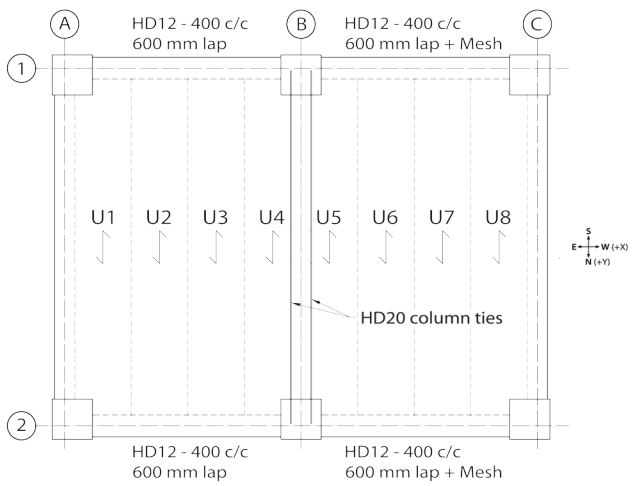

(a) TEST 1 Continuity reinforcement

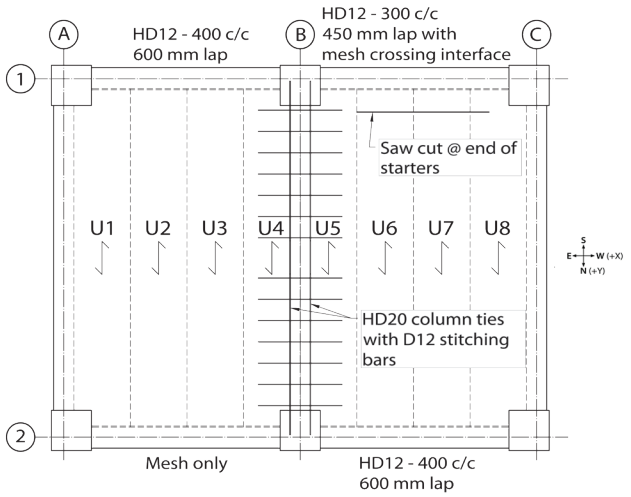

(b) TEST 2 Continuity reinforcement

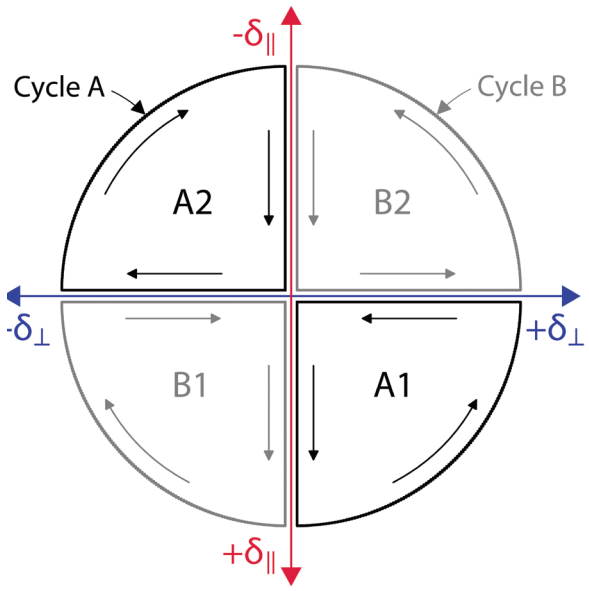

(c) TEST 1 SLP shape

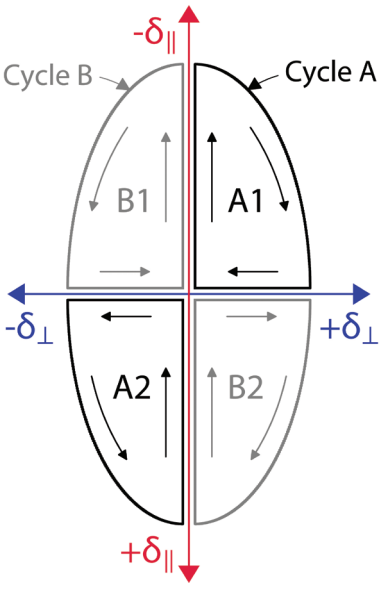

(d) TEST 2 SLP shape

Figure 2: Standard loading protocols and locations of rhomboid loading protocols for the TEST 1 and TEST 2 experiments (Büker et al. 2022)

This meant TEST 1 and TEST 2 would provide an upper and lower bound of simultaneous bi-directional actions imparted into a floor system respectively (Parr et al. 2022).

At different damage states within the floor in each test, the standard loading protocol was stopped to enforce plan shear deformation on the frame (referred to as a rhomboid loading protocol). No drift rotation was applied during the rhomboid loading as the purpose was to isolate the shear stiffness behaviour of the frame and its ability to resist warping via the floor diaphragm. The loading fixity while pushing from strong walls during the rhomboid loading protocols is displayed in Figure 3 and the force/distortion demands of each rhomboid for both tests are displayed in Table 1.

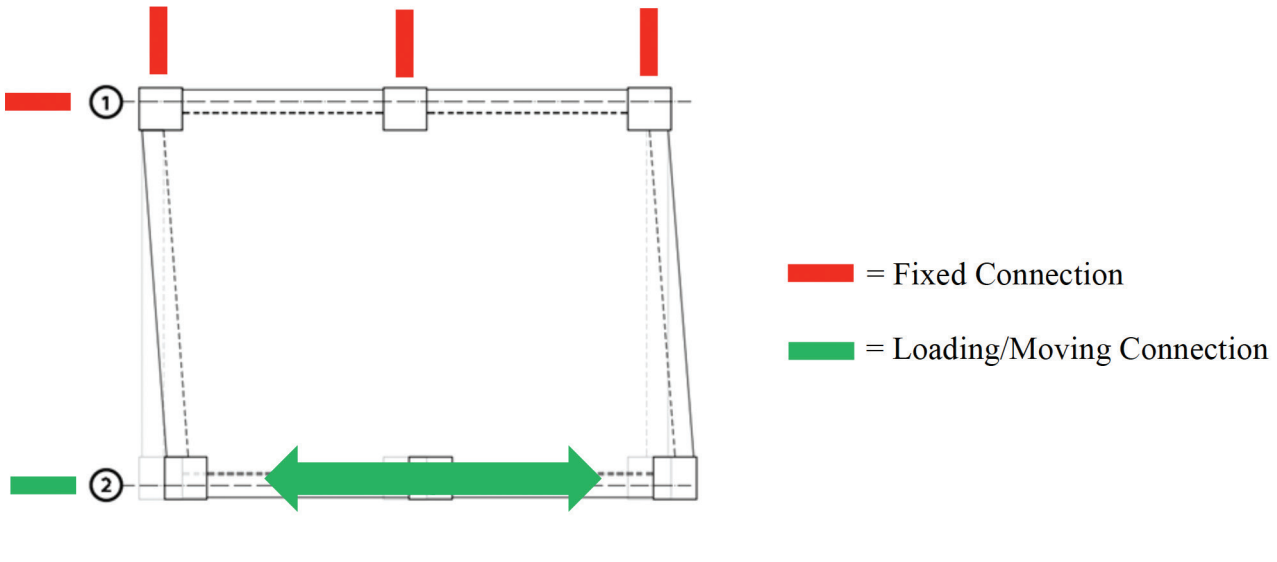

Figure 3: Fixity and loading of the specimen during rhomboid loading (positive shear distortion shown) (Parr et al. 2022)

Table 1: TEST 1 and TEST 2 Rhomboid applied displacement and shear distortion demands

Rhomboid #	+- Plan Shear Distortion, γ (%)				Targeted state of the diaphragm for testing
	Test 1		Test 2		
	± Shear Distortion, γ (%)	± Force (kN)	± Shear Distortion, γ (%)	± Force (kN)	
1	0.01	250	0.005	250	No/low damage to designed load-paths
2	0.05	500	0.02	500	Intermediate damage to design load-paths
3	0.11	450	0.06	600	High damage to designed load-paths
4	n/a	n/a	0.25	700	Extreme damage to designed load paths

Note that the magnitude of each rhomboid loading protocol was different depending on the level of damage the specimen had sustained in previous standard linearised circular loading cycles. This was done to avoid prematurely damaging the specimen before it had softened from the standard loading protocol. Doing so would have lowered the reliability of results from subsequent testing with both the standard loading protocol and rhomboid loading protocols (Parr et al. 2022).

For more detail regarding the super-assembly specimens, loading systems and loading protocols, refer to Part I (Parr et al. 2022) or the thesis (Parr 2022).

The crack maps observed at the end of TEST 1 and TEST 2 are displayed in Figure 4.

Note: The Bowstring Effect

Throughout this paper, a phenomenon known as the "bowstring effect" will be referenced multiple times. The bowstring effect describes the topping steel reinforcement of a diaphragm acting in tension to restrict beam elongation of a concrete moment frame. This creates a balance between the beams attempting to extend acting as a compression arch similar to a bow, and the diaphragm topping reinforcement restricting this by acting in tension similar to a bowstring as discussed in (Lindsay 2004) and (MacPherson 2005).

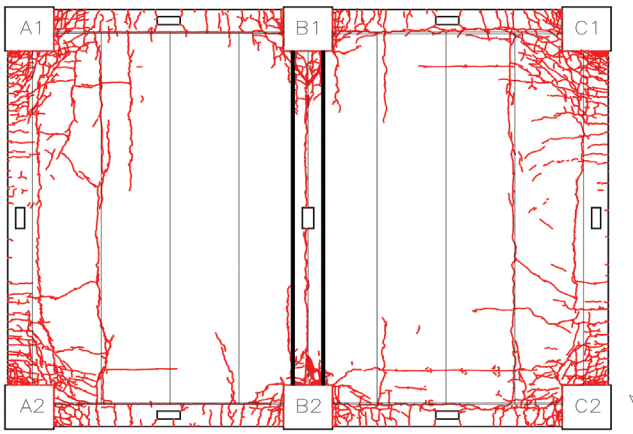

(a) TEST 1 Topping crack map after 3.0% drift

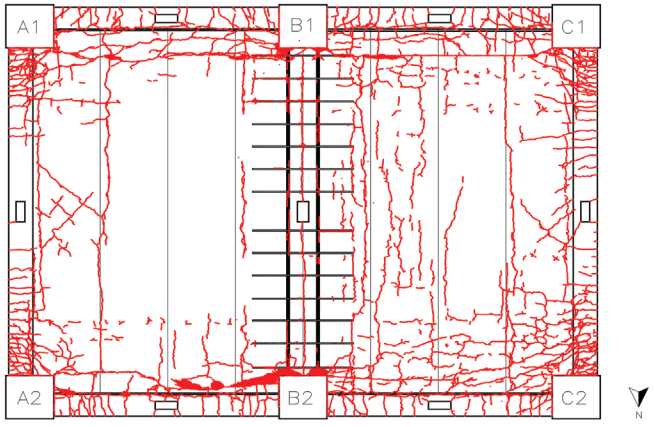

(b) TEST 2 Topping crack map after 5.0% drift

Figure 4: Topping crack maps for TEST 1 and TEST 2 at conclusion of experiments (Parr et al. 2022)

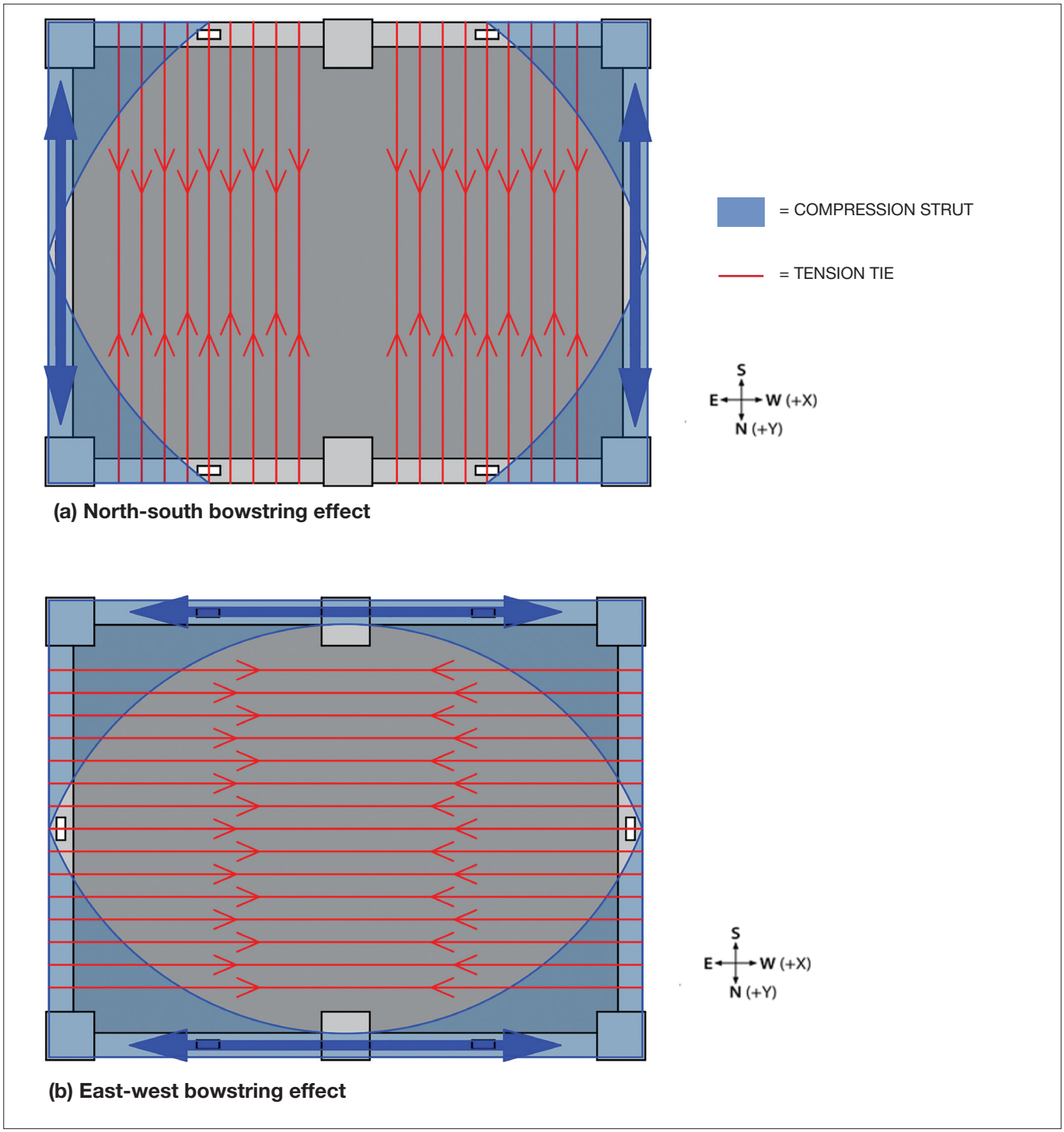

Figure 5: Directionality of the bowstring effect in the 2020 UC super-assembly experiment

If steel reinforcing in the floor topping ruptures this can reduce or even eliminate the restriction to beam elongation provided by the bowstring effect. This is a critical factor in many of the observations relating to residual load-paths discussed in this report.

Throughout the paper there will also be distinction between the bowstring effect acting in different directions across the floor diaphragm. References to a north-south bowstring effect relate to a load-path (for the specimen described in Section 1) like the one displayed in Figure 5 (a). References to an east west bowstring effect relate to a load-path like the one displayed in Figure 5 (b).

2. ANALYSIS OF SUPER-ASSEMBLY TEST RESULTS

2.1 DEGRADATION OF FRAME IN-PLANE SHEAR-MODE STIFFNESS WITH INCREASING DIAPHRAGM DAMAGE

As covered in Section 1, a core objective of the UC 2020 super assembly experiments was to determine how load-paths evolve as a diaphragm degrades during an earthquake. The observations from TEST 1 and TEST 2 provided some unexpected results.

When wide cracks form around the perimeter of a floor in an RC frame structure, the anticipated behaviour was that no compression struts would be able to form across the crack openings between both the floor and columns as well as the floor and beams until rhomboidal deformation of the surrounding frame elements in plan led to binding with the floor. When considering the force displacement response of a structure with shear deformation applied, this would have led to very low stiffness at low shear deformations until binding occurred across the diagonal. This is because the only elements contributing resistance to shear deformation before binding would be the beams orthogonal to the loading direction acting in shear and bending about their weak axis as displayed in Figure 6.

The force displacement response of this anticipated system would have looked like what is displayed in Figure 7. Based on this model, higher damage states with wider cracks would be associated with larger shear deformations in the horizontal plane (in plan) required before jamming

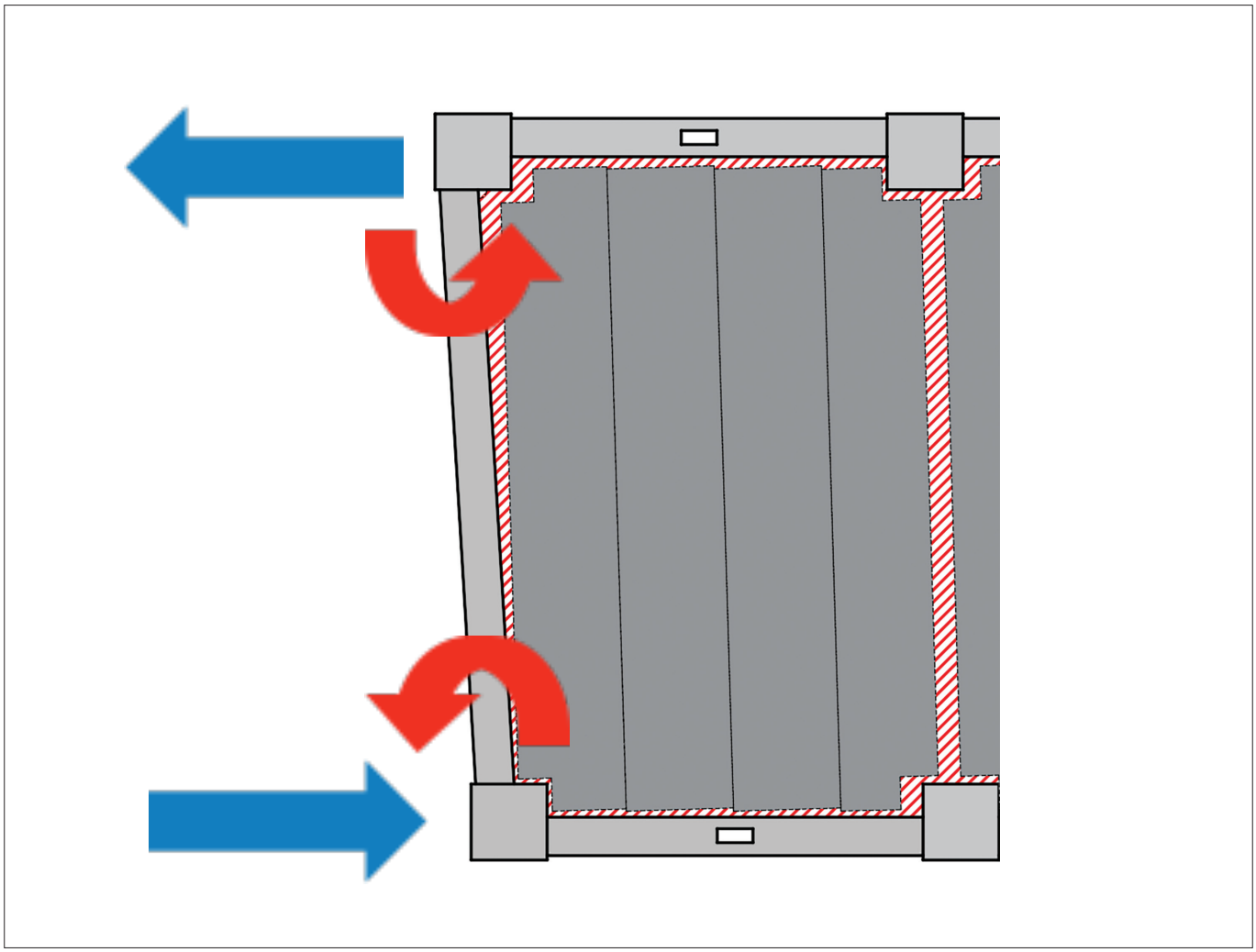

Figure 6: Expected behaviour of the diaphragm and surrounding beams prior to binding across the diagonal with stiffness contribution only provided by longitudinal beams acting in shear/moment about their weak axis

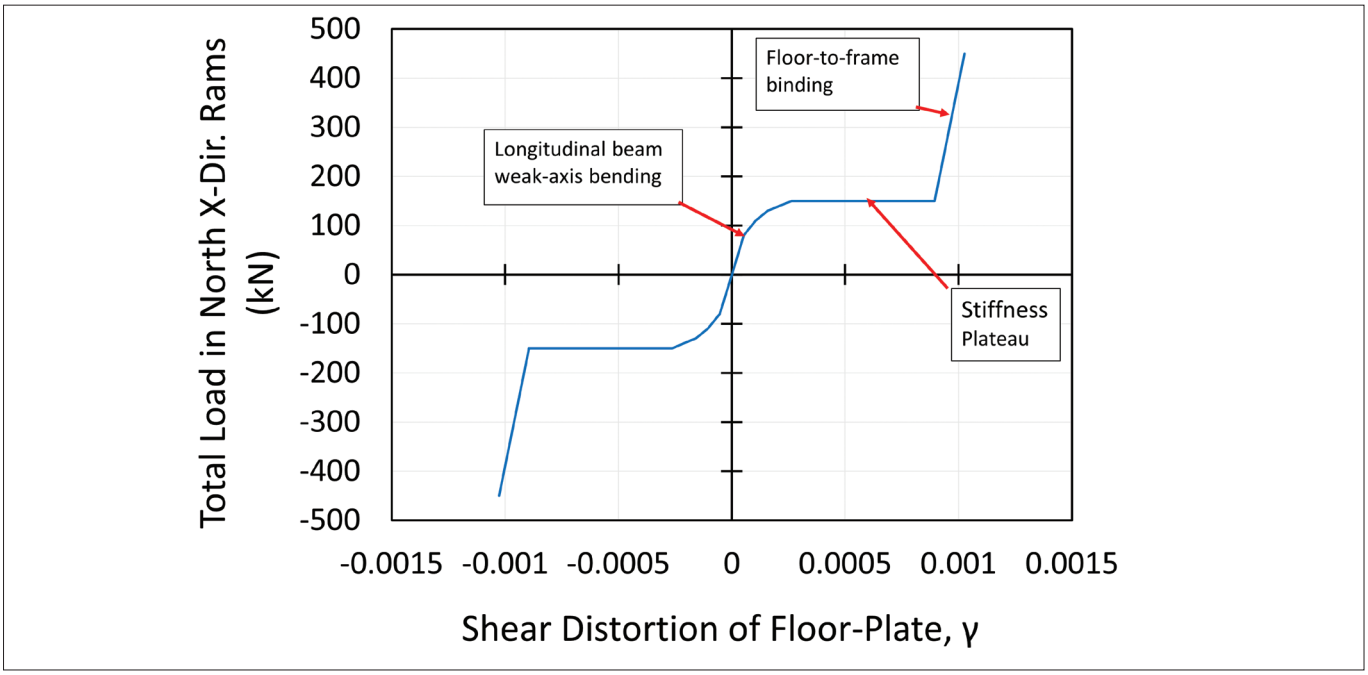

Figure 7: Expected Plan Shear Stiffness Behaviour with the Proposed "Picture Frame Effect"

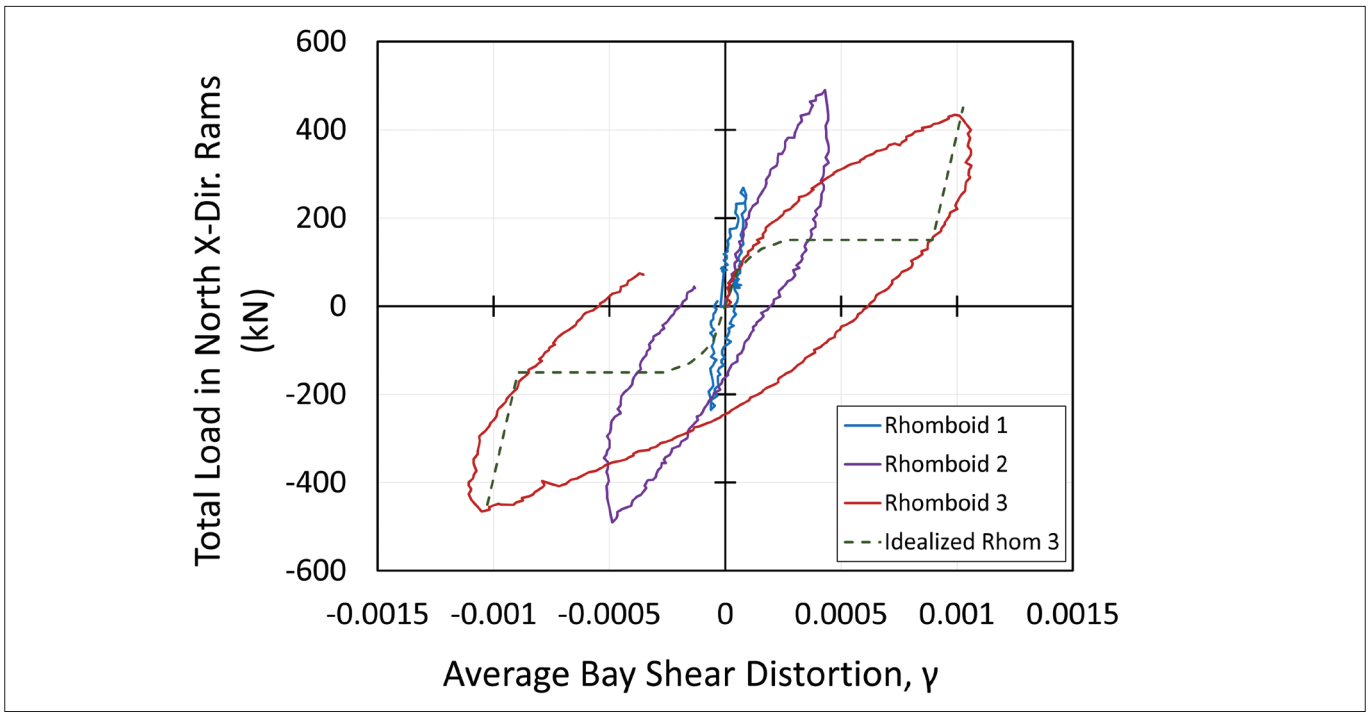

Figure 8: Observed plan shear stiffness behaviour for rhomboid loading protocols undertaken in TEST 1

occurred across the diagonals of the floor. Once jamming occurred, the stiffness would increase greatly.

The true behaviour observed in the 2020 UC super assembly experiments deviated significantly from the anticipated behaviour. The force-distortion behaviour observed in the rhomboid protocols undertaken throughout TEST 1 are displayed in Figure 8.

The force-distortion behaviour observed in the rhomboid protocols undertaken throughout TEST 2 are displayed in Figure 9.

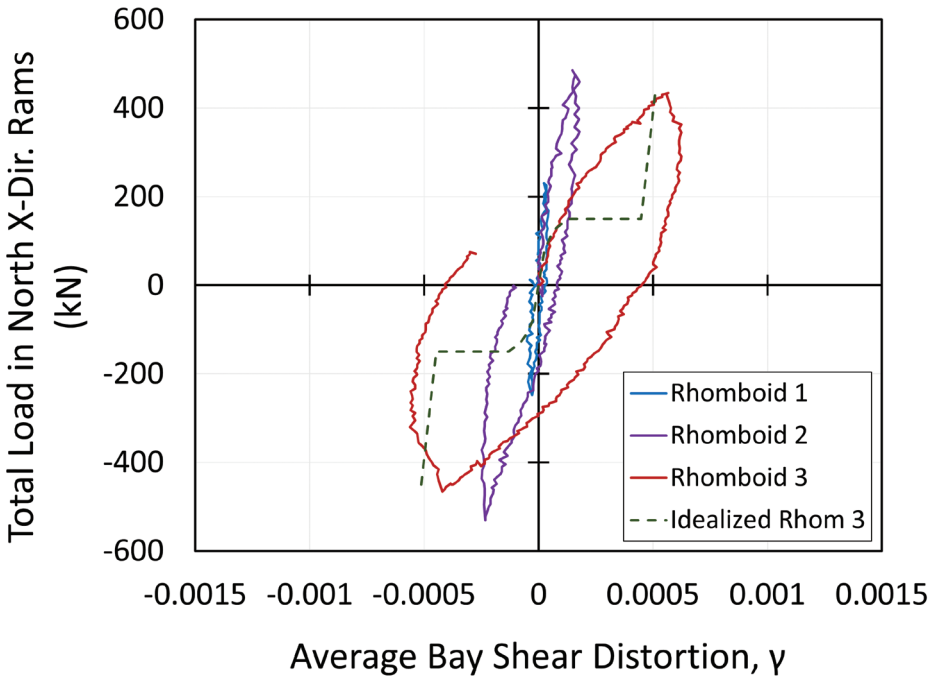

(a) Plan shear stiffness behaviour of the first three rhomboids of TEST 2 (for comparison with the TEST 1 rhomboids)

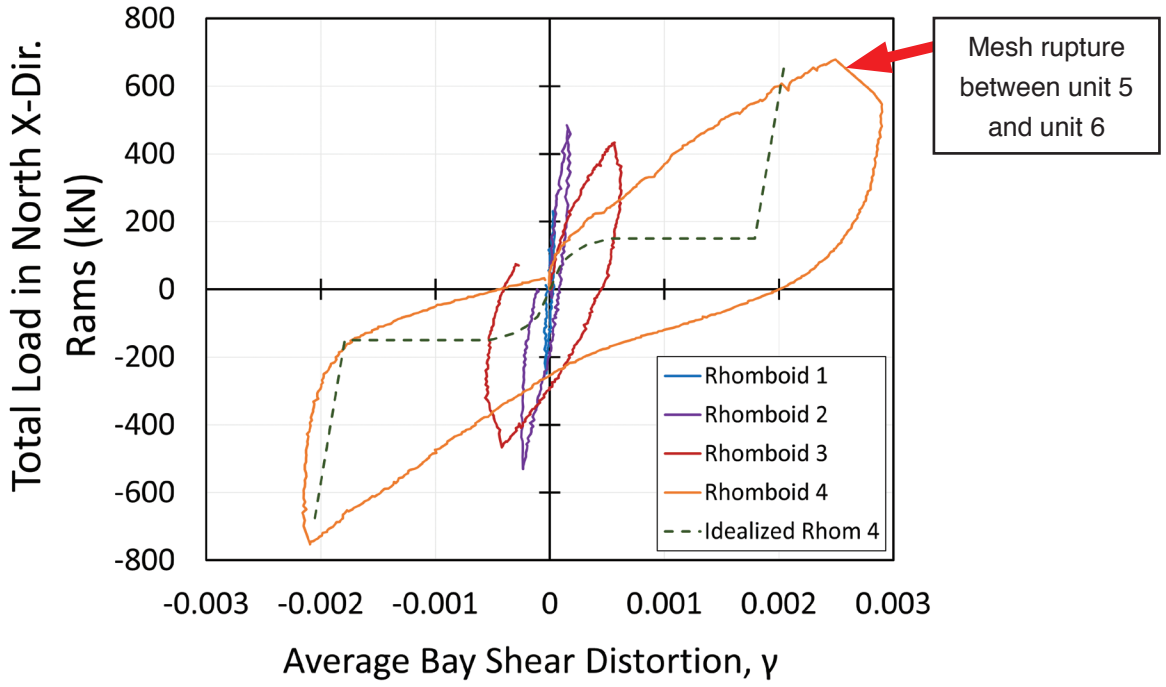

(b) Plan shear stiffness behaviour of all four rhomboids of TEST 2

Figure 9: Observed plan shear stiffness behaviour for the first three rhomboid loading protocols undertaken in TEST 2

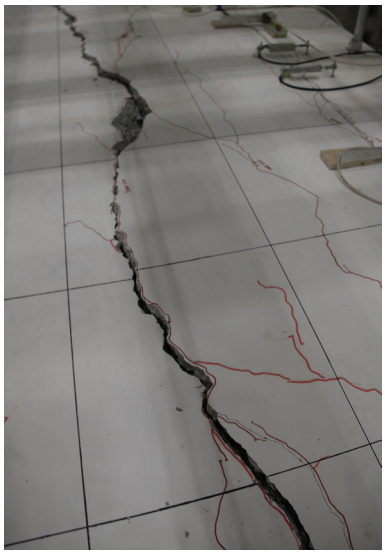

(a) Highly curved crack surface along A1B1

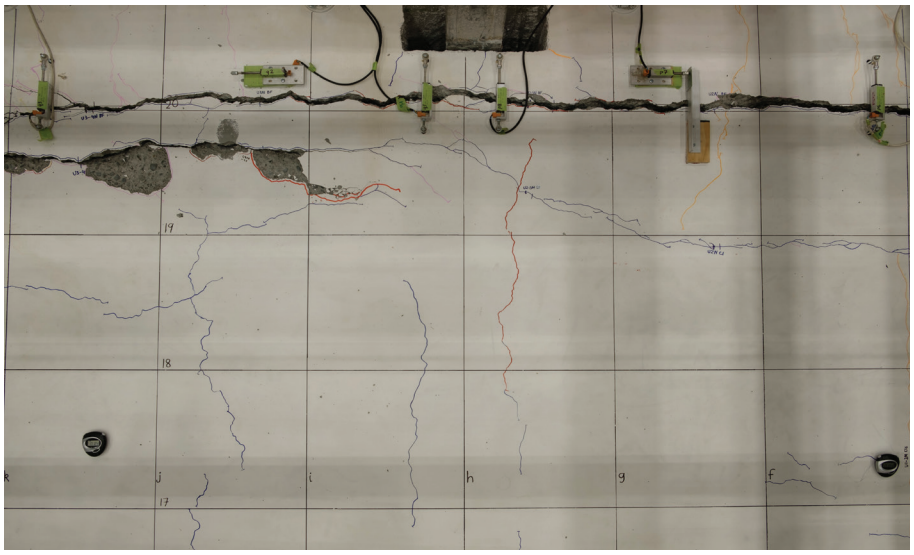

(b) Slightly curved crack surface along A2B2

Figure 10: Curved and rugged wide crack interfaces in TEST 2

There is a stark difference between the idealised and observed force-displacement results. Under real shear distortion loading there is an immediate resistance to shear deformation in plan at all damage states. The reason for the discrepancy becomes clearer when the crack patterns are considered. When considering the perimeter cracks theoretically, it was assumed that once a wide enough crack formed there would be no contact across the crack and it could be idealised as a gap similar to a saw cut, i.e., with a clean visible gap between the two sides. The reality of cracking in floors is that it does not result in clean, unobstructed cracks. Examples from the 2020 UC super-assembly experiments are displayed in Figure 10.

It is well known that aggregate interlock can transfer load at small crack widths (<0.3 mm) (Vecchio and Collins 1986). The process of aggregate interlock requires pieces of aggregate engaging with the other side of a crack. As cracks run through the weak points in the interfacial transition zones of the concrete, this creates a rugged, three-dimensional interlocking surface that can transfer compressive forces. The results from the super assembly tests showed that compressive forces can also transfer across crack widths much greater than 0.3 mm once aggregate interlock is lost. However, at this higher level of damage the process is different. For aggregate interlock, the two sides of the crack can remain mostly intact and close which contributes to compressive capacity under loading, as the gap is very small.

For the observed wide crack compressive load-path, it requires that rubble produced from grinding of the two crack sides falls into the existing gap and gets jammed at a tighter point in the crack. This means that the compressive load path at wider crack widths is a rubble aggregate contact stress compression mechanism. Reverse cyclic loading of a structure evidently provides enough grinding of the crack interfaces to create enough rubble to keep replenishing the compressive load path, up to surprisingly large crack widths. As new contact surfaces are created by jammed rubble, these new surfaces can also grind off protruding elements in the crack to generate more rubble. Also, cracks near the floor perimeter tend to be angled (such as the positive and negative moment-shear cracks that are causes for concern in hollow-core). This provides more locations for pieces of rubble to get stuck and jam than assumed clean vertical cracking would.

Cracks that form a curved surface are particularly effective at creating rubble to replenish the compressive load path. An example of this cracking layout from TEST 2 is displayed in Figure 10 (a). This cracking occurred along the ends of units near the interface with beam A1B1. It should be noted also that curved and angled cracking surfaces in the floor (relative to the primary axes of the structure) naturally developed near all corners and columns due to the simultaneous bi directionality of loading.

The most obvious case of load path replenishment from rubble was visible in TEST 2 where a large wedge of concrete at the topping near column B2 became

dislodged from both sides of the major crack and slotted into the gap, linking both sides of the crack. The concrete wedge is displayed in Part I (Parr et al. 2022). This wedge was unmoveable due to the compression it was under until 5% drift, which displayed how it was actively providing a compression load path up to this point. Over multiple cycles the wedge was pushed up by compression acting across inclined faces, so it was higher than the concrete on either side of it. Under reverse cyclic loading it would be expected that the wedge would rise and fall depending on the drift direction. Instead, it was continually pushed up. This displayed how additional grinding of the contact surfaces had created extra rubble, leading to the wedge being slowly squeezed out while remaining in compression.

The key conclusion to be drawn from these results is that diaphragm compressive load struts can be transferred across wide cracks. If there is a sustained gravity load path between the floor elements and the beam elements, a diaphragm compressive load path will also be sustained to much higher crack widths than previously anticipated. The limitation on crack width to sustain this contact stress compressive load path is unknown and would benefit from future research. A suggested assumption would be that the aggregate size used in the concrete mix is the maximum width before a reliable contact stress load path is lost, as individual pieces of aggregate are unlikely to crush. With distortion across cracks that have significant roughness and curved interfacial surfaces, cracks even wider than the aggregate size may be able to sustain intermittent struts. A depiction of compression strut formation across wide cracks due to aggregate rubble interlock is displayed in Figure 11. The aggregate size used in the TEST 1 and TEST 2 floor topping concrete mixes was 19 mm.

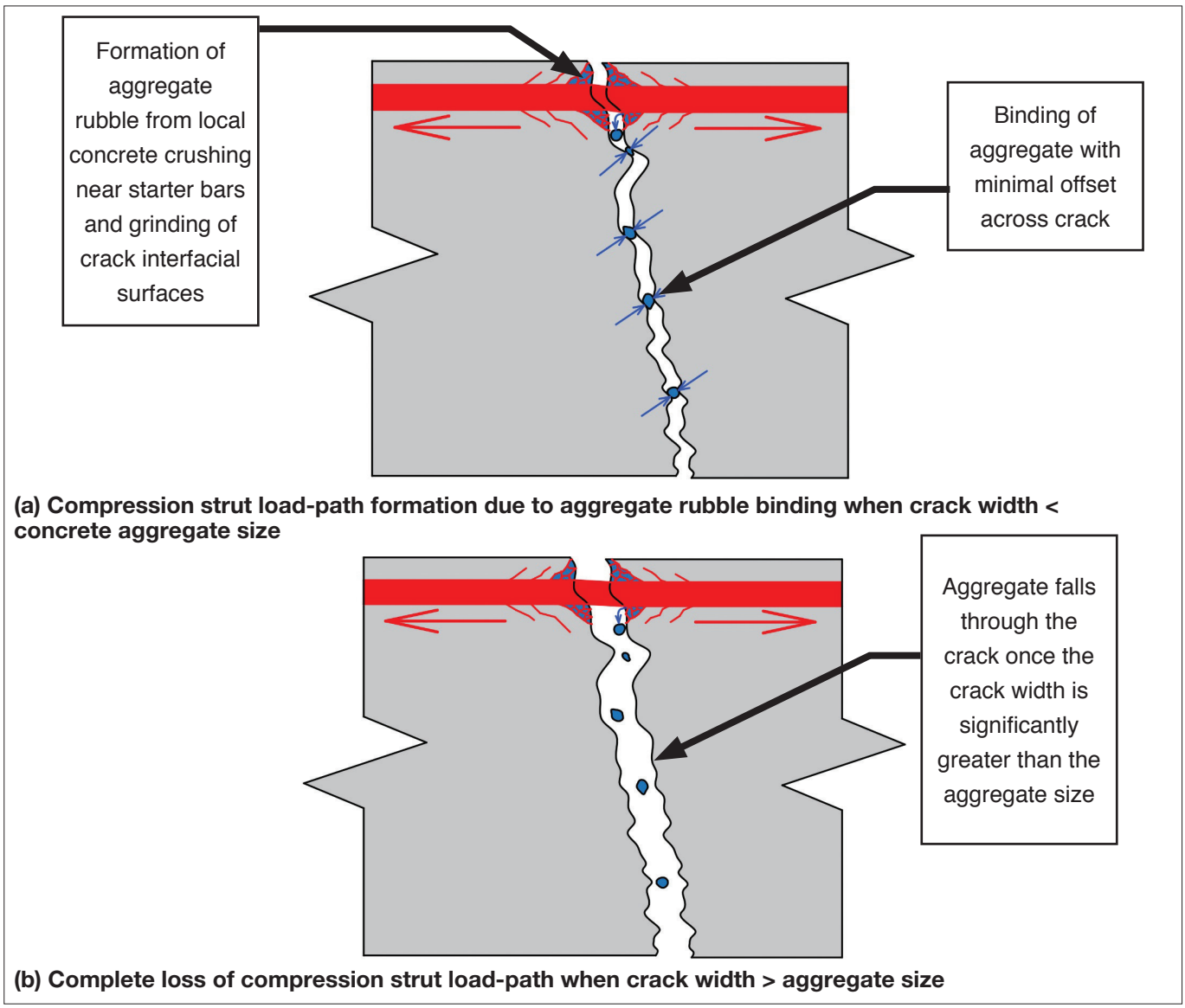

Figure 11: Residual compression strut load-paths forming across wide cracks due to aggregate rubble binding (Parr et al. 2022)

The finding that residual contact stress compressive load paths develop across wide cracks does not mean that strut-and-tie load paths remain unaffected through all damage states. If mesh rupture occurs as it did at the end of the starter bars along beam A1B1, tension tie load-paths are eliminated. Additionally, as discussed in Part I (Parr et al. 2022), gaps had opened around all the interfaces between columns and floor elements by 1% to 1.5% drift in both tests. As these interfaces were vertical and smooth, the rubble load path replenishment seen in the floors did not apply to these gaps. This meant that it would not have been appropriate to make the assumption for struts landing directly onto columns typical in strut-and-tie analysis in the case of a relatively small earthquake (the exception to this generally observed rule occurred only for the interior column to floor interfaces that were connected by tie bars as discussed later in Part I (Parr et al. 2022) and Section 2.3 of Part II).

Therefore the only remaining load-path for diaphragm compression struts to land into the rest of the structure was through the beams. While this held true for both TEST 1 and TEST 2, the exact form of the load-path degradation and rate of stiffness degradation was different. This was caused by the difference in load-path directionality between experiments and the stitching retrofit employed to keep the beta units together in TEST 2 which was not used in the TEST 1. Improved roughening of beam-column cold joint casting interfaces in TEST 2 described in Part I (Parr et al. 2022) likely also caused differences in the point diaphragm degradation initiated.

The secant stiffnesses obtained from both the TEST 1 (1:1 standard loading directionality ratio) and TEST 2 (1:2 standard loading directionality ratio) rhomboid loading sequences relative to the previous maximum drift the structure had been pushed to are displayed in Figure 12. The measured applied force divided by the shear strain, F_{rhom}/γ, is displayed in Figure 12 instead of the effective shear modulus, G_{eff}. This is because the effective shear surface area between the frame and floor elements, A_{eff}, is likely a changing variable as damage increases and requires further research. Thus a reliable value for G_{eff} cannot currently be obtained to provide a typical shear stress/strain relationship. Also note the effective shear modulus, G_{eff}, is not an elastic shear modulus (G) as elements of the system had experienced plastic deformation and cracking for all datapoints. The relationship between G_{eff} and F_{rhom}/γ is shown in Equation (1):

$$G_{eff} = \frac{\tau}{A_{eff}} = \frac{F_{rhom}}{A\gamma} \quad (1)$$

Rearranging provides the relationship in Equation (2):

$$\frac{F_{rhom}}{\gamma} = G_{eff} A_{eff} \quad (2)$$

The green dot and line in Figure 12 (a) depict the first rhomboid of TEST 2. At this stage in testing only uni-directional drift demands of 2% in the -Y drift direction

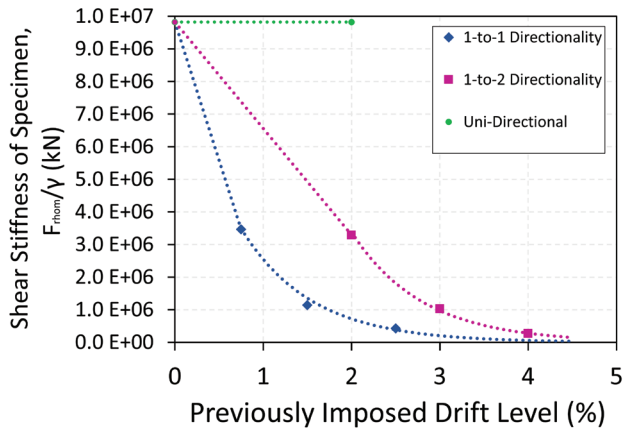

(a) Absolute values of plan shear stiffness

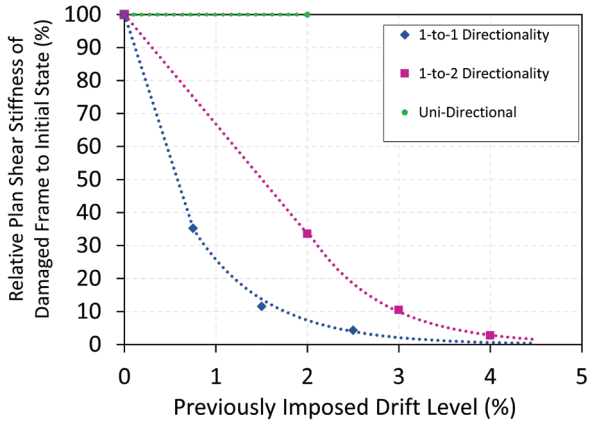

(b) Relative values of shear stiffness ($\%G_{initial}$) compared to the initial observed stiffness in TEST 2 rhomboid #1

Figure 12: Residual compression strut load-paths forming across wide cracks due to aggregate rubble binding (Parr et al. 2022)

and 1% in the +Y, -X and +X directions had been applied to the specimen. As discussed in Part I (Parr et al. 2022), cracking had developed in the floor at this stage but there had been no signs of mesh rupture or loss of beam torsional stiffness. This is therefore the closest experimental data-point to an idealised design value that may be obtained from a strut-and-tie or grillage method. Future research should seek to compare this experimentally obtained diaphragm shear stiffness value to these commonly used modelling methods.

Figure 12 shows that the rate of plan shear stiffness degradation is heavily dependent on the directionality of the earthquake. As discussed in Part I (Parr et al. 2022), TEST 1 was designed to replicate an upper bound for earthquake directionality while the TEST 2 experiment was designed as a lower bound for realistic directionality of earthquakes. Therefore by interpolating between the 1:1 directionality and 1:2 directionality lines in Figure 12, a full range of diaphragm stiffness degradation rates relative to the earthquake directionality ratio can be obtained. The equations for the 1:1 directionality stiffness degradation relationship are provided in Equation (3) and (4), where $\%G_{\text{initial}}$ is the diaphragm shear stiffness percentage relative to the initial stiffness and θ is the maximum drift demand (% drift) experienced by the structure.

$$\%G_{\text{initial}} \approx 100 - 86\theta, 0 \le \theta \le 0.75 \quad (3)$$

$$\%G_{\text{initial}} \approx 90e^{-1.25\theta}, 0.75 < \theta \le 2.5 \quad (4)$$

The equations for the 1:2 directionality stiffness degradation relationship are provided in Equations (5) and (6), where θ is the maximum drift demand (% drift) experienced by the structure.

$$\%G_{\text{initial}} \approx 100 - 33\theta, \ 0 \le \theta \le 2 \quad (5)$$

$$\%G_{\text{initial}} \approx 416e^{-1.25\theta}, \quad 2 < \theta \le 4 \quad (6)$$

Based on these equations, a generalised set of equations for earthquake directionality is provided in Equation (7) and (8), where θ is the maximum drift demand (% drift) experienced by the structure and α is the ratio of drift demand between the drift in the primary loading direction and drift in the minimal loading direction (typically orthogonal to the primary loading direction).

Note that generalised Equation (8) is fitted to provide close alignment with Equation (7) at 1:2 (50%), 3:4 (75%) and 1:1 (100%) directionality ratios (α). There is a slight discontinuity between the two equations at other directionality ratios. This discontinuity can be removed by altering the 0.76 factor at the start of Equation (8).

Also shown in Figure 12 is the stiffness of the specimen following uni-directional pushes up to 2% in the Y-direction and 1% in the X-direction (following the initial Northridge earthquake portion of TEST 2). As seen in Figure 12 (a), this is much stiffer than the specimen when it was subjected to lower drift levels of simultaneous bi-directional loading. Due to the high stiffness and low damage at this stage in TEST 2, the value obtained from this rhomboid loading of 9.82 x 10^6kN per radian distortion was taken as the benchmark 100% plan shear stiffness to compare against in other rhomboid loading protocols. Due to the nature of the standard loading protocol used in the two tests, there was no further data obtained for the degradation of the diaphragm under uni-directional pushes. However, other research has investigated the plane shear stiffness of pre-cast floor diaphragms without pre-damaging the floor (Angel et al. 2019). The stiffness behaviour of diaphragms that are undamaged or have been subjected only to uni-directional drift demands would match the data obtained from these experiments more closely.

A limitation of the rhomboid data is the approximately 0.1 mm ±0.05 mm accuracy of the draw-wires used in measuring deformations. Particularly for rhomboid #1 of TEST 2, which saw maximum displacements of 0.4 mm, this translates to a ±12.5% error which is directly carried into the estimate of the diaphragm stiffness at its least damaged state. As the purpose of the experiment was to capture the general trends of the stiffness degradation without impacting the reliability of subsequent rhomboid loading protocols, this error is viewed as acceptable.

Additionally, as there is no data from rhomboid loading protocols conducted between 0%-0.75% drift for TEST 1 and 0%-2% drift for TEST 2, a linear interpolation has been used in this range (described in Equations 3, 5 and 7). This interpolation was from 100% stiffness for the undamaged specimen, directly to the first rhomboid stiffness result following simultaneous bi-directional demands.

It is likely that this interpolated estimate overestimates stiffness degradation at low drifts within the frame elastic response range (e.g. 0-0.25%). Future research could attempt to provide more representative results for low drift demands using methods to estimate elastic stiffness of the diaphragm .

$$\%G_{\text{initial}} \approx 100 - \frac{6.5 - 3.5(\alpha - 1)}{0.75 - 2.5(\alpha - 1)}\theta, \ 0 \le \theta \le 0.75 - 2.5\ (a - 1) \quad (7)$$

$$\%G_{\text{initial}} \approx (0.76 + 0.96|\alpha - 0.75|)*(90 - 650\ (\alpha - 1))*e^{1.25\theta}, 0.75 - 2.5(\alpha - 1) < \theta \le 4 \quad (8)$$

Finally, the exponential portion of the obtained Equations (Equations 4, 6 and 8) only have backing data up to 2.5% drift for 1-to-1 directionality and 4% drift for 1-to-2 directionality. Reliability of results is lower beyond these drift levels. However, with these drift levels the remaining diaphragm shear plan stiffness is less than 5% of the initial stiffness, so this is a minor consideration.

In TEST 1 and TEST 2, the plan shear stiffness was observed rapidly decreasing from the original diaphragm stiffness under simultaneous bi-directional loading. As the degree of simultaneous bi directionality was within realistic levels, this means the rigid diaphragm assumption may not be appropriate when modelling building response. An interesting aspect to this result is that diaphragm shear stiffness degradation was clearly not primarily driven by wide cracks in the floor as initially expected, as the largest stiffness losses occurred prior to wide cracks opening.

2.2 PRIMARY DIAPHRAGM STIFFNESS SOFTENING MECHANISM

The reason for stiffness degradation of the diaphragm was not due to the expected loss of load-path across wide cracks in the floor, but instead due to degradation of the only remaining portion of the load-path into the columns; the beam plastic hinges. After a compressive strut lands on a beam, the load must then be transferred through the plastic hinge in shear about the weak axis of the beam as displayed in Figure 13.

The beam plastic hinge degradation was driven in the form of loss of torsional stiffness. Loss of beam torsional stiffness after a frame has been subjected to earthquake loading has been observed in previous tests with frames specimens incorporating floor diaphragms, but it has not previously been identified as for a major contributor to diaphragm plan shear stiffness degradation. A depiction of a beam that has lost torsional stiffness in the plastic hinge zone is displayed in Figure 14.

Based on the TEST 1 and TEST 2 observations the process of a beam losing torsional stiffness appears to require the following events to occur:

- Beam elongation must proceed to a stage where aggregate interlock across the primary crack near the beam-column interface is reduced as shown in Figure 15.
- Weak-axis and torsional demand applied from the floor elements connected to the beam must reach a level where it overpowers the combined capacity of the beam longitudinal bars acting in dowel action across the primary crack and friction between the interfaces of the two sides of the crack acting in compression through contact stresses as shown in Figure 16. Note that there are four combinations of simultaneous bending between the two orthogonal beam directions. Based on the direction of twist and location of damage in the beams observed at the end of both tests, the critical load combination was identified as negative bending in the beam of interest (tension at the top critical beam longitudinal bars) and negative bending in the orthogonal beam (tension in the top orthogonal

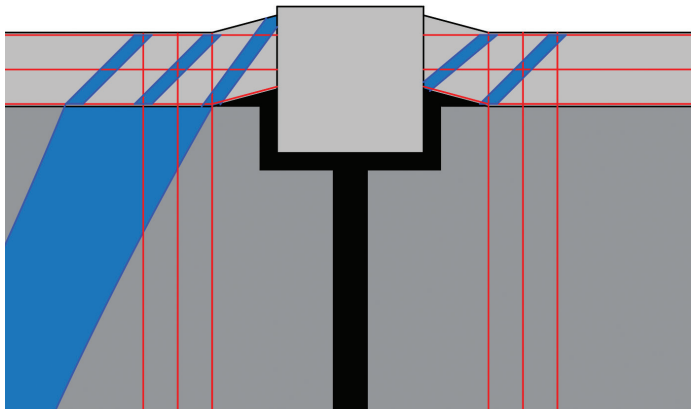

(a) Into an intermediate column

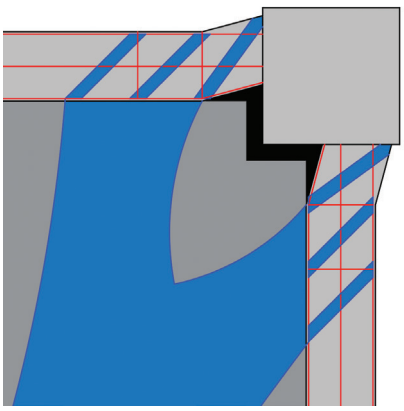

(b) Into a corner column

Figure 13: Transfer of diaphragm compressive struts through beam plastic hinges (compressive struts depicted in blue and tension ties in red)

beam longitudinal bars and starter bars). Based on which longitudinal bars were most heavily loaded in tension, the centre of torsional stiffness in the beam moved, meaning the instantaneous centre of rotation (ICR) also moved. By the end of the test, the buckling of the interior bottom beam bars depicted in yellow in Figure 16 (d) and (e) had permanently moved the ICR to the bottom outer corner of the beam, as evidenced by the torsional distortion observed.

The proposed reason that loss of beam torsional stiffness degrades the diaphragm plan shear stiffness is, as the beam twists, it buckles the interior bottom bars, thus cracking the surrounding concrete and reducing their confinement and bond with the rest of the beam. This decreases their contribution to dowel action by not having an effective, supported length determined by the stirrup spacing, which is a much weaker and less stiff contribution to the beam shear load path than the originally designed confined shear contribution. Additionally, twisting of the beam across the primary crack near the beam-column interface likely grinds the two sides of the crack smoother over multiple cycles, reducing aggregate interlock and the friction necessary to

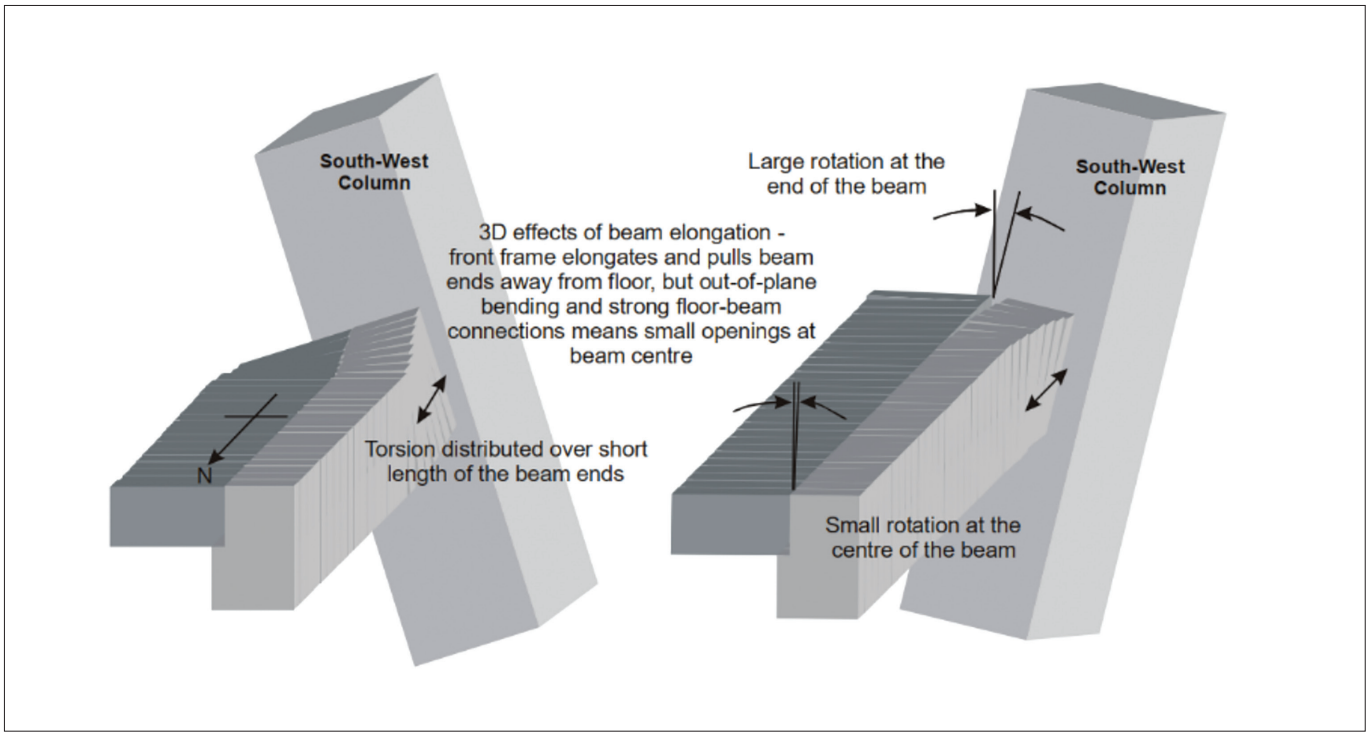

Figure 14. Beam torsion observed in previous UC super-assembly experiments (MacPherson, 2005)

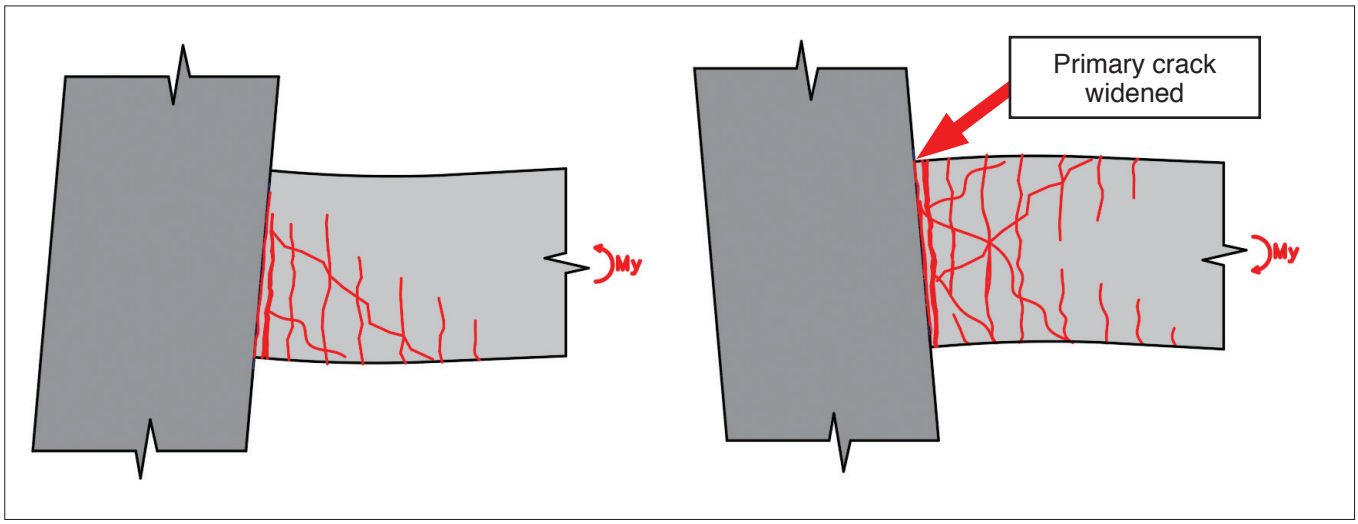

Figure 15: Primary wide crack/s forming near the beam-column interface developing due to beam elongation

maintain the compressive portion of the weak axis shear load-path. This damage would reduce the minor axis shear capacity of the beam, reducing the strength of the load-paths depicted in Figure 13.

While this appears to be a relatively simple process, there are a wide range of factors that can change the level of drift required to initiate loss of beam torsional stiffness as well as changing the level of its impact and rate of degradation once initiation occurs. These factors are a set of interconnected phenomena that can alter the order of occurrence of damage modes for the overall floor system.

The most critical interconnected factors are:

- Degree of simultaneous bidirectionality in earthquake loading.
- Amount of beam elongation.
- The ratio of beam plastic hinge cross-section strength to imposed demands from the floor-beam connection on half the beam span.

For more in-depth investigation into the inter-relationship of these and other factors on the rate of diaphragm shear stiffness degradation refer to (Parr 2022).

Figure 16: Process Leading to Loss of Beam Torsional Stiffness

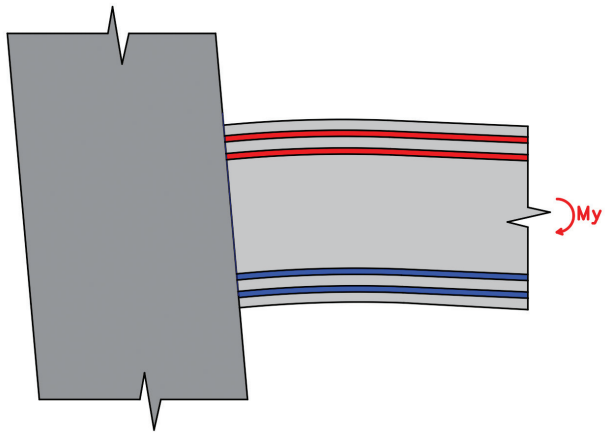

(a) Side view of the critical beam under negative drift demands (top beam bars in tension)

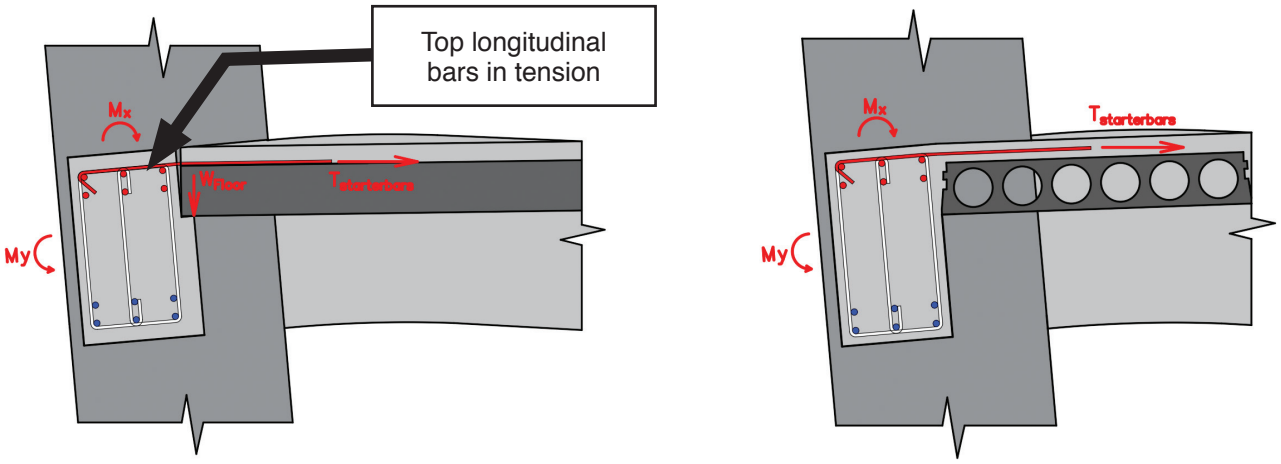

(i) Support beam variant demands **(ii) Longitudinal beam variant demands**

(b) Cross-section view of the critical beam with demands from orthogonal beam in negative bending (top beam bars and starter bars in tension)

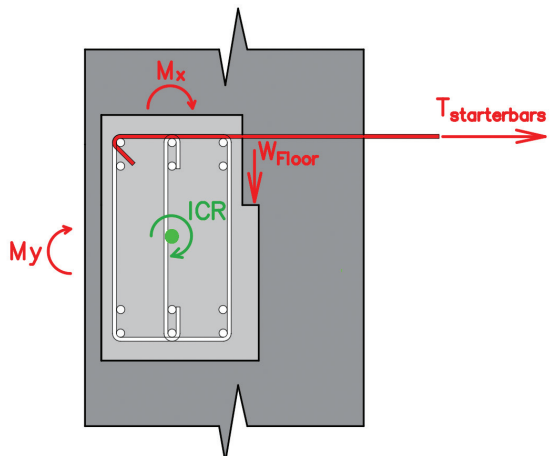

(c) Initial ICR with Critical Beam Load Combination Shown

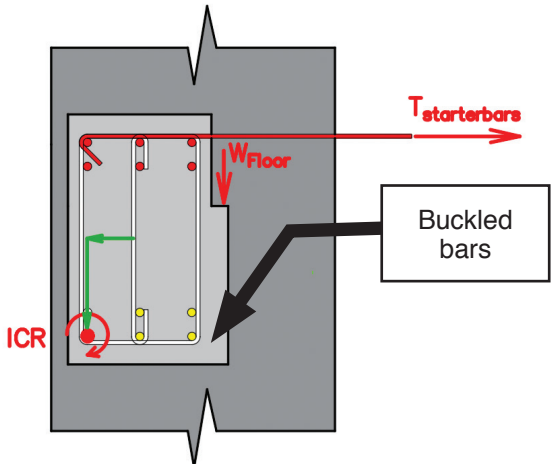

(d) Movement of ICR as Yellow Highlighted Bars Buckle Under Torsional Demands

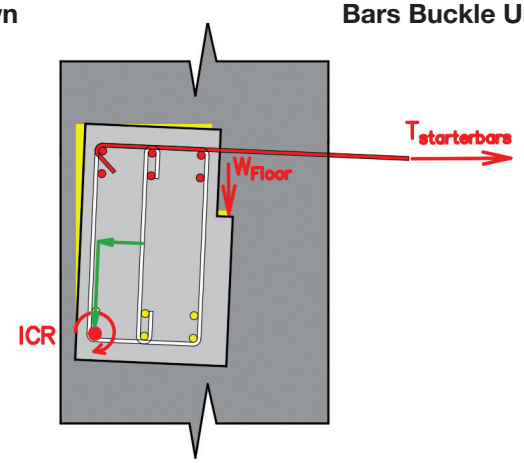

(e) Torsional Rotation of Beam Through the Plastic Hinge About the Residual ICR

2.3 EFFECTS OF THE SIMULTANEOUS BI-DIRECTIONALITY RATIO AND TENSION TIE RETROFITS ON DAMAGE MODES AND DIAPHRAGM STIFFNESS DEGRADATION

2.3.1 Test 1

As discussed in Section 2.1 TEST 1 yielded unexpected and interesting results based on the chosen directionality of the standard loading protocol. The 1:1 directionality (circular rather than elliptical) was selected primarily to provide a worst-case scenario for the individual hollow-core units by enforcing maximum realistic simultaneous strong-axis, weak axis and torsional demands along the lengths of the units via deformation incompatibility with the ductile support beams. Instead it was observed relatively early (by approximately 1.5% drift) that the beams became overloaded by the simultaneous actions caused by deformation incompatibility with the diaphragm and lost torsional stiffness. The loss of beam torsional stiffness meant the support frame for the diaphragm was no longer stiff enough to impart large enough forces through the floor starter bars to damage the floor units. In effect, the weak link in the capacity hierarchy for the system was the beams rather than the floor itself. Diagrams of the demands applied to support and longitudinal beams while experiencing simultaneous bi-directional loading are displayed in Figure 16.

Based on the loss of load-path through the beta-beta unit interface and the inability for diaphragm compression struts to land directly into columns the remaining shear deformation strut load-path in TEST 1 from 1.5% drift onward is displayed in Figure 17.

This load-path is similar to the “picture frame effect” proposed in section 1, except it requires landing of struts in the beams instead of directly between columns. Note that the compression struts displayed in Figure 17 are a simplification for clarity of the true paths a diagonal strut within the floorplate could take. As seen in the crack

patterns in Figure 4, intra-span and beta units of each bay acted as a single block. This means tension ties within and across these units were viable to allow for a truss-like strut-and tie system within each bay. Struts tend to form at an angle of less than approximately 60° (referencing the axis of the support beams), meaning it is probable that tie-backs developed in the system to provide a lower energy load-path like the one displayed in Figure 18. This applies to all subsequent diaphragm load-path figures.

The observation of concrete crushing in the plastic hinge of beam B2C2 near column C2 under positive shear distortion demands and in the plastic hinge of beam B1C1 near column C1 under negative shear distortion demands provided evidence of significant tension ties forming in the north-south direction across the floorplate as shown in Figure 17 (b). These tension ties engaged the beam plastic hinges of the support beams that were not on the short diagonals of the distorted floorplate. The ties also enforced the bowstring effect on each individual bay with elongation of the longitudinal beams restricted (in theory) by the tension ties linking the support beams.

The initial undamaged stiff diaphragm had tension ties running across the entire floorplate in both the north-south direction linking the support beams and in the east-west direction linking the longitudinal beams. This meant that in both directions the bowstring effect was restricting beam elongation (so elongation of both the support and longitudinal beams were being restrained by tension across the floor). After splitting and mesh rupture occurred between the beta units at the start of the 1.5% drift cycle, the bowstring effect in the east-west direction was eliminated. This meant beam elongation of

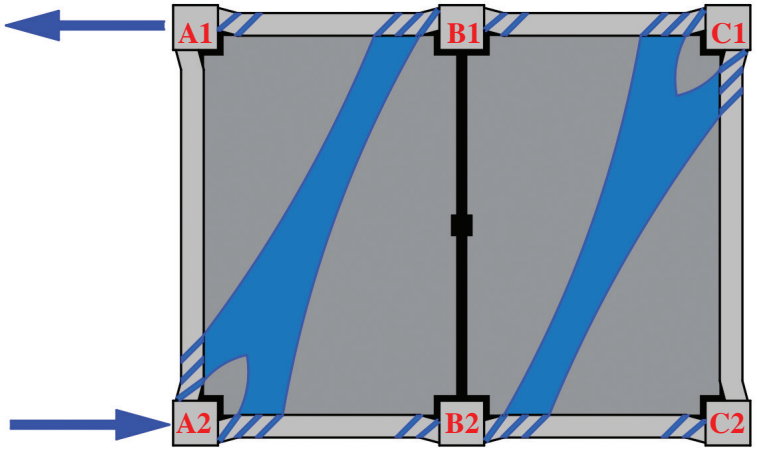

(a) Load-path with only compression struts

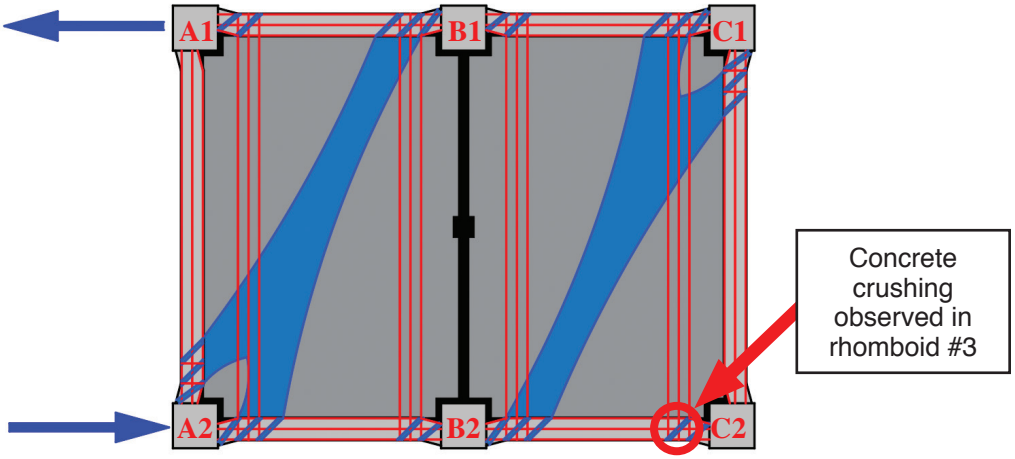

(b) Load-path with struts and tension ties

Figure 17: TEST 1 Residual diagonal compression strut load-path under positive shear distortion loading

the support beams was no longer restrained. As shown in Figure 19, beam elongation of beams A1B1 and B1C1 rapidly increased from this point on.

An unexpected outcome from this data is the finding that the longitudinal beam elongated as much as the support beams beyond 1.5% drift. With tension ties linking the support beams and the bowstring effect intact in this direction, it could be expected that elongation would be lower in the longitudinal beams from restraint through the floor. The reason this was not the case is evident if the torsional response of each beam is examined. This is displayed in Figure 20.

Figure 20 (a) and (b) show that beyond the loss of the east-west bowstring effect the support beams rotated into the span, meaning the distance between the starter bar connections of the north and south support beams was reduced. This meant the bowstring effect restricting longitudinal beam elongation was greatly reduced, because the bowstring ties were anchored in weak, flexible beams. The direct correlation between the longitudinal beam elongation and support beam rotation is clearer in Figure 21. Once the east-west bowstring effect is lost and the support beams lose torsional stiffness, each elongation of the longitudinal beam A1A2 is directly followed by inward rotation of the support beams to accommodate the growth in the orthogonal direction. This displays that once the bowstring effect is lost in one direction, the run-on effects of beam elongation and torsion of the affected beams leads to loss of effective bowstring action effects in the orthogonal direction. It also displays that while the bowstring effect restrains and stiffens the diaphragm system at low levels of damage, it is a direct driver of diaphragm plan shear stiffness degradation at higher damage levels by enforcing large torsional demands on the beams, leading to beam loss of torsional stiffness and therefore reduction of beam weak-axis shear stiffness in the plastic hinges.

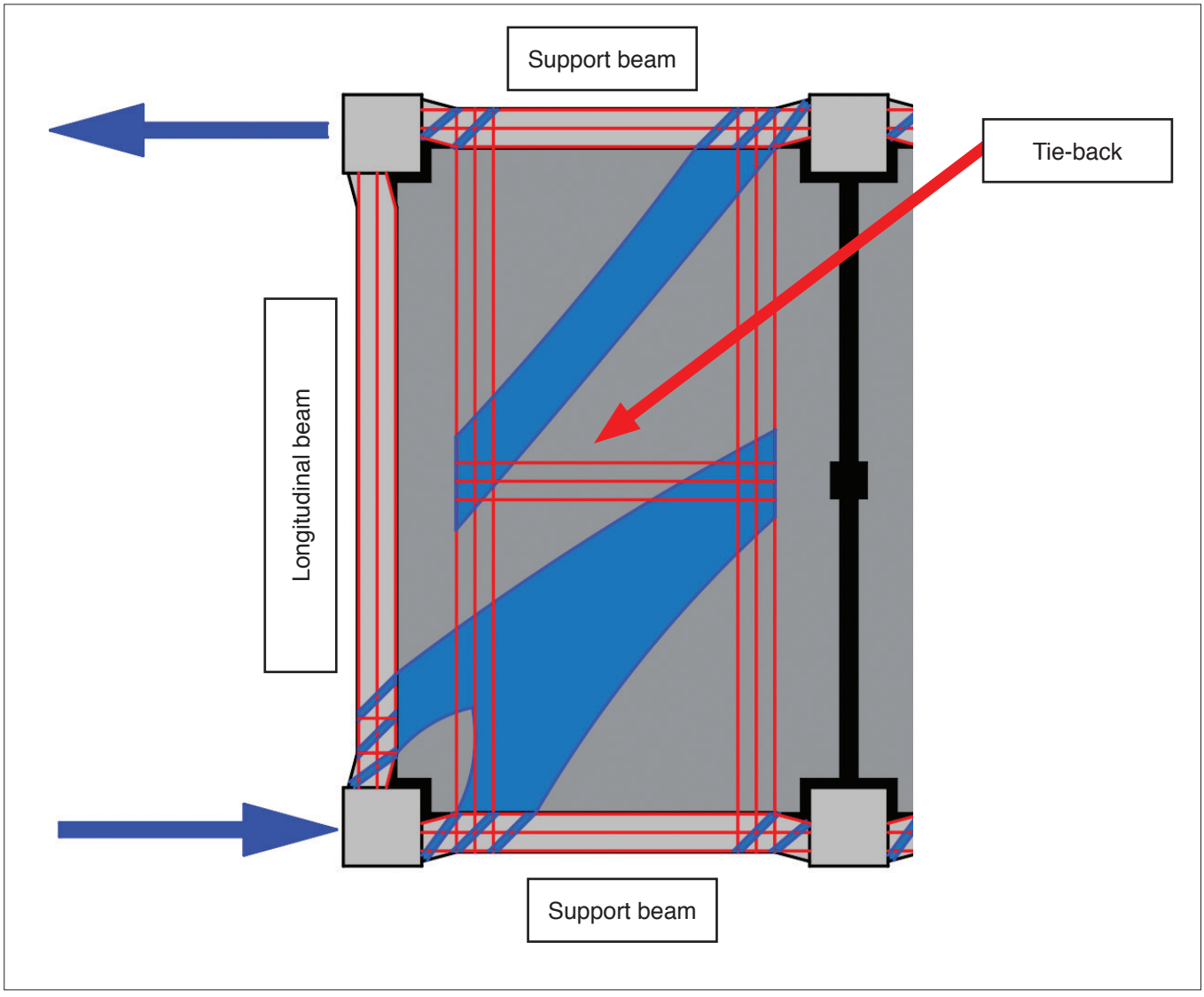

Figure 18: Diagonal struts with tie-backs to form low energy truss strut-and-tie load paths within the floor-plate

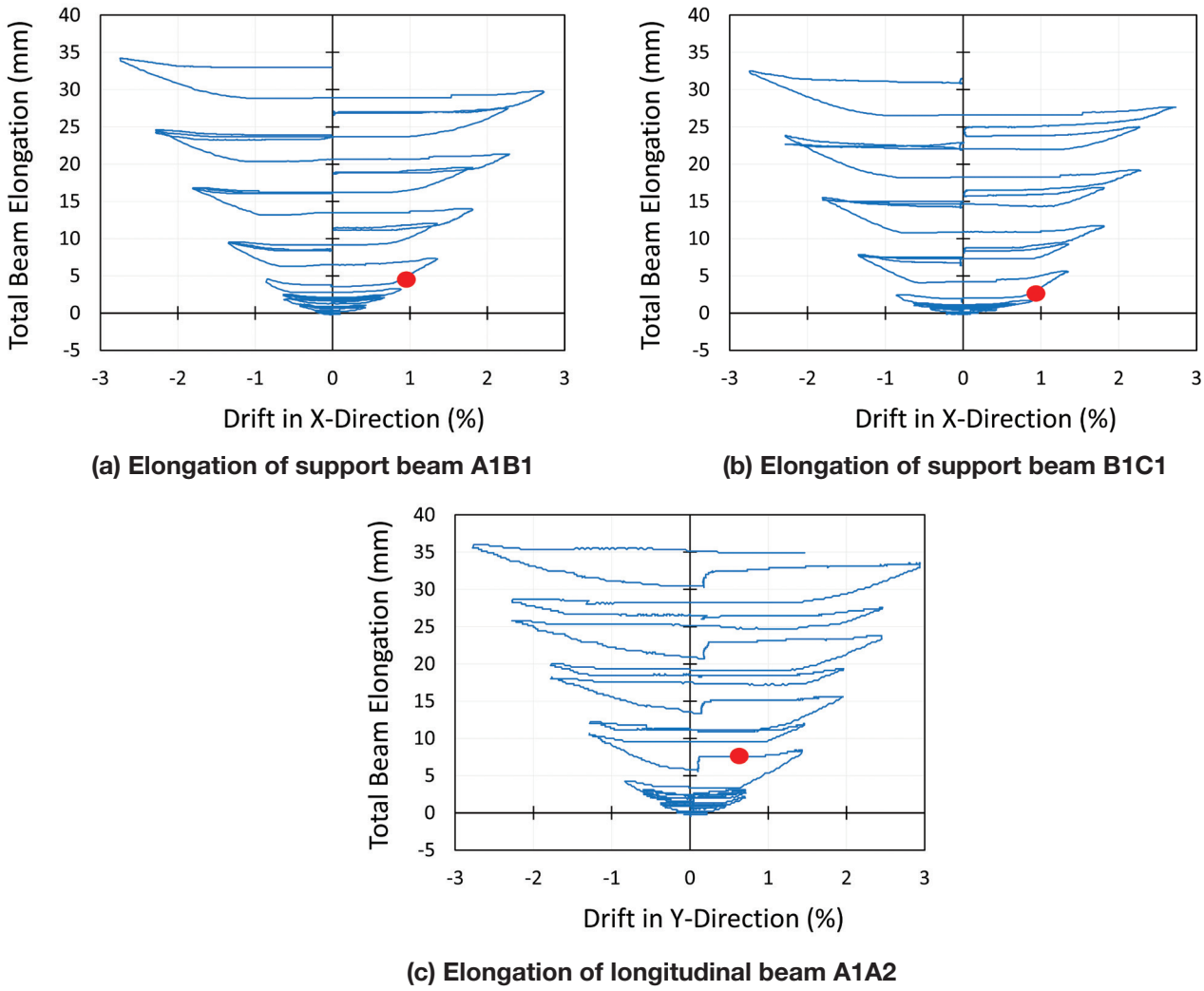

Figure 19: TEST 1 Elongation of support and longitudinal beams relative to their critical loading direction (red dots indicate where the bowstring effect was lost for support beams)

Inward rotation in Figure 21 describes the top of the beams (where they are connected to the floor via starter bars) moving inwardly towards the floorplate. A visual representation of this and the starter bar demands that cause it is portrayed in Figure 16 (e).

The torsional rotation of beam A1B1 and B1C1 is nearly identical. As discussed in Part I (Parr et al. 2022), the first (eastern) bay had only starter bars crossing the beam-floor interface whereas the second (western) bay had both mesh and starter bars crossing the interface, increasing the interface capacity and therefore the total torsional demands that could be imparted into the beam via the bowstring effect. The lack of any noticeable difference between the behaviour of the two beams suggests that the starter bar-only configuration was already overpowering the torsional capacity of the support beam and further reinforcement across the beam-floor interface had no effect on the diaphragm capacity. This suggests the standard starter bar detailing provided over-reinforcement and the amount of beam-floor continuity reinforcement could have been reduced with no negative repercussions for the diaphragm performance.

The diaphragm load-path displayed in Figure 17 assumes there is no ability to transfer compressive load struts directly into columns. This is a valid representation of the available load-paths observed at earlier stages of the test after gaps had opened around the columns, as there were clear air gaps preventing any load-path from forming

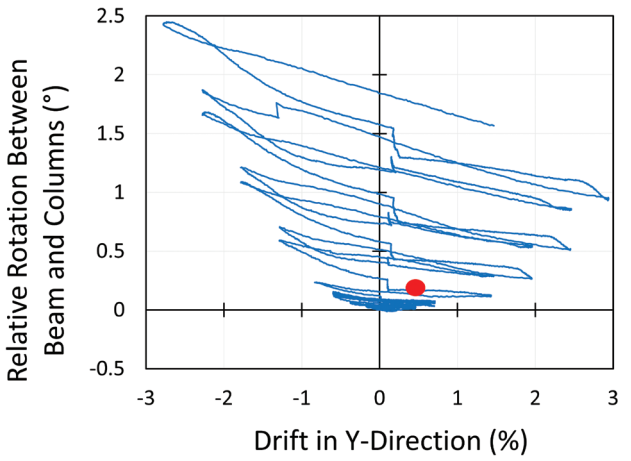

(a) Torsional rotation of support beam A1B1 relative to columns A1 and B1

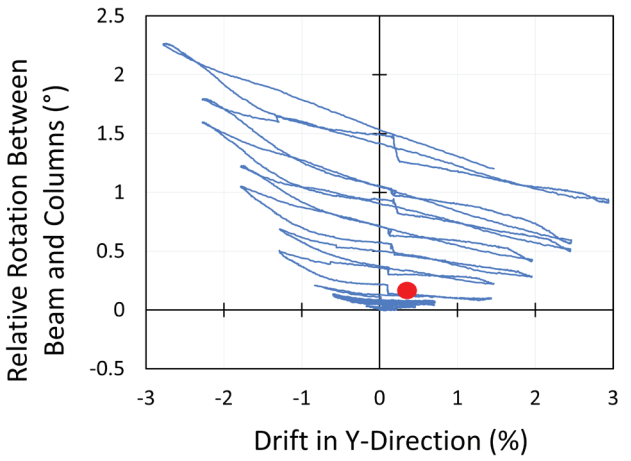

(b) Torsional rotation of support beam B1C1 relative to columns B1 and C1

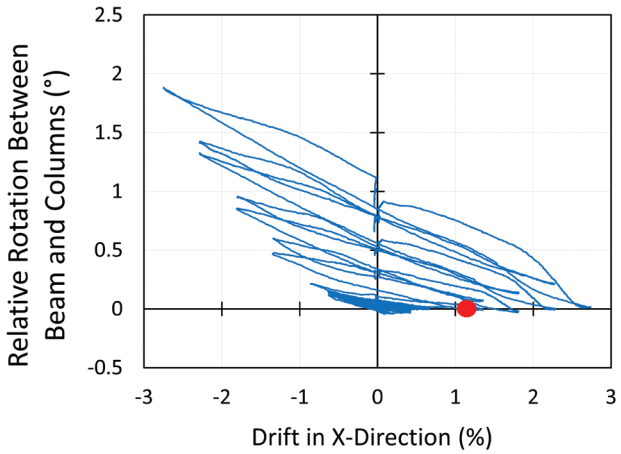

(c) Torsional rotation of longitudinal beam A1A2 relative to columns A1 and A2

Figure 20: TEST 1 Torsional rotation of support and longitudinal beams relative to their supporting columns (red dots indicate where the bowstring effect was lost for support beams)

for all columns. This applied to the intermediate columns as only the tie bars linked the two sides of the gap, which would provide a minimal strength compression/shear load-path when compared to the scale of the overall diaphragm forces.

However, in the final rhomboid loading of TEST 2 there was clear evidence of compression struts forming directly between the floor system and the intermediate (B1 and B2) columns as shown in Part I (Parr et al. 2022). The TEST 1 residual load-path with the addition of this tie-bar rubble contact stress compression load-path is displayed in Figure 22.

As the specimen was pushed to greater drifts and the diaphragm subjected to greater deformation in both tests, chunks of the floor topping slab around each tie-bar connection were popped off in a flat cone pull-out style failure mechanism as displayed in Part I (Parr et al. 2022). Pieces of the rubble formed in this way appeared to drop into the gap between the floor units and the column, instating a residual contact stress load-path (from approximately 2%-2.5% drift onwards) for compression struts, similar to the ones that had formed along the beams in TEST 2. Without the tie-bars and the rubble formation they caused, no load-path could form from

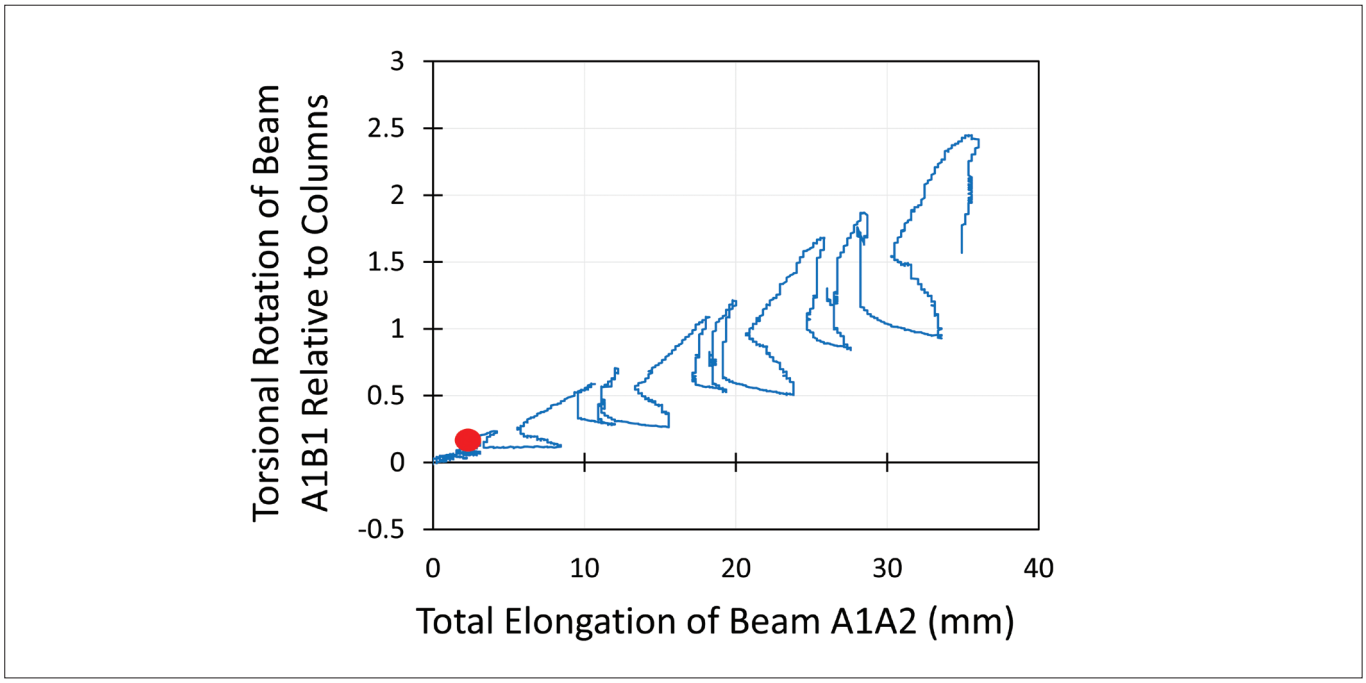

Figure 21: TEST 1 Inward rotation of support beam A1B1 driven by elongation of the orthogonal longitudinal beam A1A2

the floor directly into the interior columns. This displays a secondary positive effect caused by installation of tie-bars additional to the original intended purpose of restraining columns from pushing out of the building.

Important notes related to the tie-bar rubble residual contact stress compression strut load-path are:

- It could only form on the column face the tie-bars were anchored into.
- It required reverse cyclic behaviour to form rubble from compatibility demands between the tie-bars and floor topping.
- There may be a zone at moderate drift/damage levels where there is no load-path between the floor and column interface after the column-to-floor gap has opened but before sufficient rubble has been generated to instate the residual load-path.
- It was a stiffer load-path than struts landing in the beams, meaning higher potential for local concrete crushing damage to beta units which are already vulnerable elements of the floor system.
- It incorporated the tie-bars into the diaphragm system as tension ties.
- It incorporated the longitudinal beams into the diaphragm as anchor points for tension ties.

2.3.2 Test 2

TEST 1 displayed two critical results informing the design of TEST 2.

The first was that a high ratio of simultaneous bi-directional demands led to beams being the weak element of the system due to loss of torsional stiffness. Based on this finding, the loading protocol of TEST 2 was changed to an initial uni-directional push (based on the Northridge earthquake of 1994) followed by a lower-bound standard loading protocol simultaneous bi-directionality ratio of 1:2. This change was selected in an attempt to observe different damage modes in the hollow-core units and diaphragm by enforcing less critical demands for the beam torsional response and therefore more critical demands for the floor elements.

The second was the split in the weak zone between beta units leading to separation of the two bays of the floorplate. The removal of any diaphragm load-path linking the two bays and the destruction of the bowstring effect in the east-west direction at 1.5% drift was a defining point for the performance of the diaphragm from this point on for TEST 1. In TEST 2, “stitching bars” were post-installed in the topping between the beta units to replace the topping mesh reinforcement across the interface that was cut due to post-installation of tie-bars between column B1 and B2. This also provided the opportunity to compare the performance of the

diaphragm if the two bays remained linked and the east-west bowstring effect remained intact.

As discussed in Part I (Parr et al. 2022), much greater damage through the development of wide cracks was observed in the floor elements in TEST 2 compared to TEST 1, particularly at the seating ends of the hollow-core units. This damage mode initiated within the uni-directional push at the start of the test and further damage concentrated at the critical cracks. Mesh rupture across the north and south critical cracks occurred at approximately 1.6% drift (in the y direction). This signalled that the simultaneous bi-directionality ratio was critical in determining the damage mode of the floor, particularly at the start of loading. In floor systems that only use non-ductile mesh for topping reinforcement within the floorplate, damage will concentrate where it first occurs as the mesh will rupture at relatively low drift levels and further damage will concentrate at the weak zone this creates.

However it was also observed that compression struts could form across wide cracks via contact stresses with pieces of rubble that fell into the cracks. The residual load-path created by the damage modes observed in TEST 2 are displayed in Figure 23. The critical wide cracks near the ends of the units are displayed in green.

Note that while compression struts could cross the wide cracks at the ends of the hollow-core units, the cracks eliminated tension ties that crossed them in the north-south direction due to mesh rupture. This meant the bow-string effect in the north-south direction was eliminated

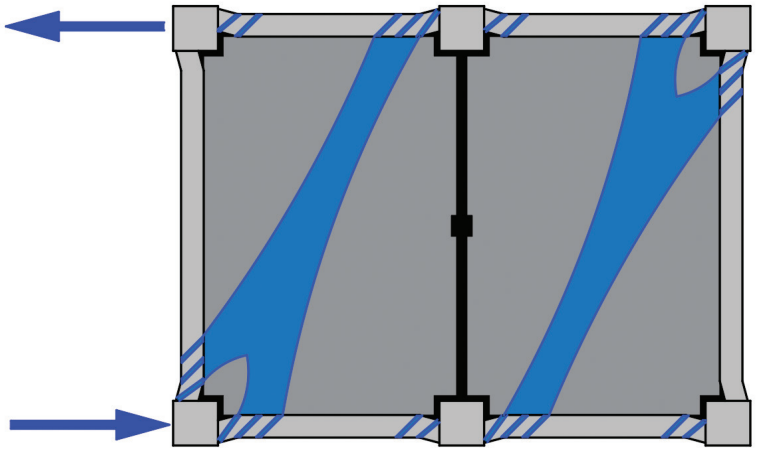

(a) Load-path with only compression struts displayed

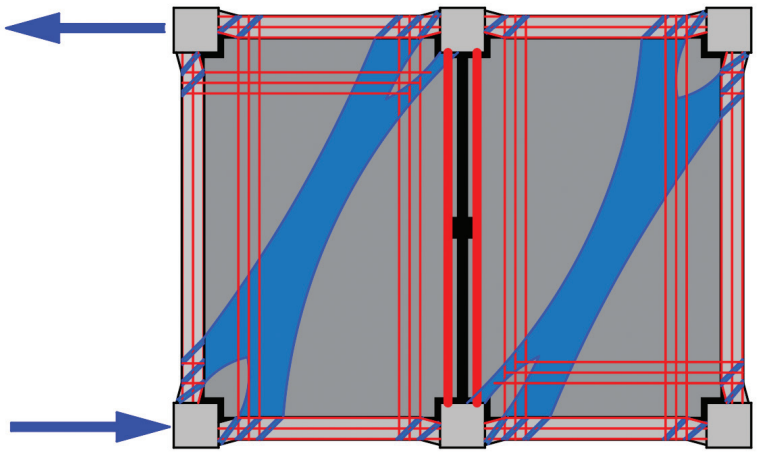

(b) Load-path with struts and tension ties displayed

Figure 22: TEST 1 Residual diagonal compression strut load-path under positive shear distortion loading after formation of tie-bar rubble contact stress compression struts

before the end of the uni directional pushes and before the standard loading protocol with a simultaneous bi-directionality ratio of 1:2 had begun.

The stitching bars were highly effective at strengthening the weak interface between the two beta units, and no significant cracking developed between the units even when drift demands of 4.0% in the N-S direction and 2.0% in the E-W direction were applied. This meant the bow-string effect in the east-west direction remained intact up to this point as shown with the ties linking the longitudinal beams in Figure 23. Without the strengthening across the weak beta-beta unit interface, this tension tie load-path would likely have been eliminated by 1.5% drift in the X-direction, greatly reducing the diaphragm plan shear strength (and therefore stiffness as a run-on effect), similar to TEST 1. Additionally, diagonal compression struts could form across both bays of the specimen with the two bays acting as a single diaphragm instead of two individual split diaphragms.

Following the 4% N-S, 2% E-W drift cycle, the 4th rhomboid of TEST 2 was conducted. At this stage in testing the cracks at the northern ends of the floor units were extremely wide, with approximately 30 - 40 mm crack widths (along the A2B2 and B2C2 beam-to-floor interface). At this crack width, even with replenishment of the compressive load-path through rubble formation, the gap was clearly wide enough to prevent effective compressive struts from forming. This led to loss of load-path across the crack as depicted in Figure 11 (b). The crack width at the southern end of the floor units at the end of the starter bars was approximately 20 mm wide

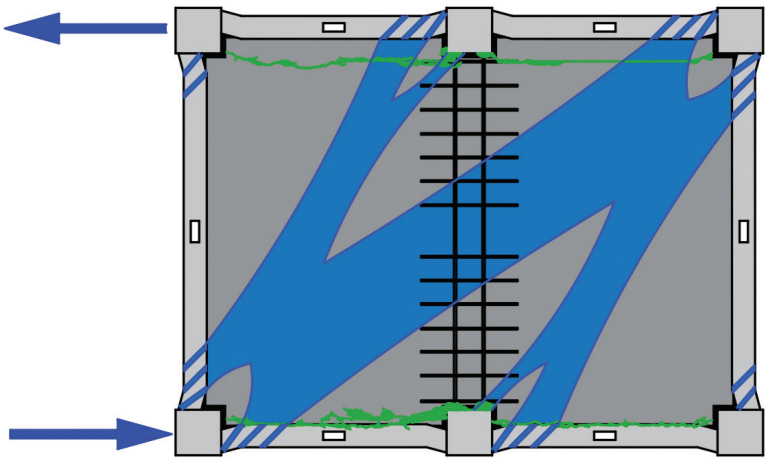

(a) Load-path with only compression struts displayed

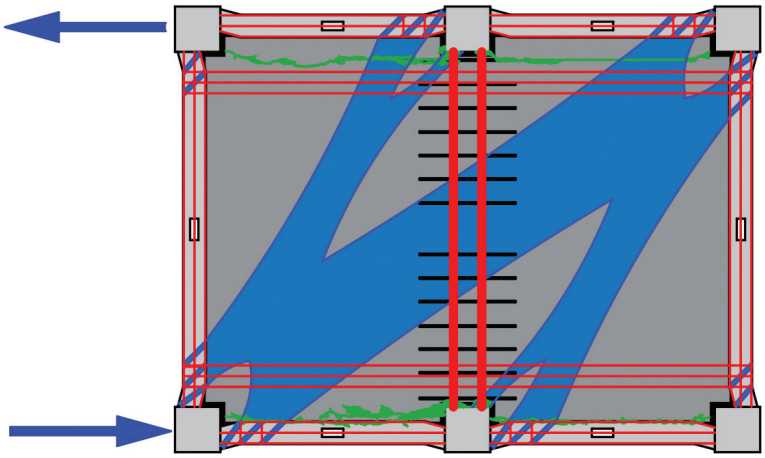

(b) Load-path with struts and tension ties displayed

Figure 23: TEST 2 Residual diagonal compression strut load-path under positive shear distortion loading

with approximately 20 mm vertical offset. Note that the critical crack along the southern end of the floor units traced a sinusoidal curve as shown in Figure 10 (a) that created clear compressive binding when shear distortion demands were applied.

The specimen diaphragm load-path at the initiation of the rhomboid #4 loading protocol is displayed in Figure 25 (a). At the northern end of the units the compressive struts could not land in the support beam A2B2 and B2C2 due to the very wide crack at the beam-to-unit interface. This meant the horizontal component of the strut force instead had to be tied back into the northern plastic hinge of beam C1C2 as shown in Figure 25 (a). The tie force in tie 2 of Figure 25 (a) was greatly increased compared to the regular force sustained in tie 1, as it collected force from the struts that could not land in the support beams moving west. The critical weak unit-to-unit interface, where most forces from the compression struts had accumulated within tie 2, was between unit 5 and unit 6, directly on the west side of the beta-beta unit stitching bar retrofit. At approximately 0.25% positive shear distortion of the floorplate, the tie force in tie 2 exceeded the mesh capacity, leading to mesh rupture at the north end of the unit 5 to unit 6 interface which then unzipped approximately 2/3rds of the mesh along the interface running southward. This led to the cracking displayed in Figure 25 (b) with the width of the north end of the crack being approximately 7 mm and the width of the south end of the crack being approximately 3 mm. Therefore, the loss of compression strut load-paths from the floor units into the northern beams explains why there was significantly more damage at the north end of the unit 5

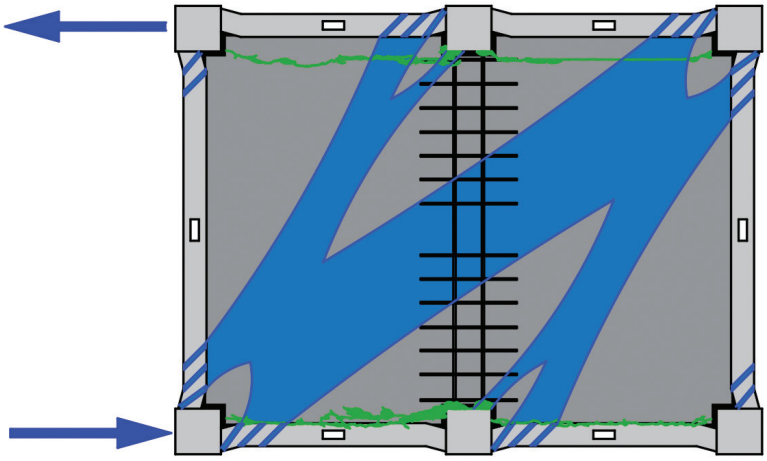

(a) Load-path with only compression struts displayed

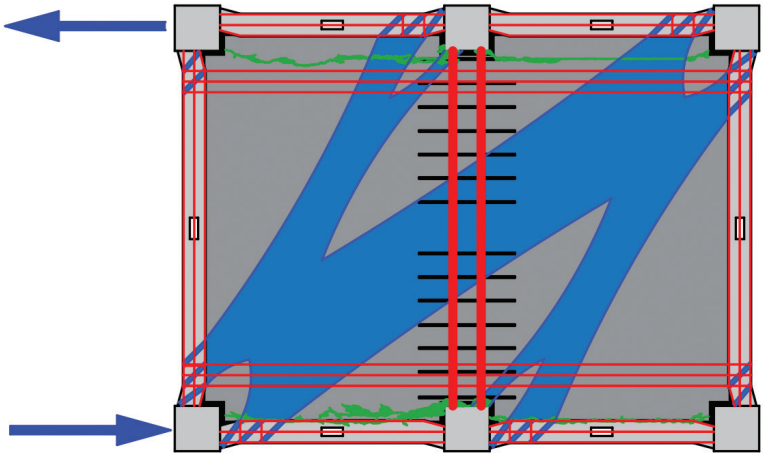

(b) Load-path with struts and tension ties displayed

Figure 24: TEST 2 Residual diagonal compression strut load-path under positive shear distortion loading

to unit 6 split in a system that was otherwise symmetrical. The crack caused an instant loss of plan shear stiffness and capacity under positive shear distortion as displayed in Figure 9 (b), with a drop in plan shear capacity of 100 kN (down to 580 kN from 680 kN) and an increase in shear distortion of 0.03% (up to 0.28% from 0.25%).

Interestingly, the loss of plan shear stiffness under positive shear distortion demands (following the unit 5 to unit 6 split occurring) was not observed when the floorplate was subjected to negative shear distortion demands. The reason for this becomes apparent when observing the different load-paths available between positive and negative plan shear distortion as shown in Figure 25 (b) and (c).

Under positive shear distortion, the split mesh between unit 5 and unit 6 meant a strut could not form from the floor to the intermediate column B2 near the tie bar anchor rubble. This meant tie forces needed to develop to link the strut and tie system back to where there was ability to cross the unit 5 to unit 6 split at the south end where the crack was not as wide and mesh was still intact. The contribution to plan shear stiffness from the western bay was greatly weakened by this.

Under negative shear distortion, while the inter-bay strut visible in Figure 25 (a) was still destroyed, the primary strut of the western bay could still form directly to the intermediate column B1 and the support beam B1C1 across the thinner end of the unit 5 to unit 6 split as shown in Figure 25 (c). This meant the plan shear stiffness and capacity was generally unaffected by the split under negative shear distortion, as the eastern bay primary strut was also unaffected by the unit 5 to unit 6 split.

The unit 5 to unit 6 split also greatly reduced the east-west bowstring effect following the rhomboid #4 loading protocol, as approximately 2/3rds of the tension ties linking the longitudinal beams were eliminated.

With the destruction of the north-south bowstring effect near the start of TEST 2 the longitudinal beams A1A2 and C1C2 had no restraint against beam elongation. This led to significant beam elongation throughout the test, reaching a maximum of approximately 30 mm elongation per plastic hinge by the end of the test following 5% drift demands as shown in Figure 26 (a). A similar effect of weakened bowstring effect restraint observed in TEST 1 was also observed for the surviving east-west bowstring effect in TEST 2, with the support beams only displaying slightly less elongation with respect to drift compared to the longitudinal beams as shown in Figure 26. Note that the red and orange dots in Figure 26, Figure 27 and Figure 28 all relate to the same points where bowstring effect actions were eliminated in the north-south direction (red) and severely weakened in the east-west direction (orange).

The cause of the reduction in the east-west bowstring effect beam elongation restraint is again evident when observing the torsional rotation of the beams that the floor tension ties of the bowstring were anchored into. Longitudinal beam A1A2 rotated into the floor-span with permanent deformation as displayed in Figure 27 (a), relieving tension forces in the east-west bowstring tension ties. The direct correlation between total elongation of the support beams A1B1 and B1C1 and plastic inward torsional rotation of the longitudinal beam A1A2 from the engaged east-west bowstring effect is displayed in Figure 28.

Note that the torsional rotation of support beams A1B1 and B1C1 was greatly reduced in TEST 2 as shown in Figure 27 (b) and (c) due to the elimination of the north-south bowstring effect at the start of the test. This is one of the primary drivers for the improved plan shear stiffness observed in TEST 2 at moderate to design level drift demands. Diaphragm compression struts were able to cross the wide cracks at the ends of the hollow-core units to link the frames, but tension ties were not. This meant the bowstring effect was not able to exceed the torsional capacity of the beams through the starter bars and therefore weaken the diaphragm diagonal strut load-path by reducing the capacity of the critical link of the beams in shear about their weak axes. Improved roughening of the beam-column casting joint in TEST 2 also likely had a positive effect on the torsional capacity of the beams compared to TEST 1, particularly at low drift and damage levels.

The unit 5 to unit 6 split and the weakening of the east-west bowstring effect it caused had a clear impact on the torsional rotation of longitudinal beam A1A2. Following the significant damage to the east-west bowstring effect, the rate of torsional rotation in A1A2 significantly decreased. This provides further evidence that the bowstring effect is the primary driver of beam plastic hinge torsional damage when applied simultaneously with major axis bending demands and therefore it is the primary driver of diaphragm shear stiffness degradation at moderate to design level drift demands.

Again, note that inward rotation in Figure 28 describes the top of the beams (where they are connected to the floor via starter bars) moving inwardly towards the floorplate. A visual representation of this and the starter bar demands that cause it is portrayed in Figure 16 (e).

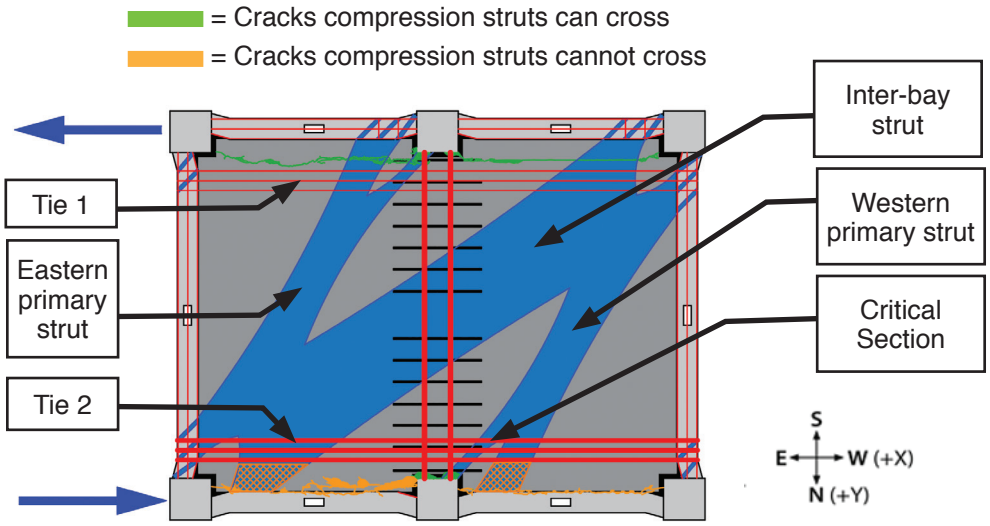

(a) Diagonal compression strut load-path at beginning of rhomboid #4

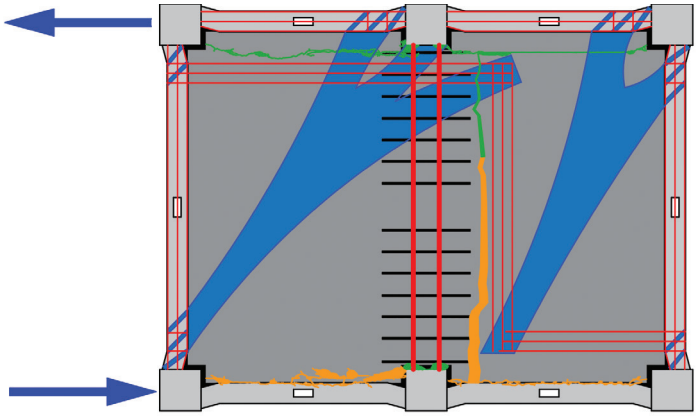

(b) Residual load-path after unit 5-unit 6 split under positive distortion demands

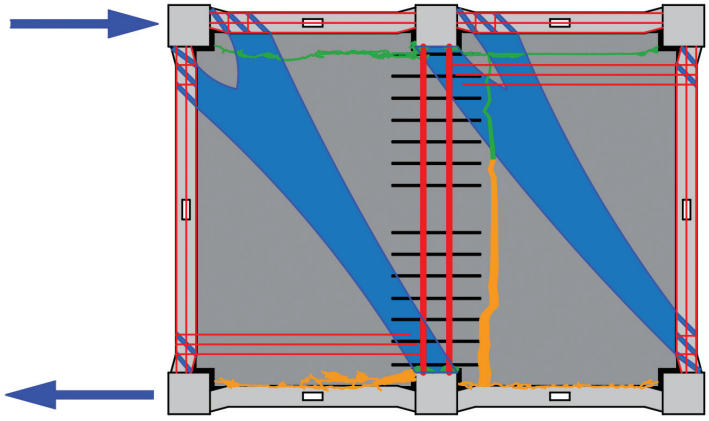

(c) Residual load-path after unit 5-unit 6 split under negative distortion demands

Figure 25: Tie force build-up leading to split between unit 5 and unit 6 during rhomboid #4 loading protocol

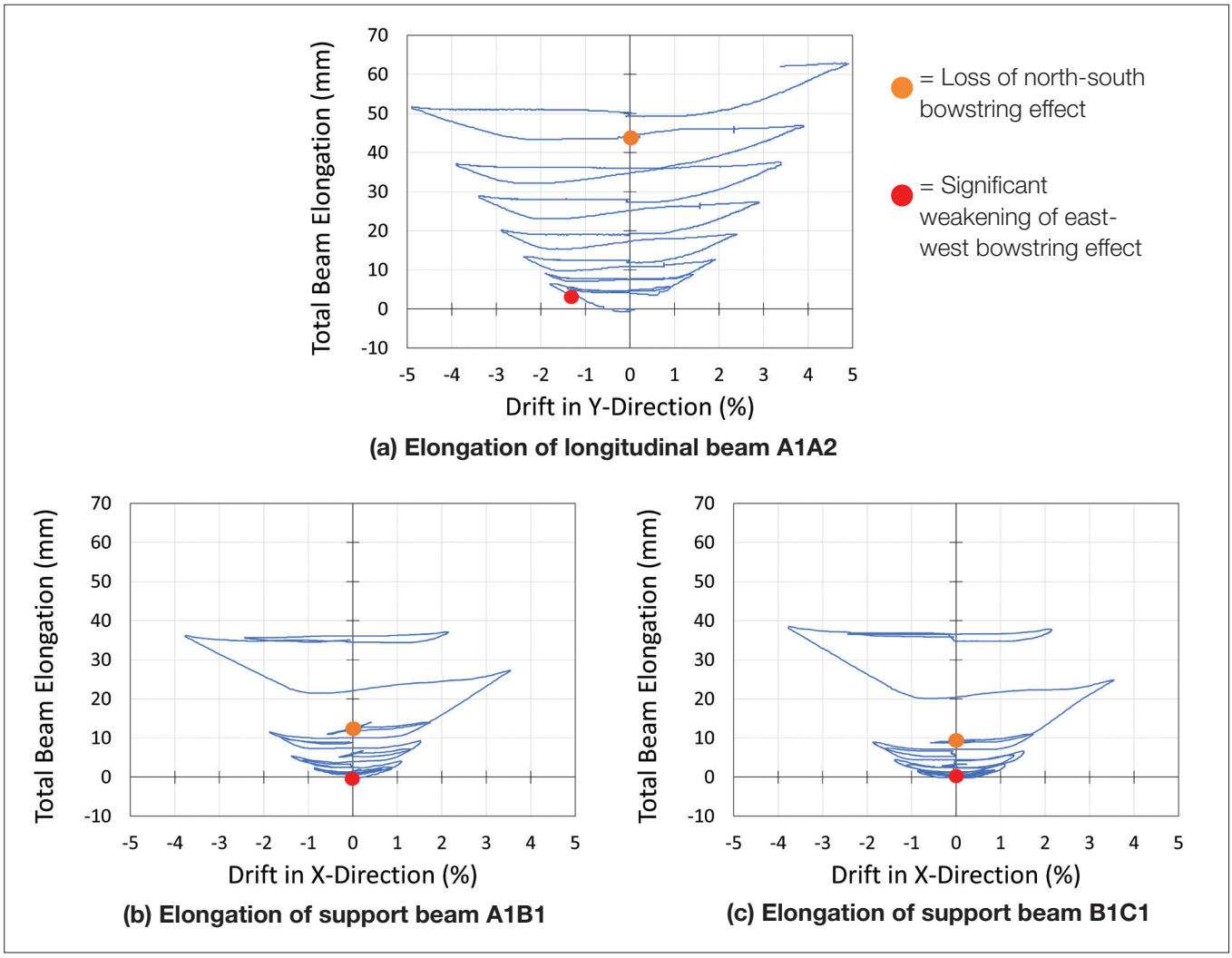

Figure 26: TEST 2 Elongation of support and longitudinal beams relative to their critical loading direction

3 CONCLUSIONS

The described analysis has led to the following conclusions and recommendations related to precast floor units and floor diaphragms:

3.1 QUALITATIVE DIAPHRAGM BEHAVIOUR CONCLUSIONS:

- Residual floor diaphragm load-paths will exist even at high damage states with very wide cracks if there is a viable gravity load path for the floor and there is adequate continuity reinforcement. However, there is high potential for the designed strut-and-tie load-paths to break down across beta-unit-to-beta-unit interfaces where precast flooring systems are used. Additionally, struts and ties can only reliably land in beams of the support frame and must be transferred into columns via the beam plastic hinge, rather than landing directly into columns. However, for column faces of intermediate columns where tie-bars were anchored, struts were observed landing into the column face only after large amounts of damage had occurred to the floor topping.
- Contact stresses form across wide concrete cracks in floors due to rubble replenishment (a process of aggregate rubble forming and falling into the gap as the crack interfaces become more damaged). These contact stresses provide a stiff connection resistant to plan shear deformation that can allow diaphragm compressive struts to land on beams. Rubble formation appears to primarily initiate near

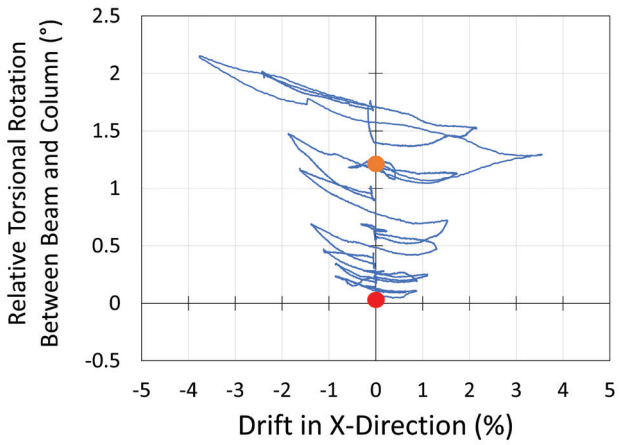

(a) Torsional rotation of longitudinal beam A1A2 relative to columns A1 and A2

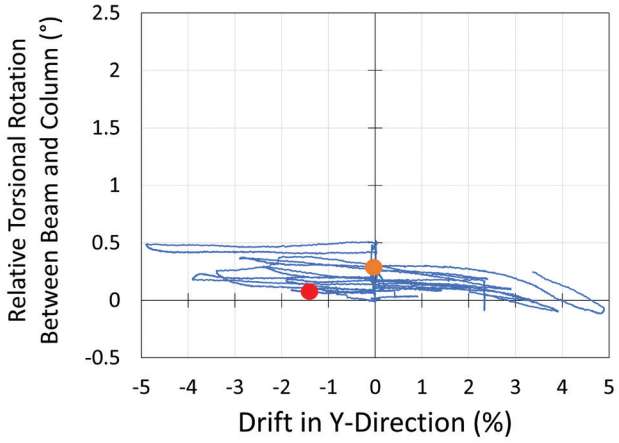

(a) Torsional rotation of support beam A1B1 relative to columns A1 and B1

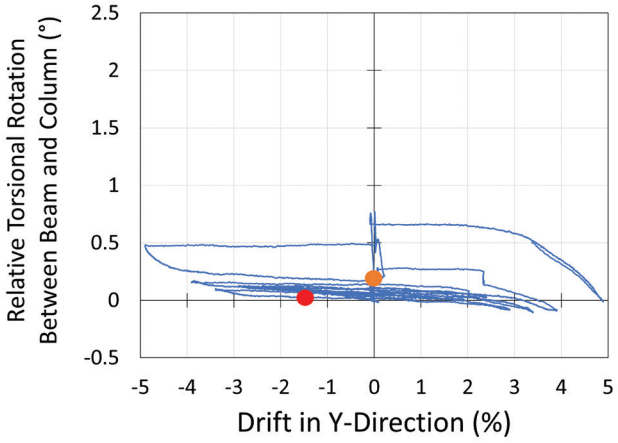

(b) Torsional rotation of support beam B1C1 relative to columns B1 and C1

Figure 27: TEST 2 Torsional rotation of support and longitudinal beams relative to their supporting columns

steel reinforcing, particularly deformed rebar. This is likely due to the bond with the bar causing substantial local cone-type cracking in the concrete when the more ductile bar deforms. Based on limited test data presented herein, starter bar spacing of 400 mm centre-to-centre crossing the crack interface appears to provide adequate rubble formation to transfer load across wide cracks. Smaller starter bar spacing should increase rubble formation, further ensuring a residual load path develops. It is proposed that the maximum reliable crack width a compression strut can form across is dependent on the aggregate size used in the topping concrete mix. This is because aggregate rubble is what wedges between the crack interfaces, and individual pieces of aggregate are unlikely to crush under compressive demands.

- The limiting factor determining floor diaphragm in-plane shear stiffness is the surrounding beam resistance to torsional deformation within their plastic hinges. Once the beams are torsionally overloaded due to a combination of elongation, simultaneous strong and weak axis bending and torsional moment, the frame beam elements become weaker and more flexible than the floor diaphragm elements. The primary driver of this damage mode (when simultaneously applied with other demands) is the bowstring effect.

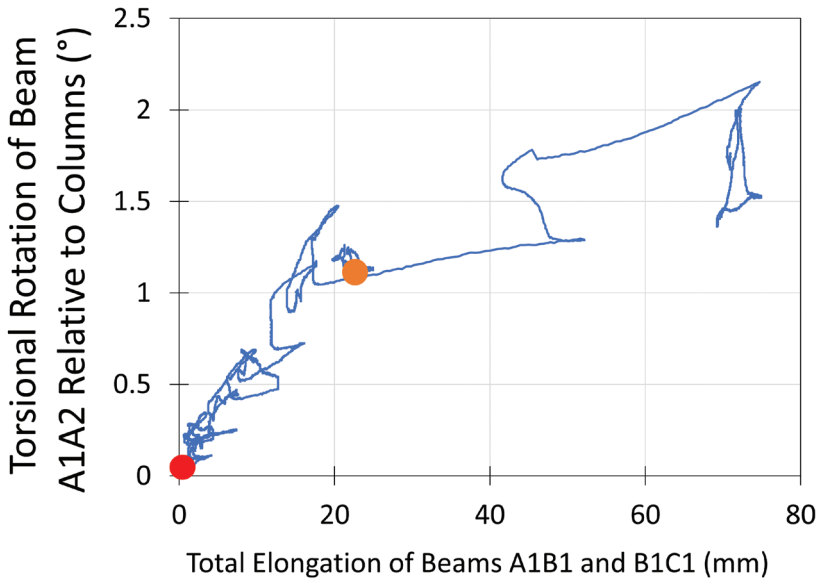

Figure 28: TEST 2 Inward rotation of longitudinal beam A1A2 driven by elongation of the orthogonal support beams A1B1 and B1C1

As tension ties in the floor resist beam elongation of beams in the orthogonal direction, these tie forces are applied to the critical beam through the starter bars which enforces significant torsional demands on the critical beam. This diaphragm degradation mechanism leads to a much lower diaphragm in-plane shear stiffness than the initial stiffness at moderate to design level drifts as displayed in Figure 12. This means the rigid diaphragm assumption may not be valid when modelling structural response under earthquake loading.

- Beam loss of torsional stiffness impacts the diaphragm stiffness because struts must pass through the beam in a weak-axis shear mode through the plastic hinge to reach columns. As the beam twists it may deform the interior bottom bars, cracking the surrounding concrete and reducing their confinement and bond with the rest of the beam. This decreases their contribution to dowel action with an unsupported length to resist shear determined by the stirrup spacing, which is a much weaker and less stiff contribution to the beam shear load path. Additionally, twisting of the beam across the primary crack near the beam-column interface likely grinds the two sides of the crack smoother over multiple cycles, reducing aggregate interlock and the friction necessary to maintain the compressive portion of the weak axis shear load-path.
- A positive of the beam torsional softening effect for hollow-core floor systems is that it may mitigate, to some extent, undesirable local failure modes such as negative moment and positive moment failure of individual floor units. This is because the deformation incompatibility demands are capped at this point as the support beam deforms plastically about its torsional twisting axis. The negative of this effect is the differential twisting of support and longitudinal beams which heavily damages the ends of alpha units (hollow-core end units positioned next to longitudinal beam) in the floorplate corners.
- Test data indicates that the diaphragm can lose as much as 75% of initial stiffness after drift demands exceed approximately 1% (in an earthquake with a directionality ratio of 1:1). In an earthquake with a directionality ratio of 1:2 (Test 2), stiffness can degrade 50% by 1.5% drift. As support frame beam elements lose torsional stiffness, load sharing between columns via floor diaphragm in-plane shear (or compression

struts) decreases. This leads to a more flexible structural response as the rigid diaphragm assumption becomes less accurate as damage progresses. The impact of this would differ depending on the structural layout and ground motion with respect to whether this amplifies or damps the structural response at moderate damage levels. Further experimental research, preferably using shake tables to provide inertial and damping response, would be required to quantify this effect.

- Directionality of earthquake loading plays a large role in determining the rate that in-plane stiffness contribution from a floor diaphragm degrades. The closer an earthquake record is to exhibiting equal displacement demands in all directions (i.e. circular bidirectional loading pattern), the earlier the diaphragm in-plane shear stiffness will degrade. This is because larger amounts of simultaneous action overpower the beam plastic hinge capacity earlier, by introducing larger weak axis bending and torsional demands while the longitudinal bar capacity is being used for strong axis bending. The converse is that the closer an earthquake is to being unidirectional (and in the direction of one of the primary frame axes of the building), the higher peak demands the supporting beams can withstand before losing torsional stiffness and therefore, the longer the floor diaphragm will remain stiff in-plane against shear deformation. This type of pulse demand would be expected in near-fault earthquakes. The downside of the stiffer diaphragm under these loading conditions is that higher deformation incompatibility demands are imparted into the floor units, making for a worse case for undesirable failure modes in hollow-core such as positive and negative moment failure modes as described in (Büker et al. 2022).
- Tie-bars are currently required between intermediate columns (with tie capacity to exceed 5% of maximum total axial compression force acting on the linked column or exceed 20% of the shear force from seismic actions in the column: Cl. 10.3.6 of NZS 3101:2006) to prevent them from bowing out of the structure which can lead to catastrophic floor failure. A secondary benefit of tie bars was observed during testing; that rubble is generated near the tie-bar anchor locations under earthquake loading due to bond stresses between the tie-bar and floor topping. However, this residual contact stress load path associated with the concrete around the column tie bars appears to require extensive diaphragm damage and is only likely to develop after the building has experienced high peak drifts.
- The interface between beta units is a critical weak point in diaphragm load-paths. This is because of deformation incompatibility between the units as the plastic hinges they are seated on undergo strong axis bending during earthquake loading, meaning the critical loading direction is orthogonal to the hollow-core unit layout. This causes one beta unit's elevation to rise and the other to fall along the beta-beta unit interface which leads to very early cracking and early rupture of the mesh along it. Additionally, this is the weak section of the bowstring effect action linking longitudinal beams, placing all mesh across the beta-beta unit interface in tension and providing further demands on the mesh across the beta-beta unit interface leading to early rupture. Being the weak section for the bowstring effect makes the beta-beta unit interface critical in determining the diaphragm performance of the floorplate. It is noted that once this connection between beta units is severed, the rate of beam elongation and degradation of beam torsional stiffness greatly accelerates in both primary frame directions.

3.2 RECOMMENDATIONS FOR PRACTITIONERS

- The findings from two super-assembly experiments provided a quantitative relationship between a structure's previously experienced drift demand (magnitude and directionality) to the degradation of diaphragm shear stiffness. In the future it would be beneficial for more experimental testing using rhomboid loading protocols to provide further data; however, as the frame and floor section sizes and steel detailing used in the two experiments were typical of mid-rise reinforced concrete buildings, the generalised Equations (7) and (8) are a useful preliminary tool to estimate diaphragm shear stiffness degradation.

  This relationship shows that diaphragm shear stiffness losses following typical ultimate limit state drift demands of 2.5% range from approximately 80% to 95% of the initial stiffness depending on earthquake directionality. Further explanation of the development of Equations (7) and (8) are shown in Section 2.1.
- In TEST 2 a retrofit referred to as "stitching bars" was used to strengthen the beta-beta unit interface. This retrofit greatly improved both the local hollow-core stability as well as maintaining the diaphragm load-path and bowstring effect across the two floor bays. It is therefore recommended that beta-unit-to-beta-unit stitching bars are added to tie-bar configurations. Even though failure of the units is delayed with the stitching bars, that failure is eventually shifted from the unit-to-unit interface to the end of the stitched

bars. To avoid failure through the unit as observed in TEST 2, it is recommended that the stitched bars be extended the full width of each beta unit. These should be deformed bars, and as an interim recommendation the strength and spacing of the stitching bars should be one sixth of the force of the tie bars (combined), at spacings equal to one third of the development length of the tie bars and these stitching bars are to be provided along the full length of the ties at this size and spacing. This ensures there is adequate strength to maintain the tension tie load-path across the beta-unit-to-beta-unit interface, removing it as a critical weak zone.

- The best way to ensure that diaphragm residual compressive strut forces can reach their landing points on beams is to provide adequate seating for the floor elements regardless of the floor system typology. In the case of hollow-core systems, seating recommendations are provided in (MBIE, et al2018) and recommendations for seating angle retrofits to improve seating lengths are provided in Büker et al. 2022. If there is a viable gravity load-path for the floor elements near the beam-floor interface, cracks that form in the floor will allow diaphragm compressive load-paths across the cracks through the rubble replenishment phenomenon observed in TEST 2 and described in Section 2.1.
- It is proposed that only column faces with tie-bar anchor points installed may be used as compression nodes in strut-and-tie analysis. This is due to the formation of rubble aggregate in the floor topping caused by deformation incompatibility demands with the tie-bars. This rubble aggregate can jam between the floor-to-column interface, bridging gaps that develop due to beam elongation.

4 REFERENCES

Angel, N., Correal, J., and Restrepo, J. (2019). "Cyclic Behaviour of Hollow-Core Diaphragm Subassemblies." PCI Journal, March-April 2019, 80-96.

Brooke, N. (2022). "Overview of Retrofit Requirements and Techniques for Precast Concrete Floors." SESOC Journal, 35(1).

Büker, F., Hogan, L., Brooke, N., Elwood, K., and Bull, D. (2022). "Design Recommendations for Seating Angles." SESOC Journal, 35(1).

Büker, F., Parr, M., De Francesco, G., Hogan, L., Bull, D., Elwood, K., Liu, A., and Sullivan, T. (2022). "Seismic Damage Observations of Precast Hollow-Core Floors From Two Full-Scale Super-Assembly Tests." SESOC Journal, 35(1).

MBIE, EQC, NZSEE, SESOC, and NZGS. 2018. Technical Proposal to Revise the Engineering Assessment Guidelines - Part C5 Concrete Buildings. Wellington, New Zealand: Ministry of Business, Innovation, and Employment.

Lindsay, R. (2004). "Experiments on the Seismic Performance of Hollow-Core Floor Systems in Precast Concrete Buildings." MEng, University of Canterbury, Christchurch, New Zealand.

MacPherson, C. (2005). "Seismic Performance and Forensic Analysis of a Precast Concrete Hollow-Core Floor Super-Assemblage." M.Eng, University of Canterbury, Christchurch, New Zealand.

Nievas, C., and Sullivan, T. (2017). "Accounting for Directionality as a Function of Structural Typology in Performance-Based Earthquake Engineering Design." Earthquake Engineering and Structural Dynamics, 46, 791-809.

Parr, M. (2022). "Retrofit Solutions for New Zealand Hollow-Core Floors and Investigation of True Floor Diaphragm Load Paths in Earthquakes." PhD, University of Canterbury, Christchurch, New Zealand - Currently in preparation.

Parr, M., Büker, F., De Francesco, G., Bull, D., Elwood, K., Hogan, L., Brooke, N., Liu, A., and Sullivan, T. (2022). "Load-Path and Stiffness Degradation of Floor Diaphragms in Reinforced Concrete Buildings Subjected to Lateral Loading – Part I, Experimental Observations." SESOC Journal, 35(1).

Paulay, T. (1996). "Seismic Design of Concrete Structures - The Present Needs of Societies." Eleventh World Conference on Earthquake EngineeringAcapulco, Mexico.

Vecchio, F., and Collins, M. (1986). "The Modified Compression-Fielf Theory for Reinforced Concrete Elements Subjected to Shear." ACI Journal, 83-22(March-April 1986), 219-231.

ISSN No. 2744-7871

STRATEGIES FOR FINITE ELEMENT MODELLING OF PRECAST PRE-STRESSED HOLLOW-CORE FLOORS

Sarkis, A.I.[1], Sullivan, T.J.[1],Brunesi, E.[2], Nascimbene, R.[2]

ABSTRACT

As part of the ReCast research programme, research has been undertaken to develop a finite element (FE) modelling approach for precast pre-stressed hollowcare (PPHC) floors. This paper summarises the modelling criteria that is considered key to analysing the behavior of PPHC floors. Comparisons of the numerical predictions with experimental results show that the proposed model is capable of capturing shear and torsional failure mechanisms. Lastly, advances towards a sub-assembly model, developed to investigate the bending behavior of PPHC slab-to-beam connections, are presented. The results indicate that the numerical approach is promising and should be developed further as part of future

1 INTRODUCTION

Extruded precast pre-stressed hollow-core (PPHC) units contain no transverse or vertical reinforcement and, given that their cross-sections contain large voids, are inherently vulnerable to brittle failure modes such as web cracking (Broo et al., 2005; Fenwick et al., 2010). Numerical and experimental research efforts have investigated the shear and torque behavior of PPHC slabs. Several previous studies have provided numerical predictions of the shear and bending behaviour of PPHC slabs at ultimate conditions based on finite element (FE) approaches, calibrated to experimental test results (Brunesi et al., 2015; Brunesi & Nascimbene, 2015; Michelini et al., 2020; Nguyen et al., 2019; Pachalla & Prakash, 2018). In addition, Pajari (2004b, 2004a) experimentally assessed the torsional behaviour of un-topped PPHC slabs under eccentric loading. The results from this experimental programme were then used by Broo et al. (2005, 2007) to numerically evaluate the shear-torsion interaction behavior in PPHC units.

While past research efforts have comprehensively studied the behaviour of PPHC slabs under gravity loads, research into the seismic performance of the slabs and the damage induced by imposed deformation demands is limited. There appears to be a need for assessment methodologies that provide estimates of the deformation capacity of the PPHC slabs. To this extent assessment methods based on numerical analysis could be useful, as it would be impractical to exhaustively investigate all aspects of precast floor behaviour in a laboratory given the expense and time required for physical testing and the difficulty of tightly controlling the properties of reinforced concrete test specimens.

As part of the ReCast research programme, research has been undertaken to test and develop finite element (FE) modelling techniques for PPHC floors. The work presented herein aims to summarise the findings and, in particular, the criteria that are considered critical for the FE modelling of PPHC floors. The presented modelling strategy could be used as part of a nonlinear analysis framework to reproduce and predict different cracking mechanisms for PPHC slabs. Results obtained for 200 mm deep slabs failing in shear and torsion are shown, and the influence of key modelling parameters is highlighted. Finally, advances towards a sub-assembly model, developed to investigate the bending behavior of PPHC slab-to-beam connections, are presented. Results from the FE models should help improve our understanding of the likely behavior of PPHC floors during earthquakes.

PAPER CLASS & TYPE: GENERAL REFEREED

1 Department of Civil and Natural Resources Engineering, University of Canterbury, New Zealand

2 Department of Construction and Infrastructure, Fondazione Eucentre, Italy

2 FINITE ELEMENT MODELLING OF PPHC UNITS

2.1 MODELLING STRATEGY

Different FE modelling and analysis trials have been undertaken using the software Midas FEA (MIDAS Information Technology, 2016), which allows both mechanical and geometrical non-linearity to be considered. 200mm deep cross-sections were considered with mean material properties typically used in New Zealand buildings. The FE modelling approach has been first developed by the authors to study PPHC slabs failing in shear (Sarkis et al., 2022b), calibrated against full-scale three-point bending tests (Sarkis et al., 2022), and then extended to study the effect of torque and twist (Sarkis et al., 2022a; Sarkis & Sullivan, 2021).

Table 1 summarises the key parameters used for the definition of the FE model. The constitutive model assumed for the concrete is the smeared total strain crack model (Selby & Vecchio, 1993; Vecchio & Collins, 1986). The Hordijk model (Hordijk, 1992; Reinhardt et al., 1986) and the Thorenfeldt (1987) model were adopted to define the uniaxial tensile and compressive behaviour of the concrete, respectively. The concrete has been modelled via three-dimensional solid/brick elements (see Figure 1), whereas the pre-stressing strands are represented as embedded line elements

Table 1: Key modelling parameters employed in the FE modelling studies of PPHC slabs.

	Parameter	Set value
Mesh (see Figure 1)	Element type:	6-node brick elements
	Cross-sectional size, x/z (mm):	15
	Extrusion size, y (mm):	30
Loading	Type of vertical loading:	Displacement
	Loading rate (mm/step):	0.02
Convergence criteria	Iteration scheme:	Newton-Raphson
	Energy norm:	5x10-3
Constitutive model concrete	Smeared crack model:	Rotating
	Tensile behaviour:	Hordijk (1992)
	Compressive behaviour:	Thorenfeldt (1987)

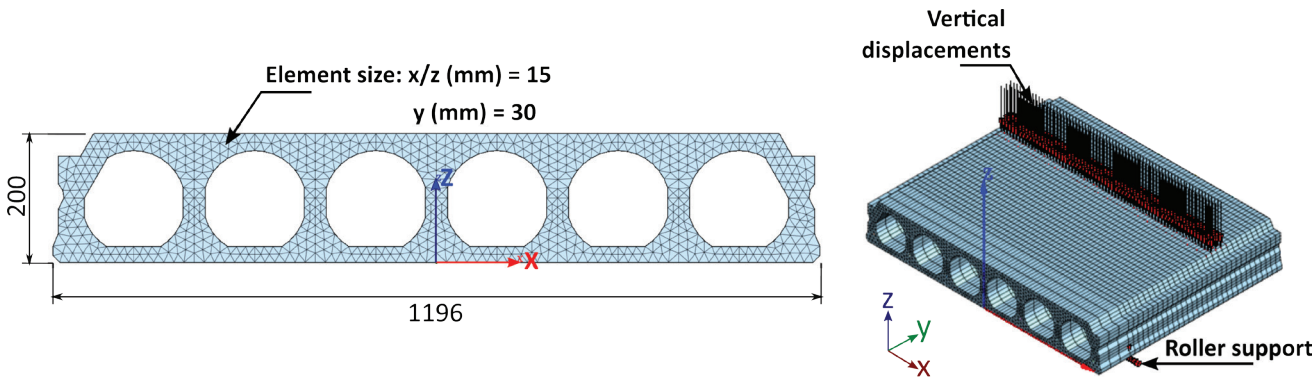

(a) Cross-sectional view of the FE mesh for a 200 mm deep PPHC unit

(b) three-dimensional sample of FE mesh

Figure 1: Mesh example of detailed solid FE model developed

2.2 MATERIAL PROPERTIES

Care must be taken to identify and specify suitable material properties for the analyses as the research found that common design values are not suitable. Table 2 summarises the material properties finally employed for the modelling of PPHC slabs. The mean compressive strength f_c, and the modulus of rupture f_r, of the hollow-core extruded concrete were obtained through material characterisation testing (Sarkis et al., 2022). Note that the values observed are significantly higher than design values and if design values were adopted (f_c = 45MPa and associated modulus of rupture) the shear capacity of the slabs would be significantly underestimated. The fracture energy G_f and the crack bandwidth h, required to define the tensile behaviour of the concrete, were deterministically estimated as shown in Equations 1 and 2 (Fib, 2013; Malvar & Fourney, 1990):

$$G_f = 73 f_c^{\,0.18} \quad (1)$$

$$h = 2.1 d_{agg} \quad (2)$$

where d_{agg} is the maximum aggregate size in mm

The stress in the pre-stressing strands can be represented as an equivalent parabolic pre-stress distribution, according to the work presented by Yang (1994), where the strand stress is postulated to be zero at the free ends of the slabs and to achieve the full effective stress at the end of the transfer length of the strands. Final pre-stressing after losses as well as the corresponding transfer length to be used in the finite element model can be calculated according to NZS3101:2006-A3 (SNZ, 2017).

3 RESULTS

3.1 FINITE ELEMENT MODEL RESULTS

The adopted modelling strategy (i.e. the FE models developed in line with the assumptions in Table 1 and the material characteristics listed in Table 2) was found to provide a consistent match with experimental test results for PPHC slabs failing in shear. The principal tensile stress distribution and predicted crack pattern at failure are in close agreement with the damage mechanism experimentally observed (Figure 2). An inclined crack emerges from both principal tensile strains and numerical crack patterns. Simultaneously an inclined compressive diagonal strut develops, resulting in diagonal cracking and the failure mode that finally occurs, which resulted in a cut-off in the shear stress flow.

The proposed FE modelling strategy was able to capture the elastic response of the PPHC slabs and torsional cracking, as well as the nonlinear behaviour of the slabs at higher displacement demands. Figure 3 provides a comparison of the principal tensile stresses on the PPHC unit at failure due to pure torsion. The numerical observations show that the cross-sectional deformations in PPHC slabs under torsion are three-dimensional and that the flow of shear stresses around the perimeter of the cross-section is non-uniform.

3.2 INFLUENCE OF KEY PARAMETERS

A detailed sensitivity study was conducted to determine the relative significance of each modelling parameter on the numerical predictions of the strength and deformation capacity. It is observed that the modulus of rupture and the crack bandwidth of the concrete and the cross-sectional size of the solid mesh element are the most important variables to be considered in reliability studies (Sarkis et al., 2022b).

Table 2: Summary of recommended material properties

	Parameter	Set value	Reference
Extruded concrete	Compressive strength, f_c (MPa)	60.5	Mean value from material testing (Sarkis et al., 2022)
	Modulus of rupture, f_r (MPa)	6.5	Mean value from material testing (Sarkis et al., 2022)
	Tensile fracture energy, G_f (N/mm)	0.16	(Fib, 2013)
	Crack bandwidth, h (mm)	25	(Malvar & Fourney, 1990)
Pre-stressing strands	Pre-stress losses	12%	Estimated according to NZS 3101:2006-A3 (SNZ, 2017)
	Transfer length strands (mm)	635	Estimated as 50db based on NZS 3101:2006-A3 (SNZ, 2017)
	Anchorage slip (mm)	2	(Brooks et al., 1988)
	Pre-stress distribution	Parabolic	(Yang, 1994)

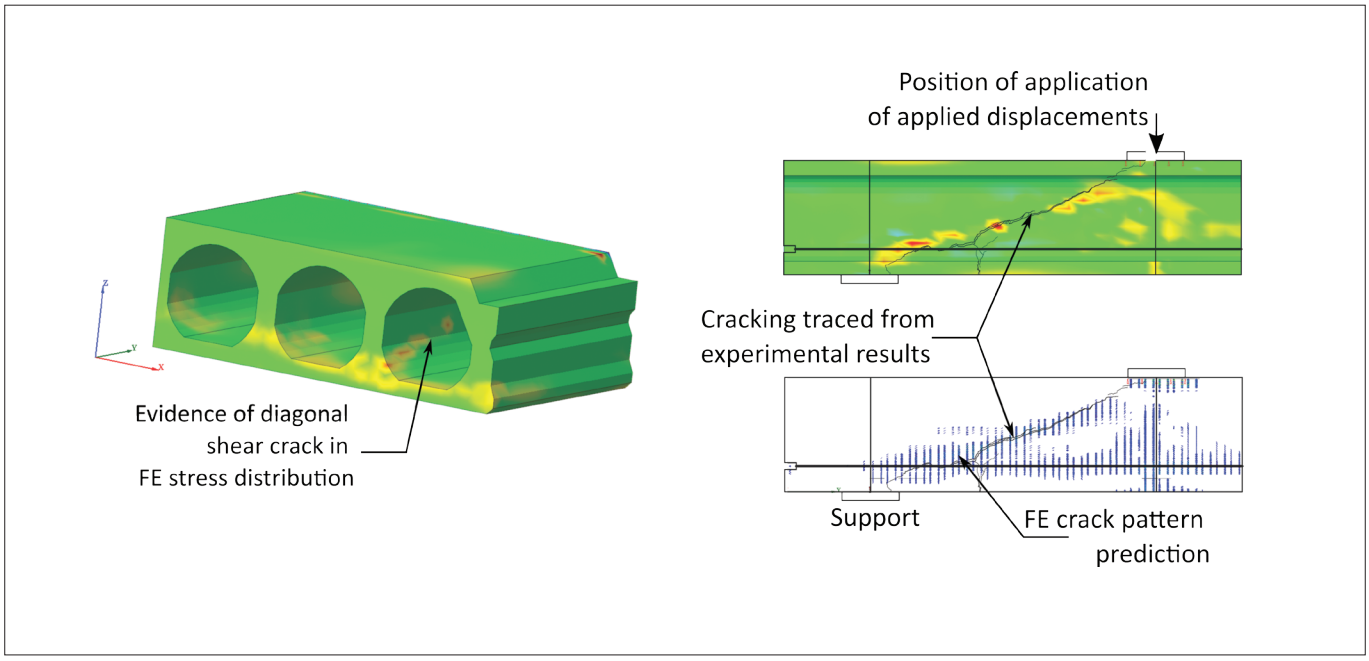

Figure 2: Principal tensile stress distribution and predicted crack pattern for a 200 mm deep PPHC unit failing in shear (the experimental testing is described in Sarkis et al. (2022)).

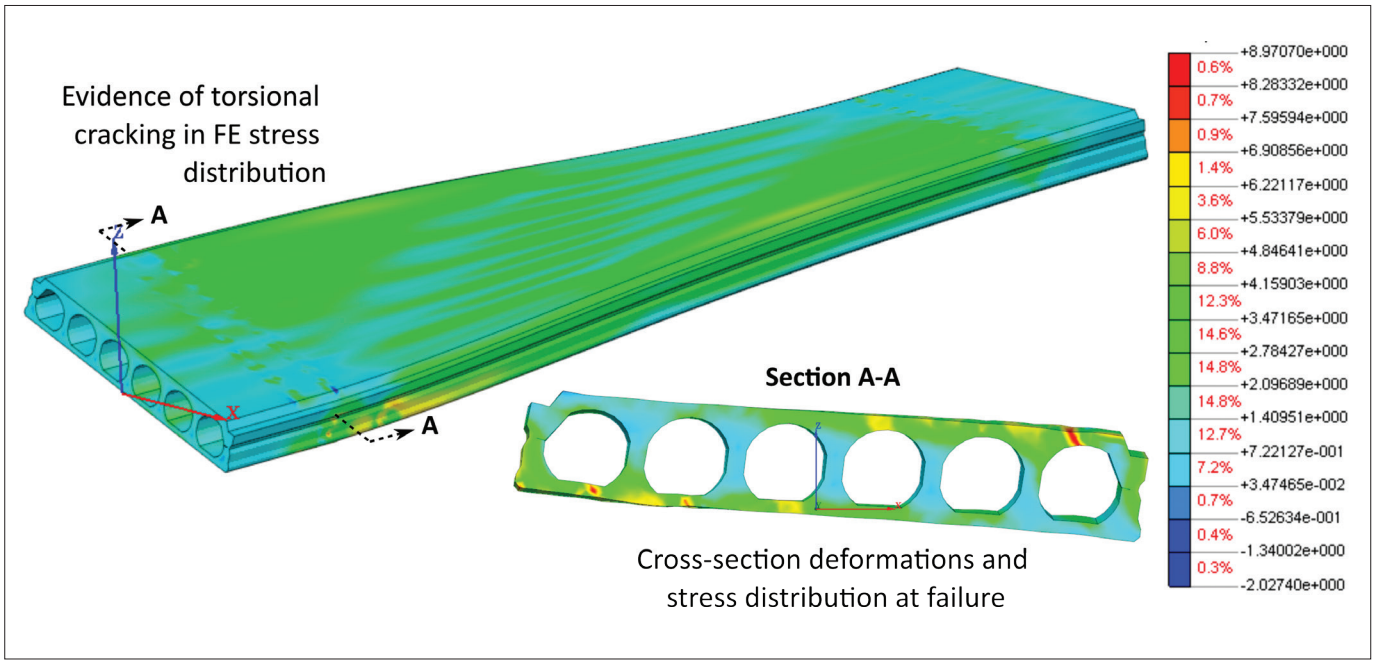

Figure 3: Principal tensile stress distribution for a 200 mm deep PPHC unit failing in pure torsion.

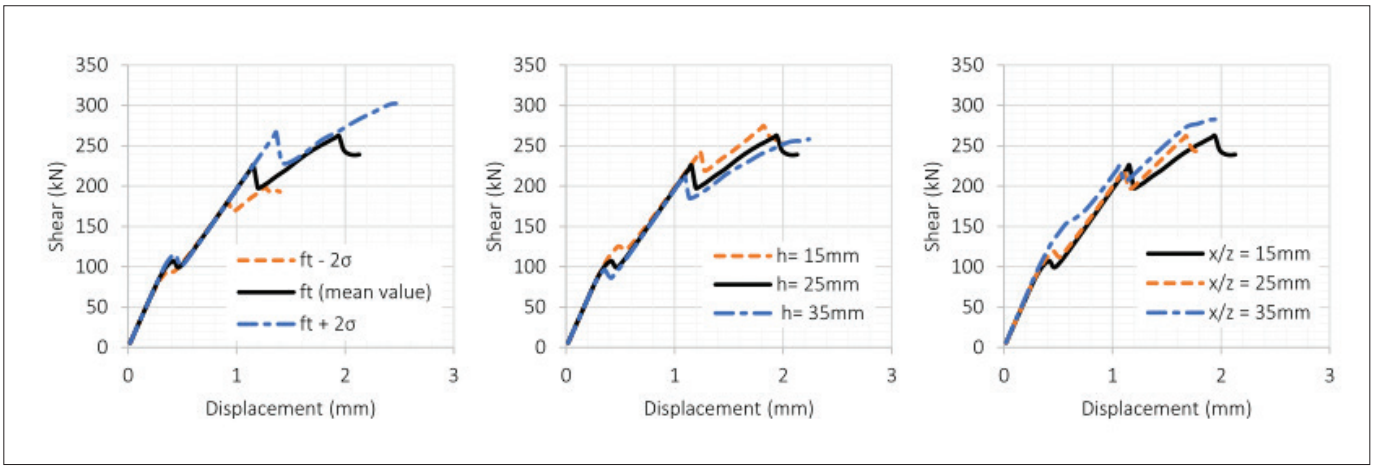

Figure 4: Impact of most significant modelling parameters on the force-displacement response: (left) modulus of rupture, (centre) crack bandwidth, and (right) mesh size.

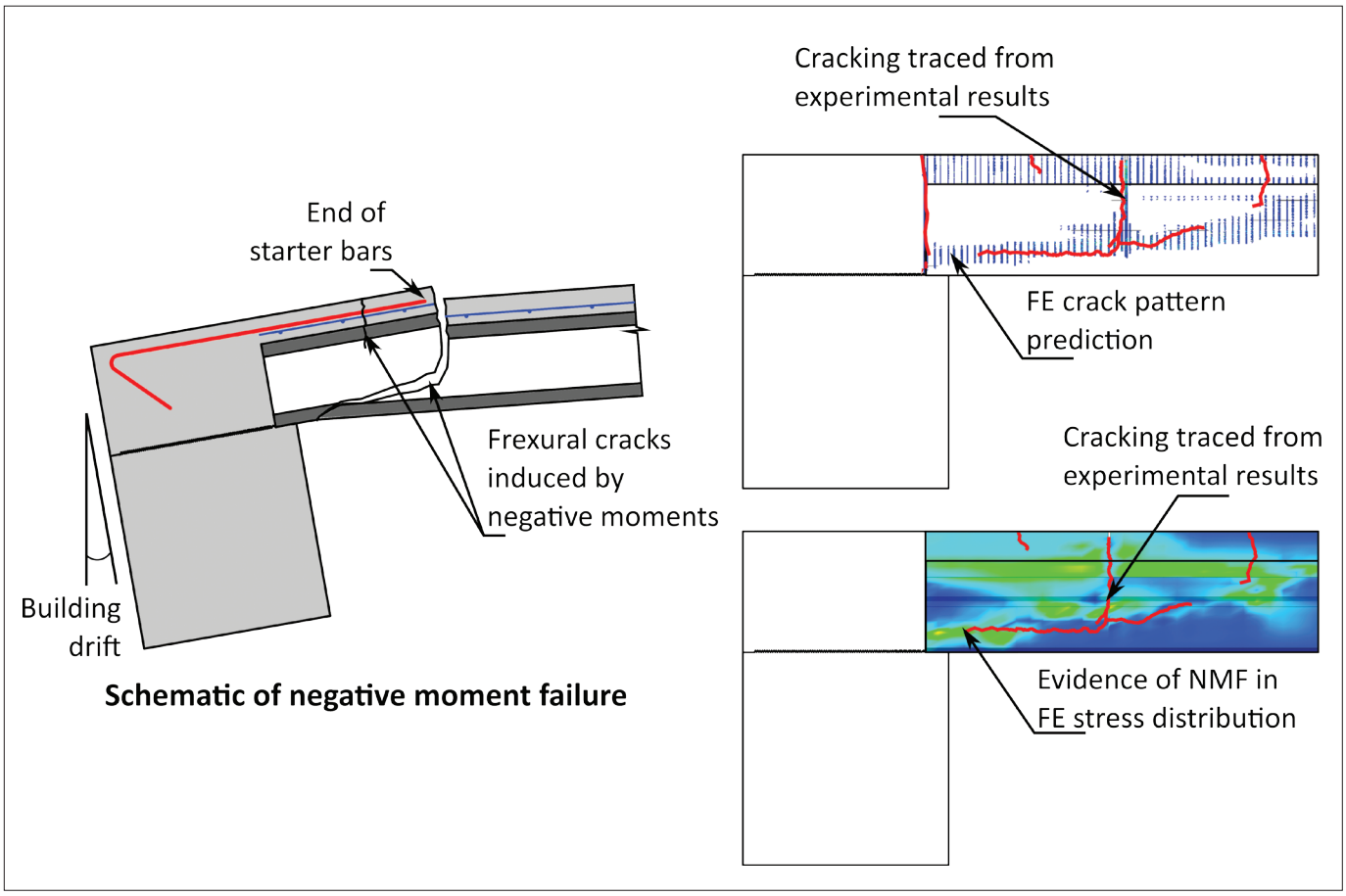

Figure 5: Preliminary results into the modelling of PPHC sub-assemblies

Figure 4 graphically shows the impact of varying the most significant modelling parameters on the force-displacement response of the PPHC slabs in shear. The three plots show the FE predictions for a 200 mm deep PPHC unit with a shear span of 300 mm. The solid black lines show the results from the model with the recommended parameters and material properties shown in Table 1 and Table 2 respectively.

The dashed blue and orange lines show alternative values for the modulus of rupture, crack bandwidth and mesh size tested during the sensitivity analysis. It can be observed that varying the modulus of rupture of the concrete resulted in greater variations in the shear strength and deformation capacity predictions.

3.3 TOWARDS A SUB-ASSEMBLY MODEL

Recent research efforts have also been looking to expand the proposed FE modelling strategy to consider the effect of bending moments on the seismic performance of PPHC floor-to-beam seating connections, or PPHC sub-assemblies. A model has been initially calibrated against existing test data to predict the failure of a PPHC slab under negative bending moments. Figure 5 shows the principal tensile stresses and predicted crack pattern against the cracking traced from the experimental testing conducted by Bueker, 2023.

When rotations were induced in the PPHC connection cracks appeared at the end of the starter bars, at the top of the slab, and then propagated vertically down the webs of the hollow-core unit before extending horizontally at the top of the bottom flange of the unit, forming a full negative moment failure (NMF) mechanism at less than 1% drift. The FE analysis results obtained allow the moment-drift response, principal tensile stresses and crack progression during loading to be compared. It is apparent from Figure 5 that good correlation was observed between the FE model predictions and the experimental crack patterns.

The FE modelling approach developed to date should permit future studies to exhaustively investigate all aspects of precast floor behaviour by varying the properties and geometry of PPHC seating connections. This work also illustrates the potential value of the FE modelling and analysis approach in gauging the impact of retrofit efforts for precast hollow-core flooring systems.

4 CONCLUSIONS AND RECOMMENDATIONS

A detailed nonlinear FE modelling strategy has been developed to represent the behavior of PPHC slabs under imposed deformations. The model has been calibrated against experimental data and then used to undertake parametric studies by varying the dimensions, properties, loading conditions and other aspects of the FE model. Results show that the model successfully predicts the PPHC floor brittle failure mechanisms.

This paper summarises the key modelling criteria employed for the FE modelling of PPHC floors. The following recommendations and conclusions can be drawn from the results presented:

- The reliability of FE modelling predictions can be greatly affected by the modelling assumptions made and the diverse user-defined input variables.
- Sensitivity analysis results reveal that the modulus of rupture and the crack bandwidth of the concrete and cross-sectional size of the solid element mesh, are the most important variables that need to be considered in reliability studies of PPHC slabs.
- The modulus of rupture of the concrete plays a dominant role in the strength and deformation capacity of the PPHC slabs, in particular for brittle fracture mechanics.
- It is recommended that characterisation of the extruded concrete properties be carefully identified (e.g. through experimental testing) and defined since actual values (obtained from experimental testing) can be significantly higher than nominal design values and capacity predictions of PPHC slabs are greatly affected by the properties adopted.

5 REFERENCES

Broo, H., Lundgren, K., & Engström, B. (2005). Shear and Torsion Interaction in Prestressed Hollow Core Units. Magazine of Concrete Research, 57(9).

Broo, H., Lundgren, K., & Engström, B. (2007). Shear and Torsion in Prestressed Hollow Core Units: Finite Element Analyses of Full-Scale Tests. Structural Concrete, 8(2), 87–100.

Brooks, M. D., Gerstle, K. H., & Logan, D. R. (1988). Effect of Initial Strand Slip on The Strength of Hollow-Core Slabs. PCI Journal, 33(1), 90–111.

Brunesi, E., Bolognini, D., & Nascimbene, R. (2015). Evaluation of The Shear Capacity of Precast-Prestressed Hollow Core Slabs: Numerical And Experimental Comparisons. Materials and Structures, 48(5), 1503–1521.

Brunesi, E., & Nascimbene, R. (2015). Numerical Web-Shear Strength Assessment of Precast Prestressed Hollow Core Slab Units. Engineering Structures, 102, 13–30.

Büker, F. (In Preparation). "Development and Experimental Validation of Hollow-core Floor Retrofits." PhD Thesis. University of Auckland, New Zealand.

Fib. (2013). Fib Model Code For Concrete Structures 2010. Ernst & Sohn, a Wiley brand. https://doi.org/10.1002/9783433604090

Fenwick, R., Bull, D., & Gardiner, D. (2010). Assessment of Hollow-Core Floors for Seismic Performance (Vols. 2010-02.;2). Department of Civil and Natural Resources Engineering, University of Canterbury.

Hordijk, D. A. (1992). Tensile and Tensile Fatigue Behaviour of Concrete; Experiments, Modelling and Analyses. In Heron (Vol. 37, Issue 1, pp. 1–79).

Malvar, L. J., & Fourney, M. E. (1990). A Three Dimensional Application of the Smeared Crack Approach. Engineering Fracture Mechanics, 35(1–3), 251–260. https://doi.org/10.1016/0013-7944(90)90203-S

Michelini, E., Bernardi, P., Cerioni, R., & Belletti, B. (2020). Experimental and Numerical Assessment of Flexural and Shear Behavior of Precast Prestressed Deep Hollow-Core Slabs. International Journal of Concrete Structures and Materials, 14(1). https://doi.org/10.1186/s40069-020-00407-y

MIDAS Information Technology. (2016). Midas FEA: Advanced Nonlinear and Detail Analysis System (v1.1). https://www.cspfea.net/prodotti/midas-fea-nx/

Nguyen, T. N. H., Tan, K. H., & Kanda, T. (2019). Investigations on Web-Shear Behaviour of Deep Precast, Prestressed Concrete Hollow Core Slabs. Engineering Structures, 183, 579–593. https://doi.org/10.1016/j.engstruct.2018.12.052

SNZ. 2017. NZS 3101:2006 - Concrete structures standard (Incorporating amendment No. 1, 2, and 3). Wellington, New Zealand.

Pachalla, S. K. S., & Prakash, S. S. (2018). Load Resistance and Failure Modes of Hollow-Core Slabs with Openings: A Finite Element Analysis. PCI Journal.

Pajari, M. (2004a). Pure Torsion Tests on Single Hollow Core Slabs.

Pajari, M. (2004b). Shear-Torsion Interaction Tests on Single Hollow Core Slabs.

Reinhardt, H. W., Cornelissen, H. A. W., & Hordijk, D. A. (1986). Tensile Tests and Failure Analysis of Concrete. Journal of Structural Engineering, 112(11), 2462–2477.

Sarkis, Ana I, Bueker, F., Sullivan, T. J., Elwood, K. J., Brunesi, E., & Hogan, L. (2022). Aspects Affecting the Nonlinear Behavior of Precast Pre-Stressed Hollow-Core Units Failing in Shear. Structural Concrete. https://doi.org/10.1002/suco.202100579

Sarkis, Ana I, Sullivan, T. J., Brunesi, E., & Nascimbene, R. (2022a). Assessment of the Torsional Behavior of Hollow-Core Slabs. Bulletin of the New Zealand Society for Earthquake Engineering. Manuscript under review

Sarkis, Ana I, Sullivan, T. J., Brunesi, E., & Nascimbene, R. (2022b). Critical Modelling Criteria for Precast Pre-Stressed Hollow-Core Slabs. Journal of Building Engineering. Manuscript under review

Sarkis, Ana Isabel, & Sullivan, T. (2021). Finite Element Analyses of Hollow Core Units Subjected to Shear and Torsion. New Zealand Society for Earthquake Engineering 2021 Annual Conference.

Selby, R. G., & Vecchio, F. J. (1993). 3D Constitutive Relations for Reinforced Concrete. Tech, Rep. 93-02, Department of Civil Engineering, Toronto, Canada.

Thorenfeldt, E. (1987). Mechanical Properties of High-Strength Concrete and Applications in Design. Symposium Proceedings, Utilization of High-Strength Concrete, Norway, 1987.

Vecchio, F. J., & Collins, M. P. (1986). The Modified Compression-Field Theory for Reinforced Concrete Elements Subjected to Shear. ACI J., 83(2), 219–231.

Yang, L. (1994). Design of Prestressed Hollow Core Slabs with Reference to Web Shear Failure. Journal of Structural Engineering, 120(9), 2675–2696.

ISSN No. 2744-7871